REPORT DOCUMENTATION PAGE

Form Approved
OMB No 0704-0188

1. AGENCY USE ONLY (Leave blank)	2. REPORT DATE	3. REPORT TYPE AND DATES COVERED
	Sept. 30, 1996	Technical 1/1/96 - 9/30/96

4. TITLE AND SUBTITLE
Higher Order Turbulence Results for a Three-Dimensional Pressure-Driven Turbulent Boundary Layer

5. FUNDING NUMBERS
N00014-94-1-0092

6. AUTHOR(S)
M. Semih Ölçmen and R.L. Simpson

7. PERFORMING ORGANIZATION NAME(S) AND ADDRESS(ES)
Dept. of Aerospace and Ocean Engineering
Virginia Polytechnic Institute & State University
Blacksburg, VA 24061-0203

8. PERFORMING ORGANIZATION REPORT NUMBER
VPI - AOE - 237

9. SPONSORING / MONITORING AGENCY NAME(S) AND ADDRESS(ES)
Office of Naval Research
800 N. Quincy St.
Arlington, VA 22217

10. SPONSORING / MONITORING AGENCY REPORT NUMBER

11. SUPPLEMENTARY NOTES

12a. DISTRIBUTION / AVAILABILITY STATEMENT
Unlimited

12b. DISTRIBUTION CODE

13. ABSTRACT *(Maximum 200 words)*

Triple and fourth-order turbulence products obtained from coincident fine-spatial-resolution three-velocity-component laser-Doppler-anemometer measurements are presented for a three-dimensional pressure-driven turbulent boundary layer from $y^+ > 3$ to the outer edge in local wall-shear-stress-direction co-ordinates. The wind tunnel flow is produced by a $Re_\theta = 5940$, $U_{ref} = 27.5$ m/s, upstream turbulent boundary layer on a flat surface that approaches a wing-body junction, although no results near the junction vortex are presented. For most of the presented locations, the mean velocities and stresses from this data set were previously discussed by Ölçmen and Simpson (1995a). New data at additional locations and for a mean two-dimensional flow are presented. Results are plotted in 6 different co-ordinate systems in Appendices A-F.

14. SUBJECT TERMS
Three-Dimensional Flow
Turbulence Structure

15. NUMBER OF PAGES
168

16. PRICE CODE

17. SECURITY CLASSIFICATION OF REPORT	18. SECURITY CLASSIFICATION OF THIS PAGE	19. SECURITY CLASSIFICATION OF ABSTRACT	20. LIMITATION OF ABSTRACT
unclassified	unclassified	unclassified	unlimited

ABSTRACT

Triple and fourth-order turbulence products obtained from coincident fine-spatial-resolution three-velocity-component laser-Doppler-anemometer measurements are presented for a three-dimensional pressure-driven turbulent boundary layer from $y^+ > 3$ to the outer edge in local wall-shear-stress-direction co-ordinates. The wind tunnel flow is produced by a $Re_\theta = 5940$, $U_{ref} = 27.5$ m/s, upstream turbulent boundary layer on a flat surface that approaches a wing-body junction, although no results near the junction vortex are presented. For most of the presented locations, the mean velocities and stresses from this data set were previously discussed by Ölçmen and Simpson (1995a). New data at additional locations and for a mean two-dimensional flow are presented.

The flow is progressively skewed in a counterclockwise direction while decelerating and then is skewed in a clockwise direction while accelerating. At the upstream locations the flow gradient angles in the outer layer persist in the upstream direction. Large $\overline{uw}$, $-\overline{vw}$ are produced, which change sign at the downstream locations. The Reynolds shearing stresses lag the mean velocity gradients.

At all velocity profile stations, in the nearest wall region ($y^+ < 15$) sweeping motions ($u > 0$) produce substantial positive $\overline{u^3}$, $\overline{uv^2}$, $\overline{uw^2}$, $\overline{-u^2v}$ values. As the upstream near-wall mean flow is skewed progressively in a counterclockwise direction relative to the local freestream, wallward motions of outer layer fluid produce positive $\overline{u^2w}$, $\overline{v^2w}$, $\overline{-uvw}$, $\overline{w^3}$; generally $\overline{v^3}$ is negative nearest the wall. At later stations where the near-wall flow is being skewed clockwise back toward the original direction, $\overline{u^2w}$, $\overline{v^2w}$, $\overline{-uvw}$, $\overline{w^3}$ are negative; $\overline{v^3}$ is positive where the flow is being skewed clockwise. Positive $\overline{vw^2}$ indicates the importance of motions away from the wall ($v > 0$). Only at stations where the skewed flow is returning to the original direction is $\overline{vw^2} < 0$ and wallward motions dominant. In the outer layer, motions away from the wall ($v > 0$) generally account for the triple-product behavior. Selected fourth-order products are presented which influence the turbulent diffusion of turbulent kinetic energy equation triple products.

Results are plotted in 6 different co-ordinate systems in Appendices A-F.

Table of Contents

NOMENCLATURE

C_p	static pressure coefficient
$(\partial C_p/\partial x)_{FS}$	static pressure coefficient gradient
C_{ij}	$\frac{\partial \overline{u_i u_j}}{\partial t}+U_l\frac{\partial \overline{u_i u_j}}{\partial x_l}$, Reynolds' stress convection tensor
FA	$\arctan(W/U)$, flow angle
FGA	$\arctan(\frac{\partial W/\partial y}{\partial U/\partial y})$, flow gradient angle
p	fluctuating pressure component
$P_{ijk\,1}$	$\overline{u_i u_j}(\overline{u_k u_m})_{,m}+\overline{u_j u_k}(\overline{u_i u_m})_{,m}+\overline{u_k u_i}(\overline{u_j u_m})_{,m}$, triple product transport production tensor
$P_{ijk\,2}$	$-(\overline{u_i u_j u_m}\ U_{k,m}+\overline{u_k u_i u_m}\ U_{j,m}+\overline{u_j u_k u_m}\ U_{i,m})$, triple product transport production tensor
PR_{ij}	$-(\overline{u_i u_l}\frac{\partial U_j}{\partial x_l}+\overline{u_j u_l}\frac{\partial U_i}{\partial x_l})$, Reynolds' stress production tensor
PD_{ij}	$-\frac{1}{\rho}(\frac{\partial(\overline{pu_j})}{\partial x_i}+\frac{\partial(\overline{pu_i})}{\partial x_j})$, Reynolds' stress pressure diffusion tensor
Re_θ	Reynolds number based on momentum thickness
S_{ij}	rate-of-strain tensor
SSA	$\arctan(\frac{\overline{vw}}{\overline{uv}})$, shear stress angle
TD_{ij}	$-\frac{\partial(\overline{u_i u_j u_l})}{\partial x_l}$, Reynolds' stress turbulent-diffusion tensor
TKE	$(\overline{u^2}+\overline{v^2}+\overline{w^2})/2=(\overline{u_i u_i})/2$, Turbulent kinetic energy
U_e	velocity magnitude at the boundary layer edge
U_i	mean velocity components
$\overline{u_i u_j}$	Reynolds stress tensor. i=1, 2, 3; j=1, 2, 3.
$\overline{u_i u_j u_k}$	triple velocity correlation tensor
U^+	$\frac{U}{u_\tau}$, nondimensional mean velocity
u_τ	$\sqrt{\tau_w/\rho}$, skin friction velocity

VD_{ij}	$\nu\frac{\partial^2\overline{u_iu_j}}{\partial x_l^2}$, Reynolds' stress viscous diffusion tensor
x_{TC}, y_{TC}, z_{TC}	tunnel coordinates
$y^+ = yu_\tau/\nu$	wall-law variable
β_{FS}	flow angle at the boundary layer edge
β_{WC}	wall-stress direction
δ_{ij}	Dirac delta function. $\delta_{ij}=1$ if i=j, $\delta_{ij}=0$ if i≠j.
δ	boundary layer thickness
ε_{ij}	$-2\nu\frac{\overline{\partial u_i\,\partial u_j}}{\partial x_l\,\partial x_l}$, Reynolds' stress viscous dissipation tensor
ε	$\varepsilon_{ii}/2$, dissipation of turbulent kinetic energy
θ	$\int_0^{\infty}(1-\frac{U}{U_e})\frac{U}{U_e}dy$, momentum thickness
ν	kinematic viscosity
ρ	density
σ	standard deviation
τ	$\sqrt{(-\rho\overline{uv})^2+(-\rho\overline{vw})^2}$, shear stress magnitude in the flow
τ_w	wall shear stress
Φ_{ij}	$\overline{\frac{p_l}{\rho}(\frac{\partial u_i}{\partial x_j}+\frac{\partial u_j}{\partial x_i})}$, Reynolds' stress pressure-strain tensor
Ω_{ij}	vorticity tensor
d_{ijk}	$-[\overline{u_iu_ju_ku_m}+\overline{(p/\rho)u_ju_k}\delta_{im}+\overline{(p/\rho)u_ku_i}\delta_{jm}+\overline{(p/\rho)u_iu_j}\delta_{km}-\nu\overline{(u_iu_ju_k)}_{,m}]_{,m}$, triple product transport diffusion tensor
ϕ_{ijk}	$\overline{(p/\rho)[(u_iu_j)_{,k}+(u_ku_i)_{,j}+(u_ju_k)_{,i}]}$, triple product transport pressure interaction tensor
ε_{ijk}	$2\nu(\overline{u_ku_{i,m}u_{j,m}}+\overline{u_ju_{k,m}u_{i,m}}+\overline{u_iu_{j,m}u_{k,m}})$, triple product transport dissipation tensor

List of Tables

CHAPTER I. INTRODUCTION

Recent studies of three-dimensional turbulent boundary layers (3D-TBL) have dealt with many issues related to the physics of turbulent flows. Reynolds-averaged turbulence closure models for 3D-TBLs are still a main issue. The anisotropy of the turbulence structure, the variation of the $-\overline{uv}$ *and* $-\overline{vw}$ shear stresses under the action of the major rates of strain $\partial U/\partial y$ *and* $\partial W/\partial y$, and the structural parameters relating Reynolds stresses are issues that have been examined (Ölçmen and Simpson, 1993, 1995a). Simplified 2-D calculation methods that have been extended to 3D-TBLs do not seem to work satisfactorily, especially with adverse-pressure gradients and strongly skewed flows. Simplified equations relating the shear stresses to mean flow quantities and/or relating higher order moments to lower order moments in an ad hoc fashion do not seem to reflect the flow physics in 3D-TBLs (Simpson, 1995). Not only are more data of stress and higher order moments needed, but also new relations among important Reynolds-averaged flow variables should be developed from data. Measurements in 3D-TBLs, including higher order moments, are necessary for modeling the correct nature of turbulence. Many existing data sets include only the mean velocity and Reynolds stresses since the measurement of triple or higher order products was difficult. Recent data sets include some higher order moment information. However, the very near-wall characteristics are not reported for high momentum thickness Reynolds numbers (Re_θ) due to physical limitations of the instrumentation or are available for mainly low Reynolds number flows.

Bradshaw and Pontikos (1985) made measurements on an 'infinite' swept wing configuration similar to Elsenaar and Boelsma flow (1974) at 4 locations ($Re_\theta \approx 5000$). Mean velocities, Reynolds stresses and triple products were measured with single hot-wire and cross-wire hot-wire probes above $y^+ \approx 230$ and the skin friction measurements were made with a surface fence. The shear stress angle ($SSA = \arctan(\overline{vw}/\overline{uv})$) lagged behind the flow gradient angle ($FGA = \arctan(\frac{\partial W/\partial y}{\partial U/\partial y})$). Townsend's A_1 structural parameter (the ratio of the magnitude of the shear stress to the twice the turbulent kinetic energy $A_1 = \sqrt{(-\overline{uv})^2 + (-\overline{vw})^2}/(\overline{u^2}+\overline{v^2}+\overline{w^2})$ decreased with the effect of 3-D from a value of 0.17 to 0.08 at the last station. Their turbulent kinetic energy

(TKE) balance showed that turbulent diffusion increased in magnitude in 3-D flow and is as high as the advection terms, but is smaller than the production and dissipation terms. The flatness of v fluctuations increased towards the layer outer edge with values between 15 to 20. The $-\overline{uv}$ stress progressively decreased downstream; possibly due to a tilting of the 2D vortices in the y-z plane that reduced the effectiveness of turbulent mixing (Bradshaw and Pontikos, 1985).

Driver and Hebbar (1987) studied a 3-D flow generated by a spinning cylinder ($W_{surface}=U_e$) under a zero pressure gradient. Measurements were made on a stationary section of the cylinder downstream of the spinning section using a 3 component LDV at $Re_\theta \approx 6000$. Measurements of the mean flow, Reynolds stresses, and triple products were made above $y^+ \approx 40$. The skin friction was measured using a fence gage. Computation of the flow based on the Reynolds stress model of Launder-Reece-Rodi (L-R-R) (1975) showed that the model overpredicted the $-\overline{uv}$ *and* $-\overline{vw}$ stresses throughout the layers. The eddy viscosity was anisotropic. Severely underestimated triple products were obtained using some relations of Daly-Harlow (1970) and L-R-R (1975) between triple products and lower order products. However, the pressure rate-of-strain model of Naot et al. (1973) and Launder-Reece-Rodi (1975) seemed to estimate the pressure rate-of-strain data variation reasonably well throughout the layers. Driver and Hebbar estimated the pressure rate-of-strain data from the stress transport equation balance.

Driver and Johnston (1990) studied both pressure-gradient and three-dimensionality effects on turbulence using a spinning or stationary cylinder with zero or varying streamwise pressure gradients generated by the diverging tunnel geometry and controlled with boundary layer suction at the walls. The Re_θ of the flow varied from 4000 (2D case) to 6000 (3D case D.S1). Downstream of the spinning cylinder, measurements of the mean velocity, Reynolds stress and triple products were obtained on the stationary cylinder on which the three-dimensionality decayed under an adverse pressure gradient. Measurements as close as $y^+ \approx 8$ were obtained with a 3-velocity-component LDV; and skin friction was measured with an oil-film interferometer. The TKE balance showed that the production and dissipation terms were of the same order of magnitude and convection and diffusion terms were nearly zero (case D.S1, $U_{ref} = W_{surface}$), indicating an equilibrium flow. The value of A_1 dropped to ≈ 0.11 in the outer region (case D.S1) and near-wall values were as low as 0.05. The SSA lags the FGA. Launder-Reece-Rodi (1975) and Naot-Shavit-Wolfshtein (1973) pressure-strain models were able to estimate the pressure-strain terms closely for that flow. However, the shear stress direction was estimated poorly.

Littel and Eaton (1991) studied a 3-D TBL on a rotating disk. The mean velocity was measured using a 3-hole probe and turbulence and higher order statistics were measured with

cross-wires and single-wire hot-wire anemometry at several different Reynolds numbers at different radial locations with different angular velocity of the rotating disk. For radius=0.421 meters, Re_θ was between 2645 to 6065 and, measurements were above $y^+ \approx 112$. The skin friction was calculated using a log-law fit. The value of A_1 decreased monotonically away from the wall. The ratio of the spanwise eddy viscosity to the streamwise eddy viscosity was between ≈0.8 and 1.1, indicating approximately an isotropic eddy viscosity. The TKE balance showed that turbulent diffusion was negligibly small.

Schwarz and Bradshaw (1993, 1994) studied the cross-flow development and decay generated by a 30° bend at $Re_\theta = 4100$. Data include the mean velocity obtained with a three-hole pressure probe and Reynolds stresses and triple products obtained for $y/\delta > 0.1$ ($y^+=150$) with cross-wire hot-wire probe. The shear stress angle lagged the flow gradient angle and the A_1 structural parameter was reduced with 3-D effects. The TKE energy balance showed that turbulent diffusion term is smaller than the dissipation and production terms.

Flack and Johnston (1993) studied the 3-D TBLs produced by flow in a 30° bend and flow approaching a swept 45° forward facing step in a water tunnel. The Re_θ varied from ≈ 1300 to 1700 for the 30° bend case and ≈ 1400 to 1850 for the forward facing step case. Skin friction at the wall was calculated using the total velocity gradient and the dynamic viscosity in the sublayer. Measurements of the mean velocity, Reynolds stresses and ten triple products were made with a 3-velocity-component LDV as close as $y^+ \approx 1.5$. The SSA lagged the FGA in the outer layer, while below $y^+ \approx 10$ the SSA leads the FGA. The A_1 parameter decreased with increased 3D effects, although both the TKE and shear stress magnitude increased. The distribution of some of the triple products in the layers presented in that study are qualitatively similar to the quantities presented in this study.

Here higher-order moment results are presented and discussed for a 3-D pressure-driven turbulent boundary layer generated by a 3:2 elliptic-nose/NACA 0020 tail wing (chord = 30 cm, thickness = 7.17 cm, height = 22.5 cm) perpendicular to a flat plate. The Reynolds number based on momentum thickness measured 0.75 chord upstream of the wing on the centerline is 5940 for a nominal air speed of 27.5 m/sec. LDV data were obtained at 9 stations along a line defined by translating along the flow-angle direction at the y locations in each profile where the $\overline{u^2}$ normal stress is maximum. This location was conjectured as the y location where the inner and outer layer turbulence structure overlaps. The line was defined with hot-wire measurements at 18 stations. The flow studied is a unique data set in which the lateral pressure gradients that turn the flow change their sign and thus turn the very near-wall flow back toward its initial direction.

Figure 1 shows a portion of the wing, the measurement locations, and the local free-stream x_{FS} and the local wall-stress coordinate x_{WC} directions at each location. The x_{FS} coordinate is in the direction of the local inviscid velocity immediately outside the boundary layer. The x_{WC} coordinate is in the direction of the flow angle at the first nearest-wall measurement location of each station profile. The y coordinate is normal to the surface in both coordinates and the z_{FS} and z_{WC} coordinates form right-handed systems. This figure shows that at stations 6 to 9 the wall coordinates and local free-stream coordinates are very close to each other (table 1). Mean velocities, Reynolds stresses, and skin friction values as well as the flow angle, flow gradient angle and shear stress angle at stations 1 through 7 were previously discussed by Ölçmen and Simpson (1995a) in local free-stream coordinates. For completeness, for reference and for some new insights, mean velocity components (Section II), SSA, FGA, and FA (Section III) and the Reynolds stresses (Section IV) are presented here in wall-stress coordinates. Besides these previously discussed data, 2 new additional LDV profiles at stations 8 and 9 are also presented. The new data contain the mean velocities, Reynolds' stresses, 10 triple products and 15 quadruple products, where the 3-D flow is relaxing downstream of station 7. A 2-D flow profile was also measured with the LDV in the vicinity of the station 5 without the wing present in order to document the variation of higher order terms near the wall. Data presented here satisfy the realizability conditions described by Schumann (1977). All quantities except the mean velocities and normal stresses are nondimensionalized with respective powers of the normal stresses in correlation coefficient form. Mean velocity components and normal stresses are nondimensionalized by respective powers of skin-friction velocity=u_τ ($u_\tau=\sqrt{\frac{\tau_w}{\rho}}$, τ_w=wall shear stress magnitude, ρ=density). All quantities are plotted vs. y^+ ($y^+=\frac{yu_\tau}{\nu}$, y=distance from the wall, ν=kinematic viscosity). At stations 1 through 7 the u_τ skin friction velocity was obtained with an oil-film interferometry technique by Ailinger (1990). At stations 8 and 9 skin friction is calculated using the near wall mean velocity gradient and the dynamic viscosity. For the 2-D profile Coles law-of-the-wall profile with constants κ=0.41 and C=5 was used to calculate u_τ. The uncertainties in the measured quantities with 20:1 odds are given in table 2. Measurements were made with a 3-velocity-component LDV system which is a sub-system of a 5-velocity-component LDV system designed to study near-wall turbulence (Ölçmen and Simpson, 1995 b). The probe volume diameter was 30 μm and measurements were made as close as y^+≈3 to the wall with a (+20,-5μ)

uncertainty in y location. The surface pressure distribution on the wall was measured at closely spaced locations. An oil-flow visualization technique was used to reveal the skin-friction line characteristics for this flow. Skin-friction coefficient magnitude and direction were reported from measurements by an oil-film interferometry technique. However, due to the direction uncertainty, the wall-stress direction was taken as the mean flow direction of the closest to wall point in the profiles.

For reference, the conclusions of the previous work (Ölçmen and Simpson, 1995a) are summarized here. The flow is highly anisotropic, with an anisotropy ratio (ratio of the lateral to longitudinal eddy viscosities) different than 1. In wall-stress direction coordinates, the anisotropy constant is close to 0.6, although it varies through the layers and from station to station. The shear stress angle lags behind the flow gradient angle. Townsend's structural parameter A_1 is observed to be less than 0.15 at the outer regions of the layers, and substantially less than 0.15 near the wall, with double-peaked profiles at some stations. The ratio of the vertical normal stress to the shear stress magnitude ($\overline{v^2}/|\tau/\rho|$) is about 1.6 in the $y^+ \approx 100$ to 1000 range. Also, the ratio of the shear stresses $-\overline{vw}/-\overline{uw}$ varies semi-logarithmically and the ratio of the production of these stresses $C=-\overline{vw}_{production}/-\overline{uw}_{production}$ is about constant throughout the layers, although it varies from station to station. For further details see Ölçmen and Simpson (1995a).

CHAPTER II. MEAN FLOW AND REYNOLDS STRESS RESULTS

The U/u_τ profiles at all stations follow each other closely up to $y^+ \approx 9$ (figure 2). Above this height, station 1, 2 and 3 values closely follow each other up to $y^+ \approx 100$. These are the stations where three-dimensionality of the flow starts to develop. The $U//u_\tau$ profiles overlap each other with a semi-logarithmic variation in the $y^+ \approx 30\text{-}150$ range, suggesting a similarity relation. At downstream stations there is no similarity. Starting with station 4 the profiles become fuller and the semi-logarithmic regions of the profiles shift to higher locations in the profiles, especially at stations 8 and 9 this effect is more pronounced.

This presentation of the data in wall coordinates is in the law-of-the-wall similarity variables of Coles (1956) and van den Berg (1975). Nine similarity relations including these two relations were examined with nine different data sets and no strong evidence for a law-of-the-wall similarity relation could be found (Ölçmen and Simpson, 1992). Among these relations, the Johnston (1960) similarity relation for the component $Q = U_{FS}/\cos(\beta_w - \beta_{FS})$ in the local free-stream direction seemed to fit those data better than the others:

$$Q^+ = \frac{U_{FS}}{u_\tau \cos(\beta_w - \beta_{FS})} = B_1 \ln\left(\frac{y\, u_\tau}{\nu}\right) + B_2 \qquad (1)$$

Johnston's relation also fits the present data best (figure 3) for the first 3 stations with B_1 and B_2 constants close to the Coles and Hirst (1968) constants of $\kappa = 0.41 (\approx 1/B_1)$ and $C = 5.0 (\approx B_2)$. This suggests that a law-of-the-wall semi-logarithmic profile with universal constants only exists for the initial stages of a mean 3-D flow.

The V/u_τ profile at the first station gradually increases from the wall to the layer edge (figure 4). At station 2 and downstream the maxima of the profiles are within $y^+ \approx 600$ to 1000 and grow with increasing 3-D effects as the local free-stream flow accelerates. Near the layer edge at each station the values decrease. The scale of the V/u_τ is 1/20th of U/u_τ plots and in the region below $y^+ < 100$ the mean velocity value is nearly zero for stations 1 through 7. This shows that below $y^+ \approx 100$ the vertical motion of the flow is due to turbulent fluctuations. At stations 1 through 8 up to $y^+ \approx 300$ the magnitude of V/u_τ is lower than the 2-D value. At station 9 the magnitude is twice of the magnitude at station 8 due to the effect of the horse-shoe vortex (Devenport and

Simpson, 1992) lifting the flow away from the wall.

Due to the definition of the wall-stress coordinates, W/u_τ profiles are close to each other very near the wall with a magnitude of zero (figure 5). At the first 3 stations W/u_τ monotonically increases from the wall to the layer edge since the flow in the entire layer turns in one direction. Between stations 3 and 4 the lateral pressure gradient in wall-stress coordinates changes sign. At station 4 the W/u_τ values are close to zero up to $y^+ \approx 40$. Above this y location, values monotonically increase. At stations further downstream the effect of the sign change of the lateral pressure gradient is felt most near the wall. This results in negative W/u_τ values. The magnitude of the absolute maximum progressively increases downstream and maximum points in the profiles shift upward in the layers. The Reynolds-averaged Navier-Stokes equations show that the mean flow is immediately affected by the mean pressure gradients. The pressure force is most effective on the near-wall flow where the momentum of the flow is lowest. The lateral pressure gradient in wall-coordinates increases in magnitude proceeding downstream of station 4 till station 7, and thus the effect of the pressure gradient is felt in a larger y range near the wall. At stations 8 and 9 the lateral pressure gradient is negative with smaller magnitudes. Some length scales calculated using the mean velocities are given in table 3.

II A. FLOW ANGLE, FLOW GRADIENT ANGLE, SHEAR STRESS ANGLE

The flow angle, flow gradient angle and the shear stress angle are defined as

$$FA=\arctan\left(\frac{W}{U}\right)\ ;\ FGA=\arctan\left(\frac{\partial W/\partial y}{\partial U/\partial y}\right)\ ;\ SSA=\arctan\left(\frac{\overline{vw}}{\overline{uv}}\right) \qquad (2)$$

and are plotted against y^+ in wall stress coordinates (figure 6). At the first 3 stations the flow angles monotonically increase towards the layer edge. At station 4 the flow angle is very close to zero till $y^+ \approx 40$. At downstream stations the flow angles are negative near the wall due to the crossflow pressure gradient effect and the absolute maximum value of the profiles increases till station 6. Downstream of station 6 absolute flow angle maxima decrease. The location of the absolute maximum progressively shifts upward in the layers. The flow angle at the layer edge in wall-stress coordinates increases till station 3. At downstream stations the layer edge flow angle decreases till station 9. At stations 6 through 9 the wall-stress coordinates and the free-stream coordinates are oriented in close proximity to one another. This results in a unique flow feature. While the near-wall flow and the free-stream flow are in directions close to one another, the

intralayer flow is in different directions.

At the first 2 stations the flow gradient angle is approximately a constant above $y^+ \approx 100$. Further downstream they show a maximum peak at increasing distances away from the wall. At stations 5 to 9 minima are also observed. For the first 4 stations the shear stress angle above $y^+ \approx 100$ is about constant in the tunnel co-ordinate direction (Simpson, 1995). At downstream stations, above this y^+ location the shear stress angle profiles form peaks. At every station, the shear-stress angle lags behind the flow gradient angle. Very near the wall large differences are observed for the downstream stations. At stations 8 and 9 the difference is highly increased. At station 9 SSA is approximately at -90° with respect to the FGA. The shear stress angle responds to the changes in flow gradient angle in the same direction, but with a smaller change in magnitude. At station 5 through 7 this results in the intersection of the shear stress angle and flow gradient angle profiles at 2 points, which is discussed later in the text. At station 8 the SSA and FGA follow each other closely in a region $y^+ \approx 25$ to 300. At station 9 there exists a similar region above $y^+ \approx 100$ till 450, where the main stress is in the direction of the main strain.

II B. REYNOLDS STRESSES

The $\overline{u^2}/u_\tau^2$ normal stress profiles steeply increase from the wall to their peak at $y^+ \approx 15$ to 20 and then decrease up to $y^+ \approx 60$ to 450 at different stations (figure 7). The fluctuation continuity equation dictates that nearest the wall u fluctuating velocity varies as y. The plateau region where $\overline{u^2}/u_\tau^2$ is approximately constant varies at different stations. The maximum in the profiles decreases till station 4 due to adverse pressure gradient effects and then increases back to station 1 values downstream due to the accelerating flow. However, above $y^+ \approx 100$ the values decrease monotonically downstream of station 1 till station 7. The decrease at station 7 is approximately 60% of the station 1 value. This suggests that there are two zones in the flow where $\overline{u^2}$ is distinctly different: 1) below $y^+ \approx 100$ which is highly affected by the pressure gradients and wall proximity, and 2) above $y^+ \approx 100$ where the flow relaxes with more pronounced 3-D effects. The streamwise pressure gradient is favorable downstream of station 2 until past station 6. Between stations 6 and 7 $(\partial C_p/\partial x)_{wc}$ changes sign. At downstream stations $\overline{u^2}/u_\tau^2$ increases both in the inner and the outer regions. The peak location at each profile is between $y^+ \approx 15$ to 20. The maximum values for 1, 6, and 7 are close to the peak value for 2-D flow. At stations 2 through 5 the peak value is lower and at stations 8 and 9 the peak value is higher than 2-D values. Above

$y^+ \approx 200$, the $\overline{u^2}/u_\tau^2$ values are lower than the 2-D values except at stations 1, 2 and 3.

Profiles of $\overline{v^2}/u_\tau^2$ monotonically increase to a maximum between $y^+ \approx 300$ to 400 and then decrease toward the freestream (figure 8). Downstream of station 1 up to station 5 the maximum value decreases. The station 6 maximum is higher than the maxima at stations 5 and 7. At stations 8 and 9 the profiles show two maxima: one around $y^+ \approx 60$ and one around $y^+ \approx 400$. The near wall values at these stations are higher than station 1 values below $y^+ \approx 80$, and away from the wall the values are in between the station 3 and 4 values. The $\overline{v^2}/u_\tau^2$ profiles of stations 4 through 7 are lower compared to the 2-D values and other stations have higher values compared to 2-D values throughout the layers.

The $\overline{w^2}/u_\tau^2$ profiles reach maxima at a lower y^+ location than the $\overline{v^2}/u_\tau^2$ stress profiles (figure 9). Values at station 2 are higher with respect to station 1 and station 3 values are close to station 2 values. Proceeding downstream up to station 7 values decrease. At stations 8 and 9 the values closely follow each other and are increased close to station 4 values above $y^+ \approx 100$, below $y^+ \approx 30$ the values are close to station 2 values. Compared to 2-D profile all stations except station 7 have values higher than 2-D values above $y^+ \approx 100$. However near the wall at stations 4 through 7, $\overline{w^2}/u_\tau^2$ is decreased compared to the 2-D profile, presumably due to the increased favorable pressure gradient's effect on the fluctuating velocities.

The Reynolds-stress transport equation with summation-subscript notation can be written as (Daly, and Harlow, 1970):

$$\underbrace{\frac{\partial \overline{u_i u_j}}{\partial t} + U_l \frac{\partial \overline{u_i u_j}}{\partial x_l}}_{\textit{convection}} = \underbrace{-\left(\overline{u_i u_l}\frac{\partial U_j}{\partial x_l} + \overline{u_j u_l}\frac{\partial U_i}{\partial x_l}\right)}_{\textit{production}}$$

$$\underbrace{+\overline{\frac{p}{\rho}\left(\frac{\partial u_i}{\partial x_j} + \frac{\partial u_j}{\partial x_i}\right)}}_{\textit{redistribution}}$$

$$\underbrace{-\frac{\partial(\overline{u_i u_j u_l})}{\partial x_l}}_{\textit{turbulent diffusion}} \quad \underbrace{-\frac{1}{\rho}\left(\frac{\partial(\overline{p u_j})}{\partial x_i} + \frac{\partial(\overline{p u_i})}{\partial x_j}\right)}_{\textit{pressure diffusion}} \quad \underbrace{+\nu\frac{\partial^2 \overline{u_i u_j}}{\partial x_l^2}}_{\textit{viscous diffusion}} \tag{3}$$

$$\underbrace{-2\nu\overline{\frac{\partial u_i}{\partial x_l}\frac{\partial u_j}{\partial x_l}}}_{\textit{viscous dissipation}}$$

The production rate terms for the $\overline{u^2}, \overline{v^2}$ *and* $\overline{w^2}$ stresses can be written as $(-2\overline{uv}\frac{\partial U}{\partial y})$, $(-2\overline{v^2}\frac{\partial V}{\partial y})$, and $(-2\overline{vw}\frac{\partial W}{\partial y})$, assuming that the variations in the x and z directions are much smaller than the variations in y direction. The relative magnitudes of these mean velocity gradients are $|\frac{\partial U}{\partial y}| > |\frac{\partial W}{\partial y}| > |\frac{\partial V}{\partial y}|$ and the stresses are $\overline{v^2} > |\overline{uv}| > |\overline{vw}|$. This results in the $\overline{u^2}$ production rate being much higher than that for $\overline{v^2}$ and $\overline{w^2}$. The equations for the production terms show that for the type of flow studied here while the production of $\overline{u^2}$ is never zero in the layers the $\overline{w^2}$ production is zero at locations where $\overline{vw}=0$ and/or $\partial W/\partial y$ is 0. These locations correspond to the locations where the shear stress angle is zero ($\arctan(\overline{vw}/\overline{uv})=0$) and/or the flow gradient angle is zero ($\arctan(\frac{\partial W/\partial y}{\partial U/\partial y})=0$). Production of $\overline{v^2}$ is zero at locations where $(\partial V/\partial y)=0$. At stations 2 and downstream stations this location is below $y^+ \approx 8$. The production of $\overline{v^2}$ is an order of magnitude smaller than that of $\overline{w^2}$ and two orders of magnitude smaller than that of $\overline{u^2}$. The only other stress transport equation term reported here is for the turbulent diffusion. Since $\partial(\overline{u_i u_j u_l}) / \partial x_l$ with l = 2 (in the perpendicular direction) is the main turbulent diffusion term, where it is zero corresponds to the locations where the turbulent diffusion is approximately zero.

At all stations the $\overline{uv}/(\overline{u^2}\,\overline{v^2})^{1/2}$ correlation coefficient show double peaks; one near the wall below $y^+ \approx 50$ and one around $y^+ \approx 300$ to 1000 range (figure 10). The near wall magnitude decreases till station 3. Stations 4 and 5 show the magnitude increase due to the favorable pressure gradient. Station 6 has values close to station 5. Station 7 has the highest near-wall magnitude. At stations 8 and 9 the correlation magnitude decreases again. The $\overline{uv}/(\overline{u^2}\,\overline{v^2})^{1/2}$ shows the combined effect of streamwise pressure gradient on shear stress and normal stresses. The 2-D data values reach at a plateau value of 0.3 around $y^+ \approx 30$; a value lower than vast amounts of previous data on 2-D turbulent boundary layers. To resolve this ambiguity four different profiles were taken which did not change the results presented. Re-reduction of the raw data without cleaning the noise at the skirts of individual histograms of U, V, W velocity data and without using the velocity bias weighting scheme resulted in lower correlation values. Crude

rotation of the raw data obtained in optical coordinates to tunnel coordinates without using the accurate transformation scheme also did not have any effect on the results. Also, the coincidence window of the frequency processors were varied between 0.8 μsec to 10 μsec without any changes in the measured quantities.

At the 2-D station $\overline{uv}/u_\tau^2$ is approximately a constant between $y^+ \approx$ 40 to 200 with a value of -0.9 which is a rather high value than -1.0 obtained in the literature. At station 1 $\overline{uv}/u_\tau^2$ reaches a plateau region at $y^+ \approx 40$ at about -1.2 and stays constant up to $y^+ \approx 400$. An effect of an adverse pressure gradient on 2-D TBLs is to reduce $-\overline{uv}$ near the wall and increase it in the outer region (Simpson et al., 1981). Above $y^+ \approx 100$, $-\overline{uv}/u_\tau^2$ increases as the flow moves downstream. However below $y^+ \approx 100$, $-\overline{uv}/u_\tau^2$ increases up to station 4, and is followed by a decrease at downstream stations. This decrease below $y^+ \approx 100$ and the increase above this y location, accompanied with the fact that the stresses both at the wall and at the layer edge must be zero, result in double-peaked stress distributions at stations 4 through 9. The minimum value obtained is at station 8 with a value of $\approx$-1.5 at $y^+ \approx 35$. A local minimum at $y^+ \approx 250$ with values close to that of station 7 is seen. A local maximum is observed at $y^+ \approx 550$ at the same station. At station 9 the peak minimum value is decreased, and between $y^+ \approx 300$ to 1000 a constant stress plateau with values close to that at station 7 in the same region is observed.

The $\overline{uw}/(\overline{u^2}\,\overline{w^2})^{1/2}$ correlation coefficient is positive at station 1 and increases in magnitude by station 2 (figure 11). Station 3 values above $y^+ \approx 40$ closely follow the station 2 values. Starting with station 4 the maximum positive value decreases, and near the wall correlation coefficient is negative. The negative minimum value obtained near the wall decreases at stations downstream of station 4 until station 6, and at further downstream stations it increases. The location of the minimum and the location where the $\overline{uw}$=0 shift up proceeding downstream. At stations 8 and 9 the coefficient changes its sign to become negative in the outer region. The positive peak locations in the profiles downstream of station 4 are further away from the wall. By definition the $\overline{uw}$ in a 2-D flow is zero due to the flow symmetry.

At the first station $\overline{uw}/u_\tau^2$ is constant at two-thirds the level of $-\overline{uv}/u_\tau^2$ between $y^+ \approx 25$ and 400. At station 2 this stress increases to a level higher than that of $-\overline{uv}/u_\tau^2$. At station 3 there is a slight decrease with respect to station 2. At station 4 and other downstream stations, the values change sign between $y^+ \approx 20$ to 100. At station 6 the near-wall maximum absolute value is 5/3

times higher than that of the maximum value of $-\overline{uv}/u_\tau^2$ at the same station. At station 7 the absolute maximum near the wall decreases. The minimum peak at Station 8 is as high as that at station 7. At station 9, the near wall peak value is decreased to ≈1/2 of that of station 8. The location where $\overline{uw}$ changes sign shifts to higher y^+ values at downstream stations.

The $\overline{vw}/(\overline{v^2}\,\overline{w^2})^{1/2}$ correlation coefficient is positive near the wall at all stations and changes sign further away from the wall proceeding downstream (figure 12). The minimum value of the profiles decreases proceeding downstream of station 1 until station 4 and is at $y^+ \approx 500$. At downstream stations the minimum values increase; also the near wall positive correlation region extends farther away from the wall. The maximum value is obtained at station 6. At downstream stations the maximum values decrease. The lateral pressure gradient becomes negative at station 4 and stays negative at downstream stations.

A similar development is observed for $\overline{vw}/u_\tau^2$. At stations 1 through 3 the value of the stress increases. From station 4 onwards, the near-wall values change sign. Sign change occurs at higher locations in the downstream profiles. The positive peak value locations in the profiles shift to higher y^+ values proceeding downstream. The positive peak value at station 8 is ≈0.47 which is 2.5 times higher than at station 7 and is comparable in magnitude to the minimum value obtained at station 3 which is ≈-0.55.

The $\overline{uw}$ and $\overline{vw}$ stresses have opposite signs to each other and are zero at locations close to each other. The major production terms for $\overline{uv}, \overline{uw}, \overline{vw}$ are $-(\overline{uv}\frac{\partial V}{\partial y}+\overline{v^2}\frac{\partial U}{\partial y})$, $-(\overline{uv}\frac{\partial W}{\partial y}+\overline{vw}\frac{\partial U}{\partial y})$, $-(\overline{v^2}\frac{\partial W}{\partial y}+\overline{vw}\frac{\partial V}{\partial y})$, respectively. Production of $\overline{uw}$ is zero where -tan (SSA)=tan (FGA), or where SSA=-FGA. Production of $\overline{vw}$ is zero where $\overline{vw}\frac{\partial V}{\partial y}=-\overline{v^2}\frac{\partial W}{\partial y}$. Therefore in the region where SSA=0 and/or FGA=0, the production of the stresses $\overline{w^2}$, $\overline{uw}$ and $\overline{vw}$ are approximately zero. On the contrary $-\overline{uv}$ and $\overline{u^2}$ productions are always positive in the layers while $\overline{v^2}$ production is small and negative, except in the outer layer where it is small and positive.

CHAPTER III. HIGHER ORDER PRODUCTS

The 6 stress transport equations with boundary layer approximations include only the y (vertical) derivatives of the triple products which are the Reynolds averages of the instantaneous Reynolds stresses multiplied with the instantaneous v fluctuating velocity, or the flux of the Reynolds stresses in the vertical direction. Therefore, the simplified equations do not include the $\overline{u^3}, \overline{w^3}, \overline{u^2w}, \overline{uw^2}$ triple products. The transport equation for the Reynolds-averaged triple products can be written as

$$\frac{D\overline{u_i u_j u_k}}{Dt} = P_{ijk1} + P_{ijk2} + d_{ijk} + \phi_{ijk} - \varepsilon_{ijk} \qquad (4)$$

where

$$P_{ijk1} = \overline{u_i u_j}\,(\overline{u_k u_m})_{,m} + \overline{u_j u_k}\,(\overline{u_i u_m})_{,m} + \overline{u_k u_i}\,(\overline{u_j u_m})_{,m}$$

$$P_{ijk2} = -(\overline{u_i u_j u_m}\ U_{k,m} + \overline{u_k u_i u_m}\ U_{j,m} + \overline{u_j u_k u_m}\ U_{i,m})$$

$$d_{ijk} = -[\overline{u_i u_j u_k u_m} + \overline{(p/\rho) u_j u_k}\,\delta_{im} + \overline{(p/\rho) u_k u_i}\,\delta_{jm} + \overline{(p/\rho) u_i u_j}\,\delta_{km} - \nu(\overline{u_i u_j u_k})_{,m}]_{,m}$$

$$\phi_{ijk} = \overline{(p/\rho)[(u_i u_j)_{,k} + (u_k u_i)_{,j} + (u_j u_k)_{,i}]}$$

$$\varepsilon_{ijk} = 2\nu(\overline{u_k u_{l,m} u_{j,m}} + \overline{u_j u_{k,m} u_{i,m}} + \overline{u_i u_{j,m} u_{k,m}})$$

P_{ijk1} and P_{ijk2} represent generation due to Reynolds stress, Reynolds stress gradient interaction and mean strains. d_{ijk} represents diffusion, ϕ_{ijk} represents pressure interaction, and ε_{ijk} represents dissipation (Nagano and Tagawa, 1991). ",m" denotes differentiation with respect to that direction. Locations where the Reynolds stresses or triple products are zero and/or the gradients of stresses or the mean velocity gradients are zero result in reduced production for the triple products. All the triple products at the wall are zero since the fluctuating velocities at the wall are zero. All the triple correlations analyzed were found to be of the same order of magnitude. Figures 13 to 22 show the triple products nondimensionalized with respective powers of the normal stresses, rather than u_τ^3 which is not a scaling velocity for the triple products as pointed out by Murlis et al. (1982). However the discussion on the triple products nondimensionalized with u_τ^3 is included here. The figures of the shear stresses and triple products nondimensionalized with respective powers of u_τ are not presented in this paper. All the triple products except $\overline{u^2w}$, $\overline{v^2w}$, $\overline{uvw}$, $\overline{w^3}$ show similar

trends at both 2-D and 3-D stations.

The $\overline{u^2v}/(\overline{u^2})(\overline{v^2})^{1/2}$ profiles show a similar shape at every station (figure 13). A minimum at $y^+\approx8$ and a local maximum around $y^+\approx40$ and another local maximum around $y^+\approx2000$ near the layer edge are observed. Near wall minima increase from 1 to 3, decrease from 3 to 7, and increase again from 7 to 9. Maxima near $y^+\approx40$ increase until station 7 and decrease at further downstream stations. The values decrease from their peak value to form a local minimum around $y^+\approx400$, at stations 5 to 9 these minima are negative .Compared to 2-D, all 3-D station values are lower near the wall up to $y^+\approx15$. The y flux of u^2 or $\overline{u^2v}$ is contained in the turbulent kinetic energy (TKE) equation and the $\overline{u^2}$ stress transport equation and (nondimensionalized with u_τ^3) has a local minimum at $y^+\approx10$ and a local maximum around $y^+\approx40$ at every station. Above this y location, the values decrease. This decrease is more pronounced progressively downstream. Values change sign between $y^+\approx15$ to 20. Below this y^+ location negative v fluctuating velocities are dominant and above it positive v fluctuations are dominant. This indicates that below $y^+\approx15$ to 20, where maximum TKE production occurs, the $\overline{u^2}$ energy on the average is carried towards the wall and above that y location away from the wall. The slope of $\overline{u^2v}/u_\tau^3$ in this region becomes larger due to increased production of $\overline{u^2}$ with acceleration of the flow at the last several stations. The production of $\overline{u^2}/2$ is also the major TKE production term, which means that the TKE contained in $\overline{v^2}/2$ and $\overline{w^2}/2$ mainly come from redistribution of $\overline{u^2}/2$ (Rotta, 1962). Consequently, it is expected that the turbulent diffusion of v^2 and w^2 will be much smaller than that for u^2.

The $\overline{vw^2}/(\overline{w^2})(\overline{v^2})^{1/2}$ values are between 0 to 0.1 for $y^+<1000$ (figure 14). This shows that the positive v fluctuations on the average occur with the w fluctuations. All 3-D station values are slightly lower than the 2-D values. At stations 6 and 7 around $y^+\approx20$ to 25 negative minima are observed. The y flux of w^2 or $\overline{vw^2}$ is small in magnitude with respect to other triple products. Qualitatively the values increase towards the boundary layer edge and then decrease to zero. Except at stations 6 and 7 near the wall all the values are positive, indicating that w fluctuations occur more strongly together with positive v fluctuations.

The skewness

$$S_{(\,)} = \frac{\overline{(\,)^3}}{[\overline{(\,)^2}]^{3/2}} \qquad (5)$$

shows the asymmetry of the probability distribution function (p.d.f) of a fluctuation quantity. For a symmetric distribution such as a Gaussian the skewness is zero. A positive skewness indicates a greater number of occurrences of a quantity for large positive values as compared to large negative values. The correlation form $\overline{v^3}/(\overline{v^2})^{3/2}$ which is also the skewness of v fluctuations shows a similar trend at all the stations away from the wall (figure 15). However, near the wall (below $y^+\approx20$) the variation is not similar. The quantity increases from a negative value around $y^+\approx20$ to a positive maximum around $y^+\approx80$ with higher values at downstream stations. Positive S_v indicates motions away from the wall that are occasionally strong. Around $y^+\approx300$ the values are close to each other and are between 0 and 0.1. Above this height the values monotonically increase till $y^+\approx2000$ due to outward motions and then decrease toward zero at the boundary layer edge. For 2-D flow near the wall the values are positive around ≈0.2 and monotonically decrease to ≈-0.2 at $y^+\approx20$. The values once more become positive around $y^+\approx40$. The skewness S_v of v fluctuations below $y^+\approx20$ at stations 1 through 4, and at 9 is negative, indicating the strength of wallward motions. At stations 5 through 8 the near-wall S_v is slightly positive. However, these values are relatively uncertain because of the small $\overline{v^3}$ and $\overline{v^2}$ values in the nearest-wall region. The y flux of v^2 or $\overline{v^3}$ has similar trends as $\overline{vw^2}$ but with less scatter. Small negative values occur very near the wall due to transport of v^2 toward the wall. In the range $y^+\approx40$ to 250 a decrease in the next two stations is accompanied by an increase at accelerating downstream stations in the same region. Values at each station separately increase between $y^+\approx30$ and $y^+\approx1000$ to 1500; near the layer edge they decrease. In the outer layer the levels first increase as the flow decelerates and then decrease due to the acceleration at subsequent stations.

The correlation $\overline{uv^2}/(\overline{u^2})^{1/2}(\overline{v^2})$ shows similar trends for all stations (figure 16). The profiles form maxima at $y^+\approx8$ and decrease to values near or below zero at $y^+\approx20$ to 30, and above $y^+\approx400$ they decrease till $y^+\approx2000$, and increase till the layer edge. Near wall values are higher than the 2-D values. In the $y^+\approx30$ to 400 range, while the decelerated flow stations have higher values than the 2-D, accelerating flow stations have lower values. The quantity shows that on the average the positive u fluctuating velocities, whether they are low in count or not, result in the flux of the $\overline{v^2}$ towards the positive u fluctuation direction near the wall. The y flux of the shearing stress uv or $\overline{uv^2}$ (nondimensionalized with u_τ^3) has a local maximum between $y^+\approx15$ to 20 and a progressively lower and negative local minimum between $y^+\approx40$ and 60 proceeding downstream. Values are close to zero and positive and pass through zero between $y^+\approx200$ and 300 at stations

1 through 7, and for the 2-D profile. At stations 8 and 9 values are negative above $y^+ \approx 20$ to 30. In the outer layer the values are negative at all stations and the magnitude increases, including the second station. Further downstream the magnitude of the negative values decreases. Since v^2 is a positive definite quantity, this means that near the wall below $y^+ \approx 20$ stronger v and stronger positive u fluctuations occur together. Above this y location v fluctuations are more related to negative u fluctuations, resulting in negative $\overline{uv^2}$ values. However above $y^+ \approx 20$ $\overline{u^2 v}$ is positive which shows that u fluctuations occur more strongly together with positive v fluctuations. These observations taken together show that in this region stronger negative u fluctuations and positive stronger v fluctuations occur. Around $y^+ \approx 200$ the v fluctuations and $\pm$u fluctuations are evenly distributed.

Negative $\overline{v^3}$ and positive $\overline{uv^2}$ values near the wall show a flux in the average towards the wall where sweeps are dominant. Away from the wall ejection motions play a more important role.

At the first 3 stations below $y^+ \approx 100$ the $\overline{v^2 w}/(\overline{v^2})(\overline{w^2})^{1/2}$ values are positive, showing that the fluctuating w velocity on the average persists in the direction closer to the tunnel coordinates (figure 17). At downstream stations especially at stations 5, 6 and 7 this process results in negative values of $\overline{v^2 w}/(\overline{v^2})(\overline{w^2})^{1/2}$. Above $y^+ \approx 200$ all station values are close to or below zero. This is again due to the persistence of w fluctuating velocities in the tunnel direction. Near wall positive values and large negative values are believed to be due to the deflection of the flow from the direction of the upstream location where it originated from near the wall as a result of the pressure gradient being more effective in this region. At stations 1 through 4 the y flux of the spanwise shearing stress vw or $\overline{v^2 w}$ (nondimensionalized by u_τ^3) shows a positive maximum below $y^+ \approx 100$ which is followed by a negative maximum in the outer layers. At station 3 the positive maximum is at $y^+ \approx 50$ and negative maximum is at $y^+ \approx 900$. Proceeding downstream until station 4 the near wall values are negative. Stations 7, 8, and 9 show a negative peak at $y^+ \approx 30$. The $\overline{v^2 w}$ changes sign twice for station 4 and at downstream stations. For stations 1 through 3, the near wall v fluctuations occur together with stronger (+)w fluctuations and in the outer layer they occur simultaneously with stronger (-)w fluctuations. For downstream stations where the near wall flow is turning back towards the undisturbed free stream flow direction the (-)w fluctuations occur more frequently. At the outer layers of different stations flow above $y^+ \approx 200$ to 300 (-)w fluctuations occur more frequently together with the v fluctuations. More (-)w or stronger (-w) fluctuations indicate that on the average $\overline{v^2}$ momentum is carried away from the wing. However

at every station there is a y^+ range where $\overline{v^2w}$ is positive.

The $\overline{uvw}/u_\tau^3$ is positive when most of the two of the fluctuating velocities with the same order of magnitude have same signs provided that the third fluctuation is positive. The $\overline{uvw}/(\overline{u^2})^{1/2}(\overline{v^2})^{1/2}(\overline{w^2})^{1/2}$ is also positive when two of the fluctuating velocities are large in magnitude and of the same sign and outweigh the effect of the opposite signed fluctuating velocities in the average, provided that the third fluctuating velocity is positive. At all stations above $y^+\approx400$, $\overline{uvw}/(\overline{u^2}\,\overline{v^2}\,\overline{w^2})^{1/2}$ is close to or larger than zero (figure 18). At the first 3 stations the near-wall values below $y^+\approx200$ are negative showing one or all of the fluctuating velocities are negative in the Reynolds average sense. At downstream stations the values are increasingly positive till station 6. At further downstream stations the values decrease but they are still positive. The value of this quantity helps characterize the near-wall motions. While the w fluctuating velocity tends to stay in its original direction, u and v fluctuating velocities on the average have opposite signs to each other (sweep and ejection motions). At the first 3 stations the $\overline{uvw}/u_\tau^3$ below $y^+\approx200$ is negative, and above this y location it is positive and increases downstream of station 1. Including station 4 below $y^+\approx25$, $\overline{uvw}/u_\tau^3$ is positive. Above this y location the values are negative until $y^+\approx200$ to 300. For $y^+ > 300$ the values are positive with magnitudes close to zero.

The $\overline{u^3}/(\overline{u^2})^{3/2}$ shows the skewness (S_u) of the u fluctuating velocity (figure 19). The quantity shows a maxima at every station below $y^+\approx7$ due to the wallward motions, and decreases towards zero at y locations closer to the wall. The maximum value is in-between 0.7 and 1.1. The values quickly decrease until $y^+\approx40$ to form a local minimum. A local positive maximum is also obtained in $y^+\approx100$ to 400 region at different y locations at the various stations. Further away from the wall a local minimum at $y^+\approx2000$ is obtained. Towards the layer edge, values increase towards zero. At the first three stations the minimum obtained at $y^+\approx40$ is positive. At downstream stations the values are negative. The peak minimum value is obtained at station 7 and decreases at further downstream stations. As regards the 2-D profile, very close to the wall, the maximum is ≈0.9 at $y^+\approx4.5$, and local minimum and local maximum obtained at $y^+\approx40$ and $y^+\approx200$ are ≈-0.1 and ≈0.1 respectively. High positive near wall values are due to wallward motions which carry high speed fluid towards the wall, and high negative values near the layer edge are due to the turbulent non-turbulent interface. The near wall limiting value of S_u for a channel flow as calculated by Kim et al. (1987) using a direct numerical simulation (DNS) is ≈0.85. In the current study, very near wall values show a decrease. This decrease was also seen in the measurements

of Durst, Jovanovic and Sender (1995). Gad-el-Hak and Bandyopadhyay (1994) summarize the Reynolds number effects on S_u for 2-D TBLs. The discrepancies found among the measurements of several researchers were attributed to the size of the probe dimensions. However, measurements of Andreopoulos (1984) below $y^+ \approx 6$ show that S_u values are as high as ≈ 1.7 and do not change with the Reynolds number. The $\overline{u^3}/u_\tau^3$ has a positive peak at all stations at $y^+ \approx 10$, which denotes that most of the u fluctuating velocities are positive. Downstream of station 3 where the three dimensionality of the flow is more pronounced, below $y^+ \approx 200$ the values decrease to a negative peak value at $y^+ \approx 30$. At the third station a local minimum is positive at the same y^+ location. At $y^+ \approx 200$ and at stations 1 through 7, $\overline{u^3}/u_\tau^3$ values are closer to one another. At the last 6 stations $\partial U/\partial y$ near the wall in wall coordinates is steeper than the first three stations. Below $y^+ \approx 10$ very near the wall the flow is energized by the flow moving faster in the region close to but away from the wall which results in positive u fluctuations. Between $y^+ \approx 10$ and 30 the energized flow very near the wall lifts up and results in higher negative fluctuations until $y^+ \approx 30$ to show a peak. The effect of this lifted up low momentum fluid decreases further in the layers and at $y^+ \approx 200$ this process does not have any effect in the layers. The $\overline{u^3}$ *and* $\overline{u^2v}$ complement each other in explaining this process. At $y^+ \approx 10$, $\overline{u^2v}/u_\tau^3$ reaches a minimum at all stations and a maximum between $y^+ \approx 30$ to 40 indicating that u fluctuations are more accompanied with increasingly positive v fluctuations till this latter y location. Measurements of Murlis, Tsai ,and Bradshaw (1982) in a zero pressure gradient 2D TBL in a Re_θ range of 800-4750 in the outer layers of the flow show that the $\overline{u^3}/u_\tau^3$ triple product decreases with increasing Re_θ. Their shear stress and TKE balances in this outer region showed that the turbulent transport mechanism did not change qualitatively with the Reynolds number; $\overline{uv^2}$, especially, changed very small in streamwise direction. They further discuss that in this region triple products are related to shear stresses rather than shear stress gradients and that turbulent transport assumptions made in calculation methods need not be adjusted for local Re_θ. However the very large variations below $y^+ \approx 100$ especially in $\overline{u^2v}$ *and* $\overline{u^3}$ suggest a closer look in the near wall region.

The distribution of $\overline{u^2w}/(\overline{u^2})(\overline{w^2})^{1/2}$ shown in figure 20 also supports the observations made for $\overline{v^2w}/(\overline{v^2})(\overline{w^2})^{1/2}$. At the first four stations $\overline{u^2w}/(\overline{u^2})(\overline{w^2})^{1/2}$ is positive near the wall below $y^+ \approx 300$. At the downstream stations this quantity decreases until station 7 and increases at stations 8 and 9. Above $y^+ \approx 300$, at all stations, the values are negative except for values the near

layer edge at stations 8 and 9. The $\overline{u^2w}/u_\tau^3$ shows that at the first 4 stations where the three-dimensionality of the flow is developing, the u fluctuations occur accompanied by more (+)w fluctuations. Starting at station 5 the (-)w fluctuations are dominant below $y^+\approx25$. Above this y location mostly positive w fluctuations accompany the u fluctuations. Above $y^+\approx400$ the quantity is negative at all stations with larger magnitudes at stations 1, 2, and 3 than the other stations. Positive $\overline{u^2w}$ in the $y^+\approx30$ to 400 range for all the stations indicate that $\overline{u^2}$ momentum is associated with the flow closer to the undisturbed flow direction. For station 9, the values are negative until $y^+\approx100$.

The $\overline{uw^2}/(\overline{w^2})(\overline{u^2})^{1/2}$ profiles show a maximum at $y^+\approx7$ (figure 21). The location where the profiles cross zero value changes from station to station. At stations 6 and downstream stations, the profiles cross zero at a lower y^+ value. Values monotonically decrease until $y^+\approx2000$, and then increase toward the layer edge. This quantity shows that near the wall, w fluctuating velocities on the average occur together with stronger positive u fluctuating velocities. The $\overline{uw^2}/u_\tau^3$ has a positive peak at $y^+\approx15$ to 20 at different stations and the magnitude of the peak decreases proceeding downstream until station 7. Station 8 and 9 have peak values that are close to these for station 1. Station 1 through 7 values are approximately equal to each other at $y^+\approx300$. Above this y location this quantity shows a minimum peak which decreases in magnitude proceeding downstream of station 1 until 7, and increases at stations 8 and 9. At stations 8 and 9 $\overline{uw^2}/u_\tau^3$ is negative above $y^+\approx40$-60.

The $\overline{w^3}/(\overline{w^2})^{3/2}$ is the skewness of w fluctuations (figure 22). Far upstream, the skewness is near zero, since the mean flow is almost 2D. For stations 1 and 2, the mean flow turns a bit (table 1) while some turbulence effects lag and cause S_w to become positive in the local wall-stress co-ordinates. The skewness S_w is progressively more negative very near the wall at downstream stations. The S_w in the $y^+ = 100$ region lags the inner region, i.e., S_w is still positive until station 5. At station 6 in the $y^+=100$ to 1000 range, the values are close to zero. At station 7, 8 and 9 all the values are below zero, except that they are above $y^+\approx1000$ at stations 8 and 9. At all stations in the outer regions, S_w decreases monotonically. At the layer edge, the values increase to near zero. The $\overline{w^3}/u_\tau^3$ does not follow any specific shape. At stations 1 through 3 increasing positive values near the wall are accompanied with decreasing negative values in the outer layer. At station 4 and at downstream stations the near wall values are negative. At stations 4 and 5 in the $y^+\approx20$ to 300 range the quantity is positive. Further decrease at station 6 and at

downstream stations result in completely negative values of the quantity which indicates that in the entire layer (-)w fluctuating velocities are dominant.

Turbulent diffusion of triple products includes derivatives of the fourth order products. The triple products involved in describing the TKE transport are $\overline{u^2v}, \overline{v^3}, and, \overline{vw^2}$. If the boundary layer approximations also hold for the triple product transport equations, i.e., the y variation is much larger than the x and z variations, and the pressure interaction and dissipation terms are negligible, the following equations for the triple products in the TKE equation can be written:

$$\frac{D(\overline{u^2v})}{Dt} = \overline{u^2}\frac{\partial \overline{v^2}}{\partial y} + 2\overline{uv}\frac{\partial \overline{uv}}{\partial y} - (\overline{u^2v}\frac{\partial V}{\partial y} + 2\overline{uv^2}\frac{\partial U}{\partial y}) - \frac{\partial \overline{u^2v^2}}{\partial y}$$

$$\frac{D(\overline{v^3})}{Dt} = 3\overline{v^2}\frac{\partial \overline{v^2}}{\partial y} - 3\overline{v^3}\frac{\partial V}{\partial y} - \frac{\partial \overline{v^4}}{\partial y} \qquad (6)$$

$$\frac{D(\overline{vw^2})}{Dt} = \overline{w^2}\frac{\partial \overline{v^2}}{\partial y} + 2\overline{vw}\frac{\partial \overline{vw}}{\partial y} - (\overline{vw^2}\frac{\partial V}{\partial y} + 2\overline{v^2w}\frac{\partial W}{\partial y}) - \frac{\partial \overline{v^2w^2}}{\partial y}$$

Among the independent 15 quadruple products, the $\overline{u^2v^2}$, $\overline{v^4}$, and $\overline{v^2w^2}$ terms involved in describing the TKE diffusion are presented as well as the statistically important quantities $\overline{u^4}$ and $\overline{w^4}$.

The $\overline{u^2v^2}/(\overline{u^2})(\overline{v^2})$ profiles show that in the $y^+ \approx 20$ to 1500 range the distribution is flat, including all the stations, with values between 1.0 to 1.4 with most of the values clustered around 1.15 (figure 23). Near-wall values are higher than those for 2-D with values reaching 1.7 at station 7. Also near the layer edge, the values increase monotonically at every station. The $\overline{u^2v^2}/u_\tau^4$ at the first 2 stations profiles has approximately the same shape and magnitude. The profiles are bell shaped and peak at $y^+ \approx 200$. The peak values decrease until station 5. The decrease at $y^+ \approx 200$ is $\approx$ 75 %. At stations 6 and 7 the profiles show another peak at $y^+ \approx 30$ to 40 resulting in double peaked profiles. These peak locations are close to the locations where $\overline{uv}/u_\tau^2$, and $\overline{u^2v}/u_\tau^3$ profiles also show peaks. At stations 8 and 9 the values are close to the values obtained at station 1. Station 8 and 9 profiles also show double peaks.

The flatness is defined as:

$$F_{(\,)} = \frac{\overline{(\quad)^4}}{[\overline{(\quad)^2}]^2} \qquad (7)$$

The flatness of a Gaussian p.d.f. is 3. If the flatness is larger than 3, the p.d.f. is more peaked than a Gaussian p.d.f.; if less than 3 it indicates a more flat top p.d.f.

The $\overline{v^4}/(\overline{v^2})^2$ denotes the flatness of the v fluctuating velocities. The profiles show that the distribution of the quantity is similar between $y^+ \approx 50$ till the layer edge (figure 24). The values decrease monotonically from ≈3.5 to ≈3 until $y^+ \approx 1000$, and increase further in the layers. Near the wall, values as high as ≈9 are observed. The DNS calculations of Kim et al. (1987) show that there is no limiting value for this quantity at the wall. However, the present data show that very near the wall the values approach the Gaussian distribution value. The $\overline{v^4}/u_\tau^4$ values are close to zero near the wall and at the layer edge. Profiles show monotonically increasing values with the peaks at $y^+ \approx 250$ to 500. At station 2, $\overline{v^4}/u_\tau^4$ increases with respect to station 1 values. Including station 5 values monotonically decrease. The decrease in the peak value at station 5 is ≈70 % of station 1 peak value. Station 6, 7 values are higher than those at station 5; with larger values at station 6. Station 8 and 9 values increase progressively, however the maximum value lies in between station 3 and 4 values; which is about 60% of station 1 maximum value.

The $\overline{v^2w^2}/(\overline{v^2})(\overline{w^2})$ values in the range of $y^+ \approx 40$ to 1000 decrease monotonically and follow each other closely at every station (figure 25). Near the wall peaks with values as high as ≈1.65 are observed at $y^+ \approx 10$. Above $y^+ \approx 1000$, the values increase monotonically until the layer edge. The $\overline{v^2w^2}/u_\tau^4$ has characteristics similar to $\overline{v^4}/u_\tau^4$. Station 2 values are higher than station 1 values. Peak values of the profiles decrease up to station 5; decrease of peak value at station 5 is ≈60% of the station 1 value. At stations 8 and 9, the values recover to 80% of the station 1 value, and follow each other closely.

The flatness F_u of the u fluctuating velocity is large near the wall and decreases to a local minima at $y^+ \approx 15$ to 20 at each station (figure 26). At downstream stations it gradually increases above $y^+ \approx 50$ to near-Gaussian distribution values. The limiting value for F_u calculated by the DNS method for channel flow (Kim, 1987) is approximately 4.1 at the wall. Near the layer edge, above $y^+ \approx 600$, F_u increases and then decreases due to the turbulence intermittency. The flatness values for 2-D TBL obtained by Andreopoulos (1984) show that F_u values very near the wall increase with decreasing Re_θ value; values as high as 6.0 were reported.

The limiting value for the flatness F_w of the w fluctuating velocity calculated by DNS at the wall is approximately 6.75 (Kim, 1987) (figure 27). The data here show near-wall values of 4 to 5, and decreases farther away from the wall towards the Gaussian value of 3. Near the layer outer edge, the values increase to about 4 in the intermittently turbulent region.

CHAPTER IV. SOME STRUCTURAL RELATIONSHIPS

IV A. FLOW CHARACTERISTICS IN THE VICINITY OF $\overline{vw}$=0 and/or $\overline{uw}$=0

In the vicinity of the locations where $\overline{vw}$ and/or $\overline{uw}$ change sign the following observations were made. The observations were made in the wall-stress coordinates:

a) Derivatives of the quantities $\overline{vw}$, $\overline{v^2}$, $\overline{uv}$ with respect to ln(y) are constants and derivatives of $\overline{uvw}$, $\overline{v^2w}$ with respect to ln(y) are approximately zero.

b) The $-\overline{vw}$ and $-\overline{uw}$ stresses vary semi-logarithmically.

c) The stresses are not zero at the same point in the profiles but are zero in the vicinity of one another. The location in the profiles where stresses are zero is co-ordinate system dependent (table 4).

IV B. SOME STRUCTURAL PARAMETERS AND COORDINATE SYSTEM DEPENDENCE

One of the main objectives of experimental research is to describe and explain the relations among flow variables in order to reduce the independent variables in the governing equations. In this section some relations observed in wall stress coordinates will be presented. The effect of coordinate system is also discussed.

Figure 10 shows the $\overline{uv}/(\overline{u^2}\ \overline{v^2})^{1/2}$ stress distribution in wall-stress co-ordinates. It was observed that the shear stress did not scale on the skin friction velocity. Near the wall the $\overline{u^2}$ normal stress is observed as the scaling stress for the longitudinal shear stress component up to $y^+\approx30$ (figure 28). The $\overline{uv}/u_\tau^2$ increases below $y^+\approx30$ and the correlation coefficient also increases towards zero value below $y^+\approx20$, which indicates that the u and v fluctuating velocities are not well correlated in this region. However $\overline{u^3}/u_\tau^3$ shows a positive peak around $y^+\approx10$

indicating the presence of inactive motion in this region (i.e, high u fluctuations but low $\overline{uv}$ stress). The quantity $(\frac{-2\overline{uv}}{\overline{u^2}-\overline{v^2}})$ in this co-ordinate system denotes the ratio of the shear stress to normal stress difference (figure 29). The ratios at each station follow each other closely in wall-stress coordinates up to $y^+ \approx 50$. This quantity is also the ratio of the average momentum transfer in the vertical direction to the difference in the average stored kinetic energy between the horizontal and the vertical directions. This ratio shows that even in wall stress coordinates the near wall structure of $\overline{uv}$ is governed by the turbulent interaction of fluctuating velocities.

Other quantities tested are the ratios of the shear stresses $-\overline{uw}/-\overline{uv}$, the ratios of the shear stresses with respect to normal stresses $-\overline{uv}/\overline{v^2}$, $-\overline{uv}/\overline{w^2}$, $-\overline{uw}/\overline{u^2}$, $-\overline{uw}/\overline{v^2}$, $-\overline{uw}/\overline{w^2}$, $-\overline{vw}/\overline{u^2}$, $-\overline{vw}/\overline{v^2}$, $-\overline{vw}/\overline{w^2}$, and the ratio among the normal stresses, $\overline{v^2}/\overline{u^2}$, $\overline{w^2}/\overline{u^2}$. Among these quantities, $\overline{uv}/\overline{v^2} \approx -0.5$ for all stations between $y^+ \approx 100$ to 1000. The $-\overline{vw}/\overline{v^2}$ is constant in the same range with varying constants for stations 1 through 5. At stations 6 and 7 the stress distribution varies throughout the layers. However $|\tau/\rho|/\overline{v^2}$ is shown to be nearly a constant (Ölçmen, and Simpson, 1995a). All other quantities did not show a collapse of the data on top of another at every station.

Different co-ordinate axes tested did not result in better presentation of the data. In the first co-ordinate system used, the x axis was aligned with the shear stress vector direction at each point of the profiles; the y axis was kept perpendicular to the surface and z axis completed a right-handed co-ordinate system and all other stresses were transformed using a tensor transformation. By definition, at each point $-\overline{vw}$ stress is zero. The $-\overline{uw}$ stress and the normal stresses did not scale on the u_τ^2 in this coordinate system and $\overline{uw}/u_\tau^2$ stress magnitude was not zero, but was smaller in this co-ordinate system compared to the wall stress coordinate values. This was also observed in simulation studies of Senstad and Moin (1992). The $-\overline{uv}/\overline{u^2}$ profiles did not correlate as well in this coordinate system as they did in wall-stress co-ordinates.

The next co-ordinate system was selected to investigate the relation between the $-\overline{vw}$ shear stress and the other stresses. For the present flow studied, due to sign change of the lateral pressure gradient, shear stresses $-\overline{uw}$ and $-\overline{vw}$, both in free-stream coordinates and wall-stress co-ordinates, are observed to change sign within the layers. It is difficult to examine

relations between the normal stresses and the $-\overline{vw}$ shear stress. In the second co-ordinate system the x axis was defined such that the minimum value of $-\overline{vw}$ at each station would be zero. The y axis was kept perpendicular to the surface. The tensor transformation uses only one angle at each station. There was not a specific distribution found between the $-\overline{vw}$ stress and any other stresses.

Principal stresses and principal stress directions were calculated using wall stress data. By definition in principal stress coordinates the shear stresses are zero. Principal stress coordinates are defined with the unit vectors along the direction of principal stress vectors and these unit vectors are orthogonal to each other. Principal stress coordinates are defined separately at each y location in the profiles. The maximum shear stress magnitude in principal stress coordinates is equal to the absolute value of half of the difference between two principal stresses. Its direction lies in the plane defined by the unit vectors of the principal stresses and makes 45° to each of the unit vectors. By definition shear stress magnitudes are positive. Also by definition the diadic ($\overline{u^2}+\overline{v^2}+\overline{w^2}$) of the Reynolds stress tensor is a constant and equals the sum of the principal stresses ($\overline{u^2}_p+\overline{v^2}_p+\overline{w^2}_p$). The profiles of the normal stresses in wall stress coordinates and the principal stresses in principal stress coordinates are similar to each other. The $\overline{u^2}_p/u_\tau^2$ values are ≈0.5 larger than $\overline{u^2}/u_\tau^2$ above $y^+\approx60$. The maximum values of $\overline{v^2}_p/u_\tau^2$ profiles are ≈0.3 less than $\overline{v^2}/u_\tau^2$ profiles and $\overline{w^2}_p/u_\tau^2$ values are ≈0.2 lower then $\overline{w^2}/u_\tau^2$ values. No new information could be extracted in this coordinate system.

Another structural parameter can be defined as

$$S_1=\frac{\overline{u^2}+\overline{w^2}}{\overline{v^2}} \tag{8}$$

The ratio shows the distribution of longitudinal and spanwise fluctuations with respect to vertical fluctuations (figure 30). In purely isotropic flow the ratio equals 2. Near the wall S_1 becomes large showing the anisotropic nature of the TKE distribution in this region. This is essentially due to the dampening of "v" fluctuations. In the viscous sublayer the ratio approaches infinity as the wall is approached since u' and w' ≈ y, and v' ≈ y^2 due to continuity requirements. However the data indicate a decrease very near the wall. At stations 1 to 3 the ratio varies semi-logarithmically from $y^+\approx100$ ($S_1\approx5$) to 1000 ($S_1\approx3.5$). At downstream stations where the three-dimensionality of the flow is increasing, the ratio decreases in this y^+ range with values higher

than 2 throughout the layers. The values observed in this range are comparable to the data of Schwarz and Bradshaw (1992). In the $y^+ \approx 100$ to 1000 range, $\overline{u^2}/u_\tau^2$ decreases at the downstream stations; however the variation of $\overline{v^2}/u_\tau^2$ and $\overline{w^2}/u_\tau^2$ are not monotonical. Littell and Eaton (1991) show the parameter calculated for several 3-D flows including Anderson and Eaton (1989), Bradshaw and Pontikos (1985), Driver and Johnston (1990), Elsenaar and Boelsma (1974), and the 2-D data of Klebanoff (1955). Their figure 4.14 shows larger values of S_1 of the order of 6 to 10 as the wall is approached. The variation of this ratio in the present flow is closer to the measurements of Anderson and Eaton, and Klebanoff.

IV C. TRANSPORT VELOCITY OF TURBULENT KINETIC ENERGY (TKE)

The convection velocity of TKE is defined as an average velocity as a means to explain the transport of the TKE as (Townsend, 1976, p.125)

$$V_{q^2}=\frac{\overline{v(u^2+v^2+w^2)}}{\overline{u^2}+\overline{v^2}+\overline{w^2}} \qquad (9)$$

The direction of the energy flux is expected to be from the regions of high intensity to the regions of low intensity. A similar definition was used by Bradshaw (1967) in order to model the turbulent diffusion term in the transport equation of TKE. If such a velocity exists the TKE of the flow can be defined to express the turbulent diffusion.

Continuity relations requires V_{q2} to be zero at the wall. Below $y^+ < 20$ the velocity is negative; the profiles show a local minima between $y^+ \approx 7$ and 10 (figure 31). Negative V_{q2} denotes that the turbulent diffusion is towards the wall. TKE production is maximum near the wall between $y^+ \approx 15$ to 20, and TKE is diffused in both directions around this location. At the first two stations between $y^+ \approx 40$ to 400, V_{q2} is nearly a constant. At stations 3 and 4 there is a decrease around $y^+ \approx 150$. At stations 5, 6, and 7 the velocity is doubled around $y^+ \approx 40$ indicating a larger penetration velocity of the diffusing TKE. Profiles at these stations show a minimum between $y^+ \approx 200$ to 300. Towards the layer edge, at all stations, V_{q2} increases; outside the boundary layer it should go to zero.

Bradshaw and Pontikos' (1985) measurements on an "infinite"" swept wing include the vertical transport velocity above $y^+ \approx 230$. Data showed that the velocity increased till the layer edge with negative numbers at the last 2 stations around $y^+ \approx 250$. The "strong decrease" of V_{q2}

with increased three-dimensionality observed for that flow is not seen in the present data. Schwarz and Bradshaw (1993) studied the development and decay of a 3DTBL generated by a 30° bend above $y^+ \approx 150$. The data show that in the development stage V_{q2} increases towards the layer edge. With increased three-dimensionality of the flow, V_{q2} is higher at the layer edge and gradually decreases below zero towards the wall. In the section where the crossflow decays, V_{q2} near the wall gradually increases and becomes positive. The flow in both regions were subjected to adverse pressure gradient conditions. However for the present measurements the streamwise pressure gradient is favorable at station 2 until station 6. The V_{q2} values obtained for those flows near the layer edge are slightly higher than the values obtained for the present flow.

V. CONCLUSIONS

Experimental results for some higher order turbulence statistics were presented for a three-dimensional pressure-driven turbulent boundary layer generated by an idealized wing-body junction. The data included the mean velocity, Reynolds' stresses, 10 triple products and selected quadruple products at 9 stations and at one mean two-dimensional flow station. The triple products indicate that the near wall region is dominated by the sweep motions (+u, -v), and above $y^+ \approx 15$ to 40 by the ejection motions.

Turbulent kinetic energy is transported towards the wall below $y^+ \approx 15$ to 20 and is transported away from the wall above this y^+ location, as shown by the TKE transport velocity. The normal stress distribution is seen to be highly anisotropic. The ratio $(\overline{u^2}+\overline{w^2})/\overline{v^2}$ is an order of magnitude different than 2, the value obtained for isotropic normal stress distribution. The ratio varies semi-logarithmically in the $y^+ \approx 100$ to 1000 range for the first three stations and for the 2-D station. The ratios $\overline{uv}/\overline{u^2}$ and $2\overline{uv}/(\overline{u^2}-\overline{v^2})$ correlate the data below $y^+ \approx 50$ at all stations.

Triple products together describe the flux of the stresses. Momentum is always positive and is transferred with fluctuating velocity components. If a triple product is positive it shows that the normal stress is transferred with a positive transport velocity. The $\overline{u^2}$ transfer is described by the $\overline{u^3}$, $\overline{u^2v}$,*and* $\overline{u^2w}$ triple products in the x, y, and z directions, respectively. Large variations of these triple products occur mostly below $y^+ \approx 200$. The $\overline{u^3}$ triple product shows a positive peak at $y^+ \approx 10$, while at the same y^+ location $\overline{u^2v}$ shows a negative peak, which together indicate that the $\overline{u^2}$ momentum is carried towards the wall with faster moving fluid in the x_{wc} direction. Above $y^+ \approx 10$ this effect is decreased. Between $y^+ \approx 15$ and 20, $\overline{u^2v}$ changes sign showing that the $\overline{u^2}$ momentum is carried away from the wall. The positive peak is located at $y^+ \approx 30$ to 40. The $\overline{u^3}$ triple product changes sign at station 4 and downstream stations between $y^+ \approx 15$ and 20, with a negative peak at $y^+ \approx 30$. At the first 4 stations the $\overline{u^2w}$ triple product is positive till $y^+ \approx$ 200 to 400, which shows that the $\overline{u^2}$ momentum transfer persists in its original direction. At the downstream stations $\overline{u^2w}$ is negative near the wall indicating that the $\overline{u^2}$ momentum is transported away from

the wing. Therefore very near the wall below $y^+ \approx 15$ to 20 the $\overline{u^2}$ momentum is transferred towards the wall and above this y^+ location it is transferred away from the wall with increased transport velocity. The three dimensionality of the flow increases this transport velocity. The $\overline{u^2}$ momentum transfer does not seem to be affected by the moderate lateral pressure gradients in the whole layers. At station 5 and downstream stations very near the wall the momentum transfer persists in its original direction however with negative w fluctuations below $y^+ \approx 30$.

The $\overline{v^2}$ flux is described by the $\overline{uv^2}$, $\overline{v^3}$ *and* $\overline{v^2w}$ triple products. At all stations the $\overline{v^3}$ triple product below $y^+ \approx 30$ is less than zero indicating that the $\overline{v^2}$ momentum is transferred towards the wall. Above this y^+ location the $\overline{v^3}$ triple product is positive, indicating that the v^2 momentum is in the average carried away from the wall. The $\overline{uv^2}$ profile has a positive peak around $y^+ \approx 15$ including all the stations, and the quantity changes sign between $y^+ \approx 20$ to 40. The $\overline{v^2}$ momentum is transported with a positive transport velocity very near the wall in the x_{wc} direction, and it is transported with a negative transport velocity above $y^+ \approx 20$ to 40. Above $y^+ \approx 150$ however the $\overline{uv^2}$ is more negative in the first three stations and recovers with the increased three dimensionality of the flow. The $\overline{v^2w}$ is increasingly positive at the first three stations up to $y^+ \approx 300$ which shows a lag is involved with the $\overline{v^2}$ momentum transfer in the lateral direction. However above this location the $\overline{v^2w}$ is negative and smaller proceeding downstream of station 1 which shows that the pressure gradients are affecting the fluctuating momentum more in the outer layer than in the inner and logarithmic layers.

The $\overline{w^2}$ transfer is described by $\overline{uw^2}$, $\overline{vw^2}$ *and* $\overline{w^3}$ triple products. The $\overline{w^2}$ momentum transfer in the x_{wc} direction is with a positive transport velocity. This transport velocity value decreases with increased three dimensionality of the flow. At stations 6 and 7 the value changes sign at $y^+ \approx 40$. All station $\overline{uw^2}$ values are approximately equal to each other at $y^+ \approx 350$, and above this y^+ location the values are negative at every station. The $\overline{vw^2}$ triple product values show that the $\overline{w^2}$ momentum is also transferred away from the wall. At stations 6 and 7 the $\overline{vw^2}$ values are negative below $y^+ \approx 40$ indicating that the momentum transfer is towards the wall, above this y^+ location the $\overline{vw^2}$ is positive. The $\overline{w^3}$ triple product shows that at the first station below $y^+ \approx 50$ and

at stations 2 and 3 below $y^+ \approx 350$ the $\overline{w^2}$ transfer in wall stress coordinates is with a positive transport velocity in the z_{wc} direction indicating that the $\overline{w^2}$ transfer is also directionally lagging. With the reversed lateral pressure gradient between stations 3 and 4 the very near wall w fluctuating velocities at station 4 become strongly negative however above $y^+ \approx 20$, the $\overline{w^3}$ is positive, indicating that the mid layer flow is associated with strong positive w fluctuations. With increasing negative lateral pressure gradients the lag in the $\overline{w^2}$ momentum transfer is clearly demonstrated. At the last three stations the $\overline{w^3}$ is negative throughout the layer except above $y^+ \approx 1000$. At all stations above $y^+ \approx 350$ the $\overline{w^3}$ values are mostly less than zero, which presumably indicates that the outer layer fluctuating velocity structure responds faster to changes in the pressure gradients. This is more clear especially at stations 1, 2 and 3 that while the $\overline{w^3}$ is increasingly positive in the inner layer the triple product becomes increasingly negative in the outer layer.

ACKNOWLEDGEMENT

The authors are grateful for the support of Office of Naval Research Grant N00014-94-1-0092, Dr. L.P. Purtell, Program Manager.

REFERENCES

Ailinger, K., 1990, "Measurements of surface shear stresses under a three-dimensional turbulent boundary layer using oil-film laser interferometry", M.S. thesis, Department of Aerospace and Ocean Engineering, VPI&SU.

Andreopoulos, J., Durst, F., Zaric, Z., and Jovanovic, J., 1984, "Influence of Reynolds number on characteristics of turbulent wall boundary layers", *Experiments in Fluids*, 2, pp. 7-16.

Bradshaw, P., and Pontikos, N.S., 1985, "Measurements in the turbulent boundary layer on an 'infinite' swept wing", *Journal of Fluid Mechanics*, vol.159, pp.105-130.

Bradshaw, P., Ferriss, D.H., and Atwell, N.P., 1967, "Calculation of boundary layer development using the energy equation", *Journal of Fluid Mechanics*, Vol. 28, Part 3, pp. 593-616.

Bradshaw, P., 1967, "Inactive motion and pressure fluctuations in turbulent boundary layers", *Journal of Fluid Mechanics*, vol. 30, part 2, pp. 241-258.

Coles, D., 1956, "The law of the wake in the turbulent boundary layers", *Journal of Fluid Mechanics*, vol. 1, part 2, pp. 191-226.

Daly, B., and Harlow, F., Nov. 1970, "Transport equations in turbulence", *The Physics of Fluids*, vol. 13, pp. 2634-2649.

Driver, D.M., and Johnston, J.P., July, 1990, "Experimental study of a 3-D shear-driven turbulent boundary layer with streamwise adverse pressure gradient", Report number, MD-57, Thermosciences Division, Department of Mechanical Engineering, Stanford Univ., Stanford, CA, 94305.

Driver, D.M., and Hebbar, S.K., 1987, "Experimental study of a three-dimensional shear-driven turbulent boundary layer", *AIAA Journal*, vol. 25, no. 1.

Durst, F., Jovanovic, J., Sender, J., 1995, "LDA measurements in the near-wall region of a turbulent pipe flow", *Journal of Fluid Mechanics*, vol. 295, pp. 305-335.

Elsenaar, A., and Boelsma, S.H., 1974, "Measurements of the Reynolds stress tensor in a three-dimensional turbulent boundary layer under infinite swept wing condition", NLR TR 74095 21.

Flack, K.A., and Johnston, J.P., 1993, "Near-wall investigation of three-dimensional turbulent boundary layers", Report number, MD-63, Thermosciences Division, Department of Mechanical Engineering, Stanford Univ., Stanford, CA, 94305.

Gad-el-Hak, M, and Bandyopadhyay, P.R., August 1994, "Reynolds number effects in wall-bounded turbulent flows", *ASME Reprint No:AMR 148, Appl. Mech. Rev.*, vol. 47, no: 8,

Johnston, J.P., 1960, "On the three-dimensional turbulent boundary layer generated by secondary flow", *Transactions of ASME, Journal of Basic Engineering*, pp. 233-248.

Kim, J., Moin, P., and Moser, R., 1987, "Turbulence statistics in a fully developed channel flow at low Reynolds number", *Journal of Fluid Mechanics*, vol.177, pp. 133-166.

Launder, B.E., Reece, G.J., Rodi, W., 1975, "Progress in the development of a Reynolds-stress turbulence closure", *Journal of Fluid Mechanics*, vol. 68, pt. 3, pp. 537-566.

Littell, H.S., and Eaton, J.K., 1991, "An experimental investigation of the three dimensional boundary layer on a rotating disk", Report No: MD-60, Thermosciences Division, Department of Mechanical Engineering, Stanford Univ., Stanford, CA, 94305.

Murlis, J., Tsai, H.M., and Bradshaw, P., 1982, "The structure of turbulent boundary layers at low Reynolds numbers", *Journal of Fluid Mechanics*, vol. 122, pp. 13-56.

Nagano, Y., and Tagawa, M., 1991, "Turbulence model for triple velocity and scalar correlations", Springer-Verlag, pp. 47-62.

Naot, D., Shavit, A., Wolfshtein, M., June 1973, "Two-point correlation model and the redistribution of Reynolds stresses", *Physics of Fluids*, vol. 16, no. 6, pp. 738-743.

Ölçmen, M.S., and Simpson, R.L., 1995a, "An experimental study of a three-dimensional pressure-driven turbulent boundary layer", *Journal of Fluid Mechanics*, vol. 290, pp. 225-262.

Ölçmen, M.S., and Simpson, R.L., 1995 b, "A 5-velocity-component laser-Doppler velocimeter for measurements of a three-dimensional turbulent boundary layer", Institute of Physics Publishing, *Measurement Science and Technology*, Special Issue on Laser-Doppler Anemometry, vol. 6, pp. 702-716.

Ölçmen, M.S., and Simpson, R.L., 1992, "Perspective: On the near wall similarity of three-dimensional turbulent boundary layers", *Transactions of ASME, Journal of Fluids Engineering*, Vol. 114, pp. 487-495.

Schumann, U., 1977, "Realizability of Reynolds-stress turbulence models", *Physics of Fluids*, Vol. 20, No: 5, pp. 721-725.

Schwarz, W., and Bradshaw, P., 1994, "Turbulence structural changes for a three-dimensional turbulent boundary layer in a 30° bend", *Journal of Fluid Mechanics*, vol. 272, pp 183-209.

Schwarz, W., and Bradshaw, P., 1993, "Measurements in a pressure-driven three-dimensional turbulent boundary layer during development and decay", *AIAA Journal*, vol. 31, number 7, pp 1207-1214.

Schwarz, W., and Bradshaw, P., October, 1992, "Three-dimensional turbulent boundary layer in a 30 degree bend: experiment and modeling", Report number, MD-61, Thermosciences Division, Department of Mechanical Engineering, Stanford Univ., Stanford, CA, 94305.

Sendstad, O., and Moin, P., 1992, "The near wall mechanics of three-dimensional turbulent boundary layers", Report number, TF-57, Thermosciences Division, Department of Mechanical Engineering, Stanford Univ., Stanford, CA, 94305.

Simpson, R.L., 1995, "Three-dimensional turbulent boundary layers and separation", 33rd Aerospace Sciences Meeting and Exhibit, Jan 9-12, Reno, NV. AIAA paper 95-0226.

Townsend, 1976, *The structure of turbulent shear flow*, second edition, Cambridge university press, England.

van Den Berg, B., 1975, "A three-dimensional law of the wall for turbulent shear flows", *Journal of Fluid Mechanics*, vol. 70, part 1, pp. 149-160.

TABLE.1 LASER-DOPPLER VELOCIMETER LOCATIONS AND FLOW PARAMETERS. Station 0 data from Ölçmen, 1990.

Stations	X (in.)	Z (in)	U_{ref} (m/sec)	U_e (m/sec)	β_{FS} (deg)	β_w (deg)	β_{NS} (deg)	u_τ (m/sec)	ν (m^2/sec) x1E05	$(\partial C_p/\partial x)_{FS}$ (1/m)	$(\partial C_p/\partial z)_{FS}$ (1/m)	$(\partial C_p/\partial x)_{WC}$ (1/m)	$(\partial C_p/\partial z)_{WC}$ (1/m)	daily pressure (millibar)	daily temperature (degrees Centigrade)
0	-4.49	-1.32	27.6	26.4	-1.68	-6.1	-4.88	1.15	1.68	0.778	0.916	0.705	0.974	938	25.4
1	-3.50	-1.45	27.5	24.9	-2.64	-11.5	-8.5	0.864	1.65	1.2	1.39	0.9614	1.562	949	24.6
2	-2.29	-1.75	27.5	24.8	-4.81	-24.0	-21.5	0.865	1.65	0.204	2.99	-0.75	2.898	949	24.3
3	-1.33	-2.04	27.5	25.3	-8.63	-33.7	-18	0.957	1.65	-3.91	4.07	-5.263	2.041	947	23.5
4	-0.47	-2.58	27.5	27.3	-9.45	-30.6	-30.2	1.11	1.65	-6.34	0.923	-6.264	-1.35	946	24
5	0.26	-2.94	27.5	29.5	-7.71	-19.7	-25.3	1.15	1.67	-6.25	-1.95	-5.797	-3.036	940	24.5
6	1.19	-3.30	27.5	30.5	-5.09	-7.17	-20.8	1.16	1.68	-4.06	-5.53	-3.999	-5.573	934	25
7	2.17	-3.53	27.5	31.0	-2.71	-3.50	-10.9	1.20	1.68	0.26	-6.69	0.58	-6.695	934	24.7
8	3.66	-3.68	27.4	30.9	0.96	2.63	.928	1.024	1.67	1.307	-4.430	1.178	-4.466	941	23.9
9	5.16	-3.66	27.5	30.5	2.78	4.71	4.68	1.011	1.68	1.188	-2.174	1.113	-2.213	935	24.1
2-D	0.36	-2.94	27.4	27.1	-	-	-	0.98	1.67	-	-	-	-	941	24

Pressure coefficient gradients are calculated from the measured pressure distribution.

U_e=Velocity magnitude at the layer edge.

TABLE 2. UNCERTAINTIES IN MEASURED QUANTITIES WITH 20:1 ODDS

U/U_τ	± 0.075	$\overline{u^2v}/(\overline{u^2})(\overline{v^2})^{1/2}$	± 0.020	$\overline{u^4}/(\overline{u^2})^2$	±0.048
V/U_τ	± 0.026	$\overline{u^2w}/(\overline{u^2})(\overline{w^2})^{1/2}$	± 0.012	$\overline{u^3v}/(\overline{u^2})^{3/2}(\overline{v^2})^{1/2}$	±0.139
W/U_τ	± 0.05	$\overline{v^2w}/(\overline{v^2})(\overline{w^2})^{1/2}$	± 0.011	$\overline{u^3w}/(\overline{u^2})^{3/2}(\overline{w^2})^{1/2}$	±0.078
$\overline{u^2}/u_\tau^2$	± 0.08	$\overline{uv^2}/(\overline{u^2})^{1/2}(\overline{v^2})$	± 0.015	$\overline{u^2v^2}/(\overline{u^2})(\overline{v^2})$	±0.039
$\overline{v^2}/u_\tau^2$	± 0.029	$\overline{uw^2}/(\overline{u^2})^{1/2}(\overline{w^2})$	± 0.009	$\overline{u^2vw}/(\overline{u^2})(\overline{v^2})^{1/2}(\overline{w^2})^{1/2}$	±0.22
$\overline{w^2}/u_\tau^2$	± 0.037	$\overline{vw^2}/(\overline{v^2})^{1/2}(\overline{w^2})$	± 0.012	$\overline{u^2w^2}/(\overline{u^2})(\overline{w^2})$	±0.034
$-\overline{uv}/(\overline{u^2}\ \overline{v^2})^{1/2}$	± 0.023	$\overline{uvw}/(\overline{u^2})^{1/2}(\overline{v^2})^{1/2}(\overline{w^2})^{1/2}$	± 0.006	$\overline{uv^3}/(\overline{u^2})^{1/2}(\overline{v^2})^{3/2}$	±0.073
$-\overline{uw}/(\overline{u^2}\ \overline{w^2})^{1/2}$	± 0.021	$\overline{u^3}/(\overline{u^2})^{3/2}$	± 0.024	$\overline{uv^2w}/(\overline{u^2})^{1/2}(\overline{v^2})(\overline{w^2})^{1/2}$	±0.023
$-\overline{vw}/(\overline{v^2}\ \overline{w^2})^{1/2}$	± 0.018	$\overline{v^3}/(\overline{v^2})^{3/2}$	± 0.052	$\overline{uvw^2}/(\overline{u^2})^{1/2}(\overline{v^2})^{1/2}(\overline{w^2})$	±0.023
		$\overline{w^3}/(\overline{w^2})^{3/2}$	± 0.022	$\overline{uw^3}/(\overline{u^2})^{1/2}(\overline{w^2})^{3/2}$	±0.020
				$\overline{v^4}/(\overline{v^2})^2$	±0.084
				$\overline{v^3w}/(\overline{v^2})^{3/2}(\overline{w^2})^{1/2}$	±0.052
				$\overline{v^2w^2}/(\overline{v^2})(\overline{w^2})$	±0.023
				$\overline{vw^3}/(\overline{v^2})^{1/2}(\overline{w^2})^{3/2}$	±0.058
				$\overline{w^4}/(\overline{w^2})^2$	±0.065

TABLE 3. SOME LENGTH SCALES OBTAINED FROM LDV DATA IN WALL-STRESS COORDINATES.								
Stations	δ (mm)	δ_1 (mm)	δ_2 (mm)	δ_3 (mm)	δ_4 (mm)	δ_5 (mm)	δ_6 (mm)	δ_7 (mm)
1	39.2	+7.14	+6.90	+4.89	-3.60	+0.57	-3.02	-0.43
2	40.2	+9.14	+7.54	+6.30	-10.43	+1.70	-8.73	-2.80
3	39.3	+9.61	+6.86	+6.84	-13.57	+2.47	-11.10	-4.79
4	39	+7.45	+5.53	+5.68	-11.43	+1.54	-9.88	-3.47
5	39.6	+5.95	+5.37	+4.66	-6.10	+0.52	-5.59	-1.08
6	39.2	+5.30	+5.24	+4.13	+0.20	-0.21	-0.01	-0.09
7	38.8	+5.24	+5.20	+4.10	+0.54	-0.19	+0.35	-0.05
8	38.4	+5.16	+5.08	+3.97	+2.03	-0.32	+1.71	-0.12
9	40.7	+5.71	+5.68	+4.33	+1.59	-0.23	+1.37	-0.06
2-D	39.1	+6.2	+6.2	+4.5	-0.29	+0.03	-0.26	0

U_e=Velocity magnitude at the layer edge.

$$\delta = y \text{ where } \sqrt{U^2+W^2}/U_e = 0.995 = \textit{Boundary Layer Thickness}$$

$$\delta_1 = \int_0^{\infty} \left(1 - \frac{U}{U_e}\right) dy = \textit{Streamwise Displacement Thickness}$$

$$\delta_2 = \int_0^{\infty} \left(1 - \frac{\sqrt{U^2+W^2}}{U_e}\right) dy = \textit{Magnitude Displacement Thickness}$$

$$\delta_3 = \int_0^{\infty} \left(1 - \frac{U}{U_e}\right)\frac{U}{U_e} dy = \textit{Streamwise Momentum Thickness}$$

$$\delta_4 = \int_0^{\infty} \left(-\frac{W}{U_e}\right) dy = \textit{Lateral Displacement Thickness}$$

$$\delta_5 = \int_0^{\infty} \frac{W}{U_e}\left(1 - \frac{U}{U_e}\right) dy = \textit{Lateral Momentum Thickness}$$

$$\delta_6 = \int_0^{\infty} -\frac{WU}{U_e^2} dy = \textit{Cross Product Momentum Thickness}$$

$$\delta_7 = \int_0^{\infty} -\frac{W^2}{U_e^2} dy = \textit{Crossflow Momentum Thickness}$$

TABLE 4. THE y^+ LOCATIONS WHERE LATERAL FLOW GRADIENT AND $-\overline{UW}$ AND $-\overline{VW}$ STRESSES ARE EQUAL TO ZERO

	locations in the profiles where $\partial W/\partial y=0$			$-\overline{UW}=0$ location	$-\overline{VW}=0$ location
station	free-stream co-ordinates	normal-stress co-ordinates	wall stress co-ordinates	wall stress co-ordinates	
1	32.9	12	6.6	-	-
2	33.4	9.7	8.1	-	-
3	38.2	28.9	8.9	5	10
4	62.1	26.2	24.9	15	25
5	81.4	56.9	65.9	45	50
6	124.0	97.9	120.5	80	110
7	175.6	153.6	173.5	95-100	140-150
8	241.3	241.1	247.5	167.3	218.5
9	340.7	348	348.1	207.5	321.8

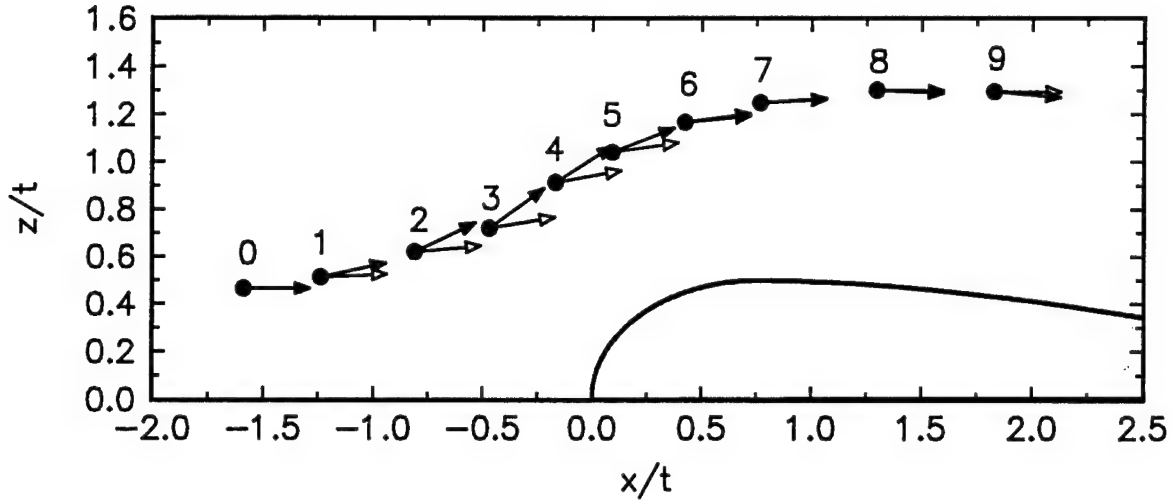

Figure 1. Wing shape and measurement locations. Full arrows wall-stress direction. Empty arrows free-stream direction.

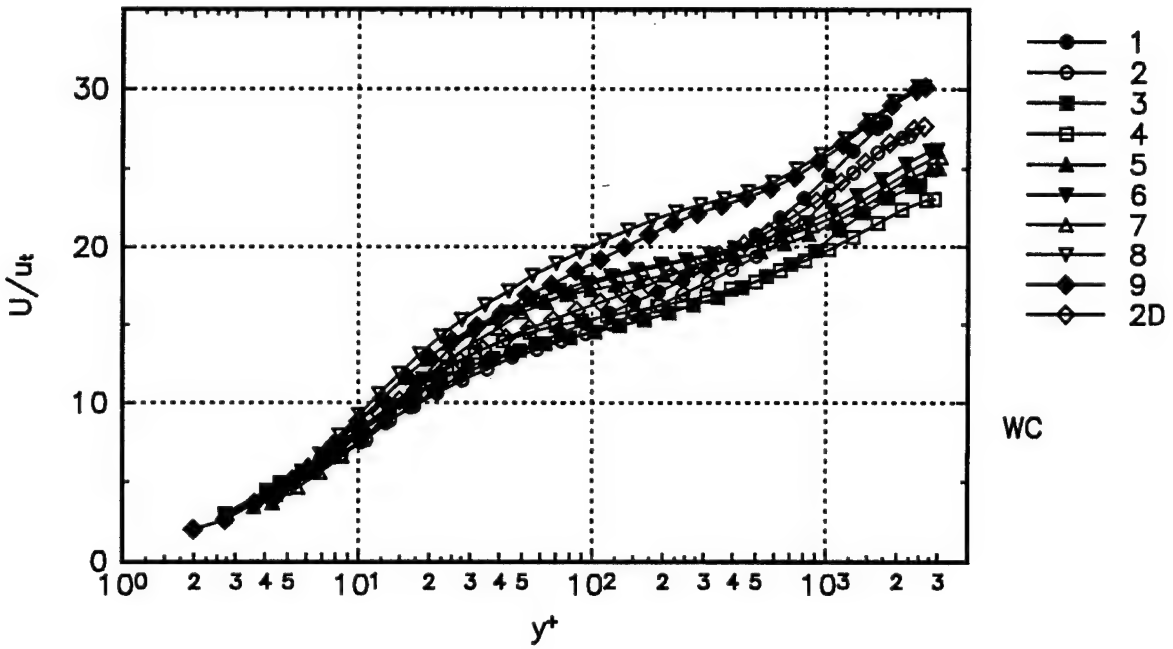

Figure 2. U/u_τ, mean velocity component in wall-stress coordinates. The uncertainties are on the order of the symbol size.

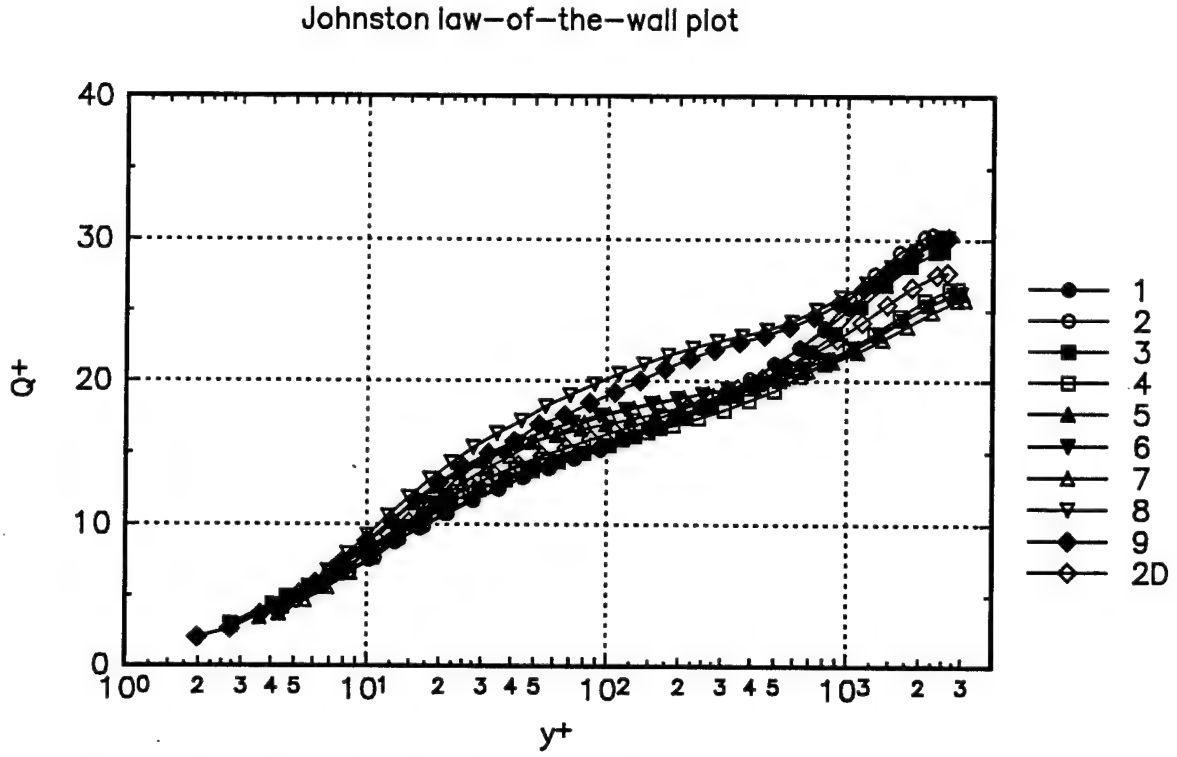

Figure 3. Present data in Johnston law-of-the-wall coordinates.

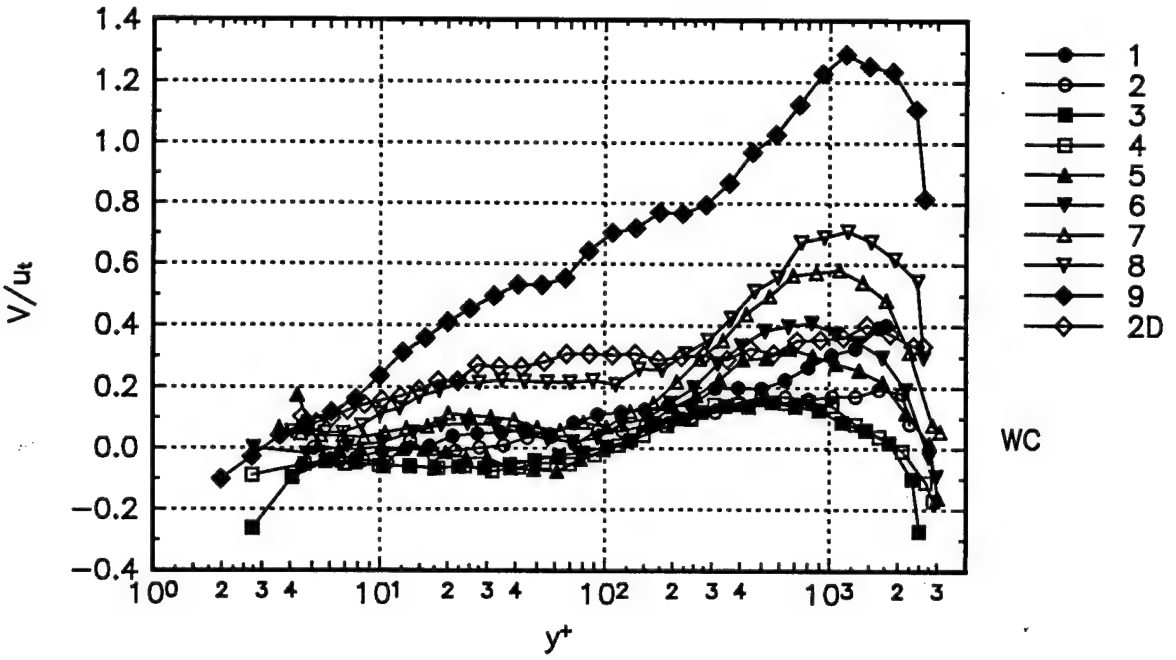

Figure 4. V/u_τ, mean velocity component in wall-stress coordinates. The uncertainties are on the order of the symbol size.

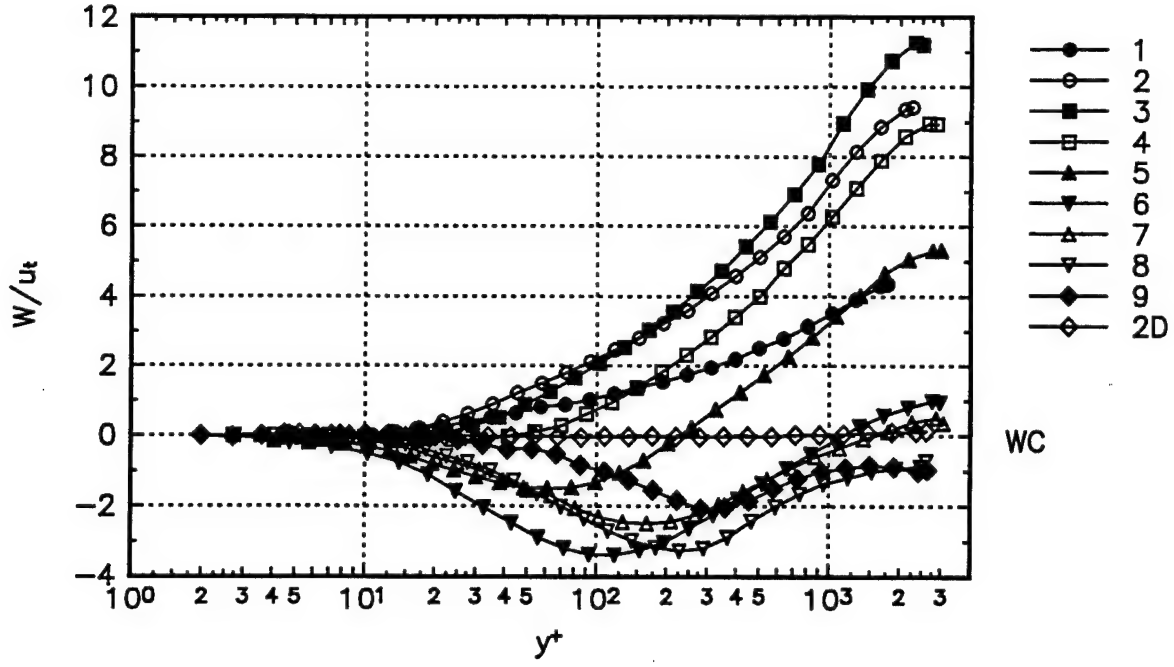

Figure 5. W/u_τ, mean velocity component in wall-stress coordinates. The uncertainties are on the order of the symbol size.

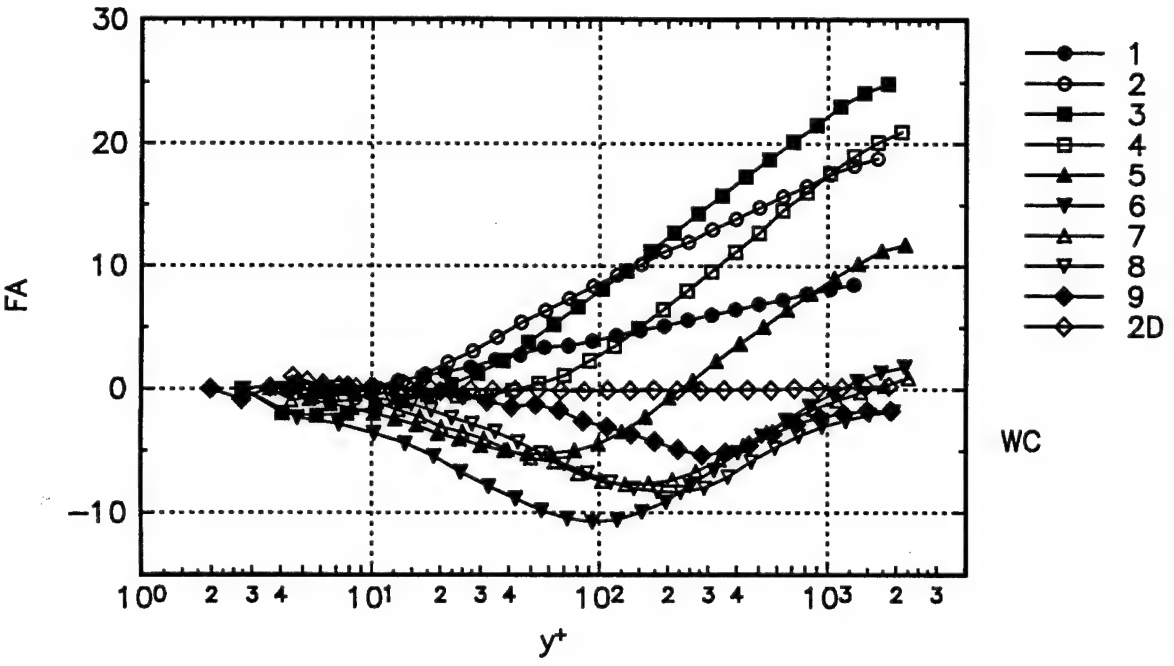

Figure 6a. Flow angle calculated in wall-stress coordinates. The uncertainties are on the order of the symbol size.

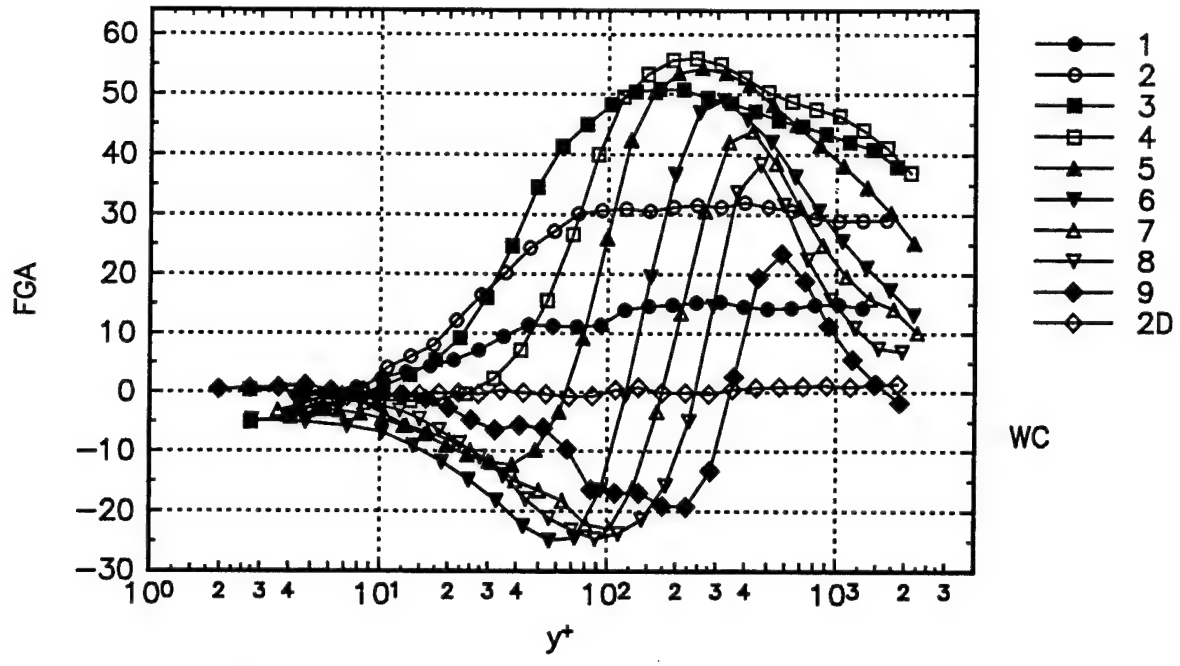

Figure 6b. Flow gradient angle calculated in wall-stress coordinates. The uncertainties are on the order of the symbol size.

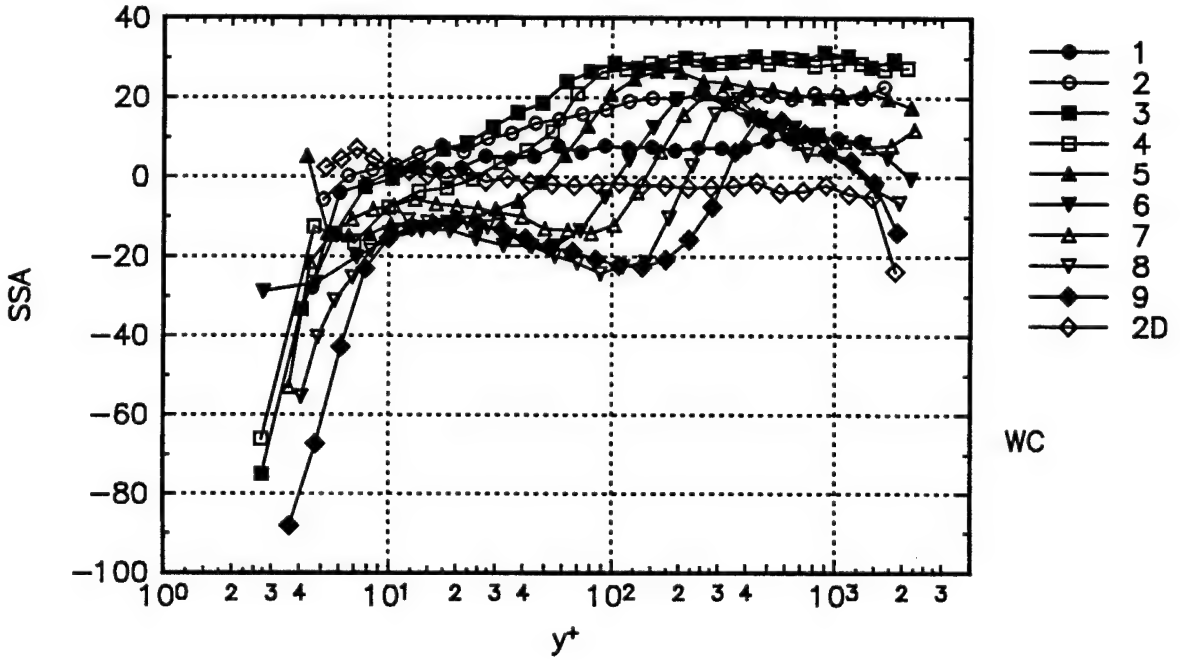

Figure 6c. Turbulent shear stress angle calculated in wall-stress coordinates. The uncertainties are on the order of the symbol size.

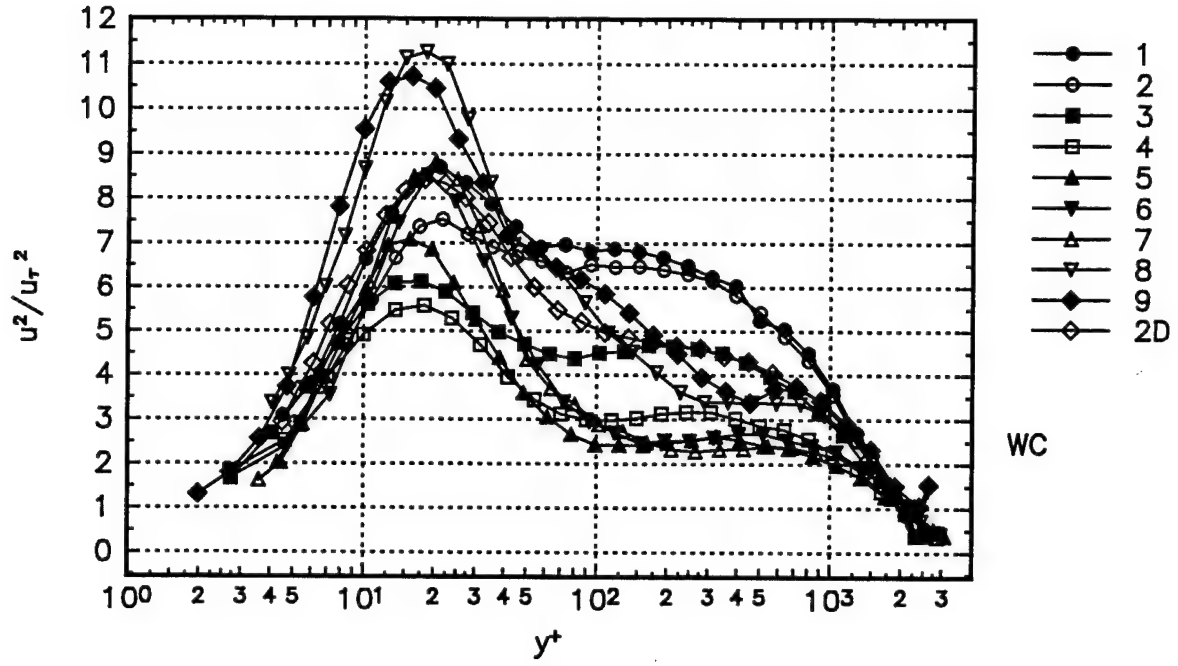

Figure 7. The $\overline{u^2}/u_\tau^2$ normal stress component in wall-stress coordinates. The uncertainties are on the order of the symbol size.

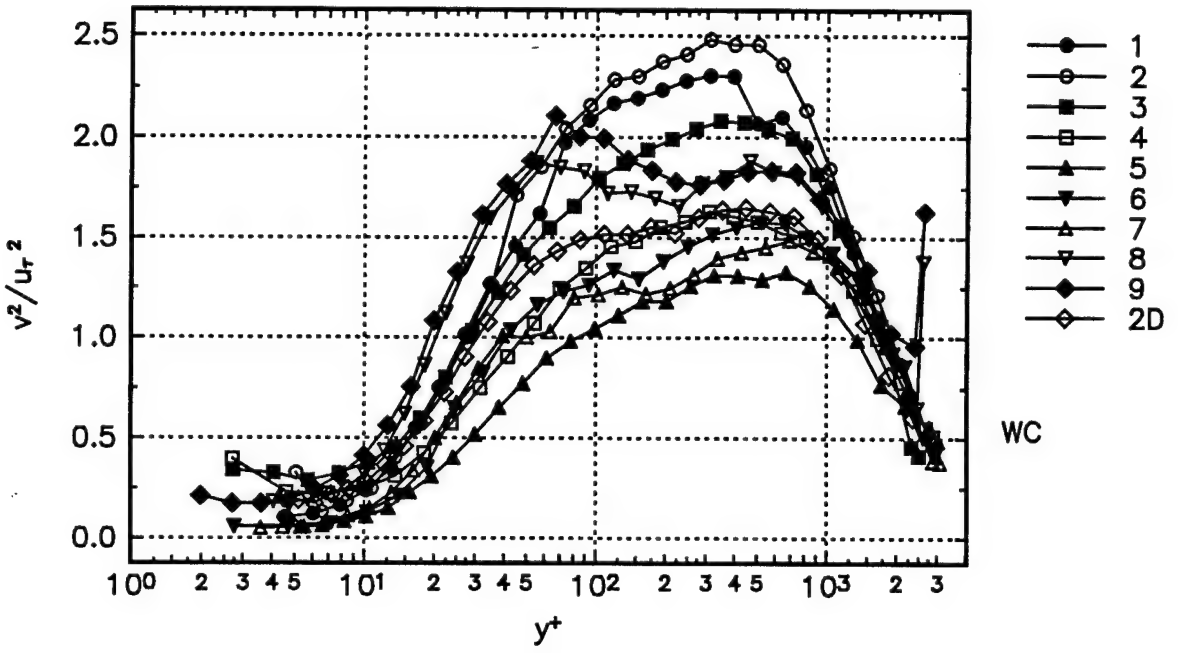

Figure 8. The $\overline{v^2}/u_\tau^2$ normal stress component in wall-stress coordinates. The uncertainties are on the order of the symbol size.

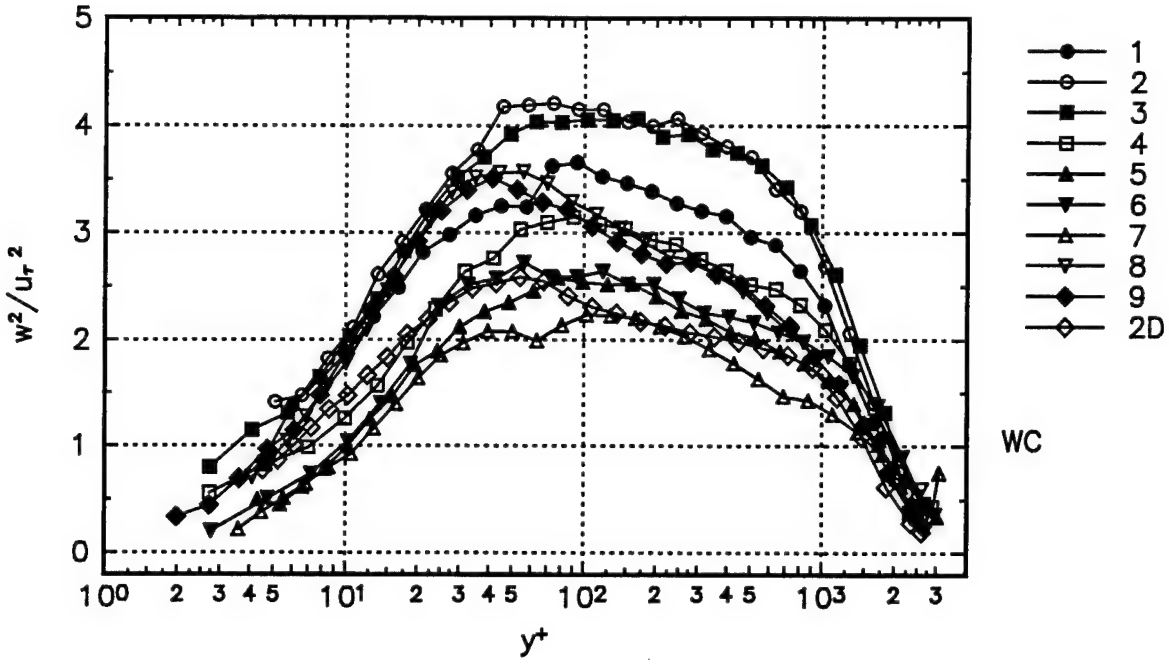

Figure 9. The $\overline{w^2}/u_\tau^2$ normal stress component in wall-stress coordinates. The uncertainties are on the order of the symbol size.

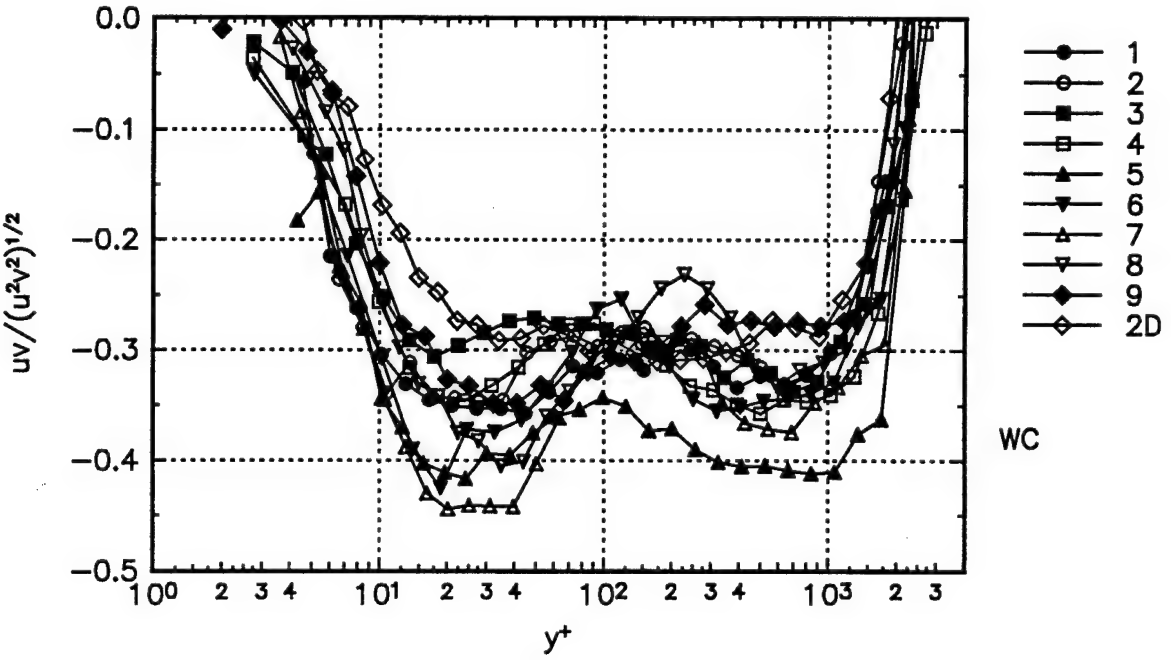

Figure 10. The $\overline{uv}/(\overline{u^2}\ \overline{v^2})^{1/2}$ shear stress correlation coefficient in wall-stress coordinates. Typical uncertainty is ±0.023.

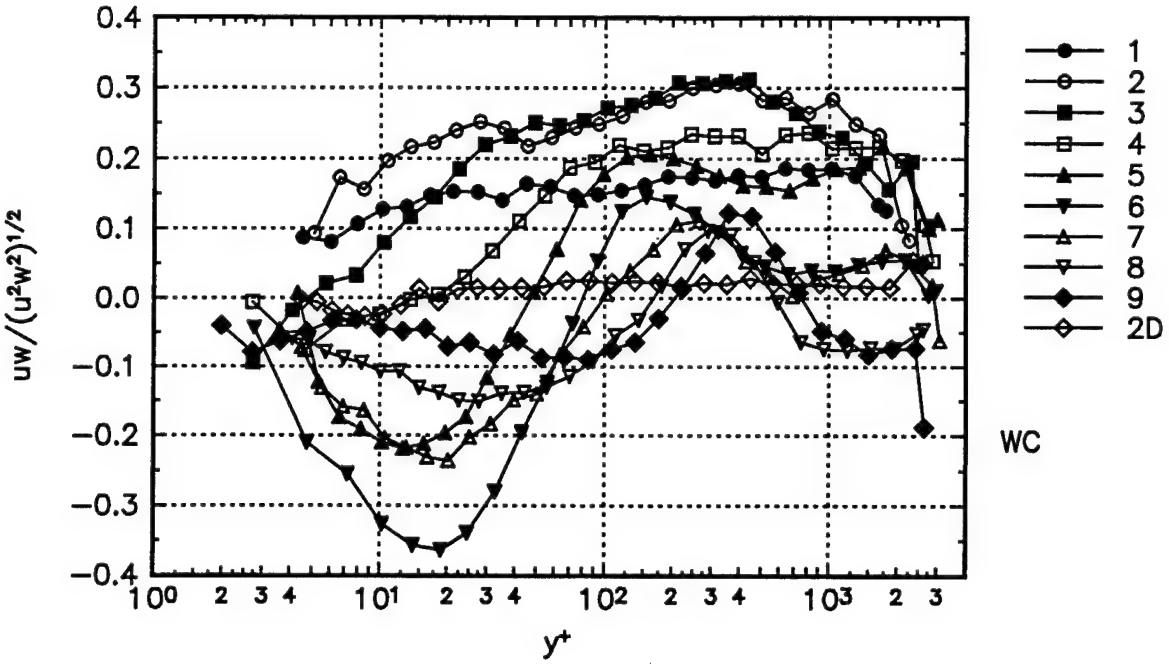

Figure 11. The $\overline{uw}/(\overline{u^2}\ \overline{w^2})^{1/2}$ shear stress correlation coefficient in wall-stress coordinates. The uncertainties are on the order of the symbol size.

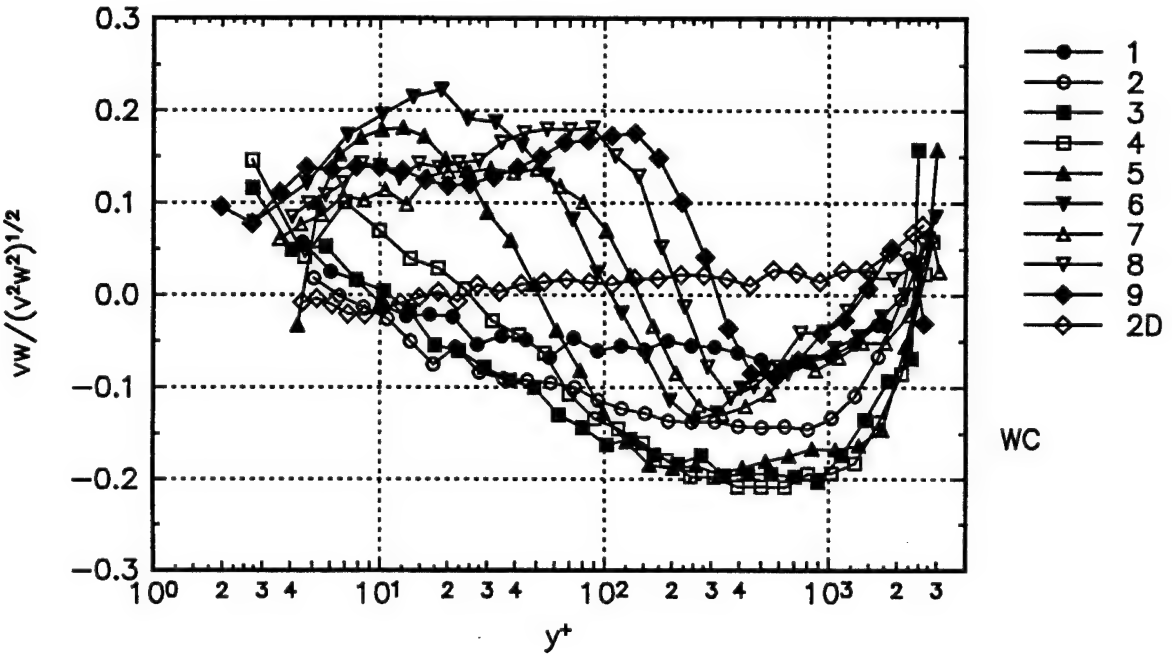

Figure 12. The $\overline{vw}/(\overline{v^2}\ \overline{w^2})^{1/2}$ shear stress correlation coefficient in wall-stress coordinates. The uncertainties are on the order of the symbol size.

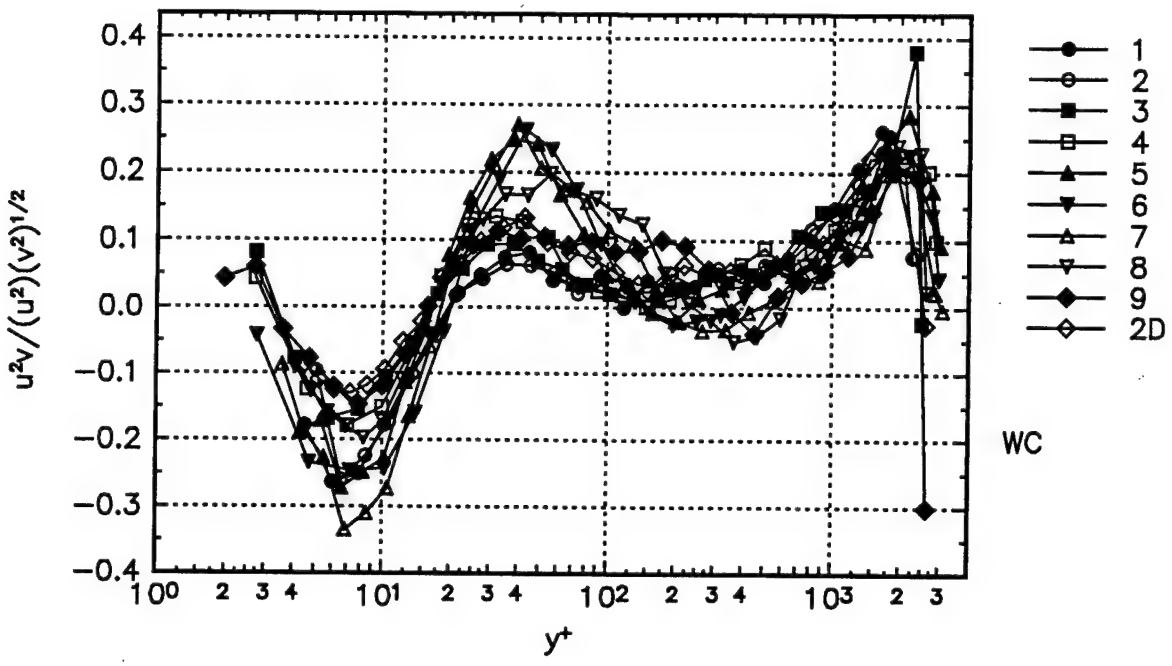

Figure 13.The $\overline{u^2v}/(\overline{u^2})\,(\overline{v^2})^{1/2}$ triple product correlation coefficient in wall-stress coordinates. The uncertainties are on the order of the symbol size.

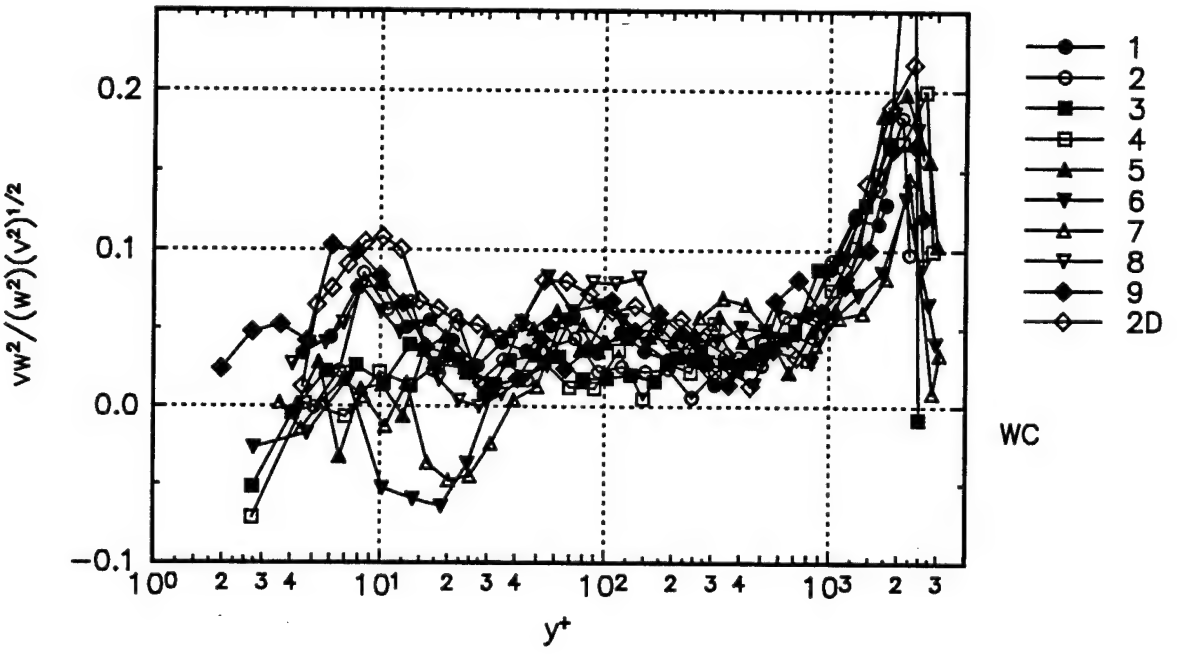

Figure 14. The $\overline{vw^2}/(\overline{w^2})\,(\overline{v^2})^{1/2}$ triple product correlation coefficient in wall-stress coordinates. Typical uncertainty is ±0.012.

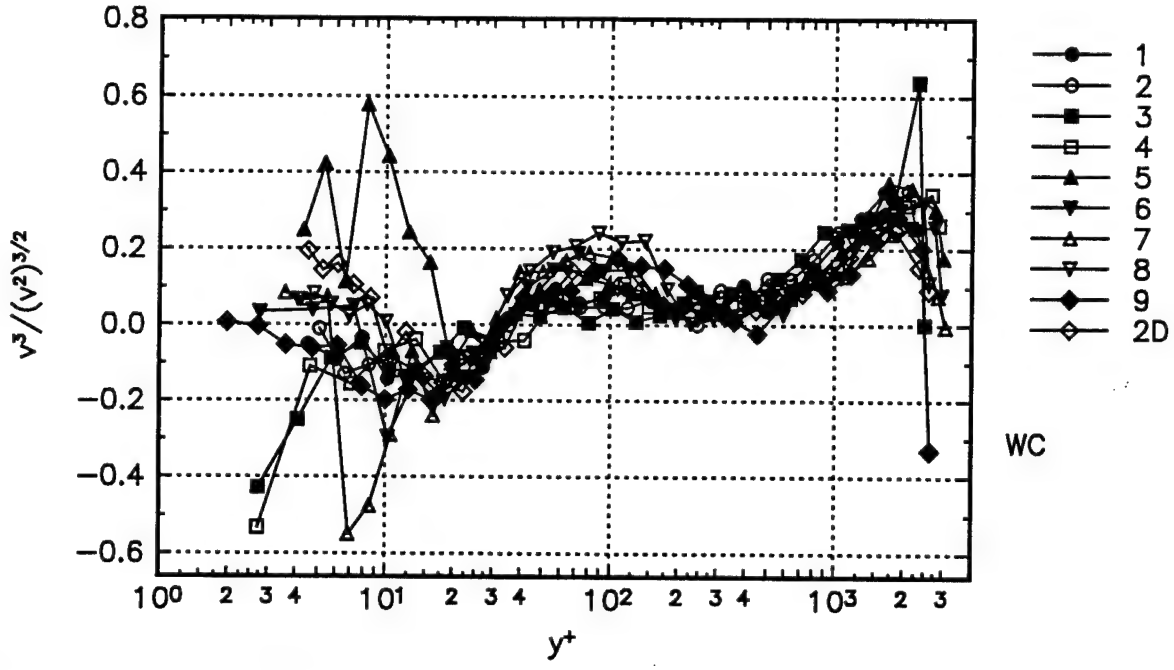

Figure 15. The $\overline{v^3}/(\overline{v^2})^{3/2}$ triple product correlation coefficient in wall-stress coordinates. Typical uncertainty is ±0.052.

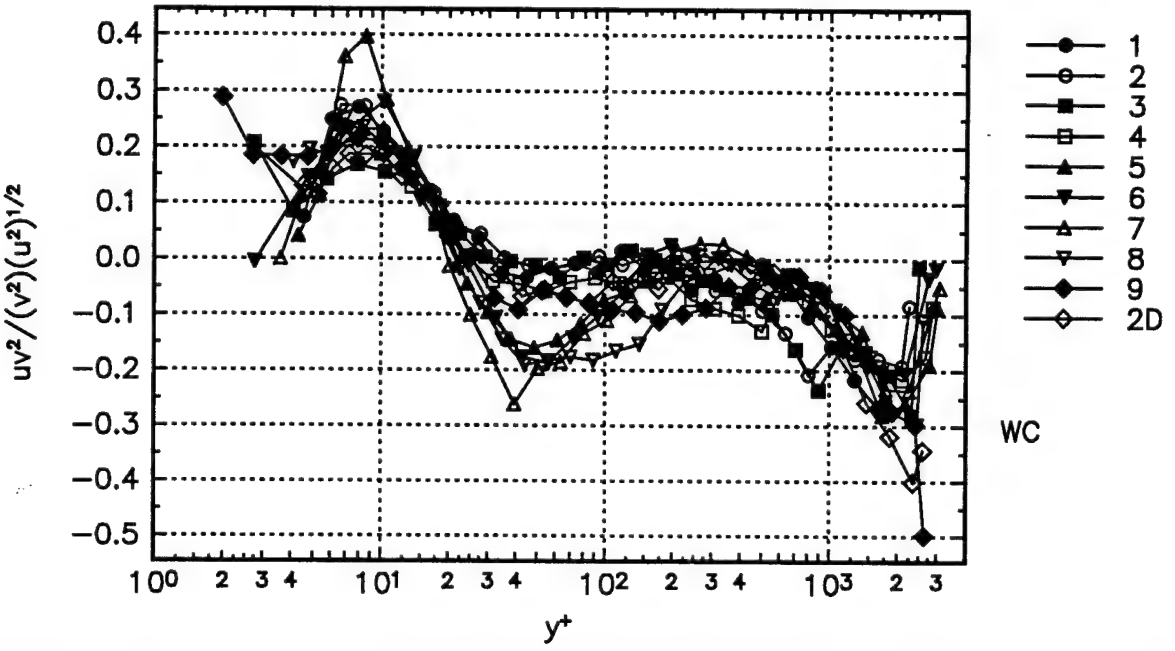

Figure 16. The $\overline{uv^2}/(\overline{v^2})\,(\overline{u^2})^{1/2}$ triple product correlation coefficient in wall-stress coordinates. The uncertainties are on the order of the symbol size.

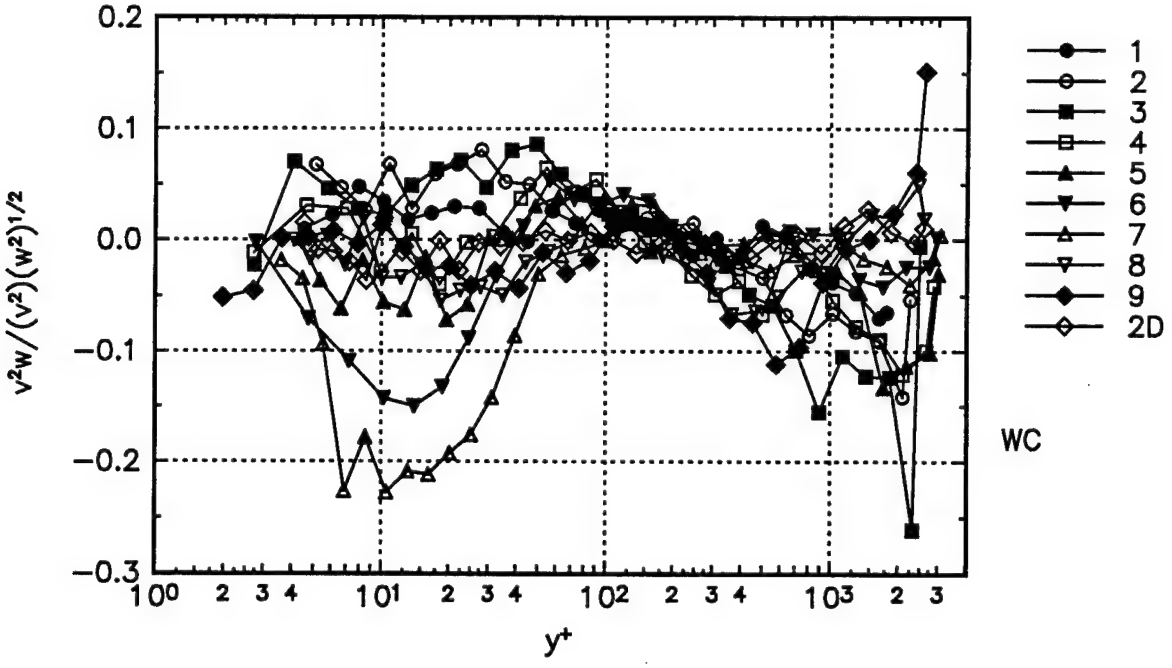

Figure 17. The $\overline{v^2w}/(\overline{v^2})\,(\overline{w^2})^{1/2}$ triple product correlation coefficient in wall-stress coordinates. Typical uncertainty is ±0.011.

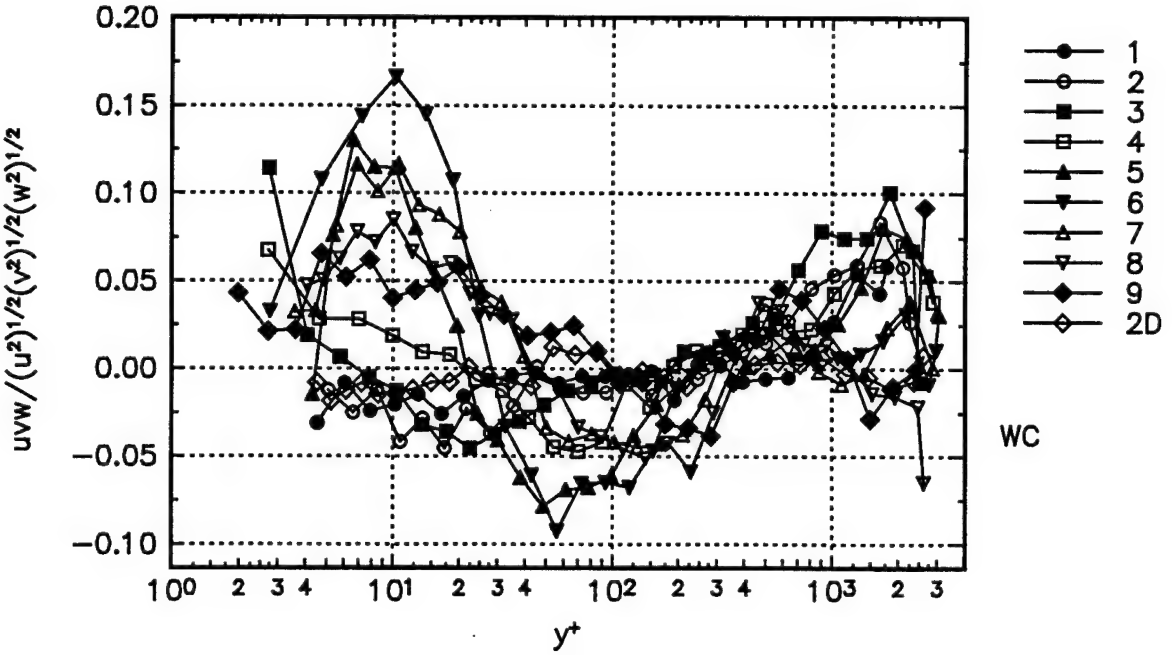

Figure 18. The $\overline{uvw}/(\overline{u^2})^{1/2}\,(\overline{v^2})^{1/2}\,(\overline{w^2})^{1/2}$ triple product correlation coefficient in wall-stress coordinates. The uncertainties are on the order of the symbol size.

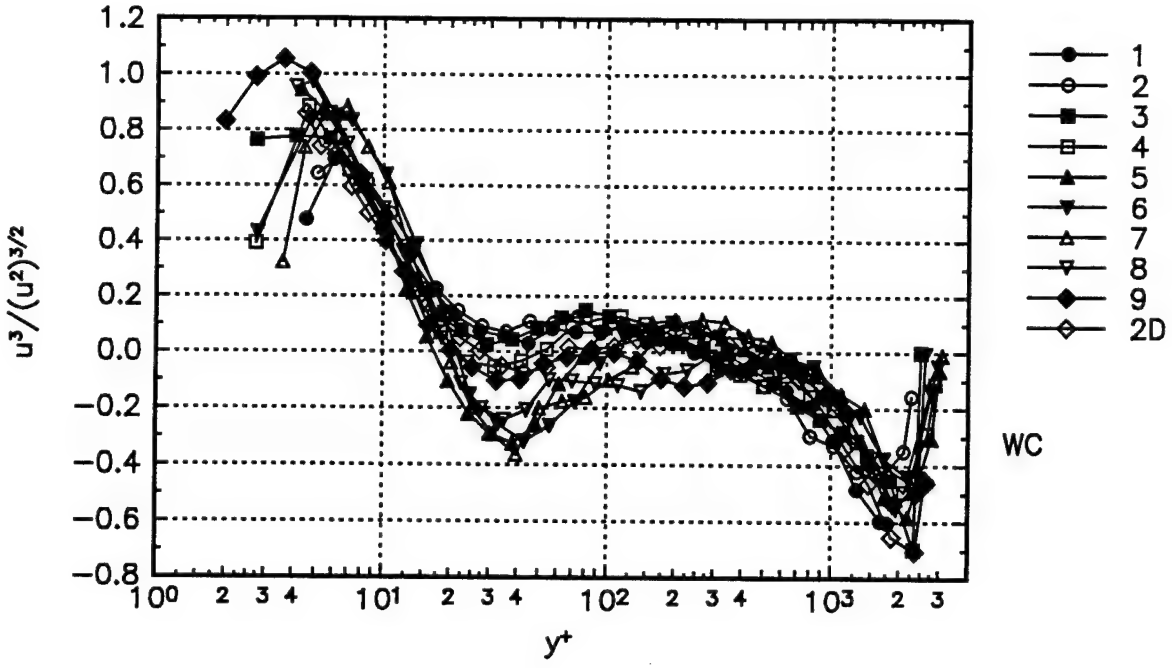

Figure 19. The $\overline{u^3}/(\overline{u^2})^{3/2}$ triple product correlation coefficient in wall-stress coordinates. The uncertainties are on the order of the symbol size.

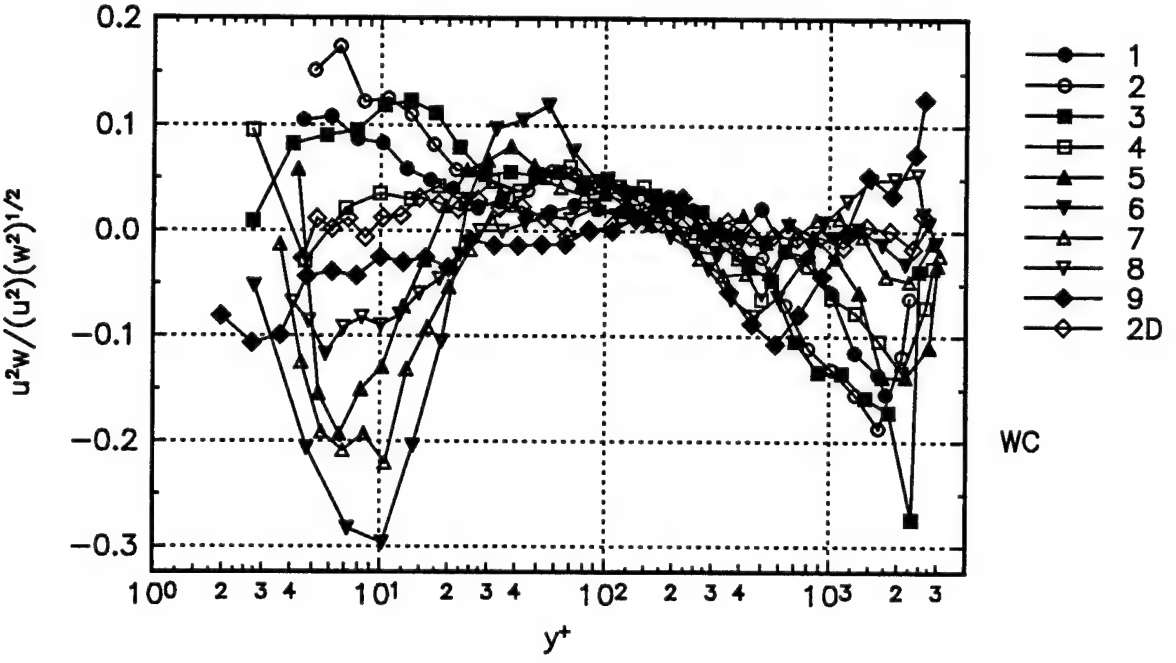

Figure 20. The $\overline{u^2w}/(\overline{u^2})\,(\overline{w^2})^{1/2}$ triple product correlation coefficient in wall-stress coordinates. The uncertainties are on the order of the symbol size.

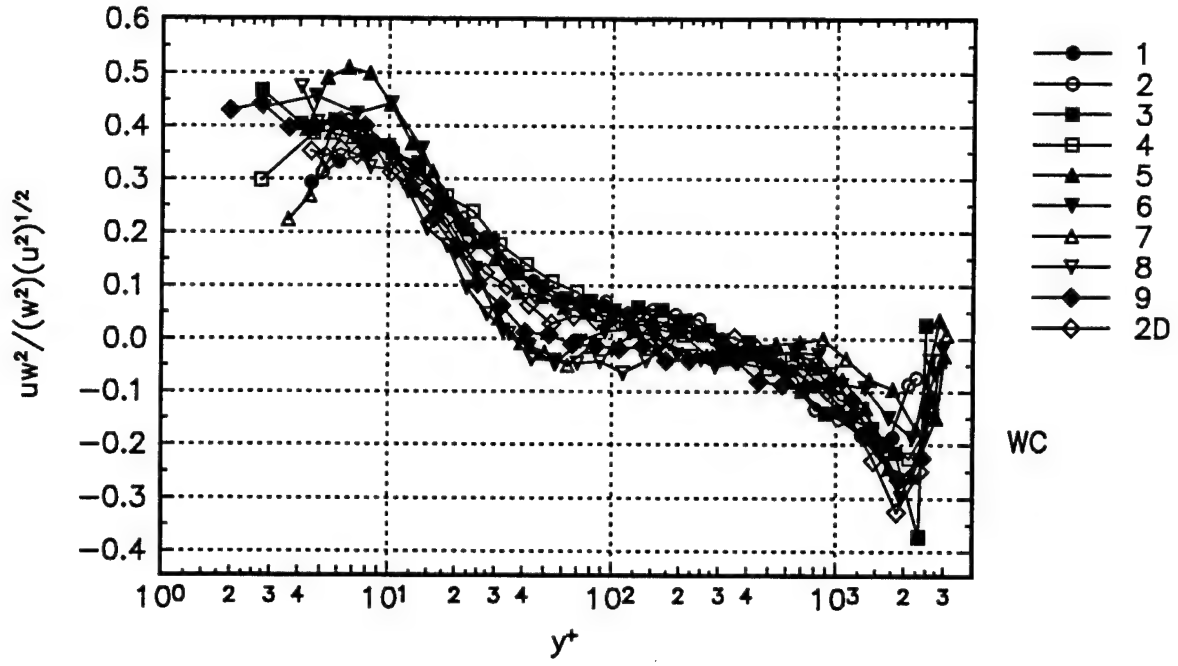

Figure 21. The $\overline{uw^2}/(\overline{w^2})\,(\overline{u^2})^{1/2}$ triple product correlation coefficient in wall-stress coordinates. The uncertainties are on the order of the symbol size.

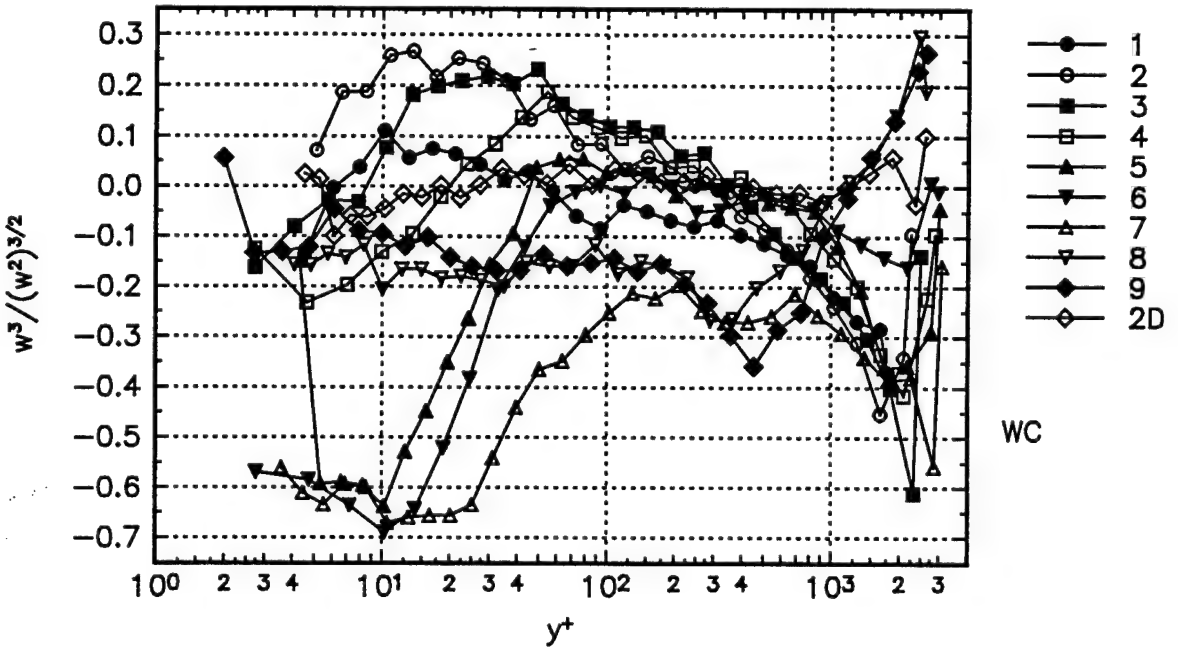

Figure 22. The $\overline{w^3}/(\overline{w^2})^{3/2}$ triple product correlation coefficient in wall-stress coordinates. The uncertainties are on the order of the symbol size.

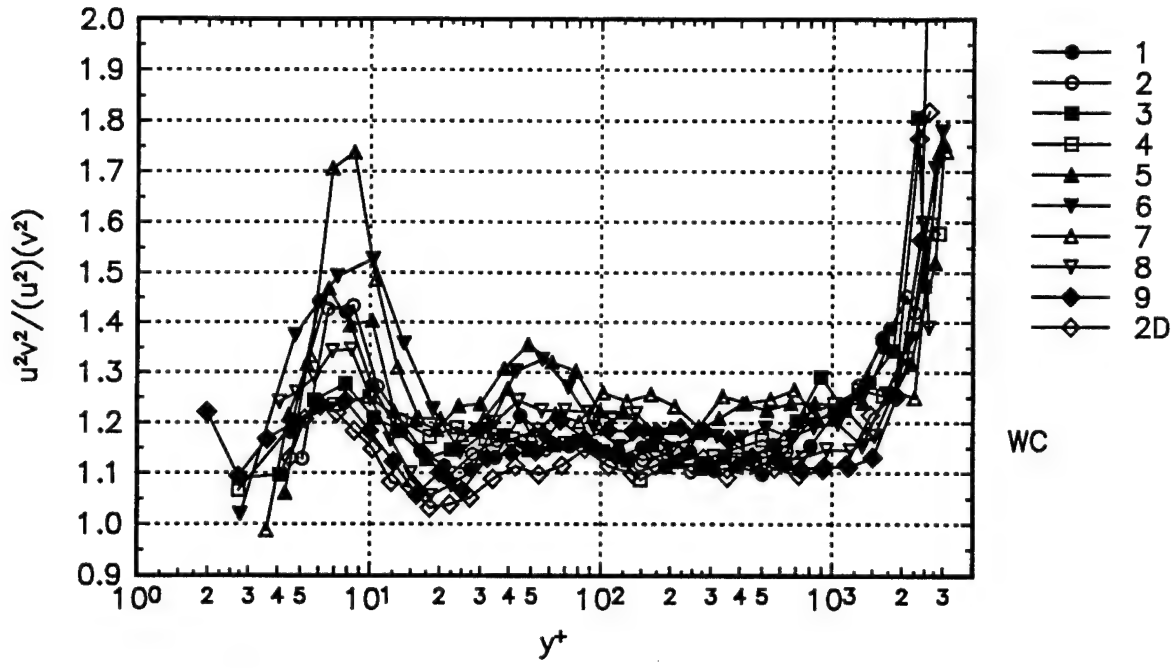

Figure 23. The $\overline{u^2v^2}/(\overline{u^2})(\overline{v^2})$ fourth order product correlation coefficient in wall-stress coordinates. Typical uncertainty is ±0.039.

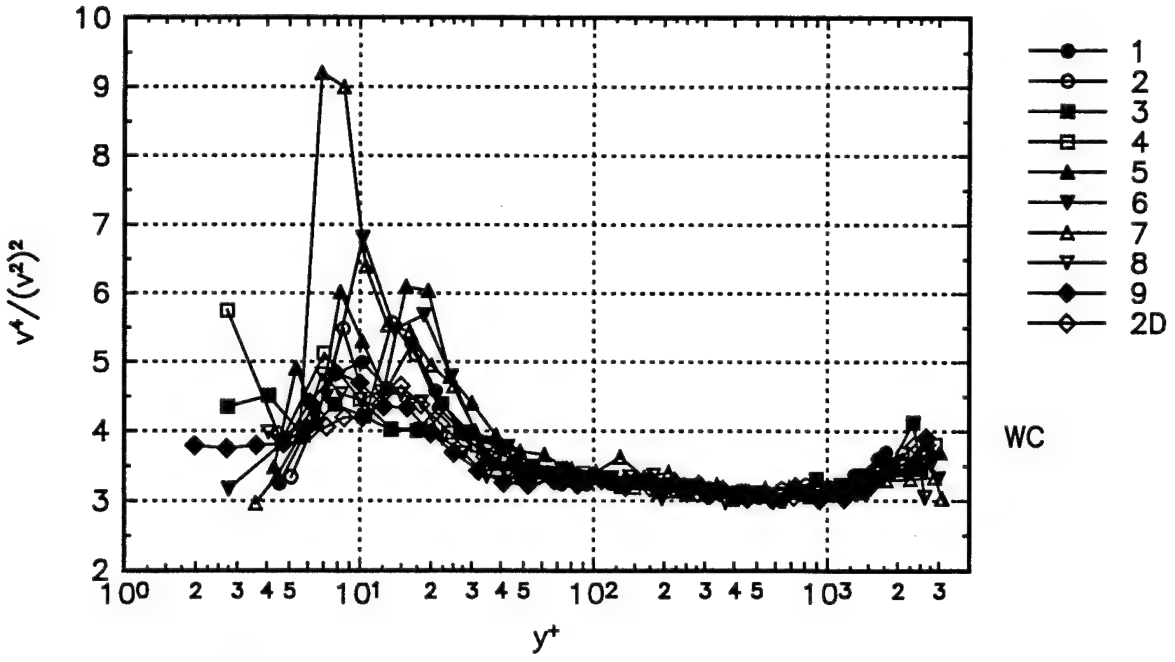

Figure 24. The $\overline{v^4}/(\overline{v^2})^2$ fourth order product correlation coefficient in wall-stress coordinates. The uncertainties are on the order of the symbol size.

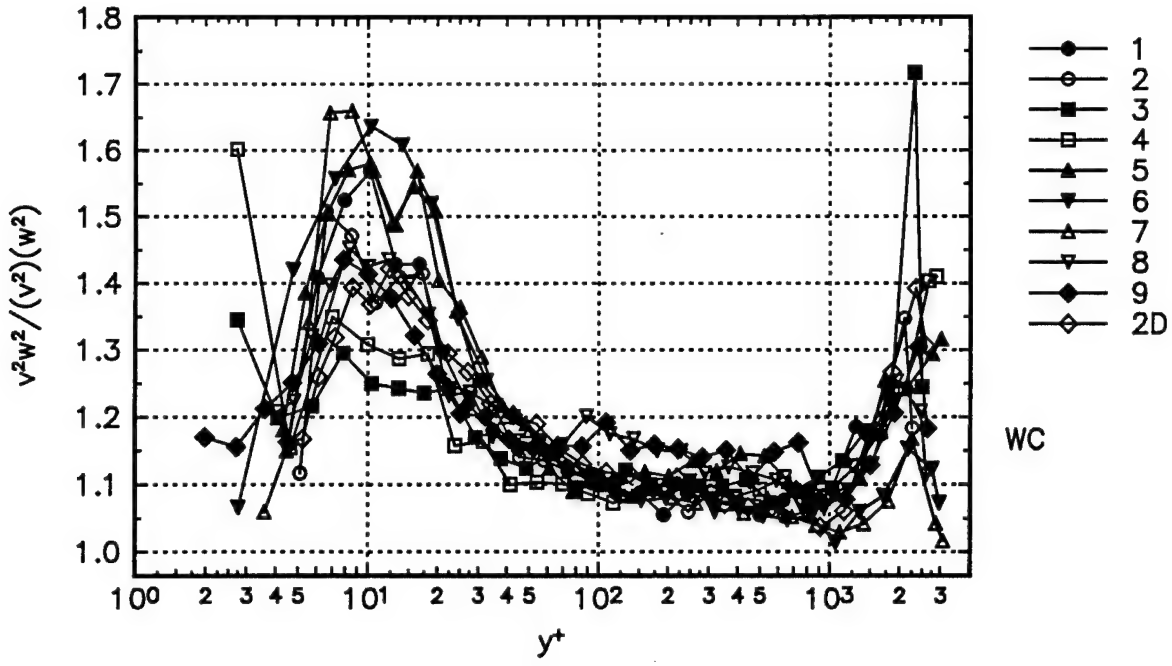

Figure 25. The $\overline{v^2w^2}/(\overline{v^2})(\overline{w^2})$ fourth order product correlation coefficient in wall-stress coordinates. The uncertainties are on the order of the symbol size.

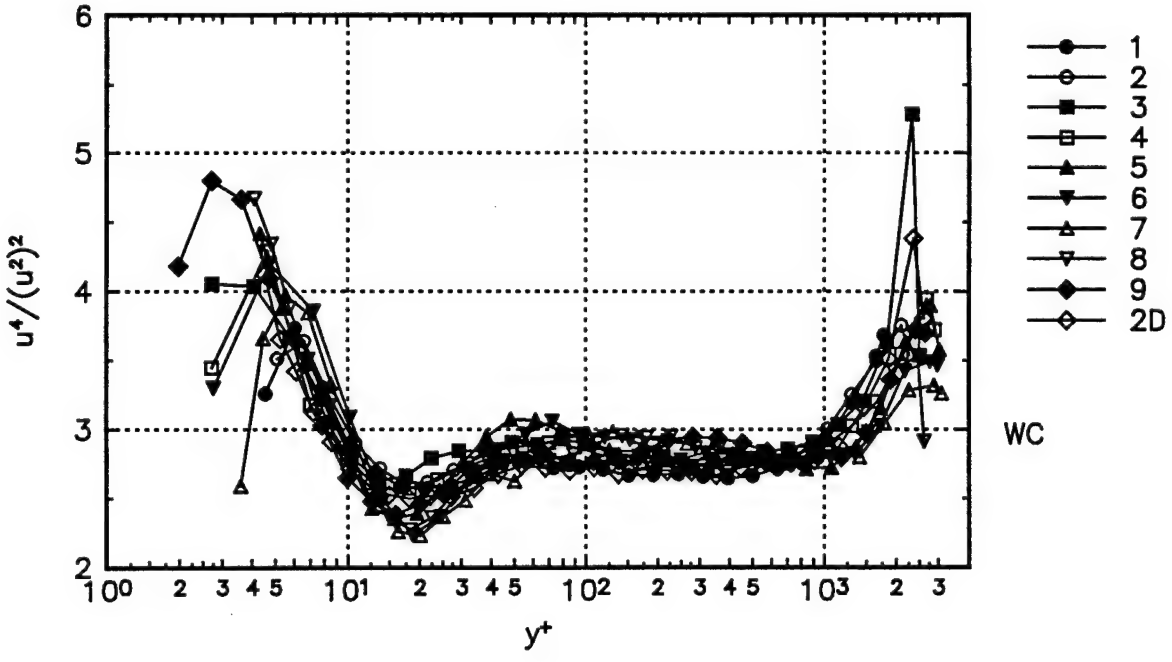

Figure 26. The $\overline{u^4}/(\overline{u^2})^2$ fourth order product correlation coefficient in wall-stress coordinates. The uncertainties are on the order of the symbol size.

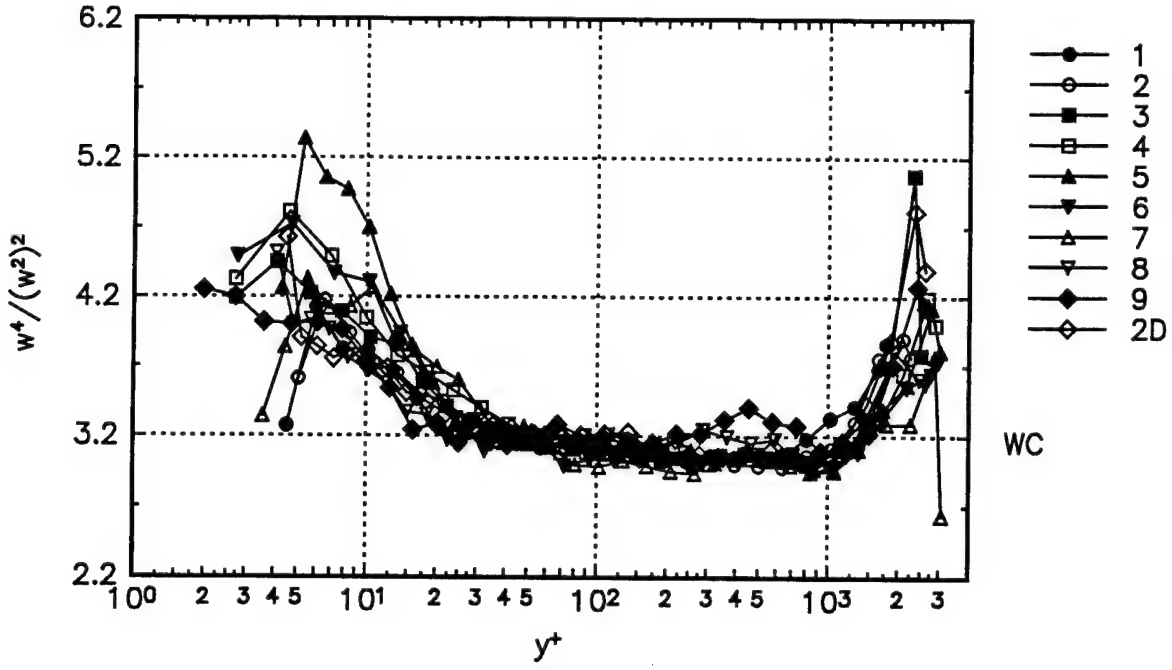

Figure 27. The $\overline{w^4}/(\overline{w^2})^2$ fourth order product correlation coefficient in wall-stress coordinates. The uncertainties are on the order of the symbol size.

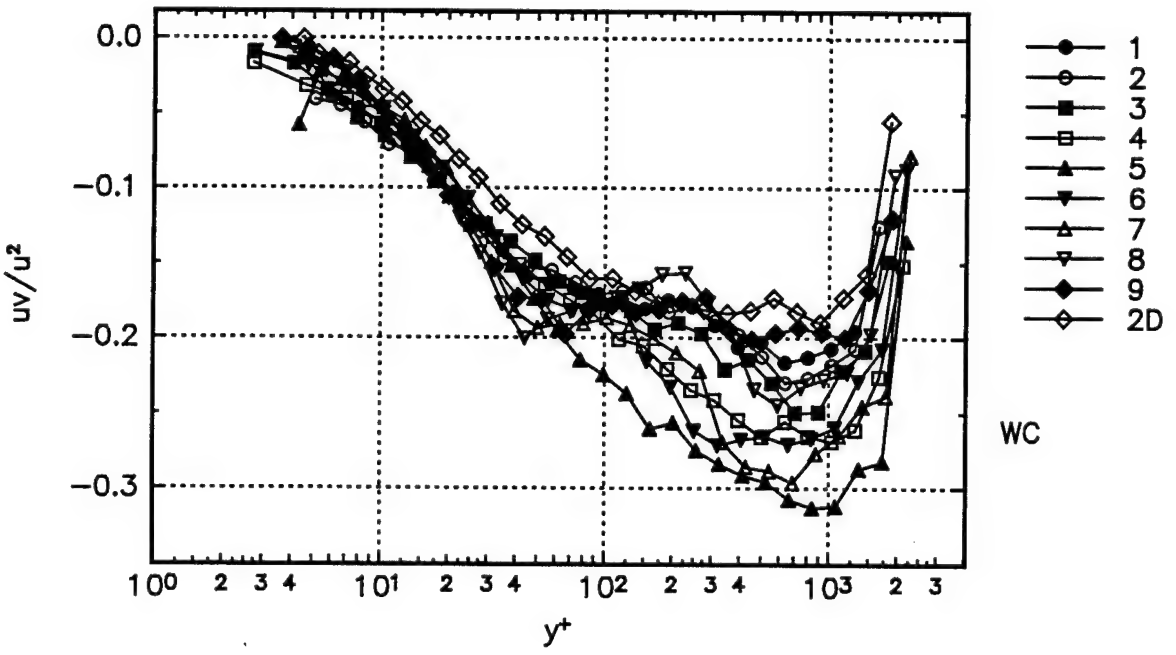

Figure 28. The $\overline{uv}/\overline{u^2}$ structural parameter calculated in wall-wall stress coordinates. The uncertainties are on the order of the symbol size.

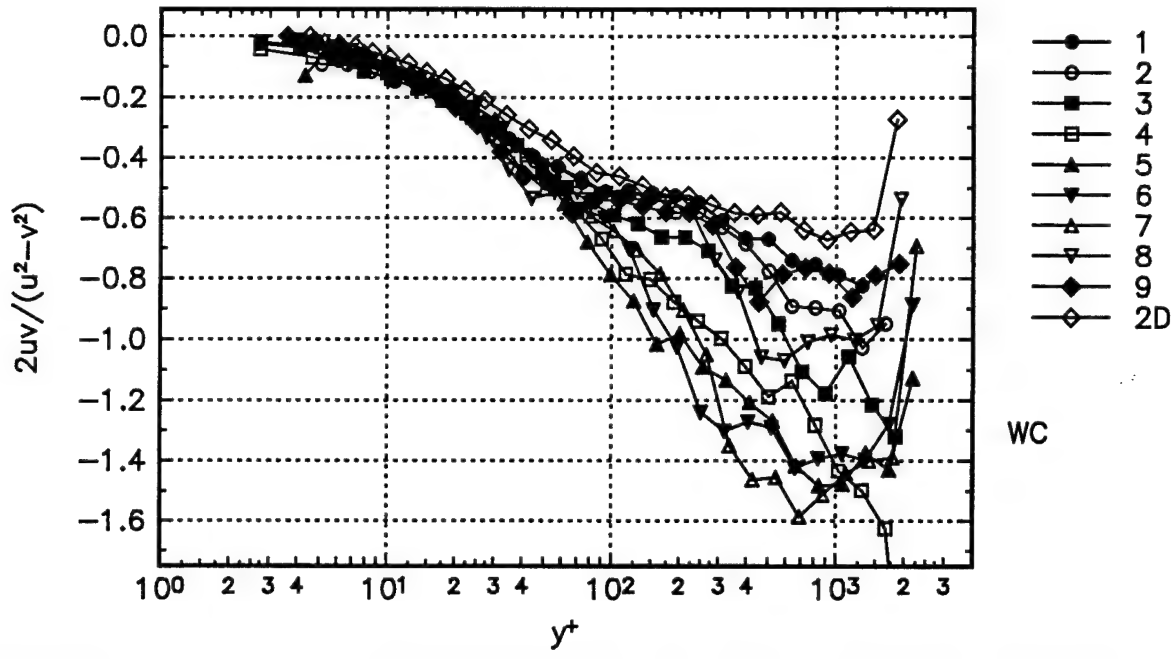

Figure 29. The $2\overline{uv}/(\overline{u^2}-\overline{v^2})$ structural parameter calculated in wall-stress coordinates. The uncertainties are on the order of the symbol size.

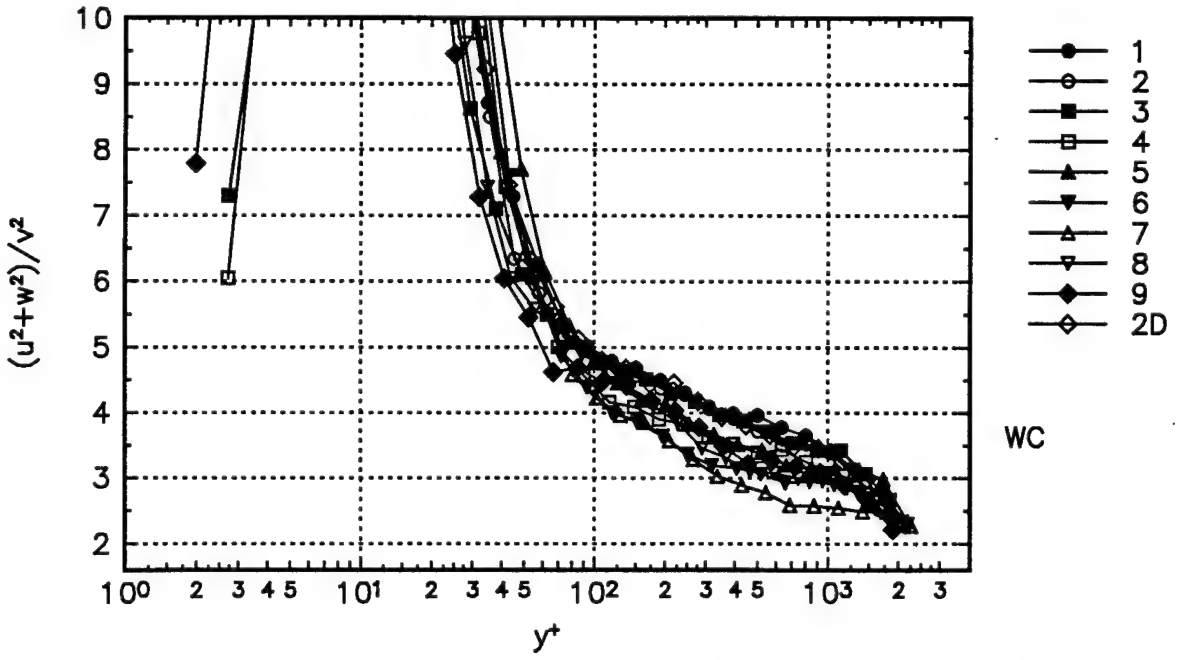

Figure 30. The $(\overline{u^2}+\overline{w^2})/\overline{v^2}$ structural parameter calculated in wall-stress coordinates. The uncertainties are on the order of the symbol size.

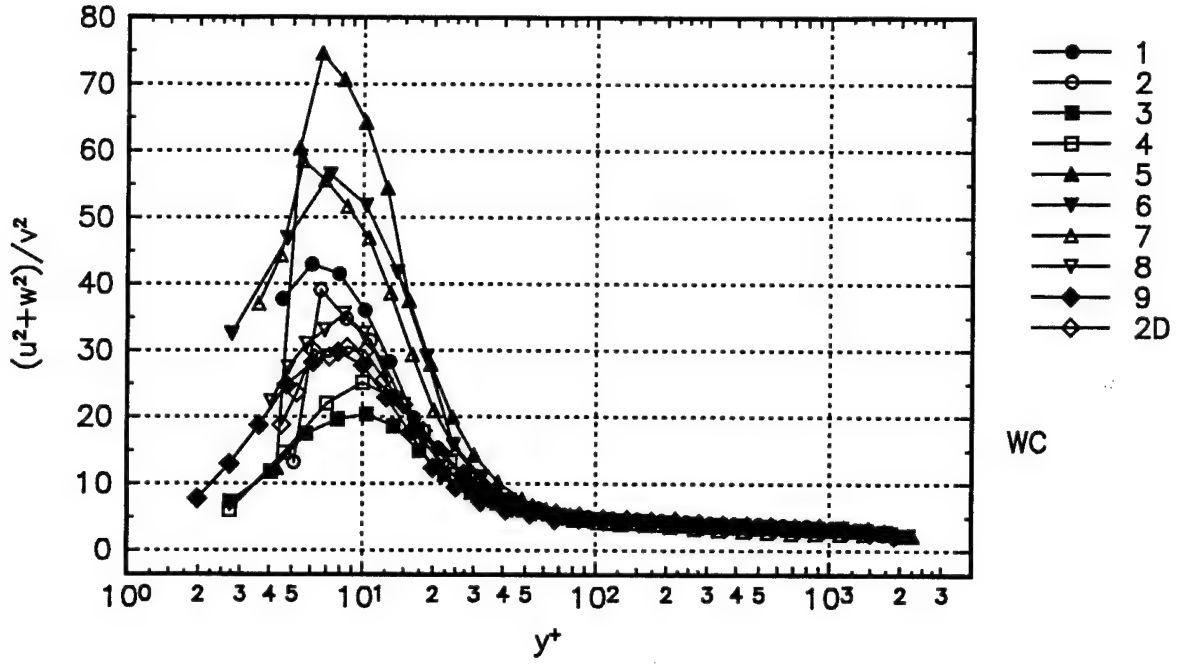

Figure 30. The $(\overline{u^2}+\overline{w^2})/\overline{v^2}$ structural parameter calculated in wall-stress coordinates. The uncertainties are on the order of the symbol size.

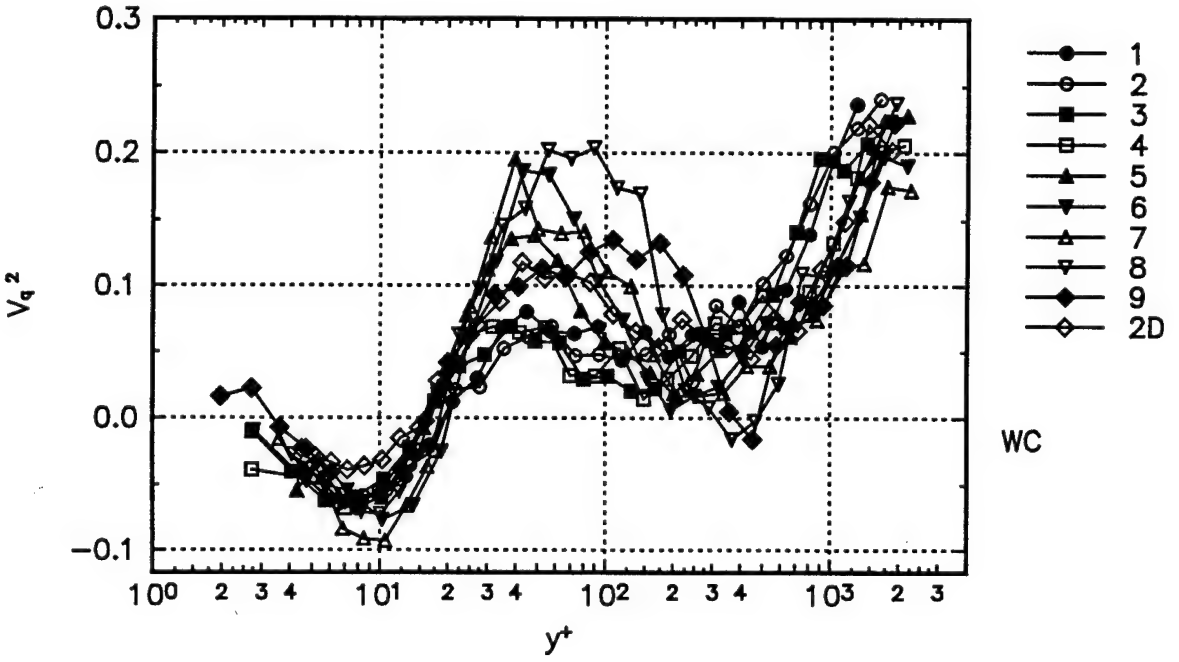

Figure 31. The V_{q2} turbulent kinetic energy transport velocity. The uncertainties are on the order of the symbol size.

TABLE 1. UNCERTAINTIES IN MEASURED QUANTITIES WITH 20:1 ODDS

U/u_τ	± 0.075	$\overline{u^2v}/u_\tau^3$	± 0.039
V/u_τ	± 0.026	$\overline{u^2w}/u_\tau^3$	± 0.066
W/u_τ	± 0.05	$\overline{v^2w}/u_\tau^3$	± 0.015
$\overline{u^2}/u_\tau^2$	± 0.08	$\overline{uv^2}/u_\tau^3$	± 0.016
$\overline{v^2}/u_\tau^2$	± 0.029	$\overline{uw^2}/u_\tau^3$	± 0.059
$\overline{w^2}/u_\tau^2$	± 0.037	$\overline{vw^2}/u_\tau^3$	± 0.012
$-\overline{uv}/u_\tau^2$	± 0.043	$\overline{uvw}/u_\tau^3$	± 0.019
$-\overline{uw}/u_\tau^2$	± 0.023	$\overline{u^3}/u_\tau^3$	± 0.189
$-\overline{vw}/u_\tau^2$	± 0.012	$\overline{v^3}/u_\tau^3$	± 0.018
		$\overline{w^3}/u_\tau^3$	± 0.05

Appendix A: Wall Stress Coordinates

In this Appendix A figures of some of the flow parameters in wall-stress coordinates that are not included in the body of the report are presented. The x coordinate of the wall-stress coordinates is aligned in the direction of the mean flow at the first point of the mean velocity profile and changes from measurement station to measurement station. The "y" coordinate is perpendicular to the wall and the "z" axis completes the right-handed coordinate system. In the first section of the Appendix figures of mean velocity, Reynolds' stresses and triple products nondimensionalized with respective powers of U_{ref} are presented. Next the transport velocities for the normal stresses and the TKE in three directions are presented. Next, the mean velocity, Reynolds' stress and triple product deivatives with respect to the "y" and the production terms for the triple product transport euqations in the vertical direction using these derivatives are presented. Some structural parameters are also presented in this Appendix.

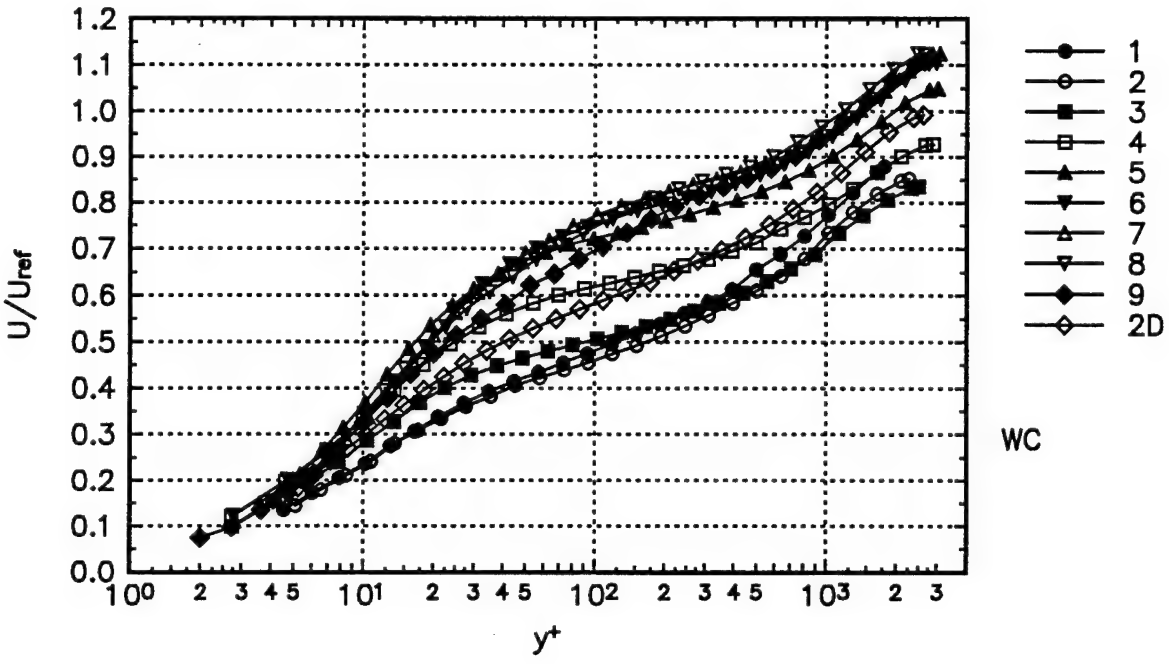

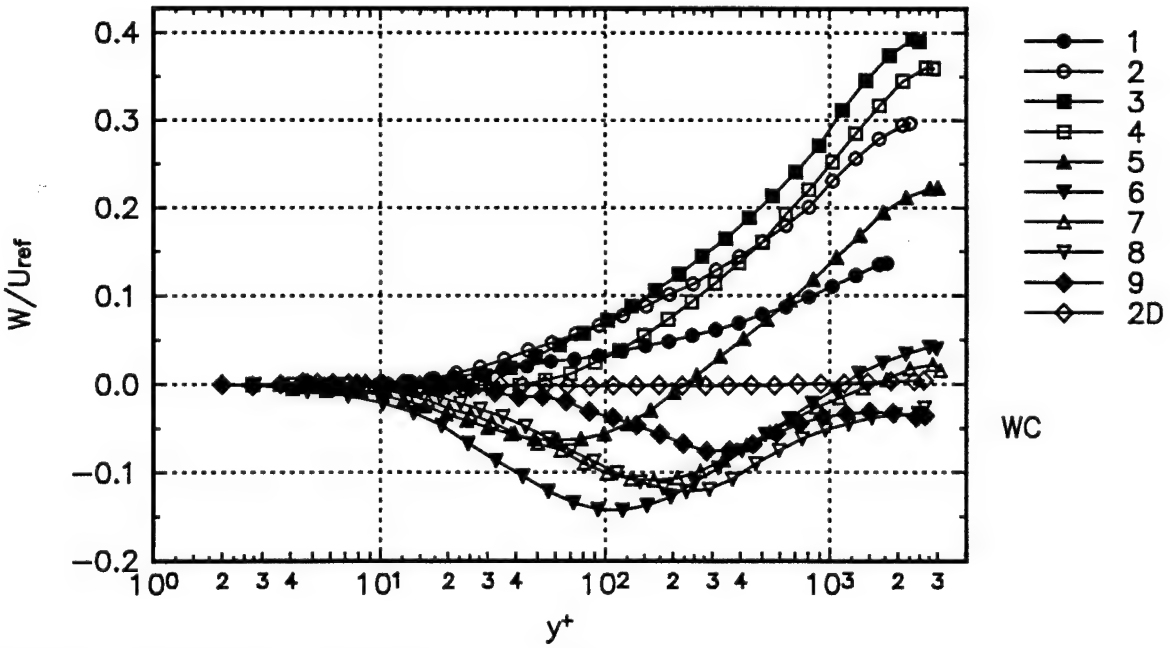

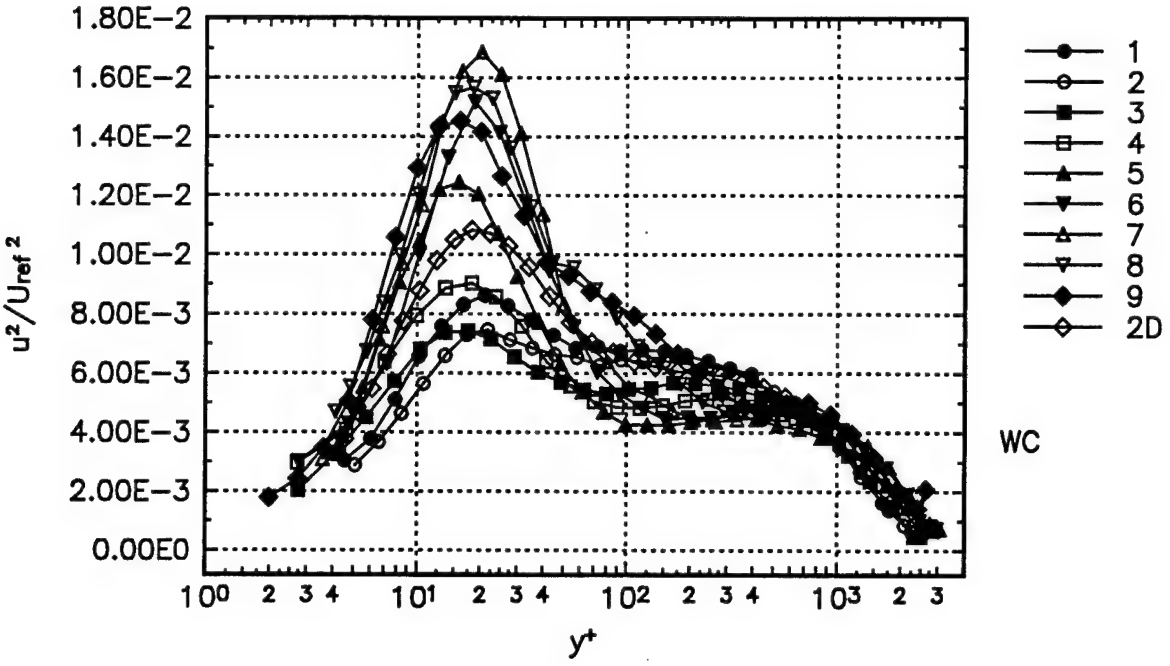
1.80E−2
1.60E−2
1.40E−2
1.20E−2
1.00E−2
8.00E−3
6.00E−3
4.00E−3
2.00E−3
0.00E0
u²/Uref²
10⁰ 2 3 4 10¹ 2 3 4 10² 2 3 4 10³ 2 3
y⁺
1
2
3
4
5
6
7
8
9
2D
WC

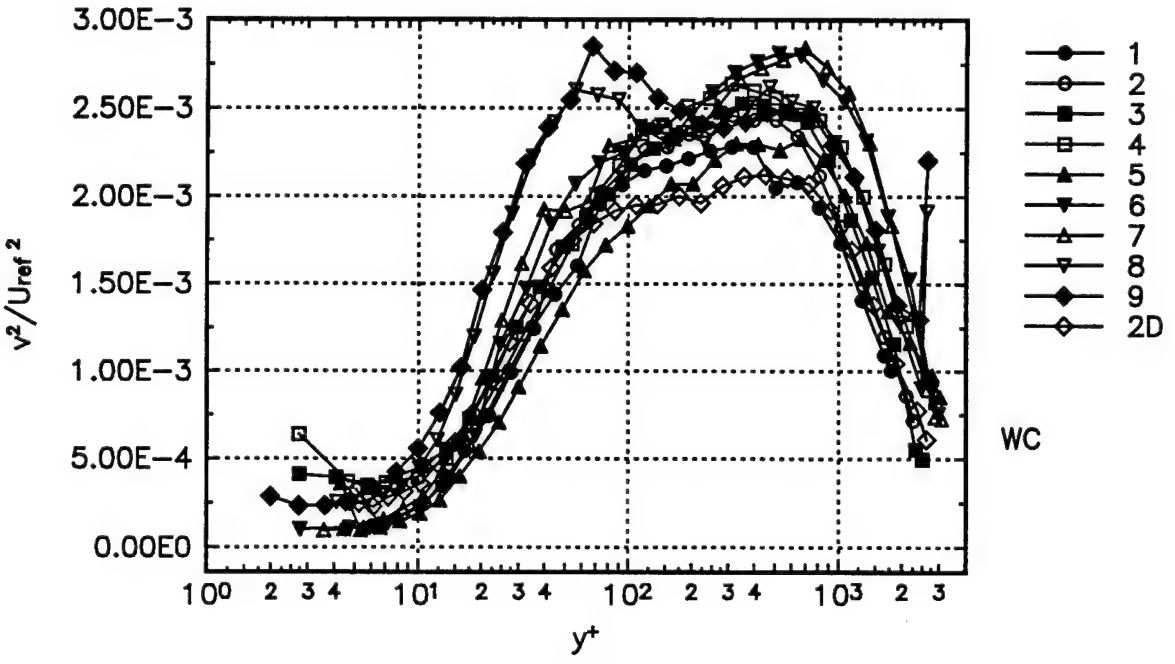
3.00E−3
2.50E−3
2.00E−3
1.50E−3
1.00E−3
5.00E−4
0.00E0
v²/Uref²
10⁰ 2 3 4 10¹ 2 3 4 10² 2 3 4 10³ 2 3
y⁺
1
2
3
4
5
6
7
8
9
2D
WC

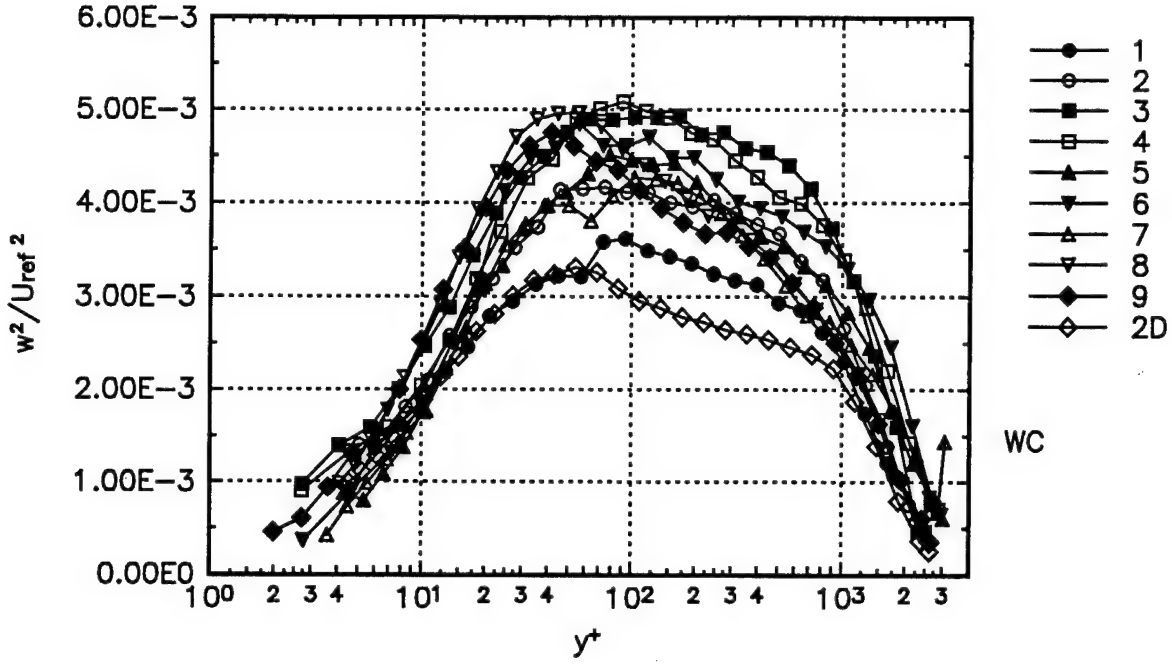
6.00E−3
5.00E−3
4.00E−3
3.00E−3
2.00E−3
1.00E−3
0.00E0
w²/Uref²
10⁰ 2 3 4 10¹ 2 3 4 10² 2 3 4 10³ 2 3
y+
1
2
3
4
5
6
7
8
9
2D
WC

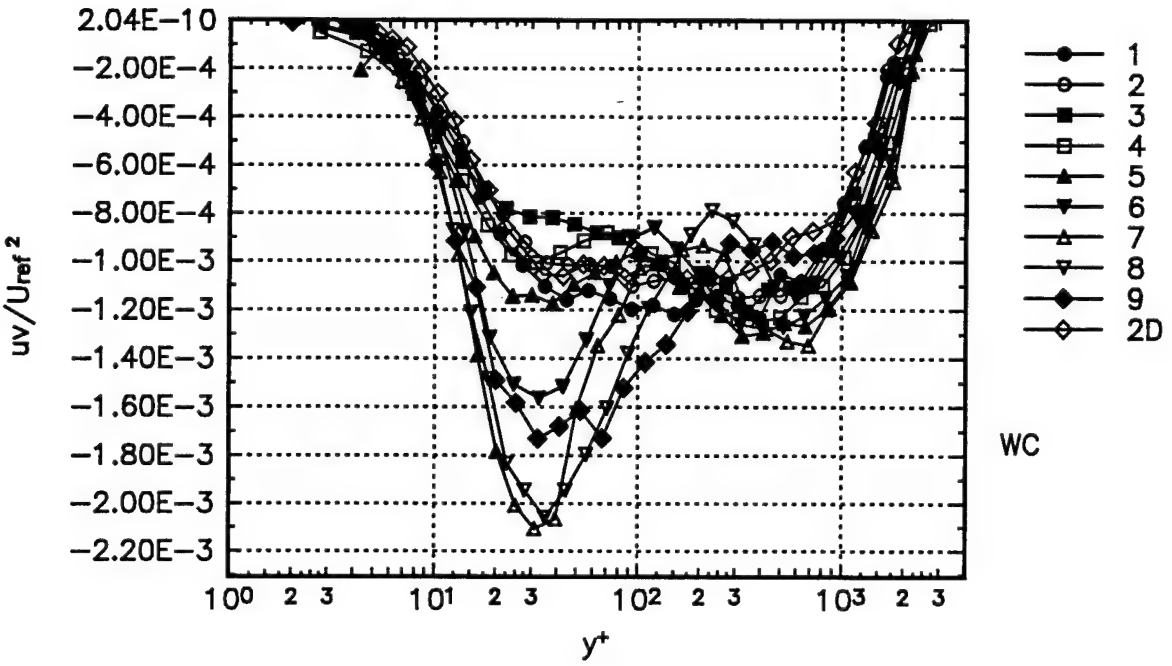
2.04E−10
−2.00E−4
−4.00E−4
−6.00E−4
−8.00E−4
−1.00E−3
−1.20E−3
−1.40E−3
−1.60E−3
−1.80E−3
−2.00E−3
−2.20E−3
uv/Uref²
10⁰ 2 3 10¹ 2 3 10² 2 3 10³ 2 3
y+
1
2
3
4
5
6
7
8
9
2D
WC

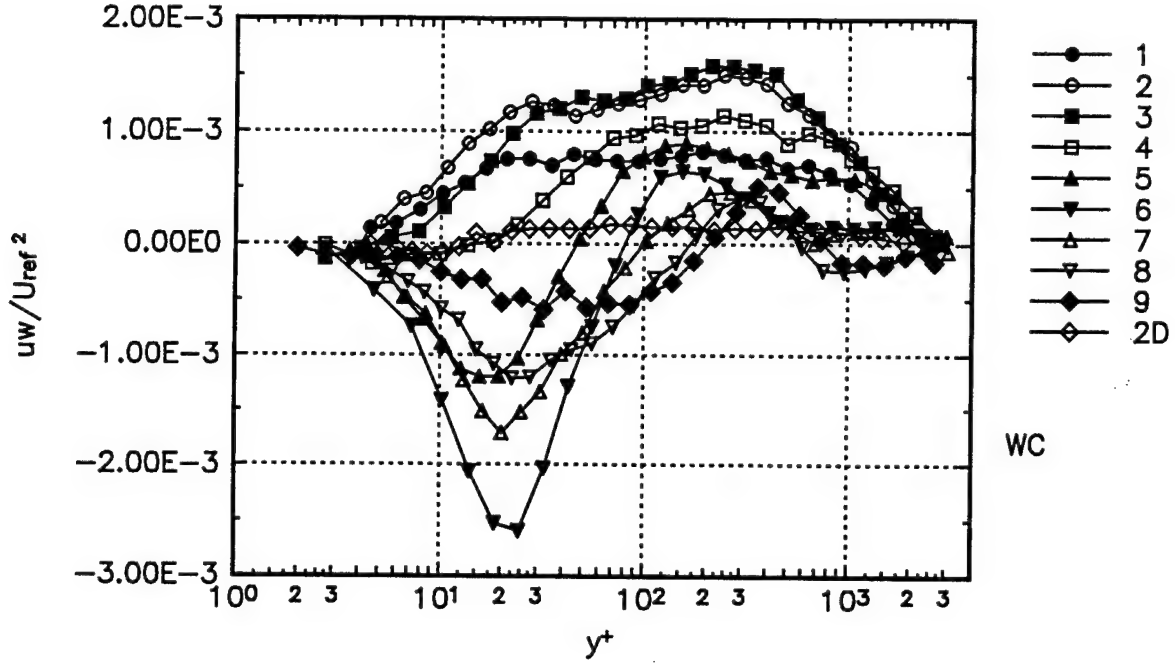
2.00E−3
1.00E−3
0.00E0
−1.00E−3
−2.00E−3
−3.00E−3
uw/Uref 2
10⁰ 2 3
10¹ 2 3
10² 2 3
10³ 2 3
y+
1
2
3
4
5
6
7
8
9
2D
WC

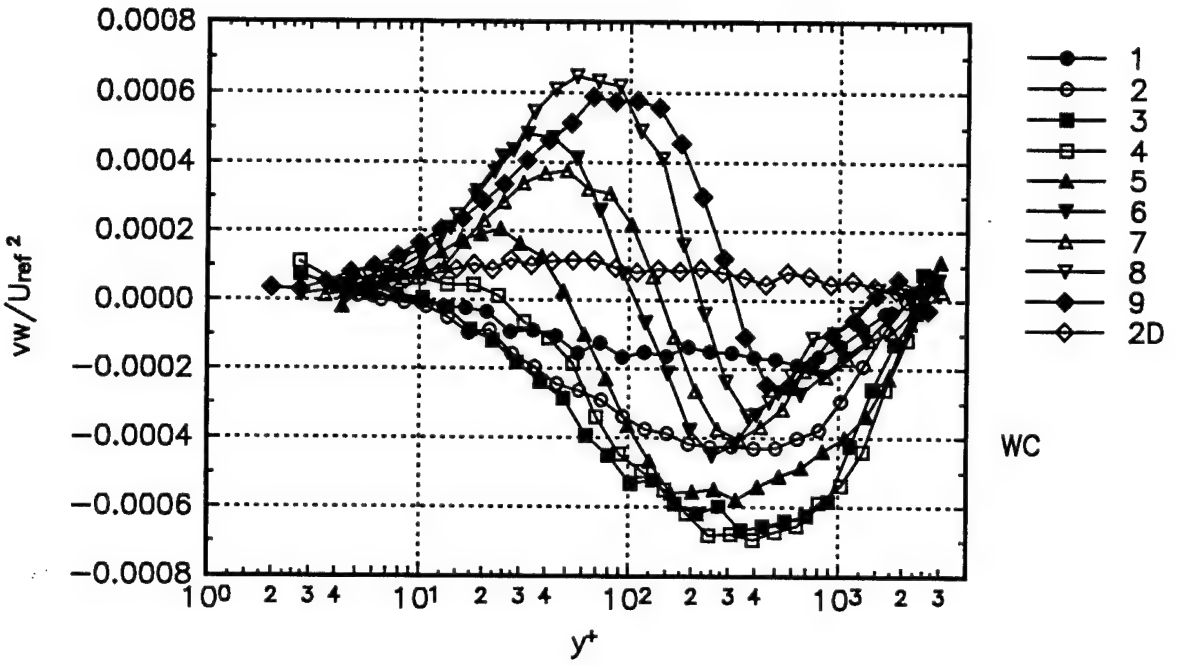
0.0008
0.0006
0.0004
0.0002
0.0000
−0.0002
−0.0004
−0.0006
−0.0008
vw/Uref 2
10⁰ 2 3 4
10¹ 2 3 4
10² 2 3 4
10³ 2 3
y+
1
2
3
4
5
6
7
8
9
2D
WC

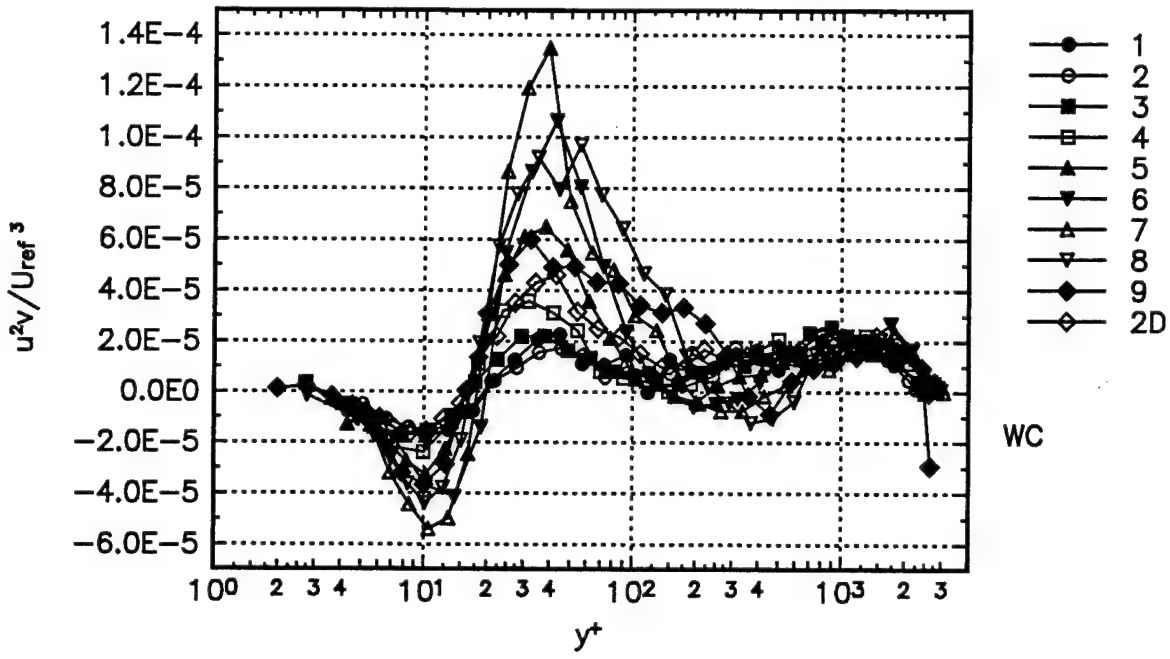
1.4E−4
1.2E−4
1.0E−4
8.0E−5
6.0E−5
4.0E−5
2.0E−5
0.0E0
−2.0E−5
−4.0E−5
−6.0E−5
u^2v/U_{ref}^3
10^0 2 3 4 10^1 2 3 4 10^2 2 3 4 10^3 2 3
y^+
1
2
3
4
5
6
7
8
9
2D
WC

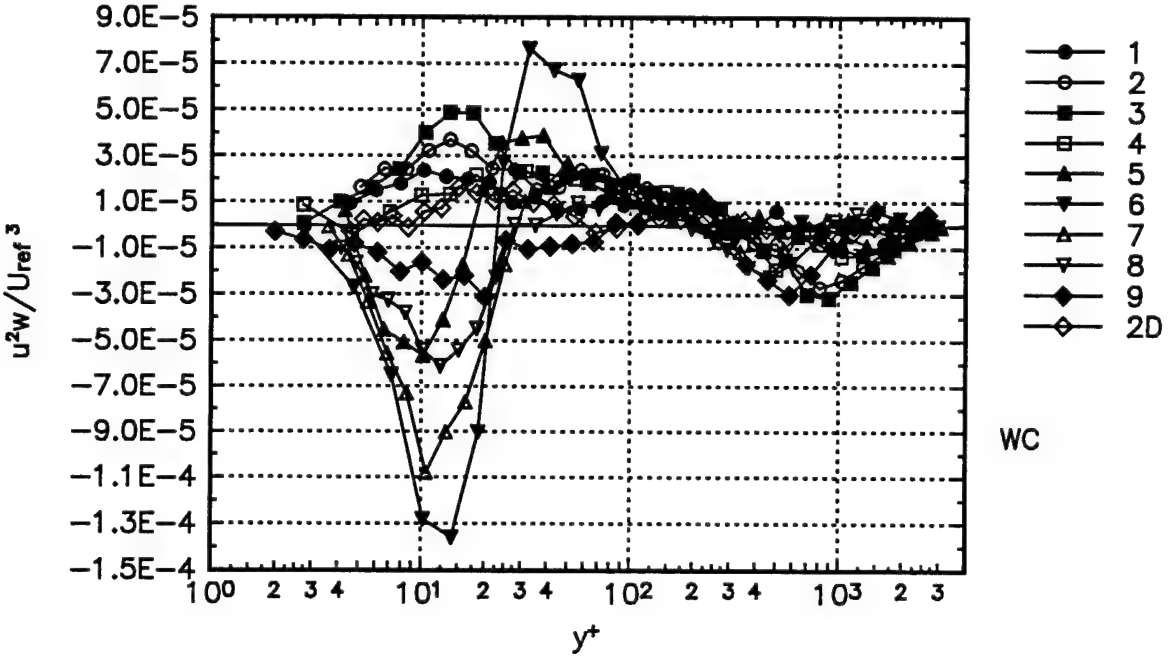
9.0E−5
7.0E−5
5.0E−5
3.0E−5
1.0E−5
−1.0E−5
−3.0E−5
−5.0E−5
−7.0E−5
−9.0E−5
−1.1E−4
−1.3E−4
−1.5E−4
u^2w/U_{ref}^3
10^0 2 3 4 10^1 2 3 4 10^2 2 3 4 10^3 2 3
y^+
1
2
3
4
5
6
7
8
9
2D
WC

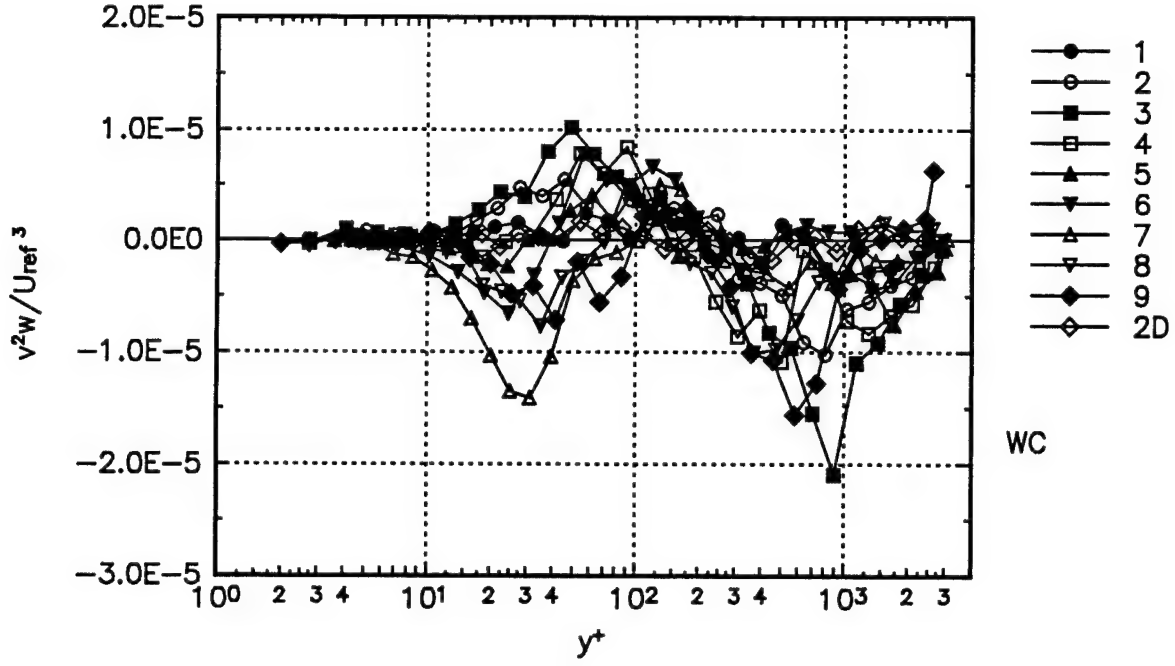
2.0E−5
1.0E−5
0.0E0
−1.0E−5
−2.0E−5
−3.0E−5
v^2w/U_{ref}^3
10^0 2 3 4 10^1 2 3 4 10^2 2 3 4 10^3 2 3
y^+
1
2
3
4
5
6
7
8
9
2D
WC

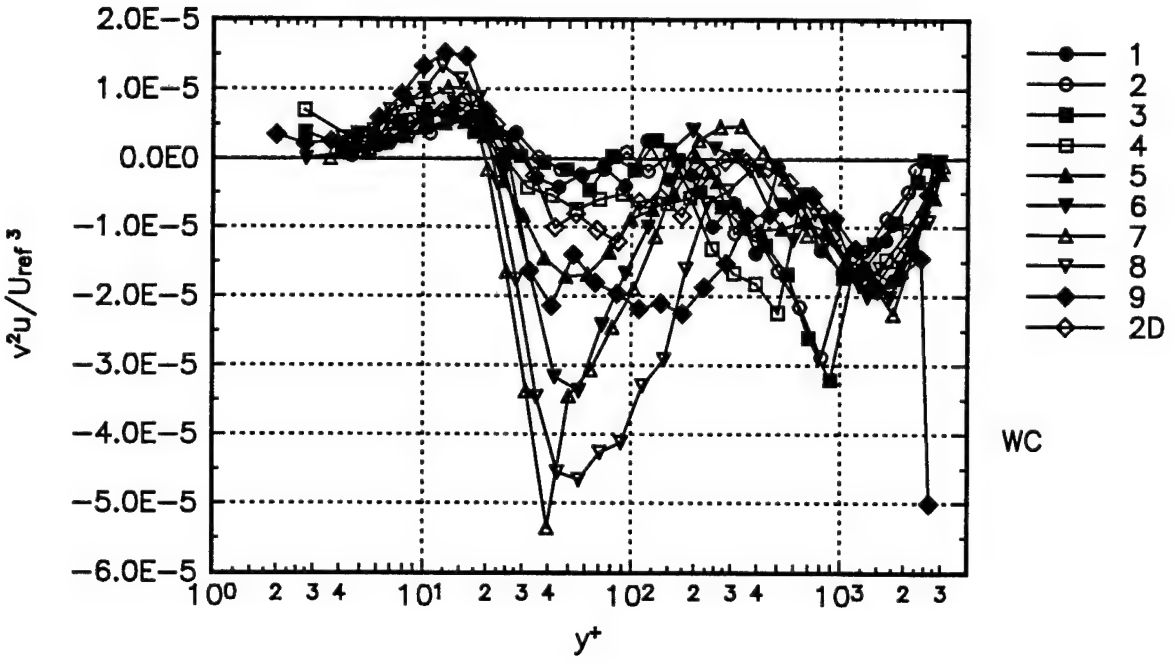
2.0E−5
1.0E−5
0.0E0
−1.0E−5
−2.0E−5
−3.0E−5
−4.0E−5
−5.0E−5
−6.0E−5
v^2u/U_{ref}^3
10^0 2 3 4 10^1 2 3 4 10^2 2 3 4 10^3 2 3
y^+
1
2
3
4
5
6
7
8
9
2D
WC

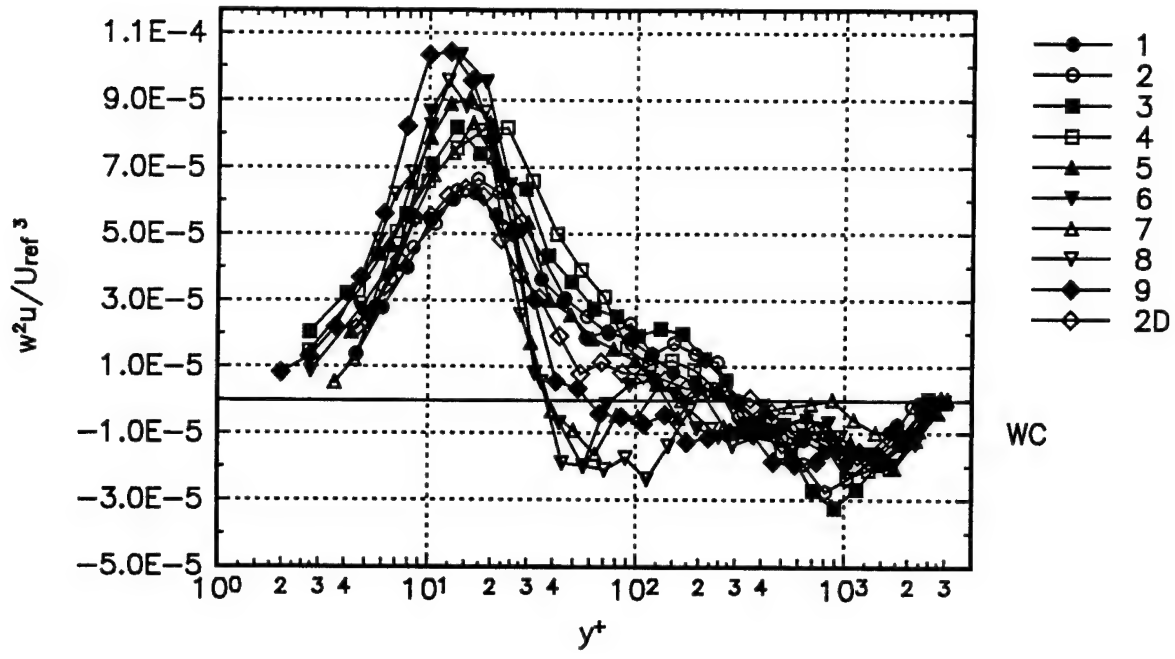
1.1E−4
9.0E−5
7.0E−5
5.0E−5
3.0E−5
1.0E−5
−1.0E−5
−3.0E−5
−5.0E−5
w^2u/U_{ref}^3
10^0 2 3 4 10^1 2 3 4 10^2 2 3 4 10^3 2 3
y^+
1
2
3
4
5
6
7
8
9
2D
WC

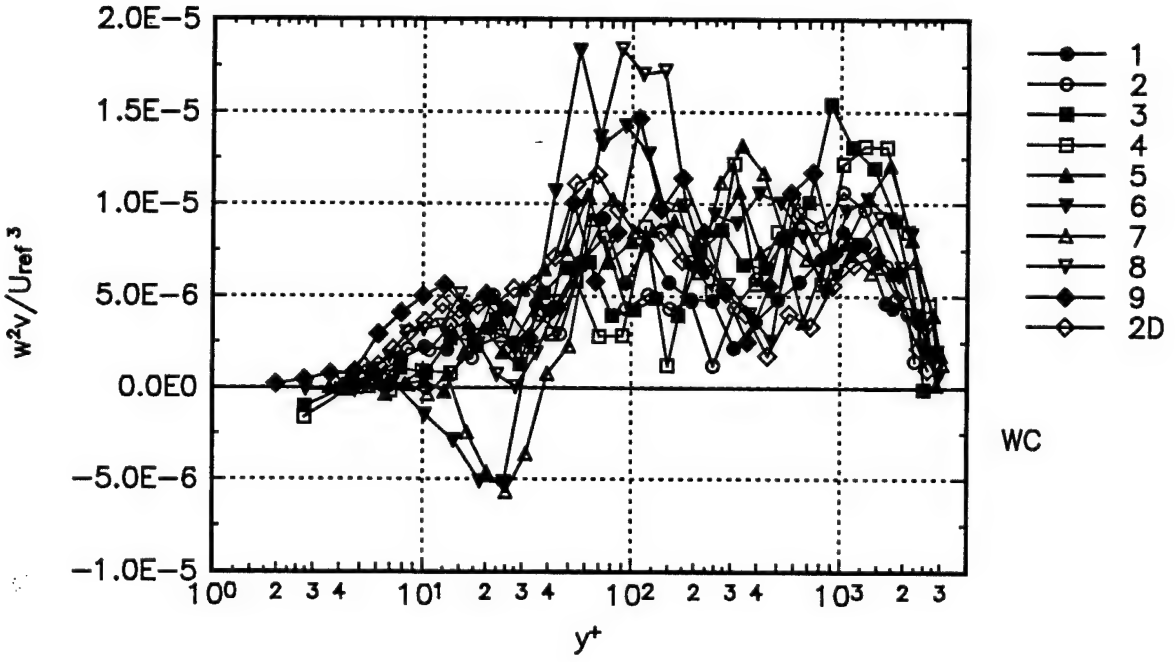
2.0E−5
1.5E−5
1.0E−5
5.0E−6
0.0E0
−5.0E−6
−1.0E−5
w^2v/U_{ref}^3
10^0 2 3 4 10^1 2 3 4 10^2 2 3 4 10^3 2 3
y^+
1
2
3
4
5
6
7
8
9
2D
WC

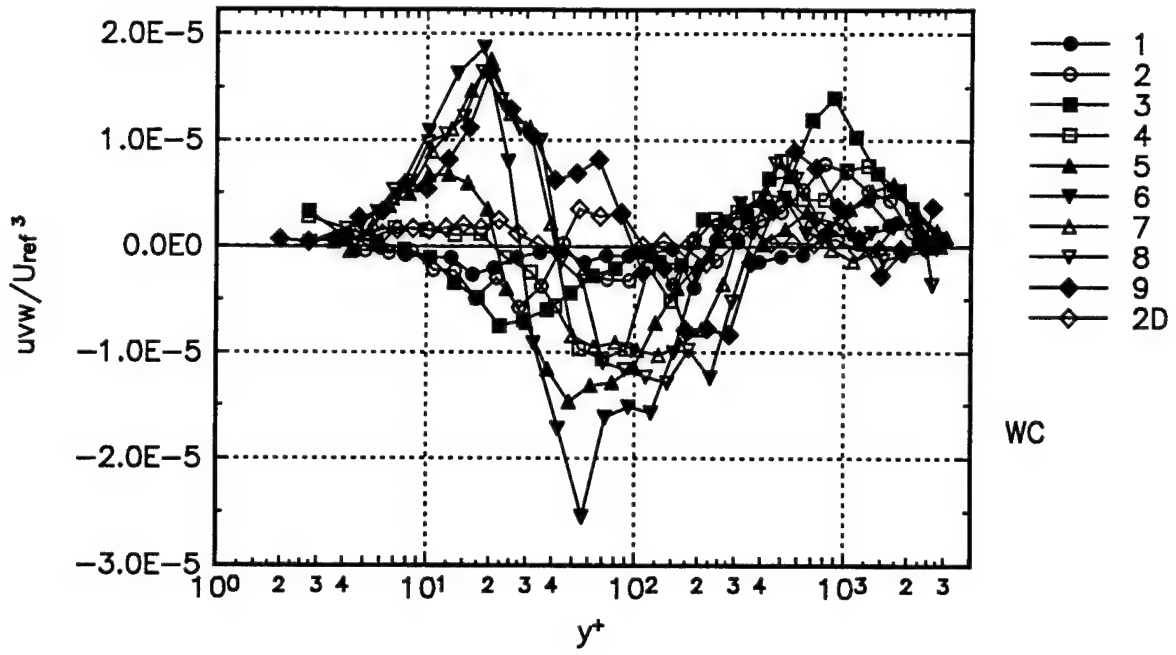
2.0E−5
1.0E−5
0.0E0
−1.0E−5
−2.0E−5
−3.0E−5
UVW/Uref 3
10^0 2 3 4 10^1 2 3 4 10^2 2 3 4 10^3 2 3
y+
1
2
3
4
5
6
7
8
9
2D
WC

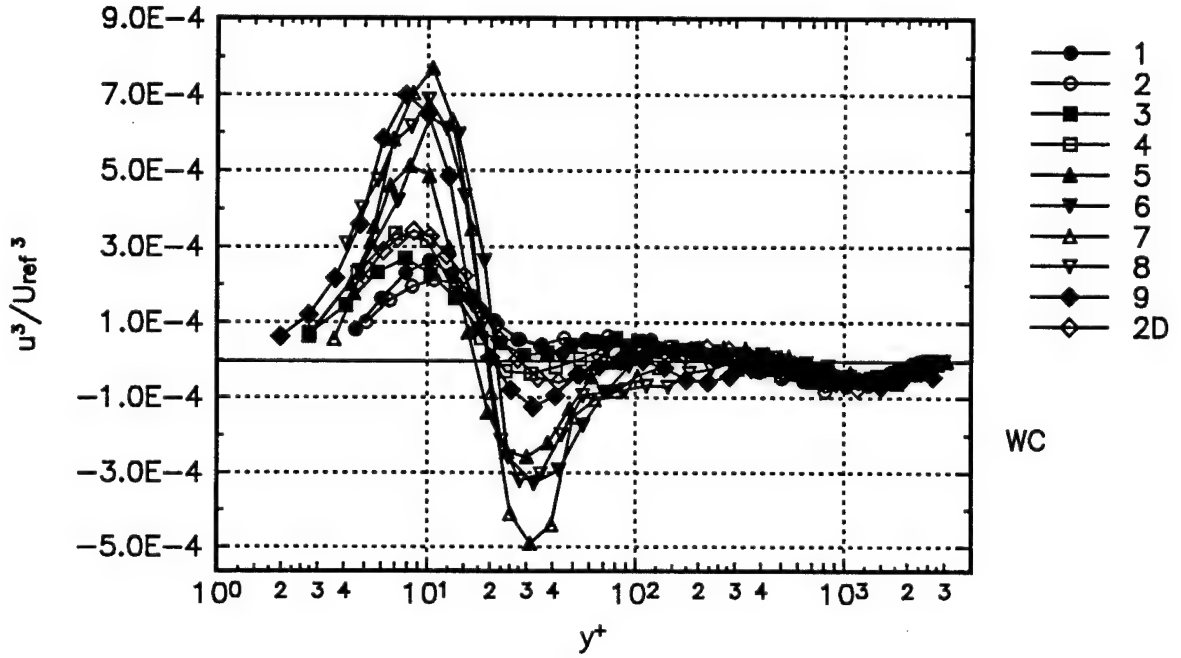
9.0E−4
7.0E−4
5.0E−4
3.0E−4
1.0E−4
−1.0E−4
−3.0E−4
−5.0E−4
u3/Uref 3
10^0 2 3 4 10^1 2 3 4 10^2 2 3 4 10^3 2 3
y+
1
2
3
4
5
6
7
8
9
2D
WC

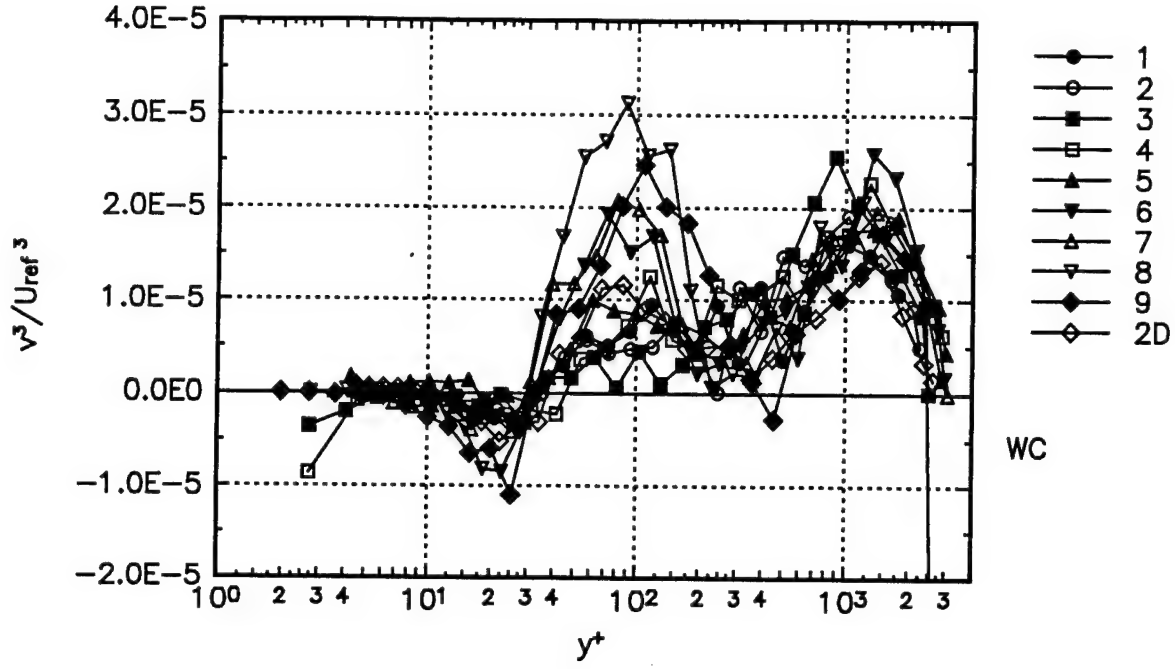
4.0E−5
3.0E−5
2.0E−5
1.0E−5
0.0E0
−1.0E−5
−2.0E−5
v³/Uref³
10⁰ 2 3 4 10¹ 2 3 4 10² 2 3 4 10³ 2 3
y+
1
2
3
4
5
6
7
8
9
2D
WC

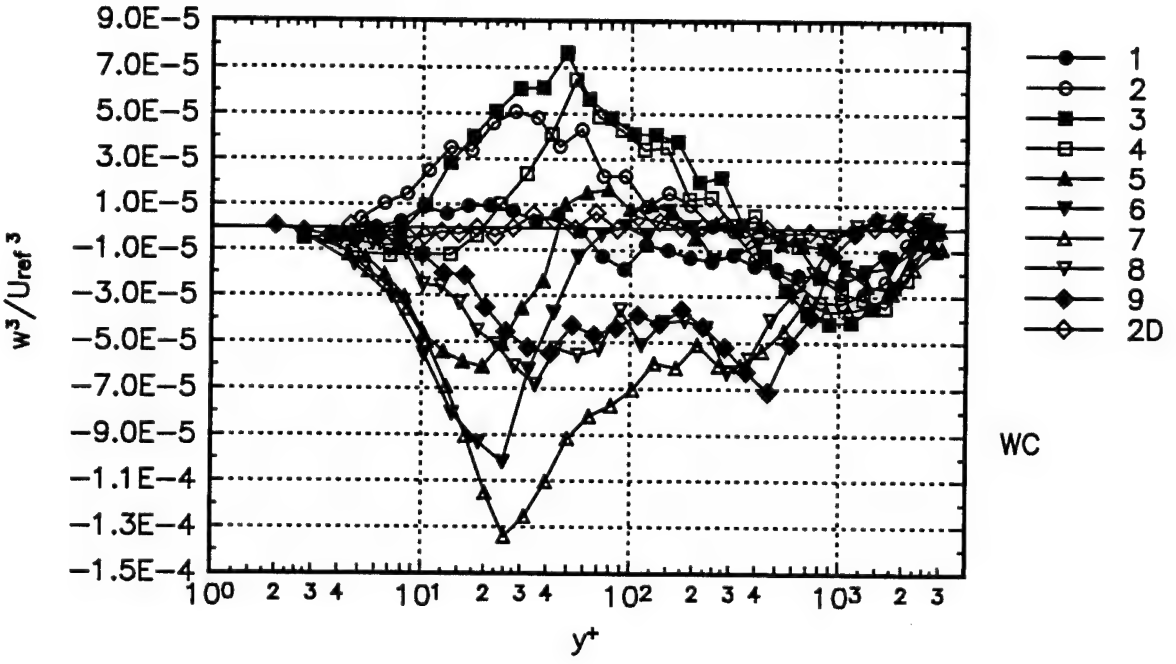
9.0E−5
7.0E−5
5.0E−5
3.0E−5
1.0E−5
−1.0E−5
−3.0E−5
−5.0E−5
−7.0E−5
−9.0E−5
−1.1E−4
−1.3E−4
−1.5E−4
w³/Uref³
10⁰ 2 3 4 10¹ 2 3 4 10² 2 3 4 10³ 2 3
y+
1
2
3
4
5
6
7
8
9
2D
WC

Figures in WALL coordinates. $\overline{u^2}$ normal stress transport velocities. The mean transport velocities are given by the following equations:

$U_{u^2}=\overline{u^3}/\overline{u^2}, V_{u^2}=\overline{u^2v}/\overline{u^2}, W_{u^2}=\overline{u^2w}/\overline{u^2}$

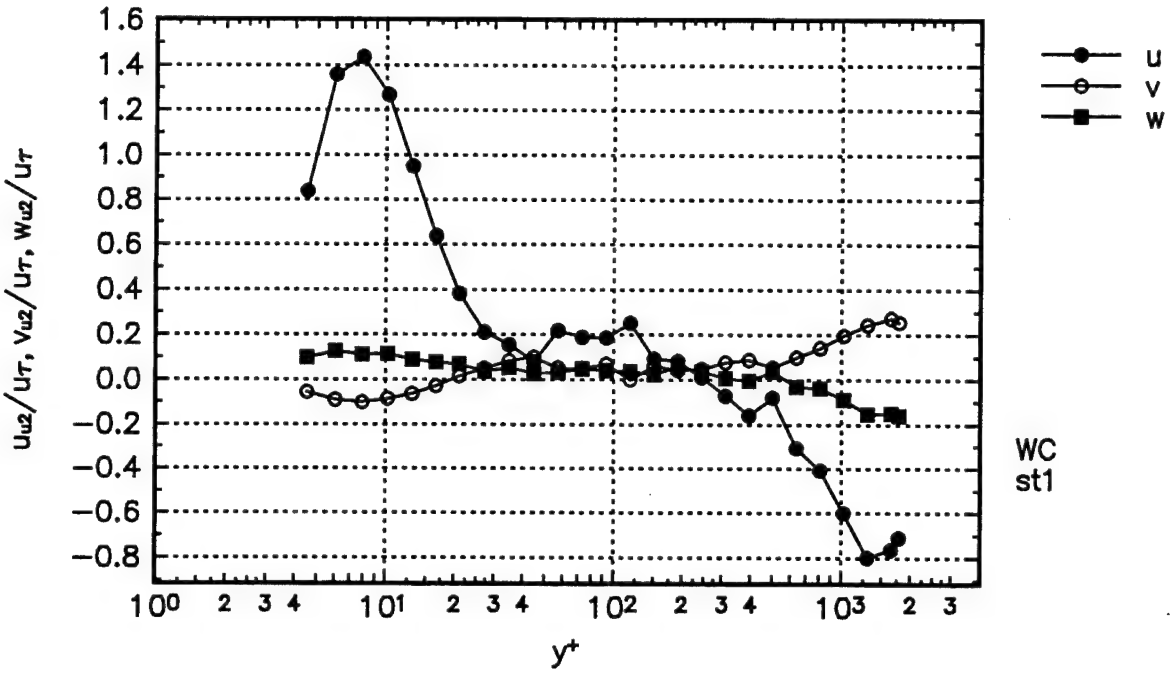

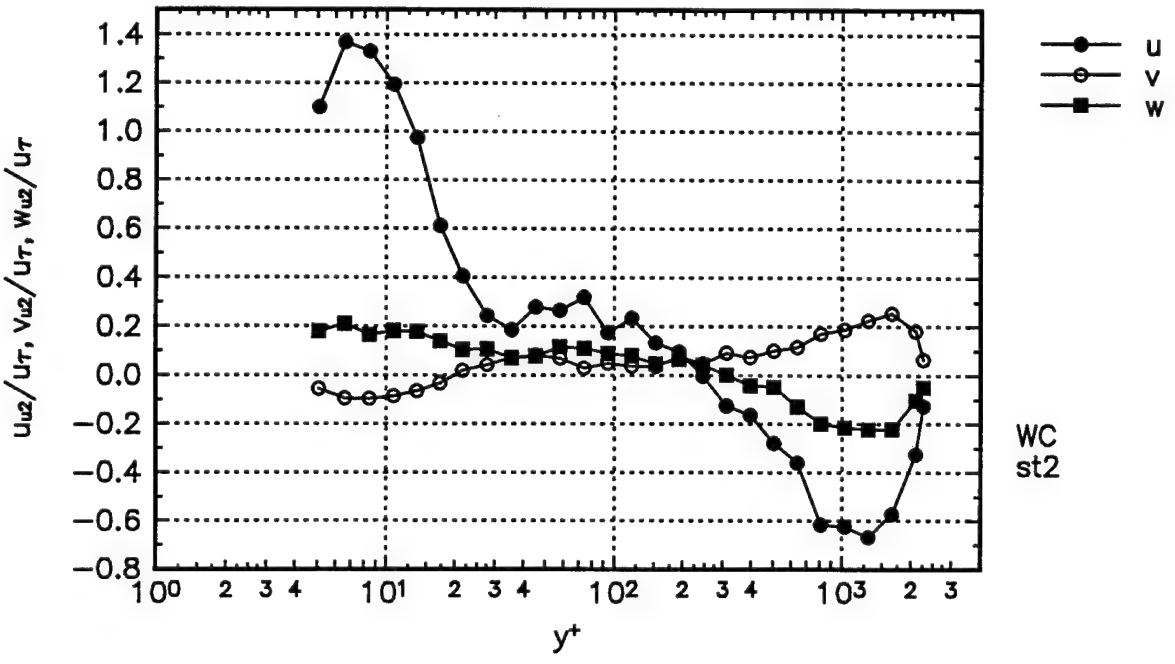

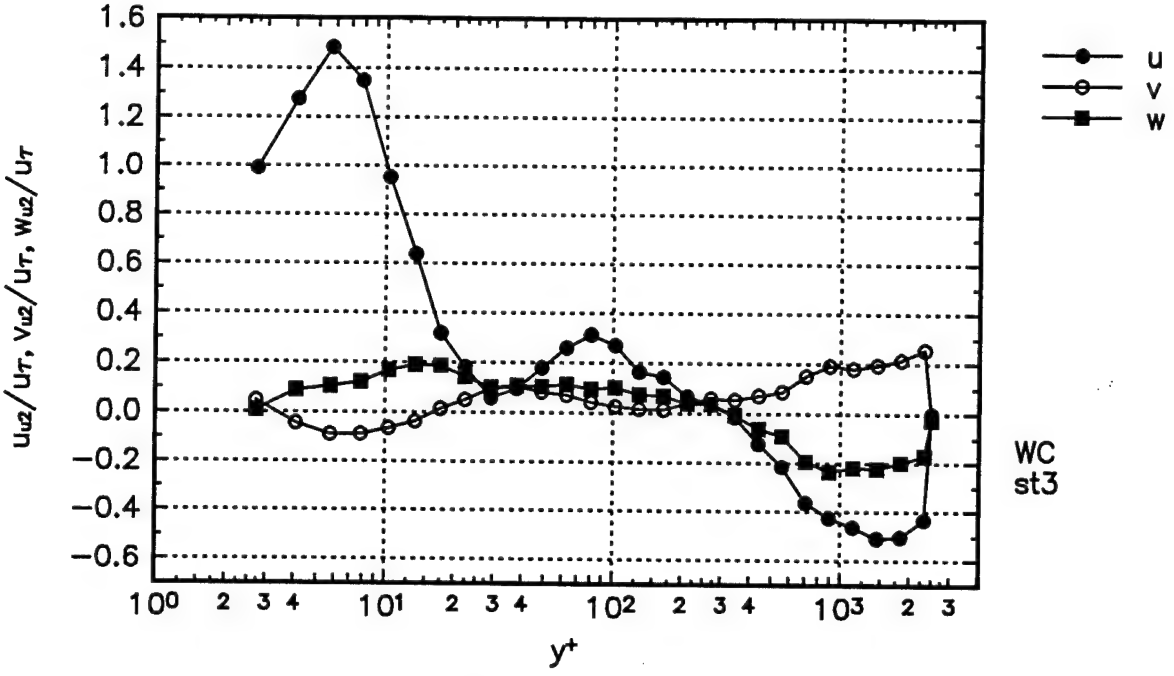
1.6
1.4
1.2
1.0
0.8
0.6
0.4
0.2
0.0
−0.2
−0.4
−0.6
$U_{\omega 2}/U_T$, $V_{\omega 2}/U_T$, $W_{\omega 2}/U_T$
10^0 2 3 4 10^1 2 3 4 10^2 2 3 4 10^3 2 3
y^+
u
v
w
WC
st3

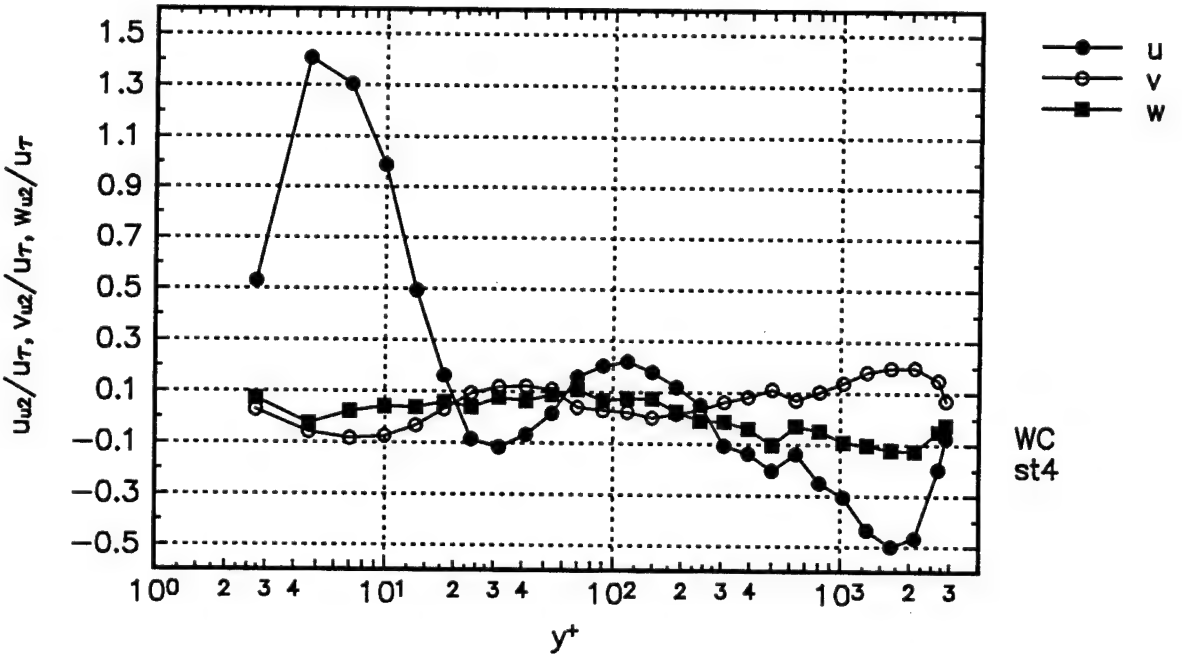
1.5
1.3
1.1
0.9
0.7
0.5
0.3
0.1
−0.1
−0.3
−0.5
$U_{\omega 2}/U_T$, $V_{\omega 2}/U_T$, $W_{\omega 2}/U_T$
10^0 2 3 4 10^1 2 3 4 10^2 2 3 4 10^3 2 3
y^+
u
v
w
WC
st4

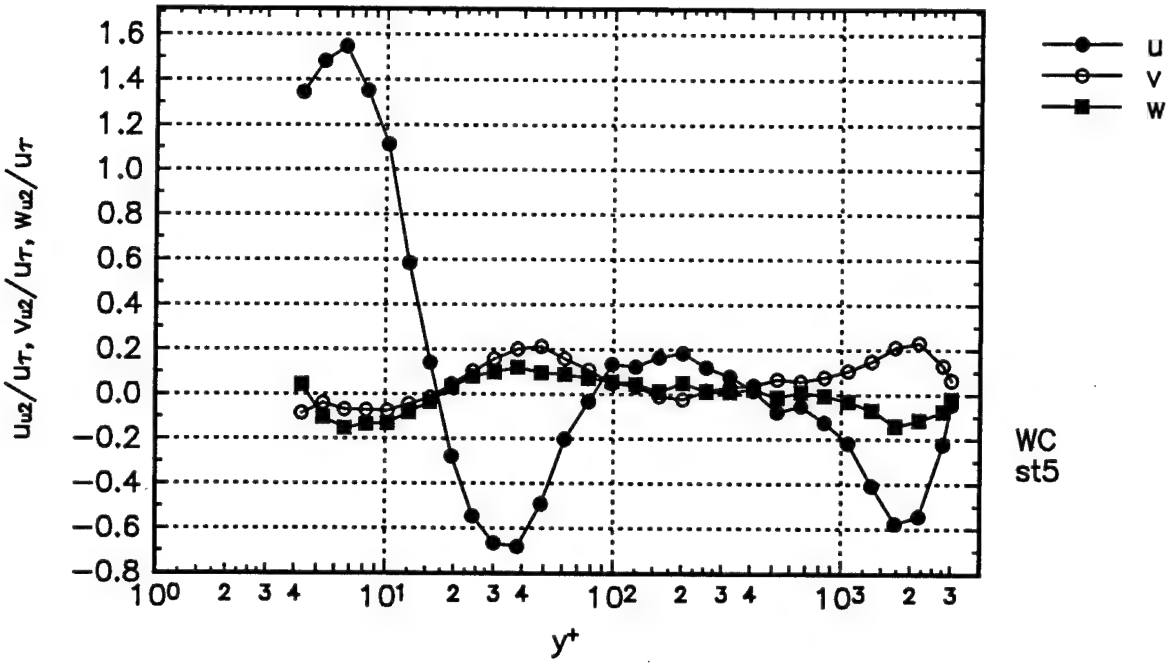
1.6
1.4
1.2
1.0
0.8
0.6
0.4
0.2
0.0
−0.2
−0.4
−0.6
−0.8
10^0 2 3 4 10^1 2 3 4 10^2 2 3 4 10^3 2 3
y^+
u_{u2}/u_τ, v_{u2}/u_τ, w_{u2}/u_τ
u
v
w
WC
st5

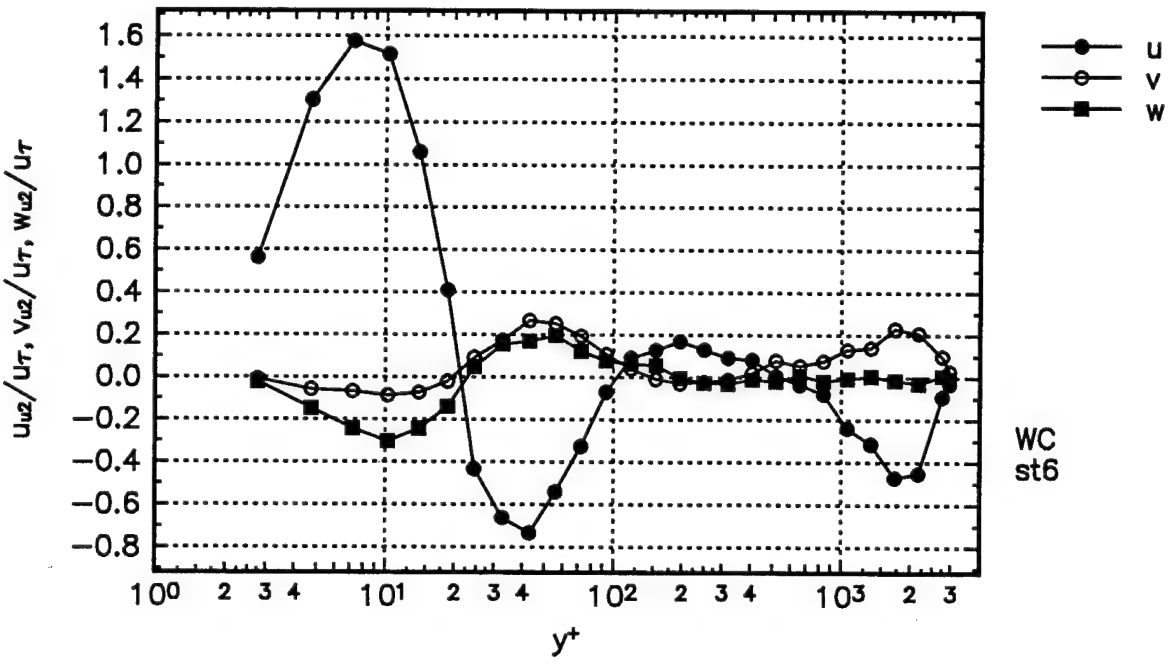
1.6
1.4
1.2
1.0
0.8
0.6
0.4
0.2
0.0
−0.2
−0.4
−0.6
−0.8
10^0 2 3 4 10^1 2 3 4 10^2 2 3 4 10^3 2 3
y^+
u_{u2}/u_τ, v_{u2}/u_τ, w_{u2}/u_τ
u
v
w
WC
st6

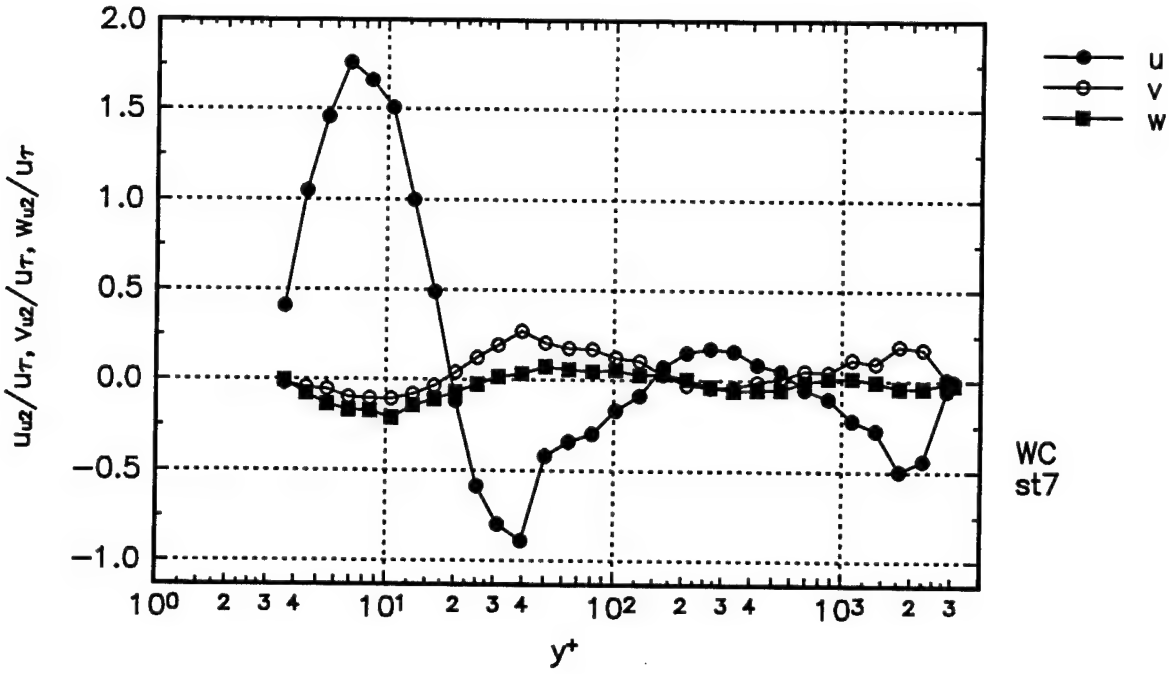
2.0
1.5
1.0
0.5
0.0
−0.5
−1.0
U_{w2}/U_T, V_{w2}/U_T, W_{w2}/U_T
10^0 2 3 4 10^1 2 3 4 10^2 2 3 4 10^3 2 3
y^+
u
v
w
WC
st7

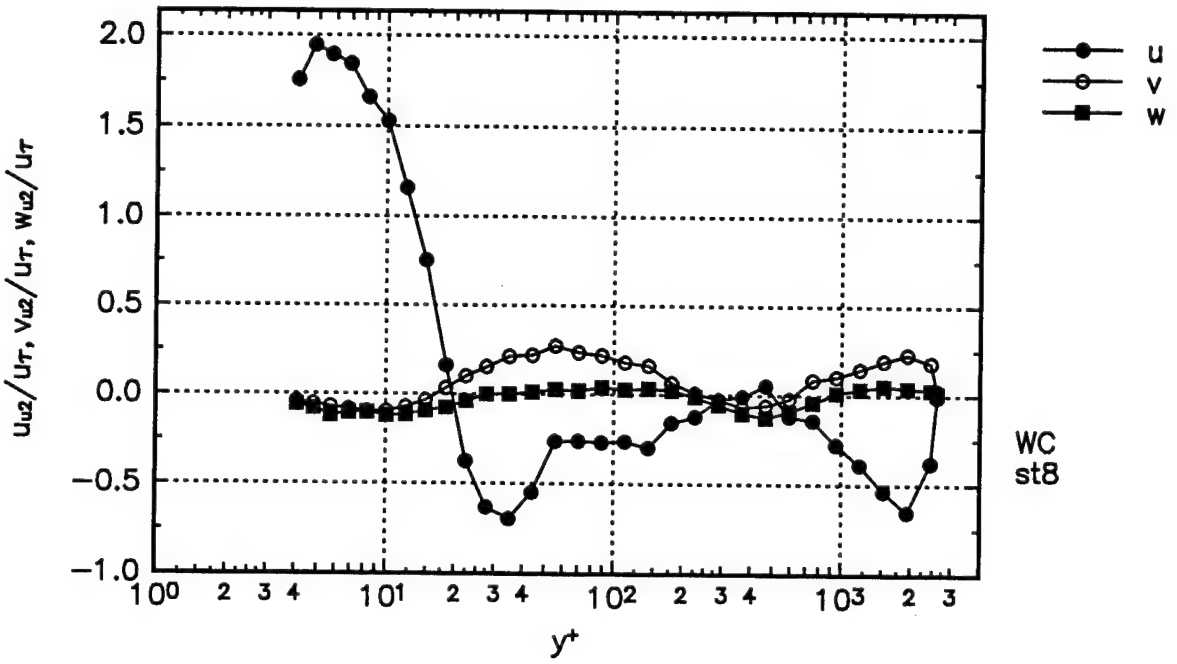
2.0
1.5
1.0
0.5
0.0
−0.5
−1.0
U_{w2}/U_T, V_{w2}/U_T, W_{w2}/U_T
10^0 2 3 4 10^1 2 3 4 10^2 2 3 4 10^3 2 3
y^+
u
v
w
WC
st8

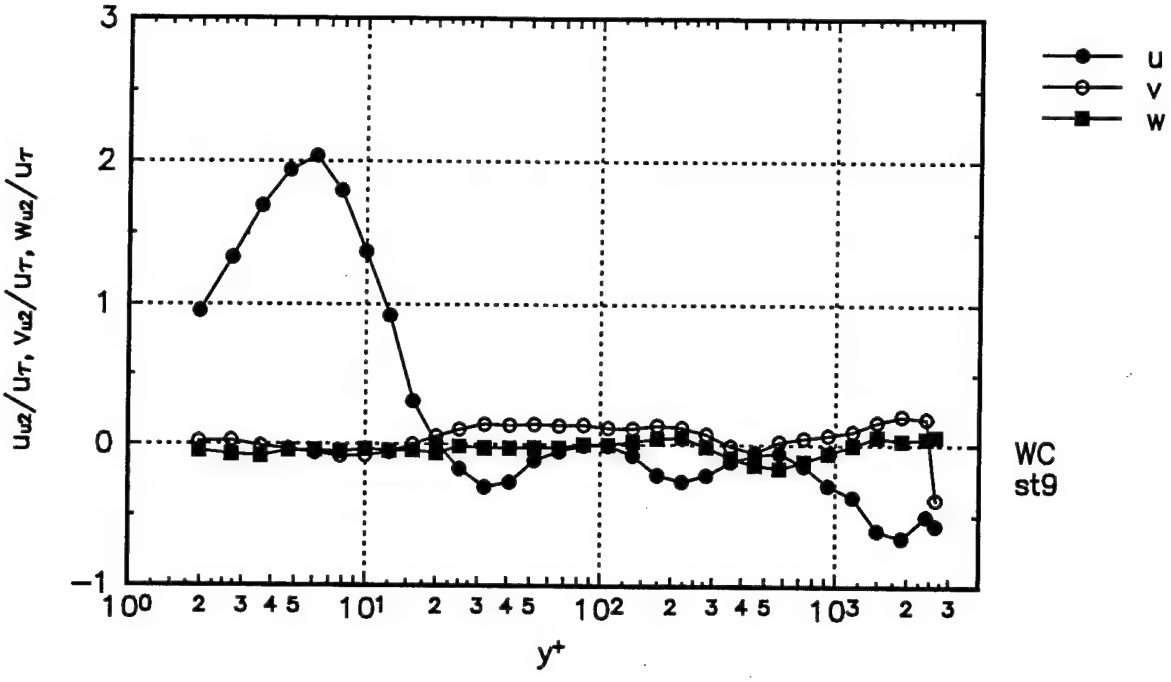
3
2
1
0
−1
$u_{\omega 2}/u_\tau$, $v_{\omega 2}/u_\tau$, $w_{\omega 2}/u_\tau$
10^0 2 3 4 5 10^1 2 3 4 5 10^2 2 3 4 5 10^3 2 3
y^+
u
v
w
WC
st9

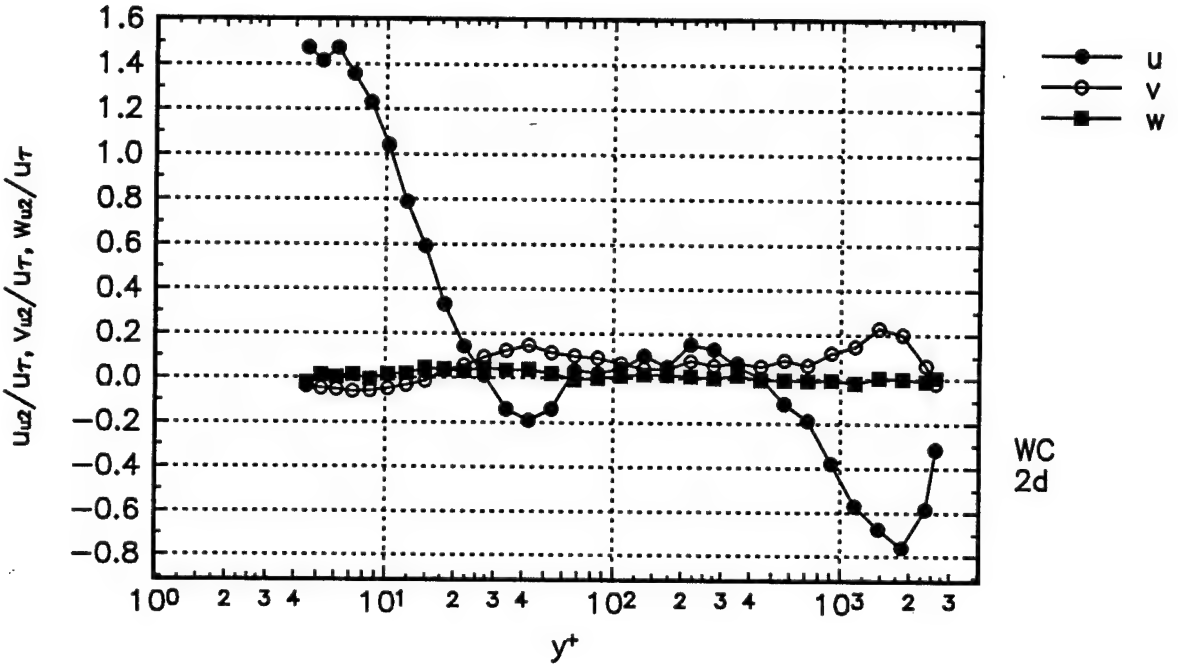
1.6
1.4
1.2
1.0
0.8
0.6
0.4
0.2
0.0
−0.2
−0.4
−0.6
−0.8
$u_{\omega 2}/u_\tau$, $v_{\omega 2}/u_\tau$, $w_{\omega 2}/u_\tau$
10^0 2 3 4 10^1 2 3 4 10^2 2 3 4 10^3 2 3
y^+
u
v
w
WC
2d

Figures in WALL coordinates. $\overline{v^2}$ normal stress transport velocities. The mean transport velocities are given by the following equations:

$U_{v^2} = \overline{uv^2}/\overline{v^2}$, $V_{v^2} = \overline{v^3}/\overline{v^2}$, $W_{v^2} = \overline{v^2 w}/\overline{v^2}$

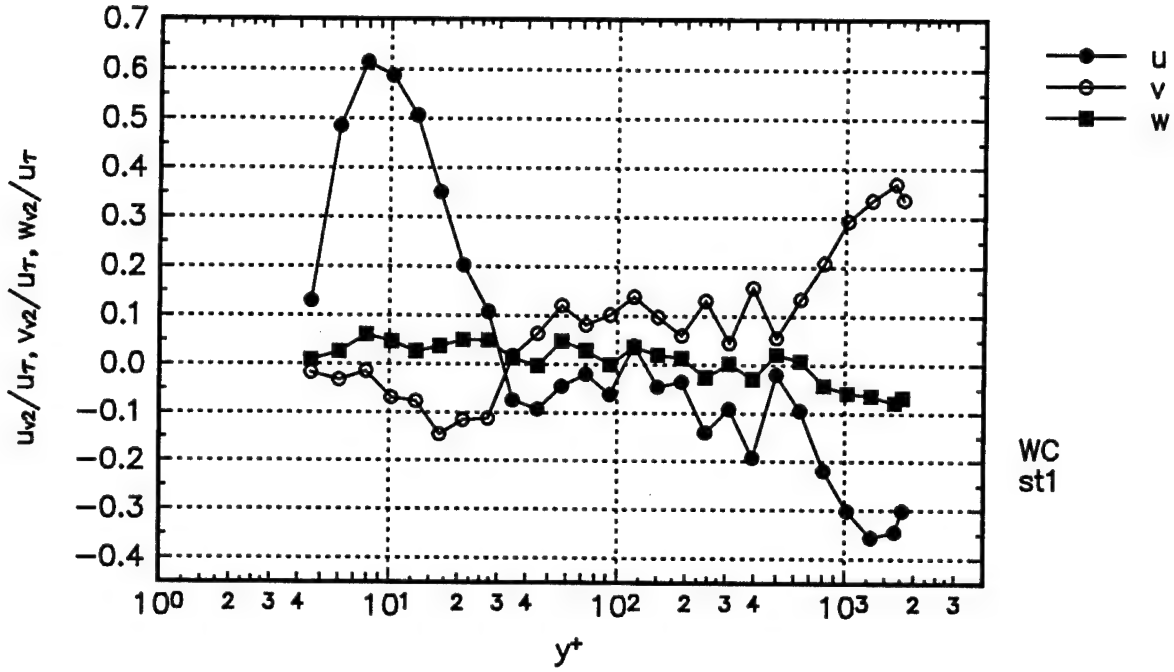

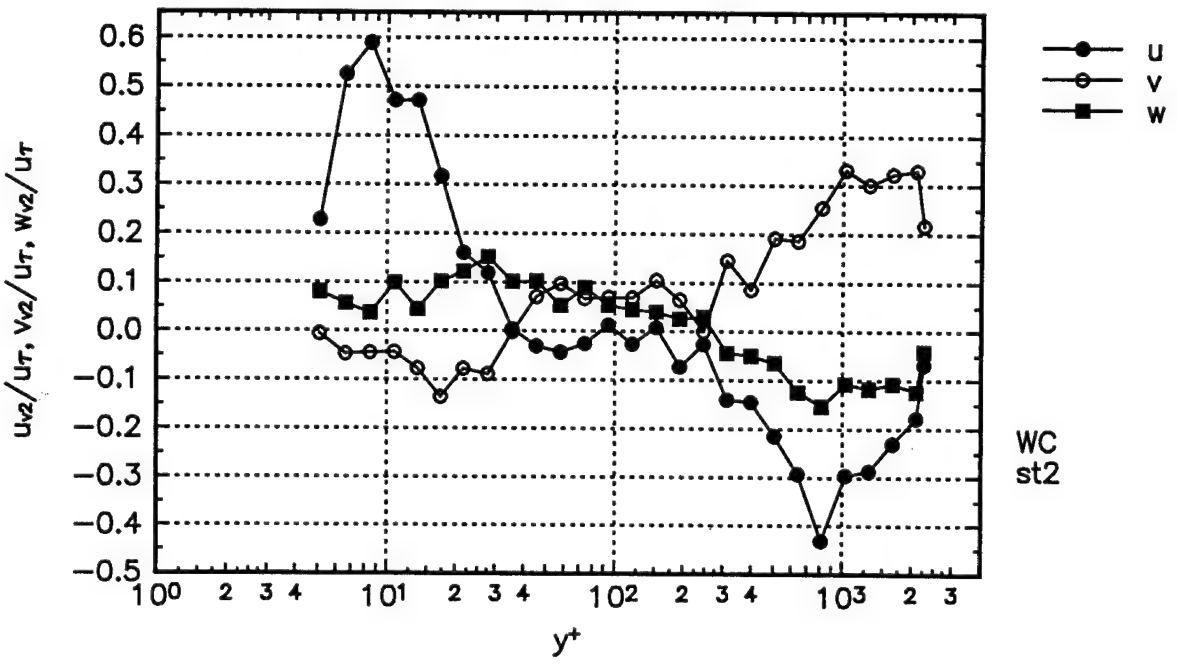

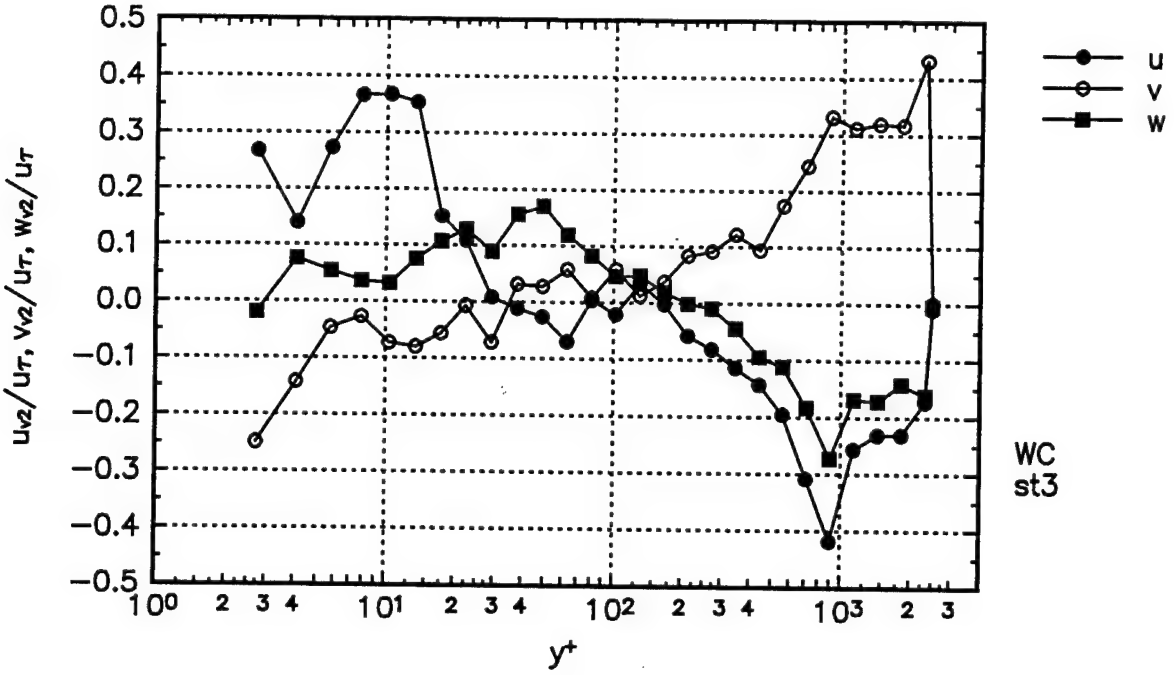
0.5
0.4
0.3
0.2
0.1
0.0
−0.1
−0.2
−0.3
−0.4
−0.5
10^0 2 3 4 10^1 2 3 4 10^2 2 3 4 10^3 2 3
y^+
u_{v2}/u_T, v_{v2}/u_T, w_{v2}/u_T
u
v
w
WC
st3

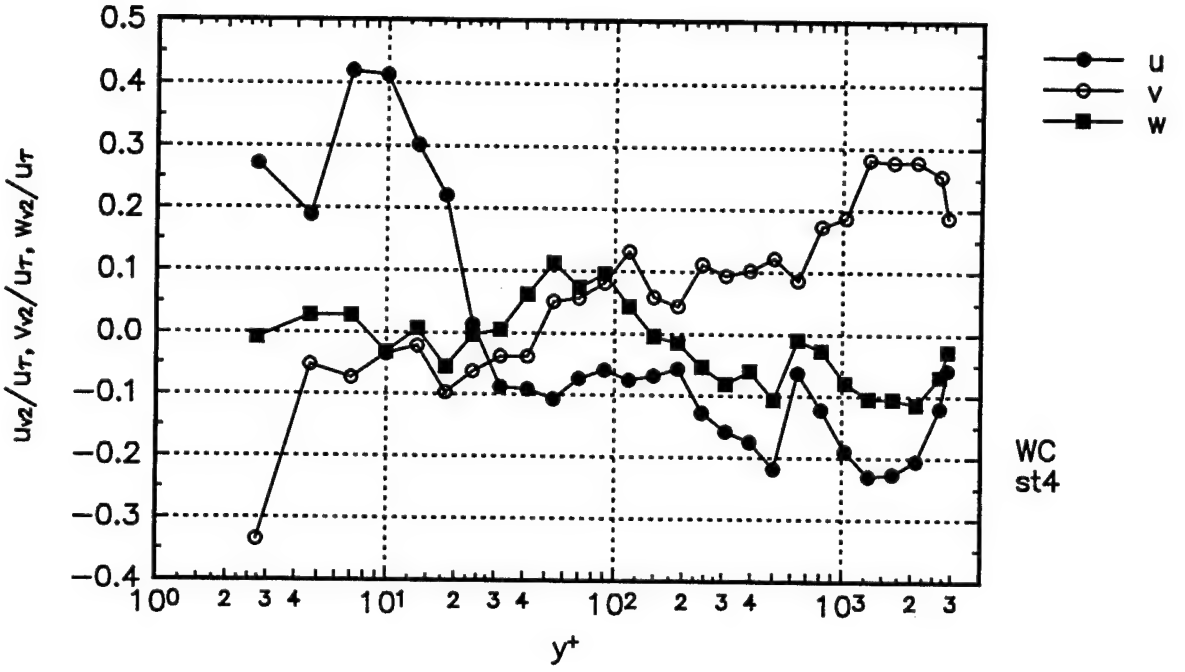
0.5
0.4
0.3
0.2
0.1
0.0
−0.1
−0.2
−0.3
−0.4
10^0 2 3 4 10^1 2 3 4 10^2 2 3 4 10^3 2 3
y^+
u_{v2}/u_T, v_{v2}/u_T, w_{v2}/u_T
u
v
w
WC
st4

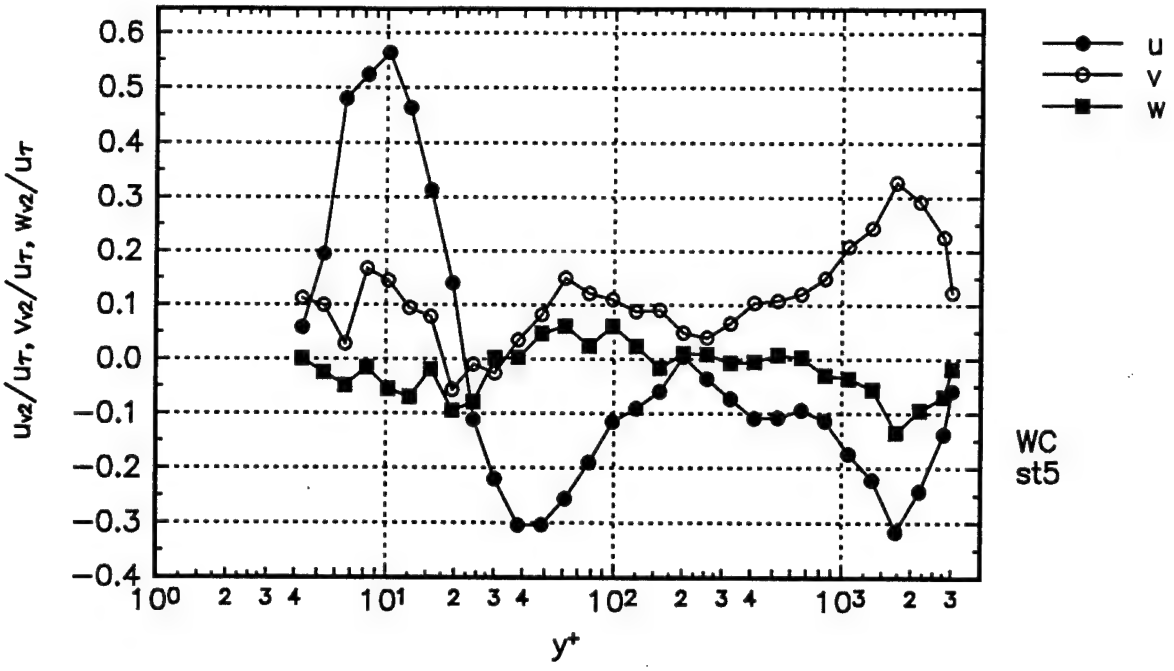
0.6
0.5
0.4
0.3
0.2
0.1
0.0
−0.1
−0.2
−0.3
−0.4
10^0 2 3 4 10^1 2 3 4 10^2 2 3 4 10^3 2 3
y^+
u_{v2}/u_τ, v_{v2}/u_τ, w_{v2}/u_τ
u
v
w
WC
st5

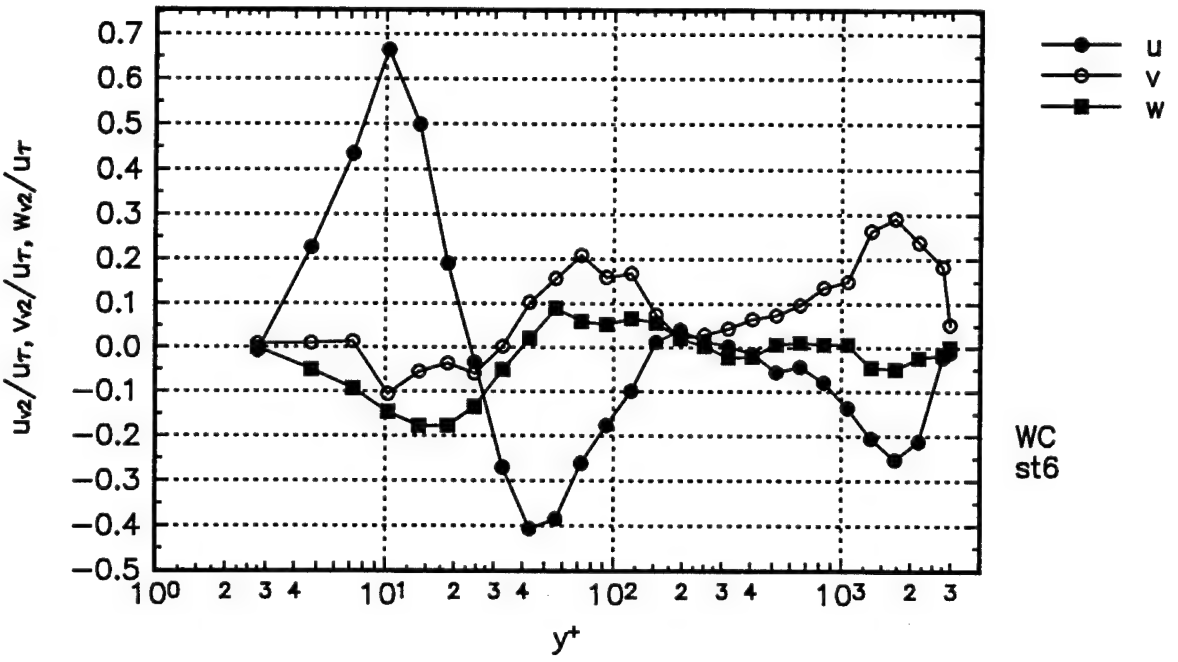
0.7
0.6
0.5
0.4
0.3
0.2
0.1
0.0
−0.1
−0.2
−0.3
−0.4
−0.5
10^0 2 3 4 10^1 2 3 4 10^2 2 3 4 10^3 2 3
y^+
u_{v2}/u_τ, v_{v2}/u_τ, w_{v2}/u_τ
u
v
w
WC
st6

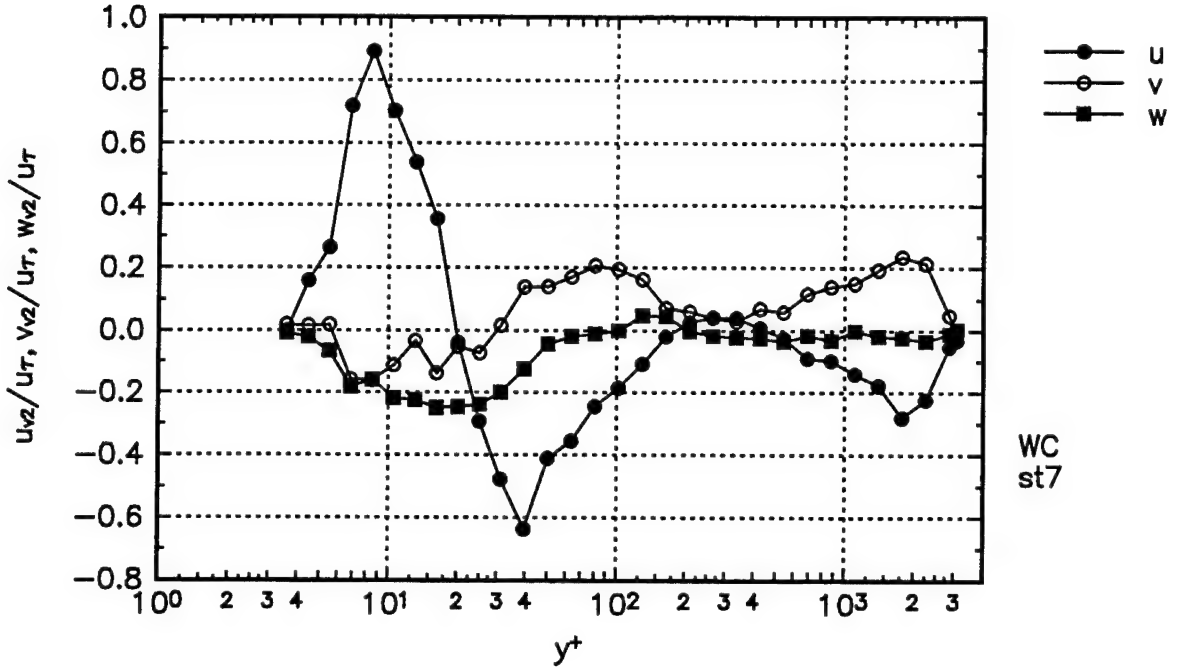
1.0
0.8
0.6
0.4
0.2
0.0
−0.2
−0.4
−0.6
−0.8
10^0 2 3 4 10^1 2 3 4 10^2 2 3 4 10^3 2 3
y^+
u_{v2}/u_τ, v_{v2}/u_τ, w_{v2}/u_τ
u
v
w
WC
st7

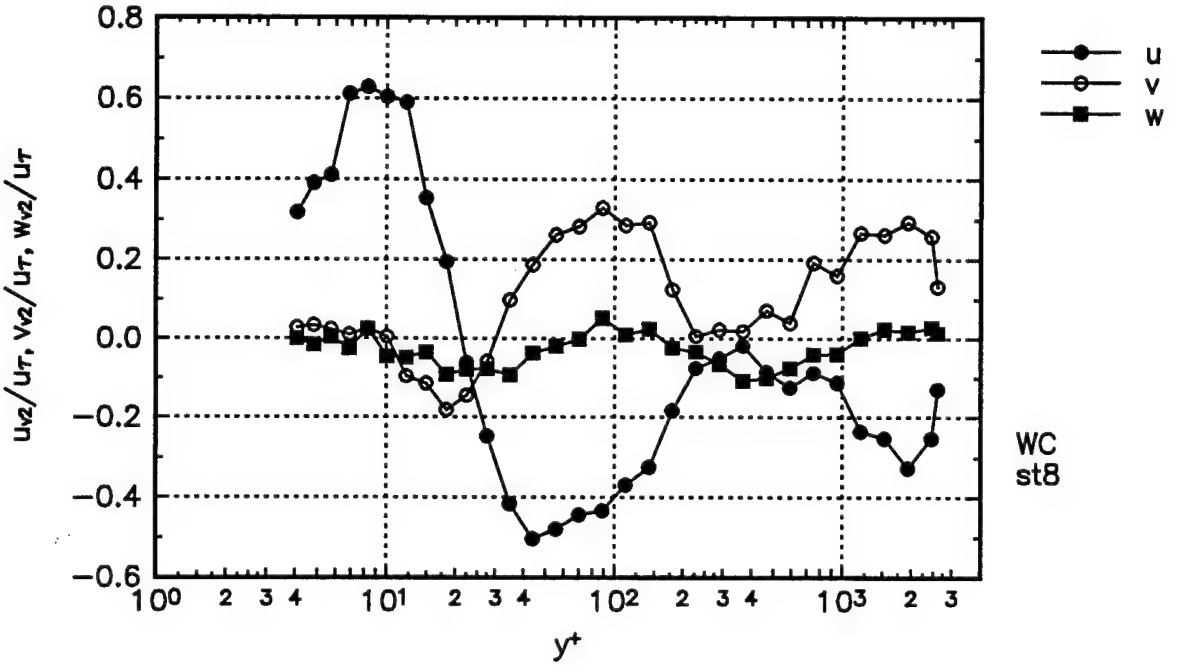
0.8
0.6
0.4
0.2
0.0
−0.2
−0.4
−0.6
10^0 2 3 4 10^1 2 3 4 10^2 2 3 4 10^3 2 3
y^+
u_{v2}/u_τ, v_{v2}/u_τ, w_{v2}/u_τ
u
v
w
WC
st8

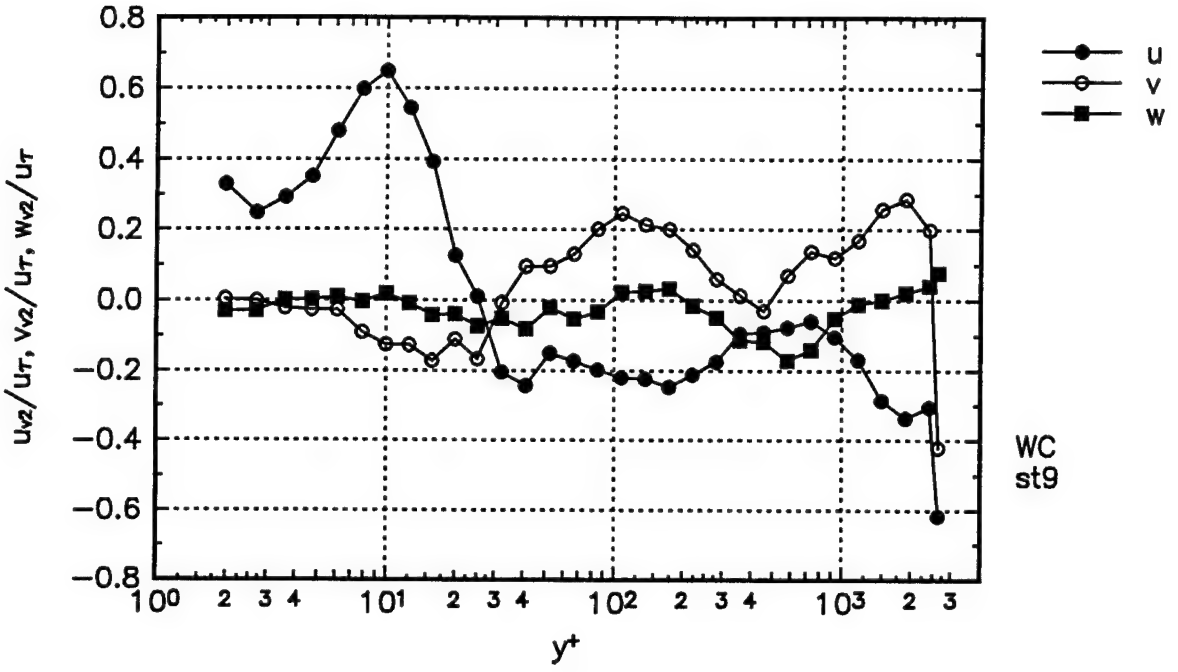
0.8
0.6
0.4
0.2
0.0
−0.2
−0.4
−0.6
−0.8
10^0 2 3 4 10^1 2 3 4 10^2 2 3 4 10^3 2 3
y^+
u_{v2}/u_τ, v_{v2}/u_τ, w_{v2}/u_τ
u
v
w
WC
st9

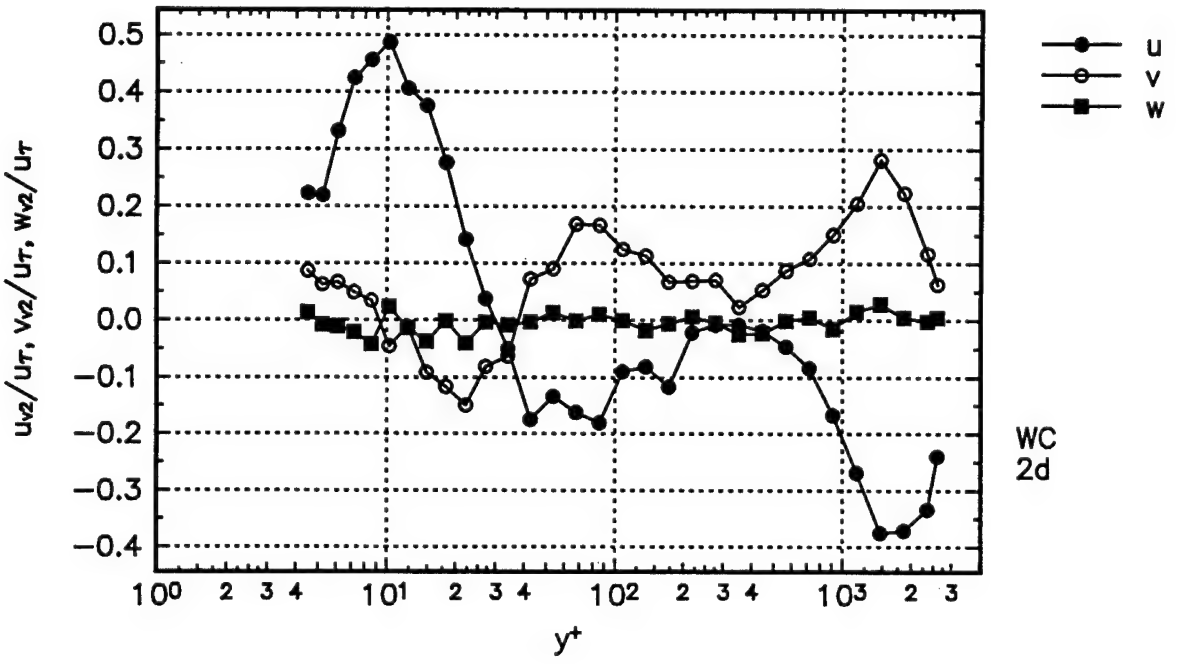
0.5
0.4
0.3
0.2
0.1
0.0
−0.1
−0.2
−0.3
−0.4
10^0 2 3 4 10^1 2 3 4 10^2 2 3 4 10^3 2 3
y^+
u_{v2}/u_τ, v_{v2}/u_τ, w_{v2}/u_τ
u
v
w
WC
2d

Figures in WALL coordinates. $\overline{w^2}$ normal stress transport velocities. The mean transport velocities are given by the following equations:

$U_{w^2} = \overline{uw^2}/\overline{w^2}$, $V_{w^2} = \overline{vw^2}/\overline{w^2}$, $W_{w^2} = \overline{w^3}/\overline{w^2}$

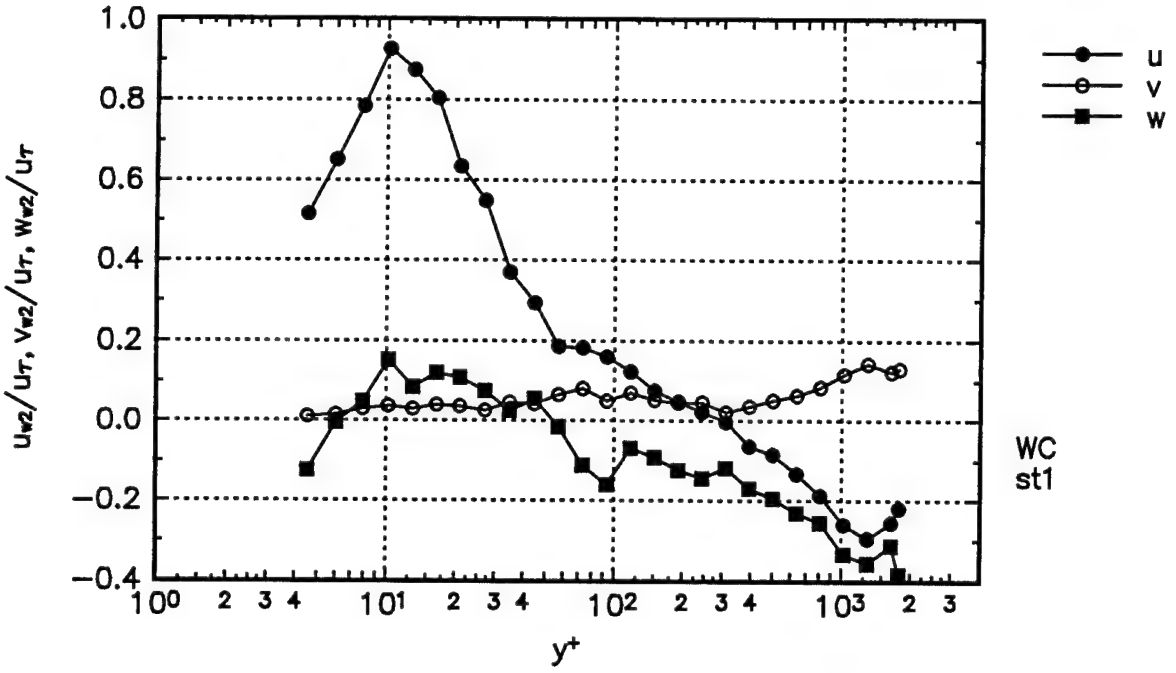

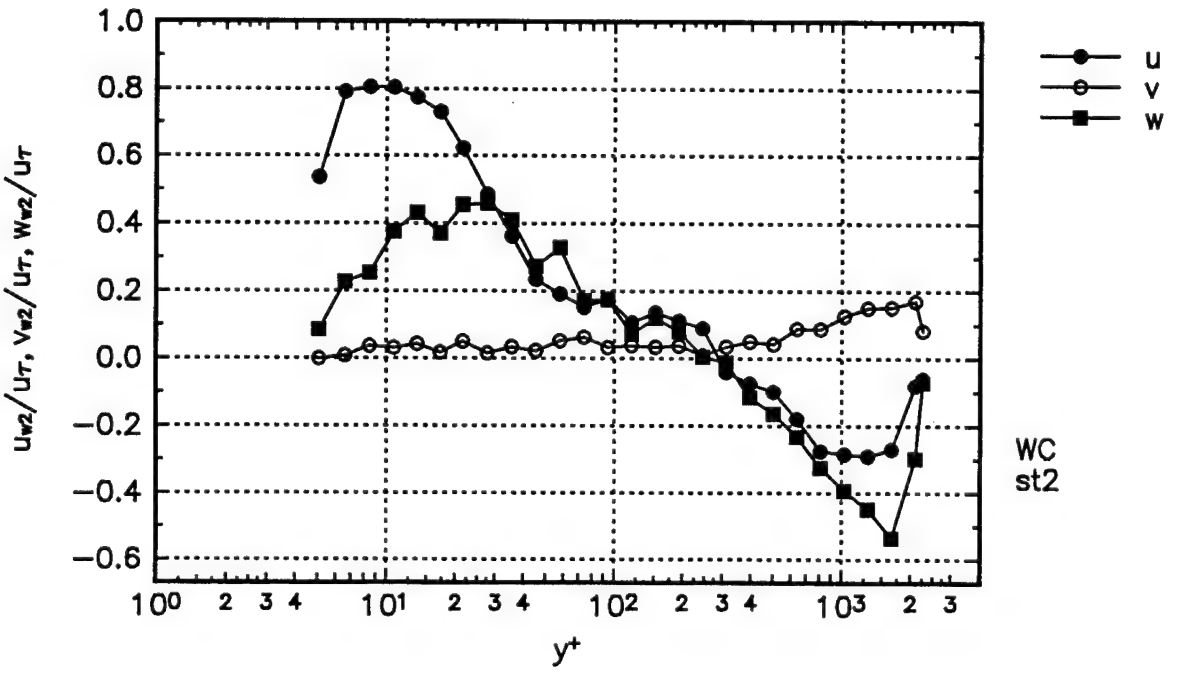

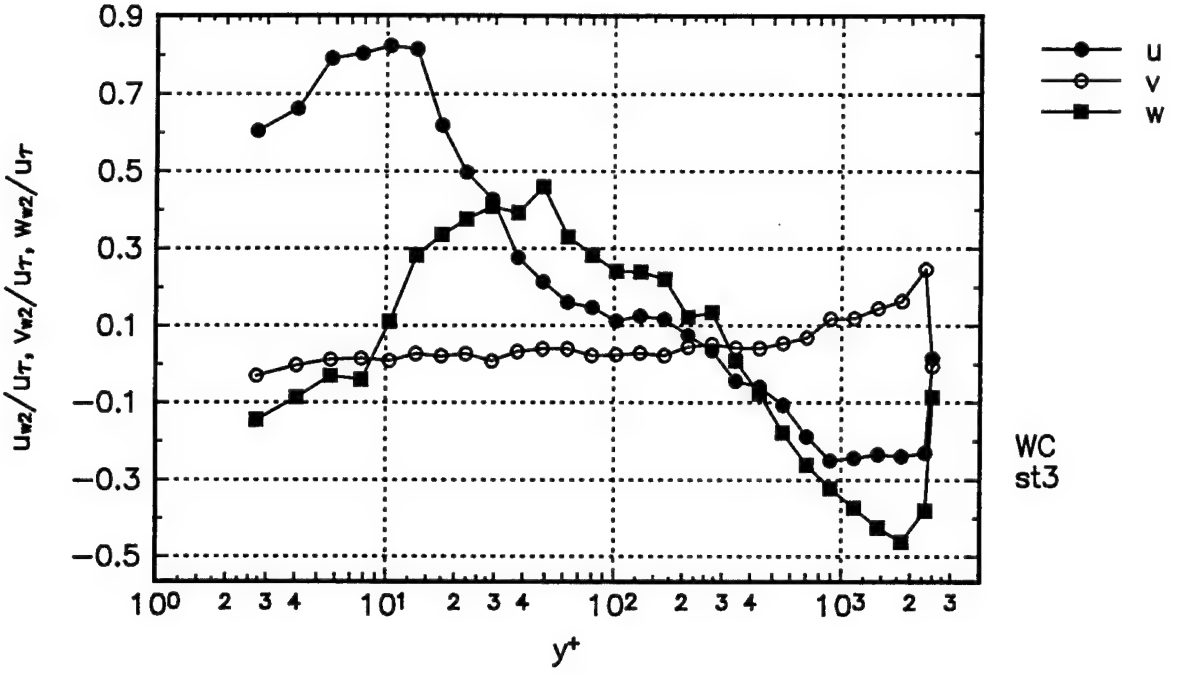
0.9
0.7
0.5
0.3
0.1
−0.1
−0.3
−0.5
10^0 2 3 4 10^1 2 3 4 10^2 2 3 4 10^3 2 3
y^+
u_{w2}/u_τ, v_{w2}/u_τ, w_{w2}/u_τ
u
v
w
WC
st3

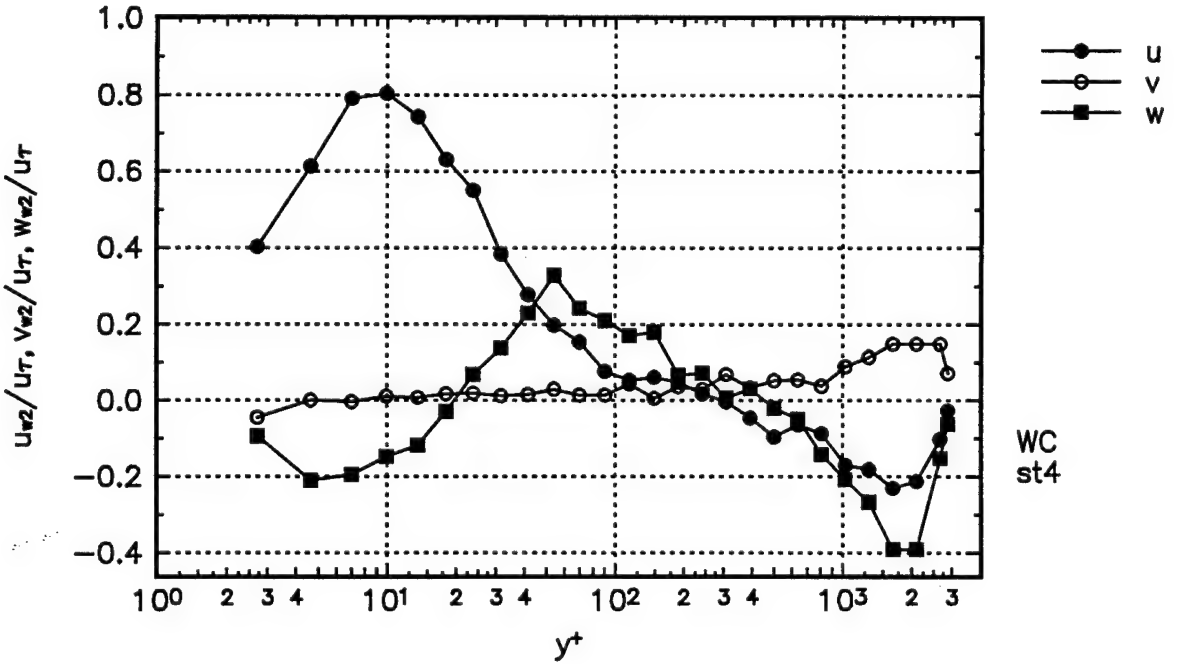
1.0
0.8
0.6
0.4
0.2
0.0
−0.2
−0.4
10^0 2 3 4 10^1 2 3 4 10^2 2 3 4 10^3 2 3
y^+
u_{w2}/u_τ, v_{w2}/u_τ, w_{w2}/u_τ
u
v
w
WC
st4

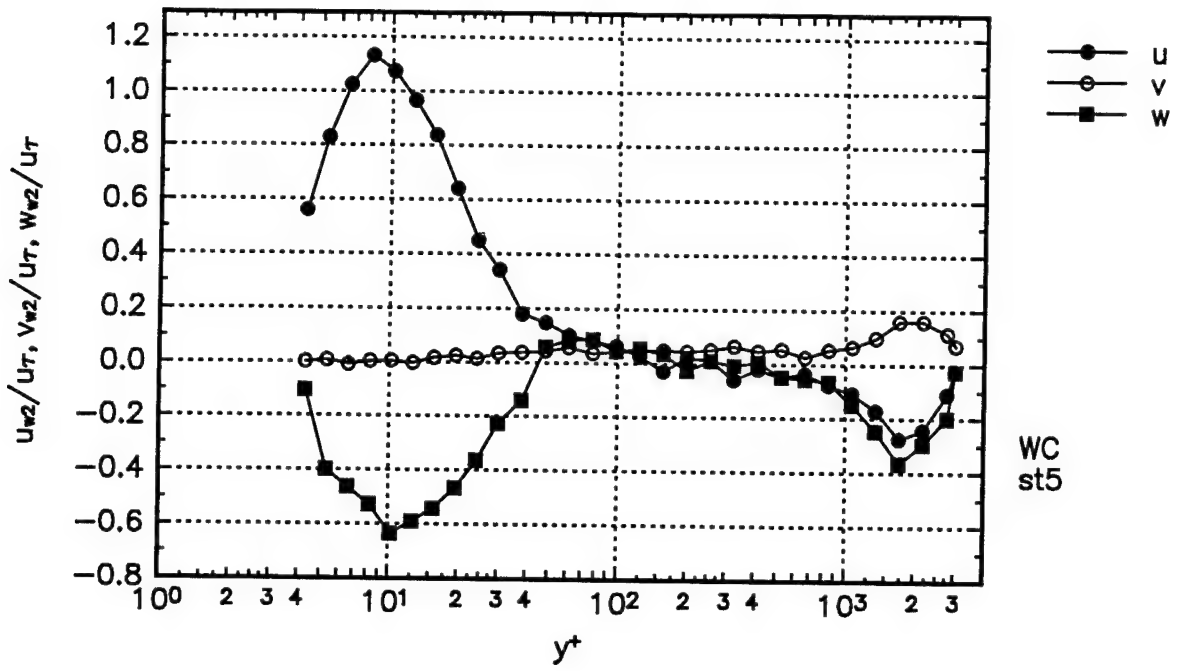
1.2
1.0
0.8
0.6
0.4
0.2
0.0
−0.2
−0.4
−0.6
−0.8
U_{w2}/U_T, V_{w2}/U_T, W_{w2}/U_T
10^0 2 3 4 10^1 2 3 4 10^2 2 3 4 10^3 2 3
y^+
u
v
w
WC
st5

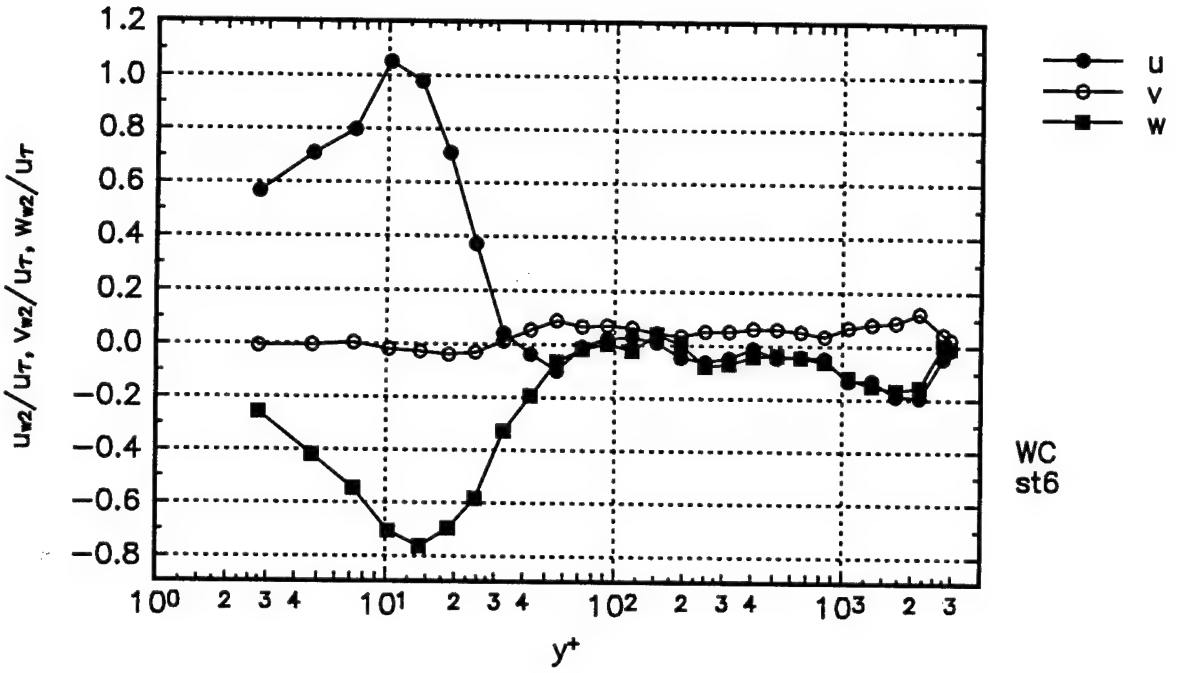
1.2
1.0
0.8
0.6
0.4
0.2
0.0
−0.2
−0.4
−0.6
−0.8
U_{w2}/U_T, V_{w2}/U_T, W_{w2}/U_T
10^0 2 3 4 10^1 2 3 4 10^2 2 3 4 10^3 2 3
y^+
u
v
w
WC
st6

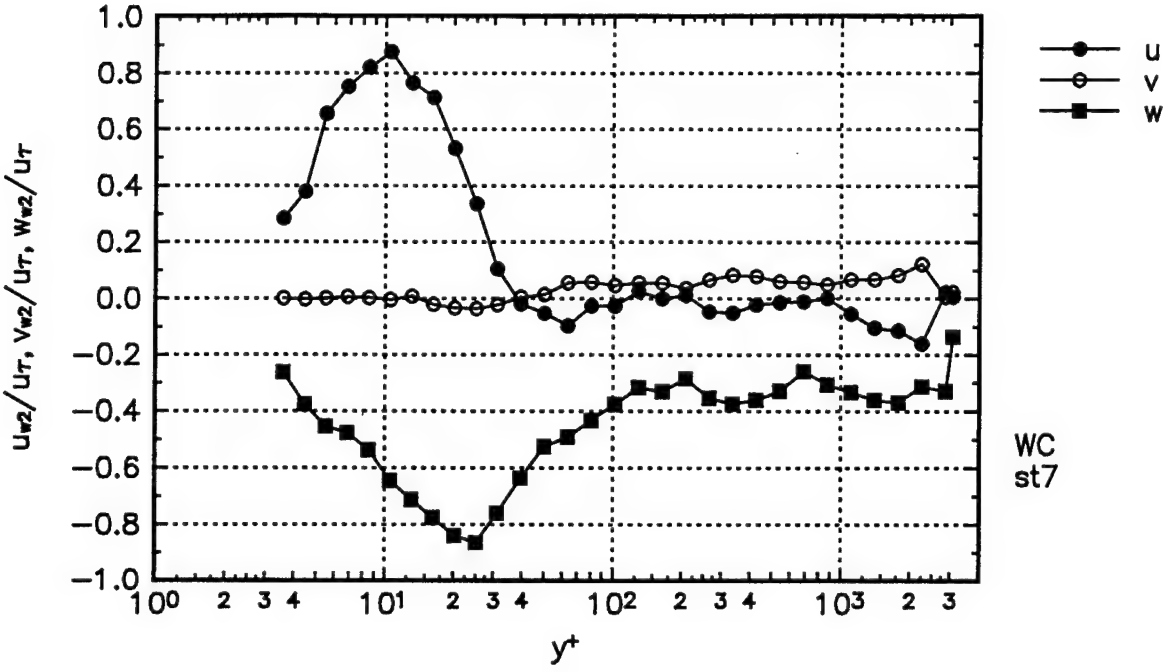
1.0
0.8
0.6
0.4
0.2
0.0
−0.2
−0.4
−0.6
−0.8
−1.0
U_{w2}/U_T, V_{w2}/U_T, W_{w2}/U_T
10^0 2 3 4 10^1 2 3 4 10^2 2 3 4 10^3 2 3
y^+
u
v
w
WC
st7

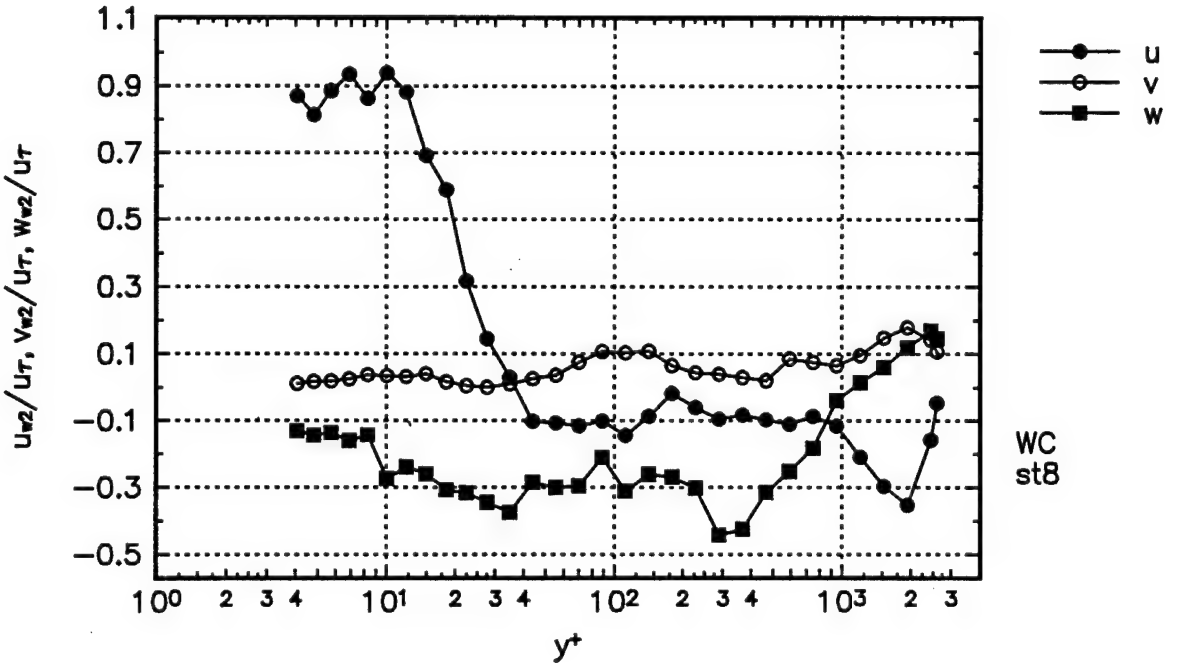
1.1
0.9
0.7
0.5
0.3
0.1
−0.1
−0.3
−0.5
U_{w2}/U_T, V_{w2}/U_T, W_{w2}/U_T
10^0 2 3 4 10^1 2 3 4 10^2 2 3 4 10^3 2 3
y^+
u
v
w
WC
st8

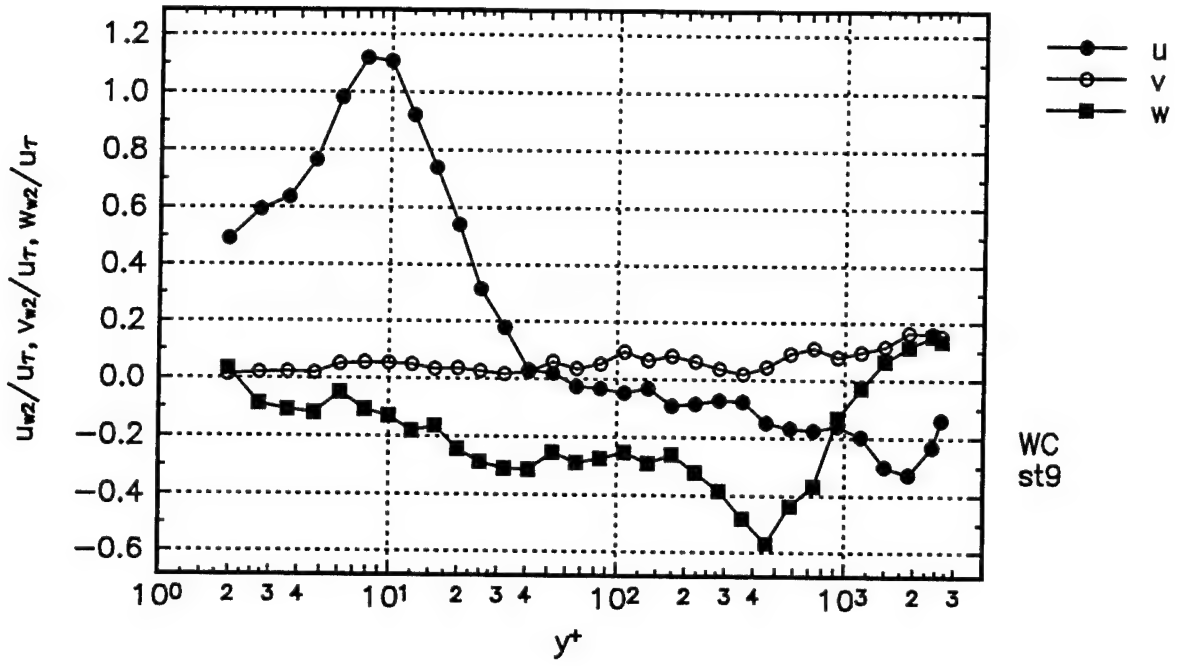
1.2
1.0
0.8
0.6
0.4
0.2
0.0
−0.2
−0.4
−0.6
u_{w2}/u_τ, v_{w2}/u_τ, w_{w2}/u_τ
10^0 2 3 4 10^1 2 3 4 10^2 2 3 4 10^3 2 3
y^+
u
v
w
WC
st9

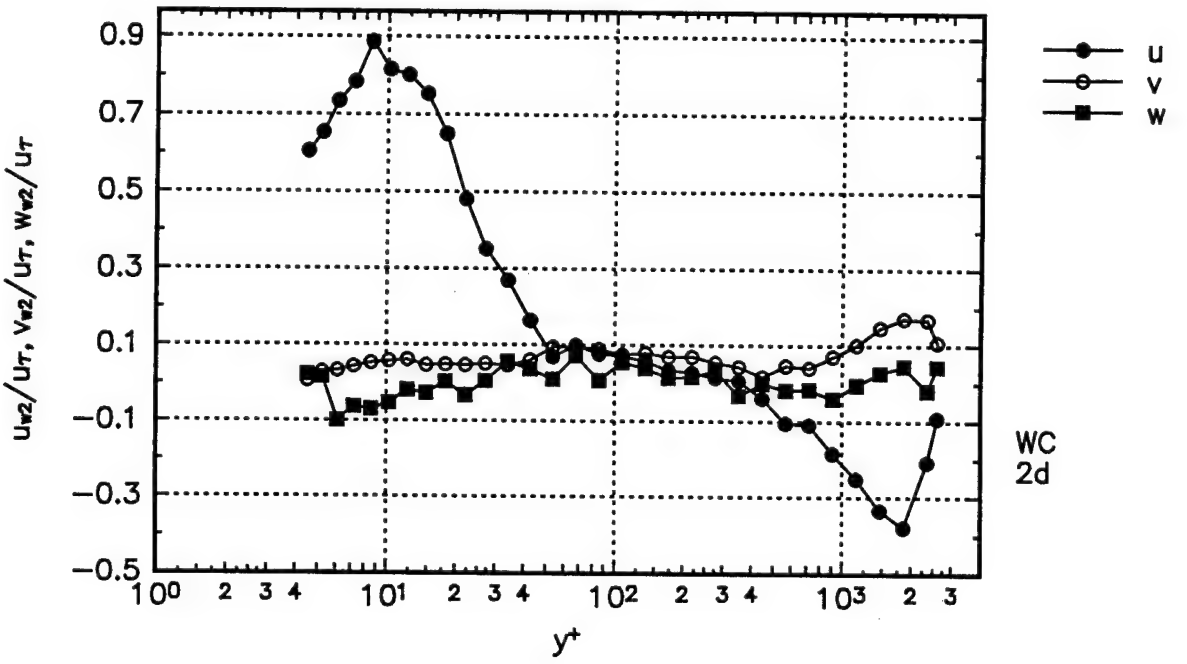
0.9
0.7
0.5
0.3
0.1
−0.1
−0.3
−0.5
u_{w2}/u_τ, v_{w2}/u_τ, w_{w2}/u_τ
10^0 2 3 4 10^1 2 3 4 10^2 2 3 4 10^3 2 3
y^+
u
v
w
WC
2d

Figure in WALL coordinates. $\overline{q^2}=\overline{u^2}+\overline{v^2}+\overline{w^2}$ transport velocities. The mean transport velocities are given by the following equations:

$$U_{q^2}=\overline{u^3}+\overline{uv^2}+\overline{uw^2}/\overline{u^2}+\overline{v^2}+\overline{w^2},\ V_{q^2}=\overline{u^2v}+\overline{v^3}+\overline{vw^2}/\overline{u^2}+\overline{v^2}+\overline{w^2},\ W_{q^2}=\overline{u^2w}+\overline{v^2w}+\overline{w^3}/\overline{u^2}+\overline{v^2}+\overline{w^2}$$

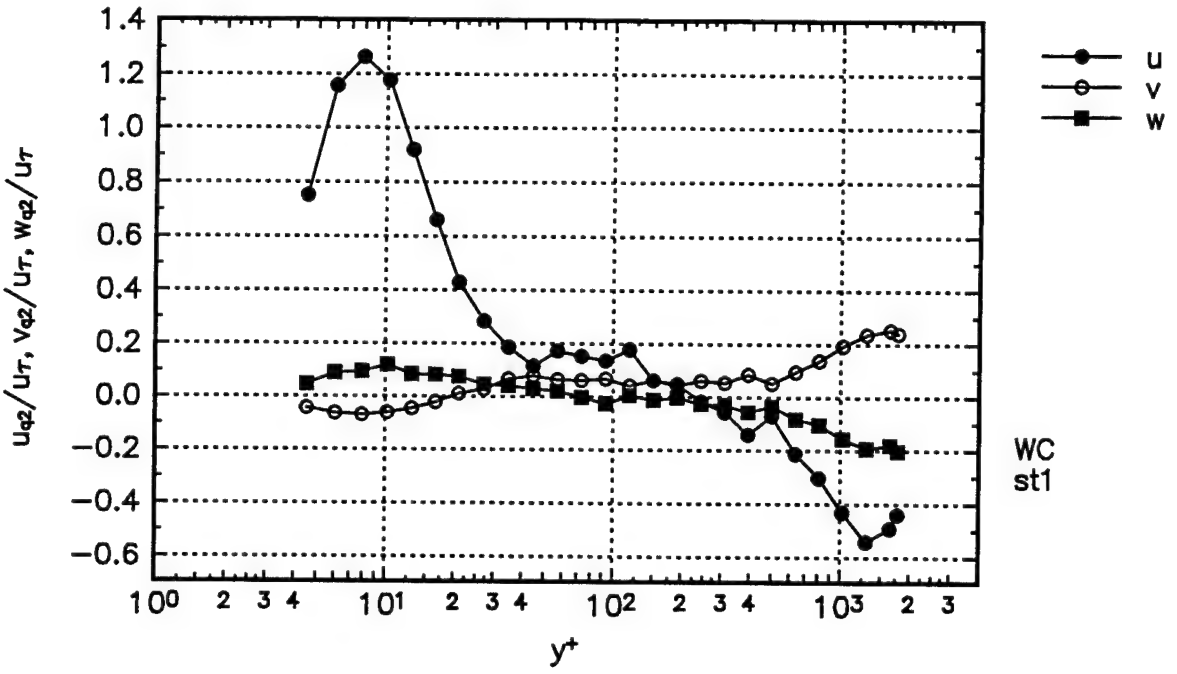

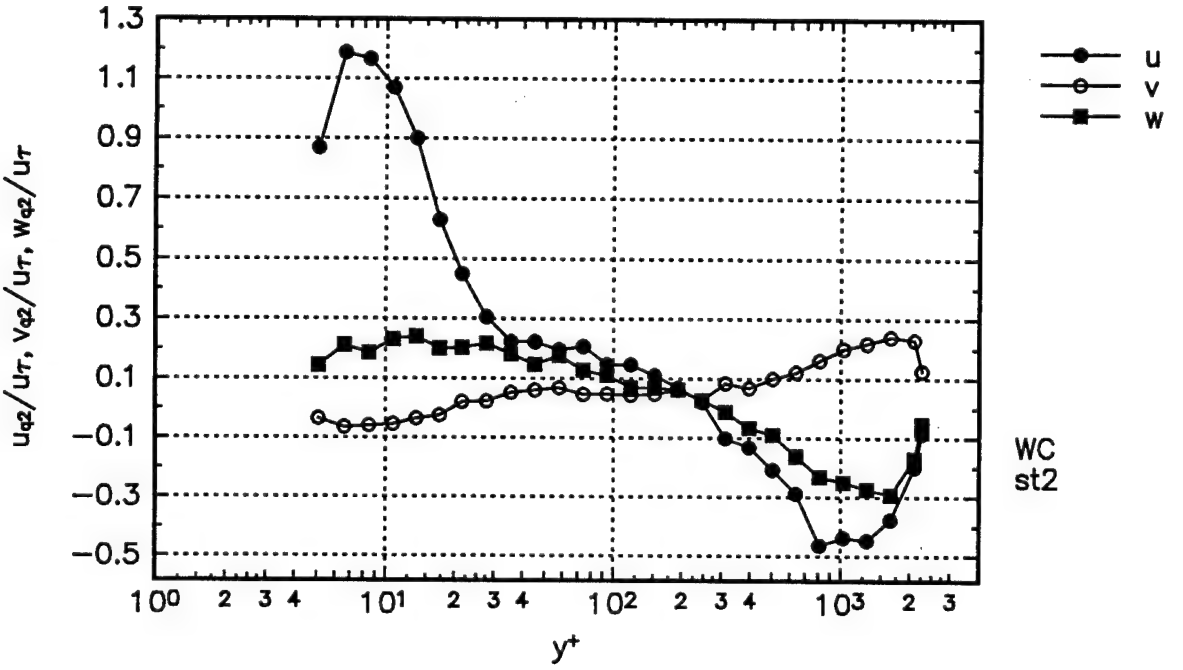

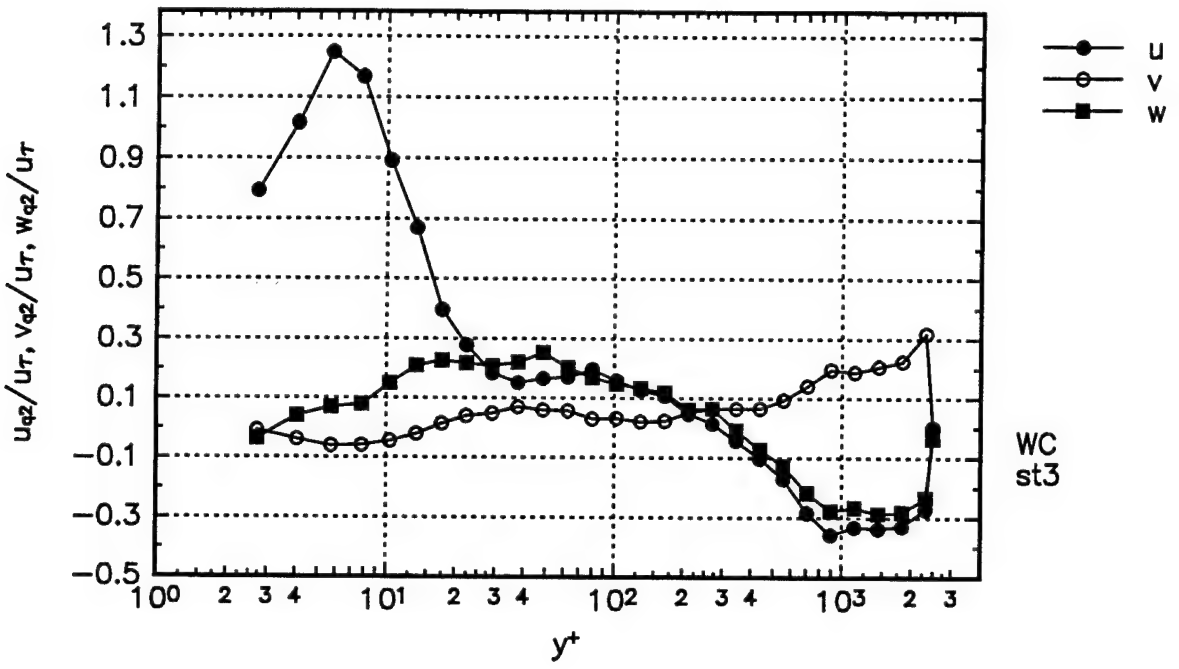
1.3
1.1
0.9
0.7
0.5
0.3
0.1
−0.1
−0.3
−0.5
u_{q2}/u_T, v_{q2}/u_T, w_{q2}/u_T
10^0 2 3 4 10^1 2 3 4 10^2 2 3 4 10^3 2 3
y^+
u
v
w
WC
st3

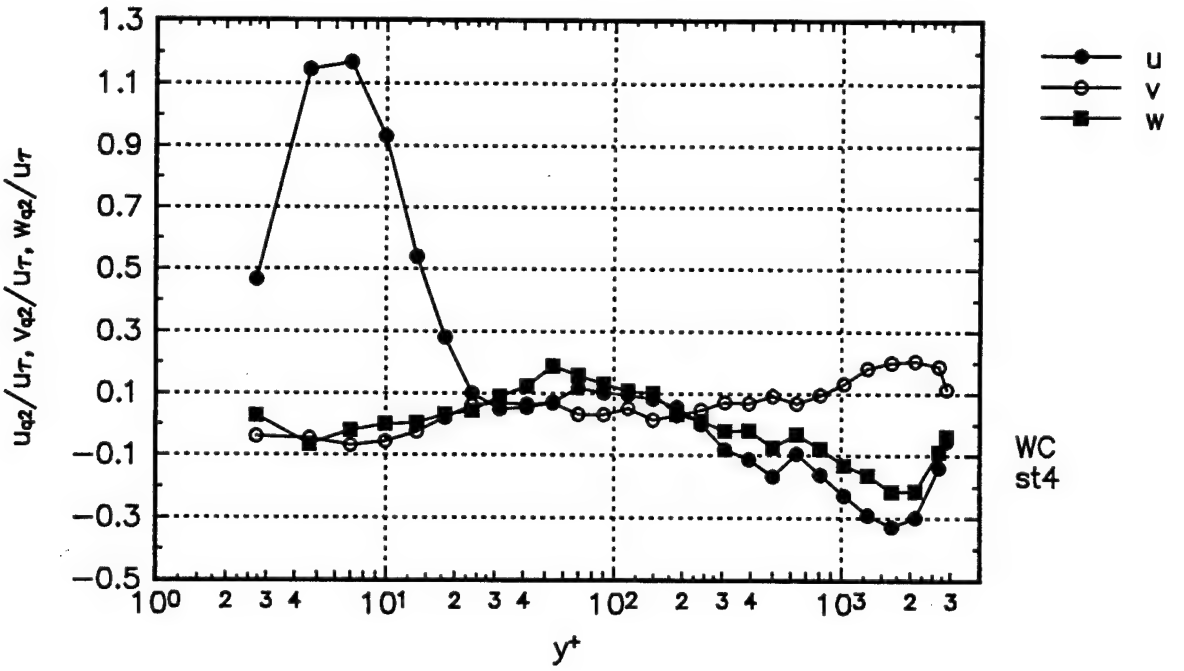
1.3
1.1
0.9
0.7
0.5
0.3
0.1
−0.1
−0.3
−0.5
u_{q2}/u_T, v_{q2}/u_T, w_{q2}/u_T
10^0 2 3 4 10^1 2 3 4 10^2 2 3 4 10^3 2 3
y^+
u
v
w
WC
st4

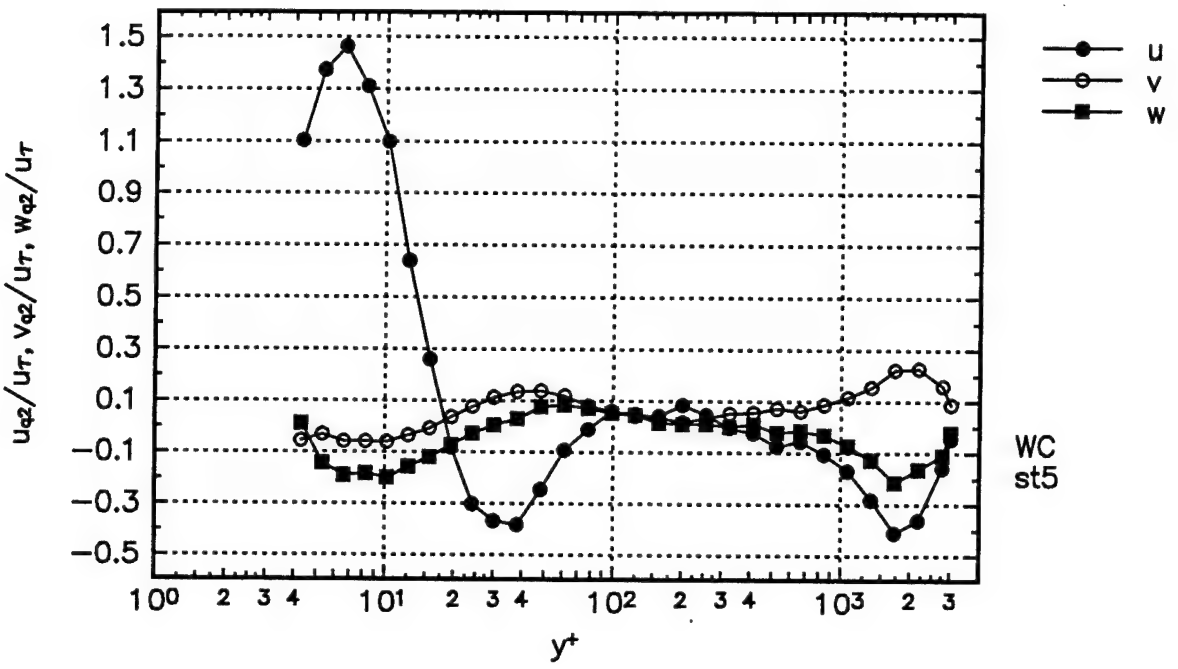
1.5
1.3
1.1
0.9
0.7
0.5
0.3
0.1
−0.1
−0.3
−0.5
$u_{\phi 2}/u_\tau$, $v_{\phi 2}/u_\tau$, $w_{\phi 2}/u_\tau$
10^0 2 3 4 10^1 2 3 4 10^2 2 3 4 10^3 2 3
y^+
u
v
w
WC
st5

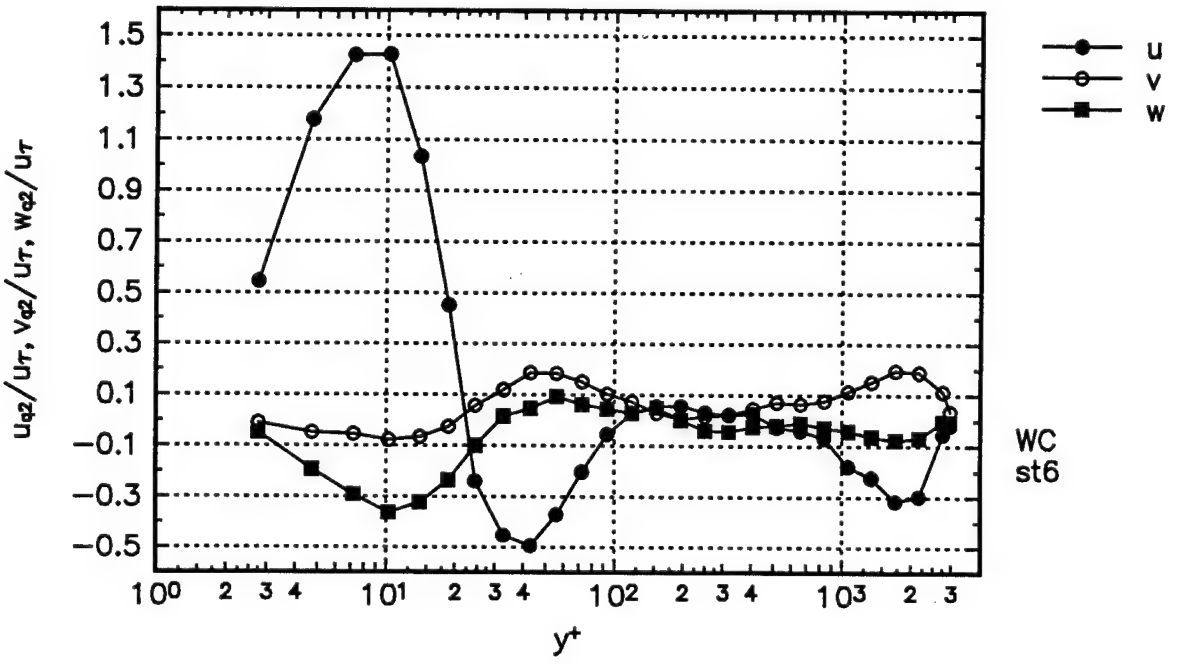
1.5
1.3
1.1
0.9
0.7
0.5
0.3
0.1
−0.1
−0.3
−0.5
$u_{\phi 2}/u_\tau$, $v_{\phi 2}/u_\tau$, $w_{\phi 2}/u_\tau$
10^0 2 3 4 10^1 2 3 4 10^2 2 3 4 10^3 2 3
y^+
u
v
w
WC
st6

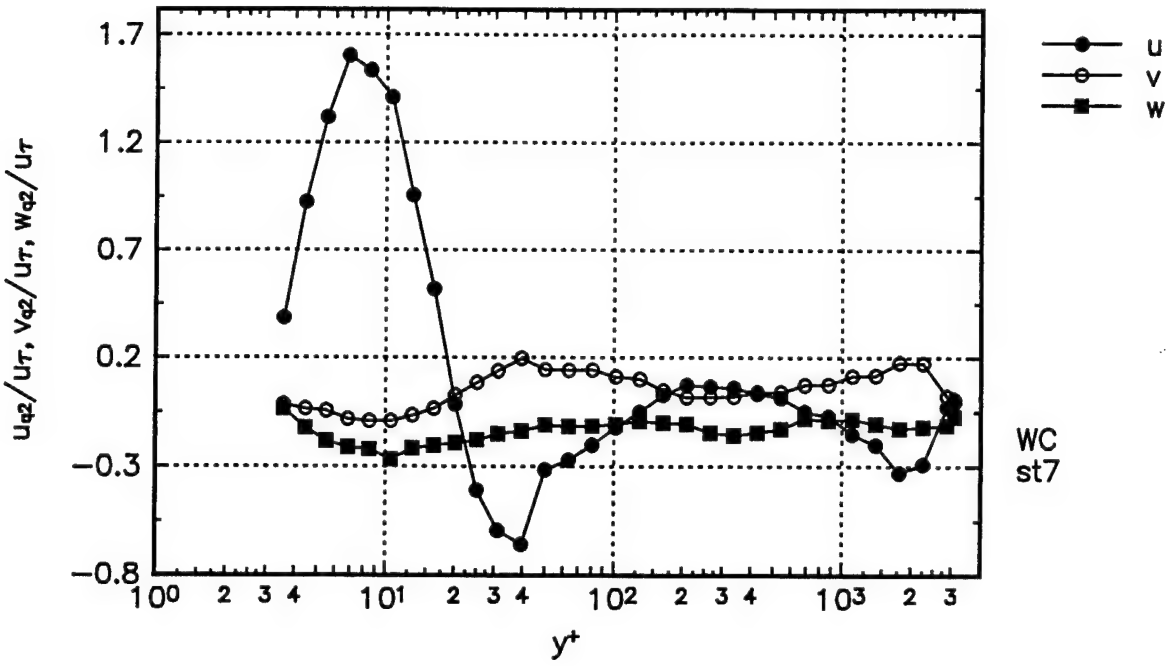
1.7
1.2
0.7
0.2
−0.3
−0.8
10^0 2 3 4 10^1 2 3 4 10^2 2 3 4 10^3 2 3
y^+
u_{q2}/u_T, v_{q2}/u_T, w_{q2}/u_T
u
v
w
WC
st7

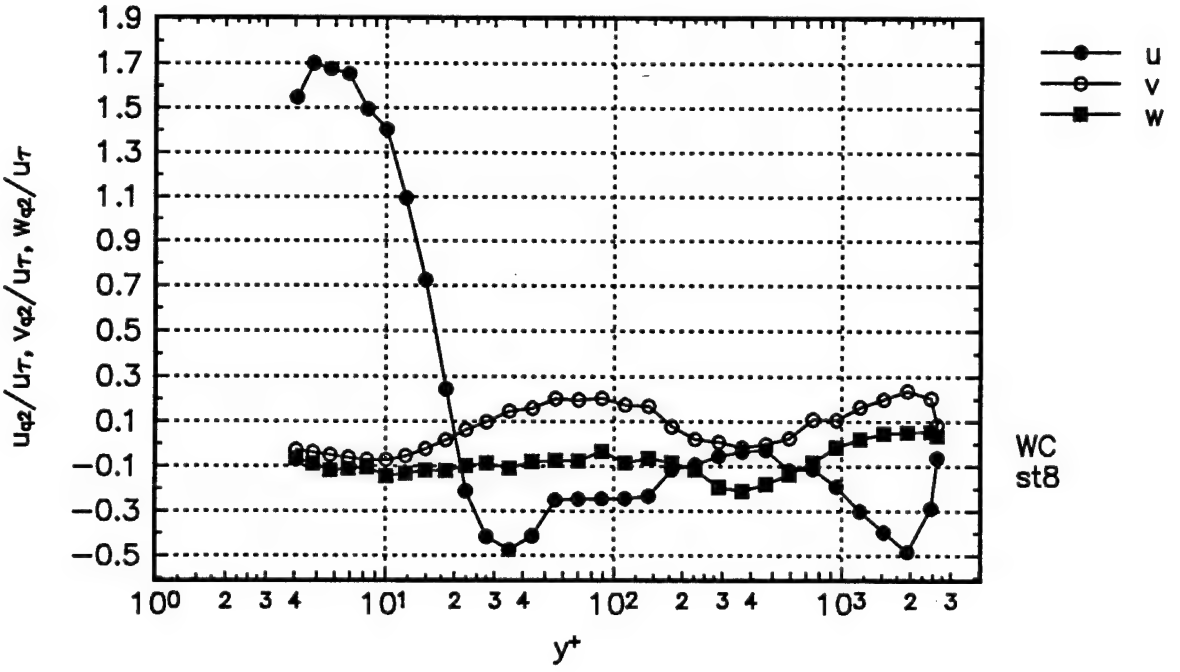
1.9
1.7
1.5
1.3
1.1
0.9
0.7
0.5
0.3
0.1
−0.1
−0.3
−0.5
10^0 2 3 4 10^1 2 3 4 10^2 2 3 4 10^3 2 3
y^+
u_{q2}/u_T, v_{q2}/u_T, w_{q2}/u_T
u
v
w
WC
st8

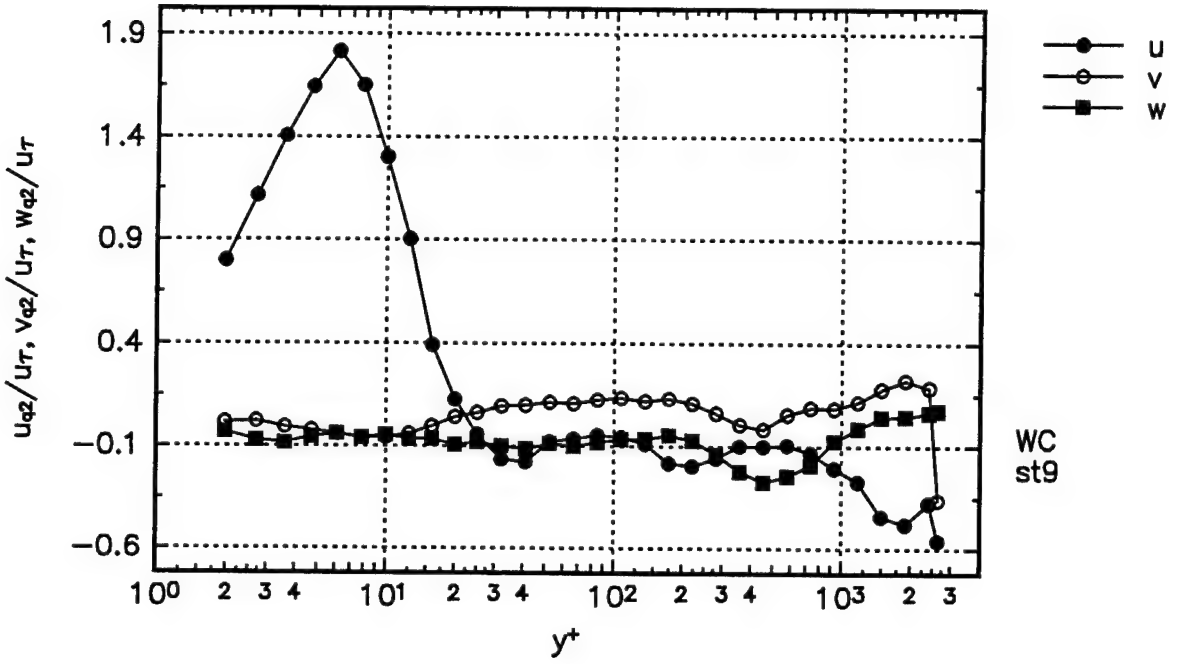
1.9
1.4
0.9
0.4
−0.1
−0.6
u_{q2}/u_T, v_{q2}/u_T, w_{q2}/u_T
10^0 2 3 4 10^1 2 3 4 10^2 2 3 4 10^3 2 3
y^+
u
v
w
WC
st9

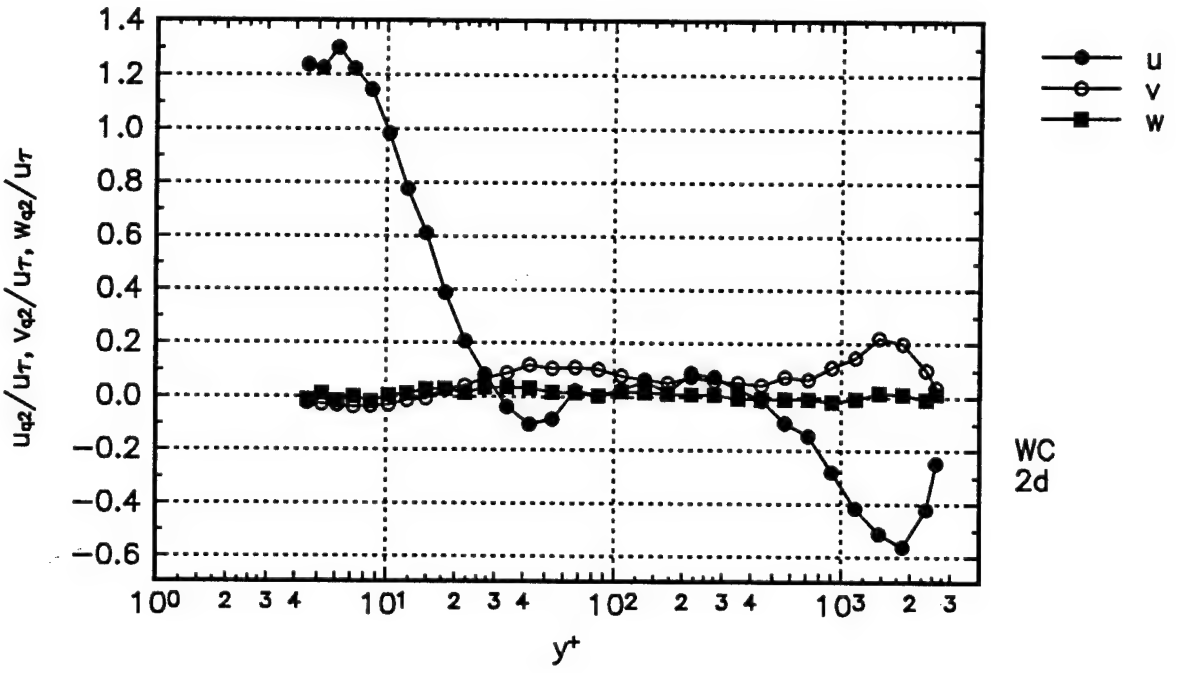
1.4
1.2
1.0
0.8
0.6
0.4
0.2
0.0
−0.2
−0.4
−0.6
u_{q2}/u_T, v_{q2}/u_T, w_{q2}/u_T
10^0 2 3 4 10^1 2 3 4 10^2 2 3 4 10^3 2 3
y^+
u
v
w
WC
2d

Figures in WALL coordinates. Transport velocity plots for all stations for $\overline{u^2}$, $\overline{v^2}$, $\overline{w^2}$, $\overline{q^2}$ on top of another. Where :

$U_{u^2}=\overline{u^3}/\overline{u^2}$, $V_{u^2}=\overline{u^2v}/\overline{u^2}$, $W_{u^2}=\overline{u^2w}/\overline{u^2}$,

$U_{v^2}=\overline{uv^2}/\overline{v^2}$, $V_{v^2}=\overline{v^3}/\overline{v^2}$, $W_{v^2}=\overline{v^2w}/\overline{v^2}$,

$U_{w^2}=\overline{uw^2}/\overline{w^2}$, $V_{w^2}=\overline{vw^2}/\overline{w^2}$, $W_{w^2}=\overline{w^3}/\overline{w^2}$,

$U_{q^2}=\overline{u^3+uv^2+uw^2}/\overline{u^2+v^2+w^2}$, $V_{q^2}=\overline{u^2v+v^3+vw^2}/\overline{u^2+v^2+w^2}$, $W_{q^2}=\overline{u^2w+v^2w+w^3}/\overline{u^2+v^2+w^2}$

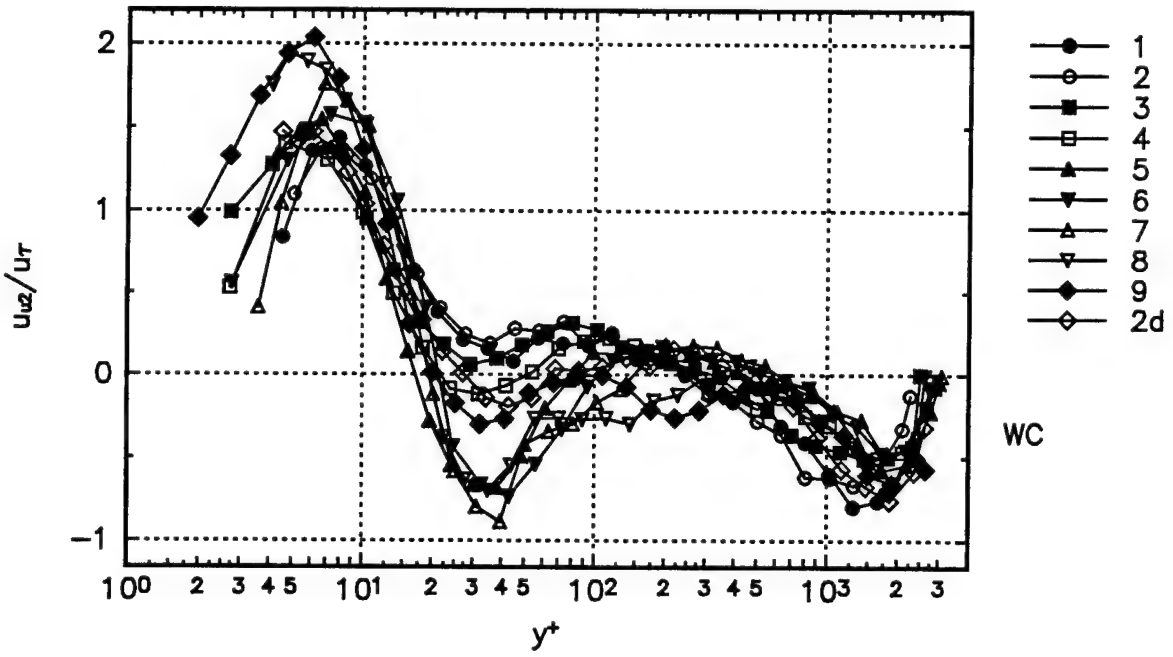

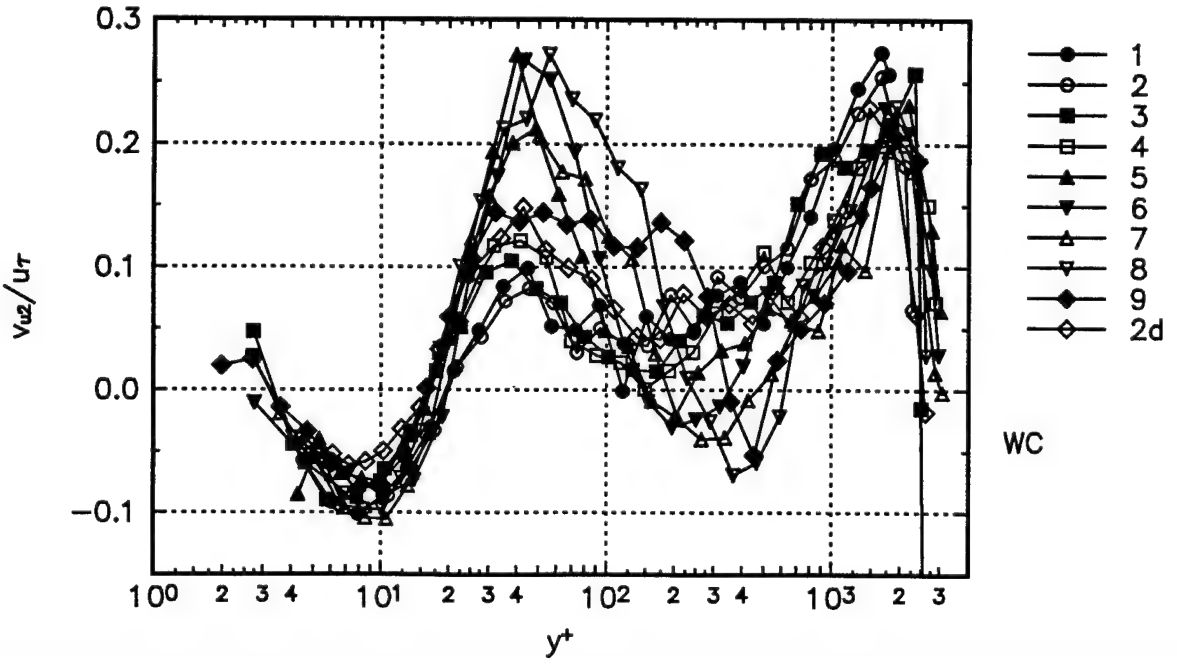

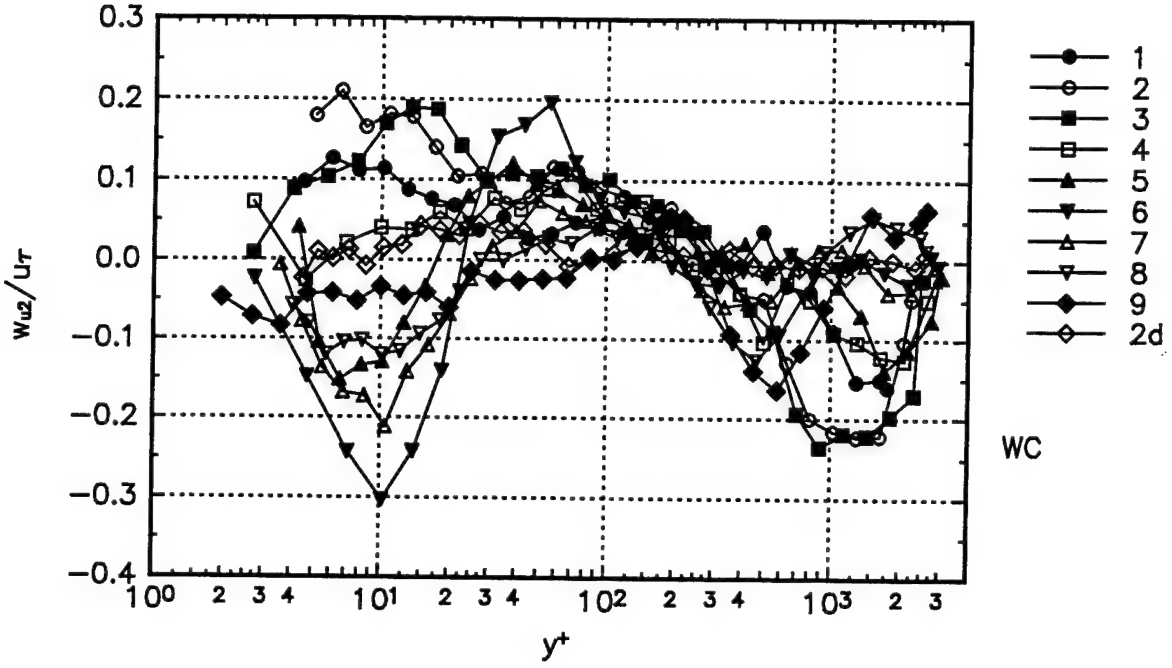
0.3
0.2
0.1
0.0
−0.1
−0.2
−0.3
−0.4
$w_{\omega 2}/u_\tau$
10^0 2 3 4 10^1 2 3 4 10^2 2 3 4 10^3 2 3
y^+
1
2
3
4
5
6
7
8
9
2d
WC

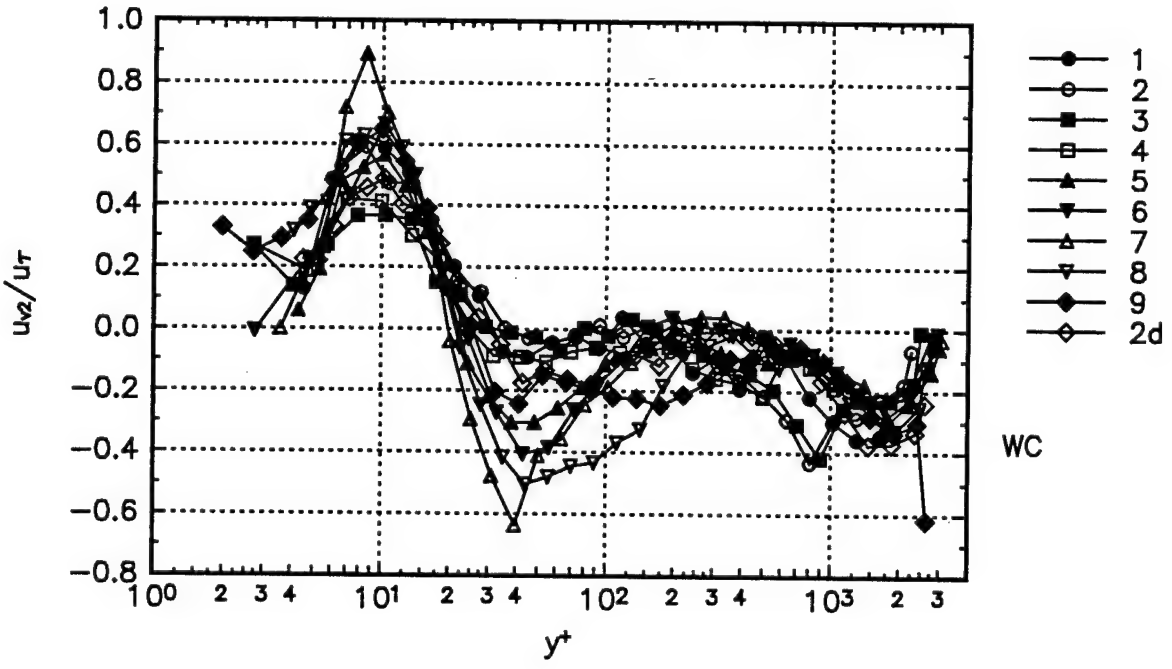
1.0
0.8
0.6
0.4
0.2
0.0
−0.2
−0.4
−0.6
−0.8
u_{v2}/u_τ
10^0 2 3 4 10^1 2 3 4 10^2 2 3 4 10^3 2 3
y^+
1
2
3
4
5
6
7
8
9
2d
WC

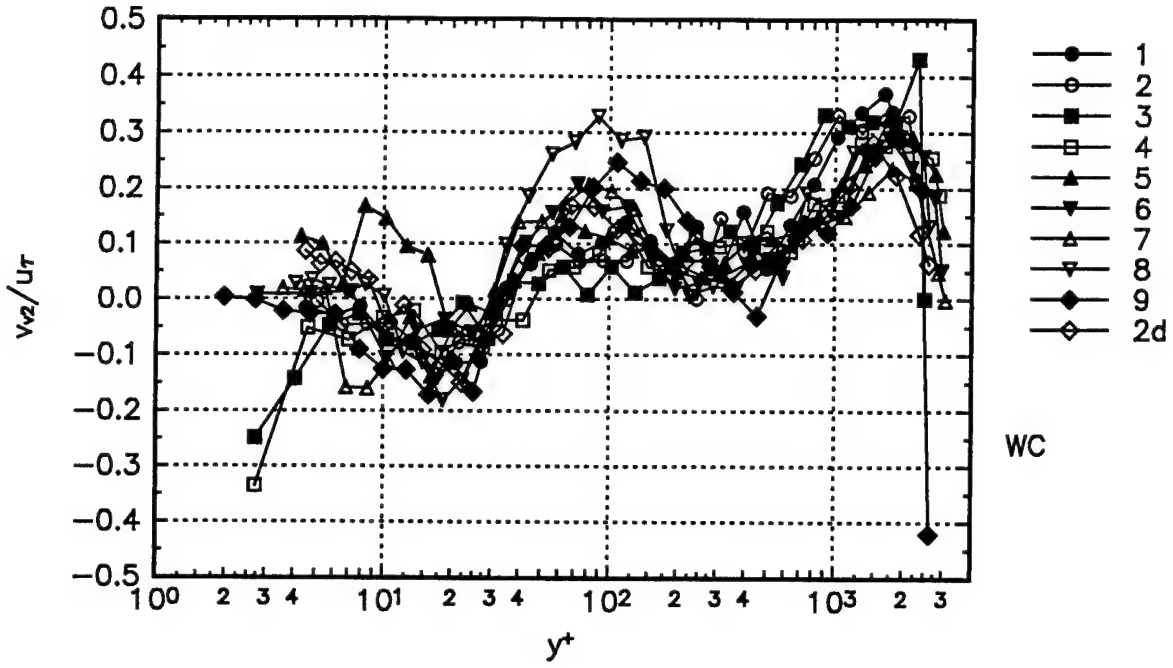
0.5
0.4
0.3
0.2
0.1
0.0
−0.1
−0.2
−0.3
−0.4
−0.5
v_{v2}/u_τ
10^0 2 3 4 10^1 2 3 4 10^2 2 3 4 10^3 2 3
y^+
1
2
3
4
5
6
7
8
9
2d
WC

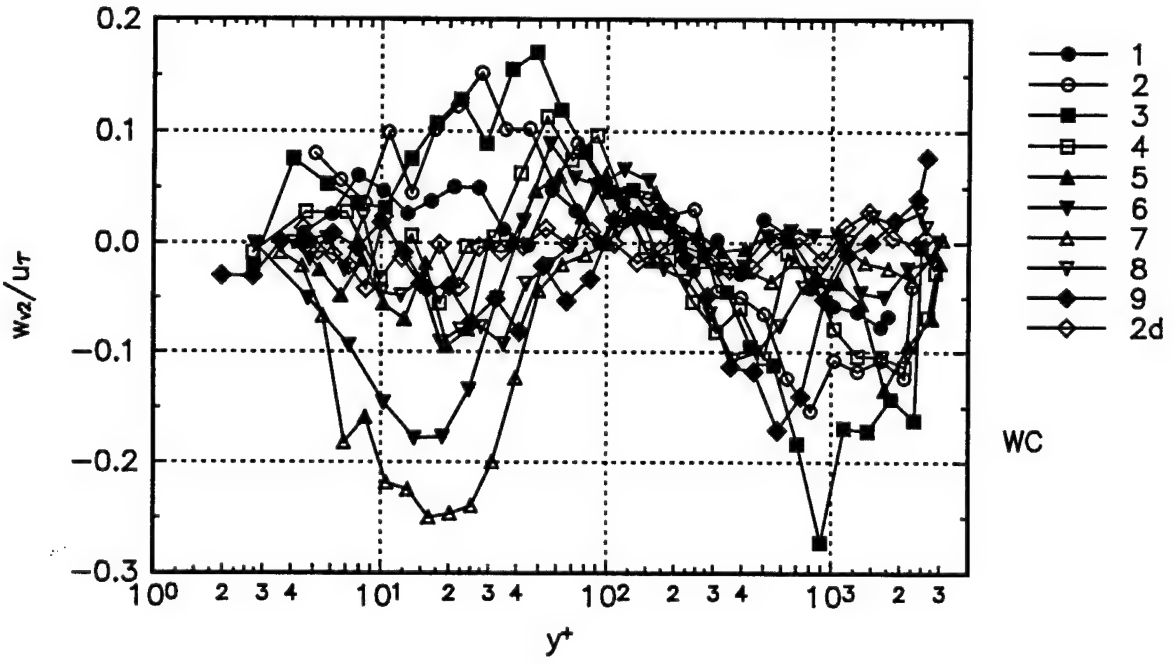
0.2
0.1
0.0
−0.1
−0.2
−0.3
w_{v2}/u_τ
10^0 2 3 4 10^1 2 3 4 10^2 2 3 4 10^3 2 3
y^+
1
2
3
4
5
6
7
8
9
2d
WC

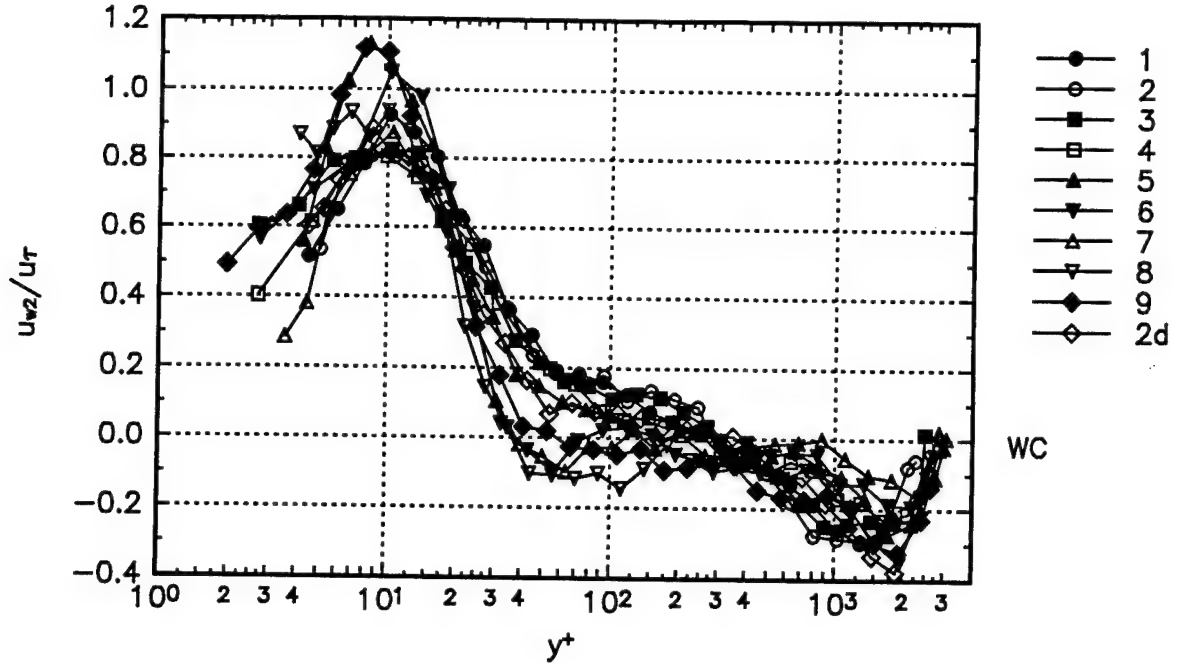
1.2
1.0
0.8
0.6
0.4
0.2
0.0
−0.2
−0.4
u_{w2}/u_τ
10^0 2 3 4 10^1 2 3 4 10^2 2 3 4 10^3 2 3
y^+
1
2
3
4
5
6
7
8
9
2d
WC

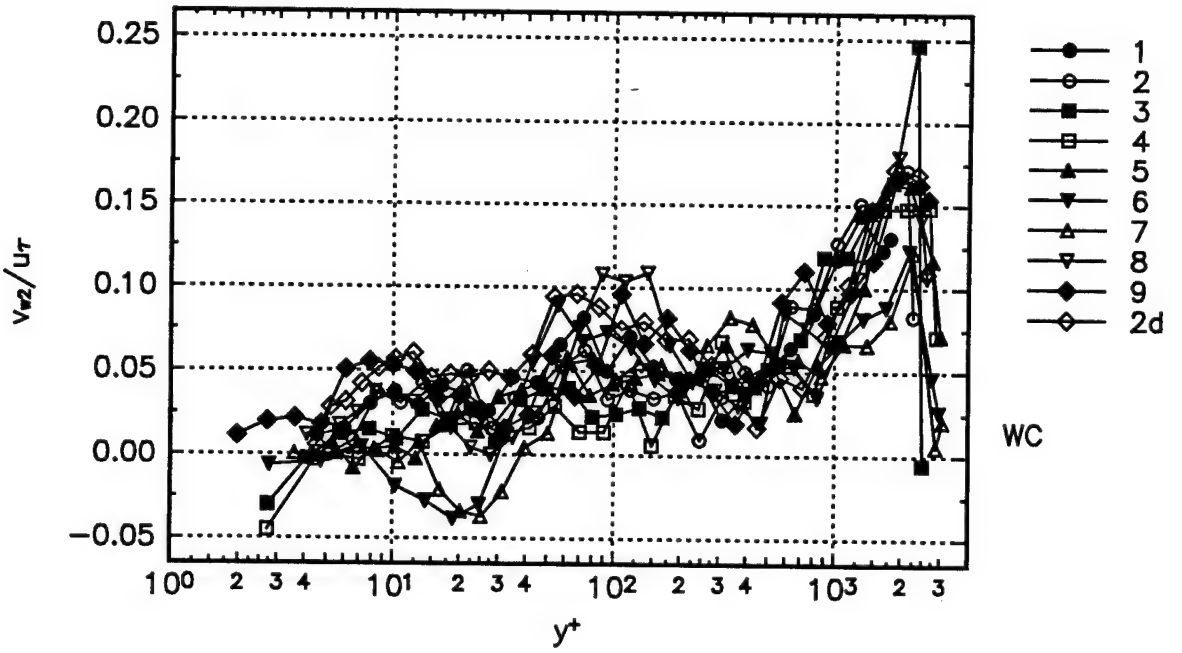
0.25
0.20
0.15
0.10
0.05
0.00
−0.05
v_{w2}/u_τ
10^0 2 3 4 10^1 2 3 4 10^2 2 3 4 10^3 2 3
y^+
1
2
3
4
5
6
7
8
9
2d
WC

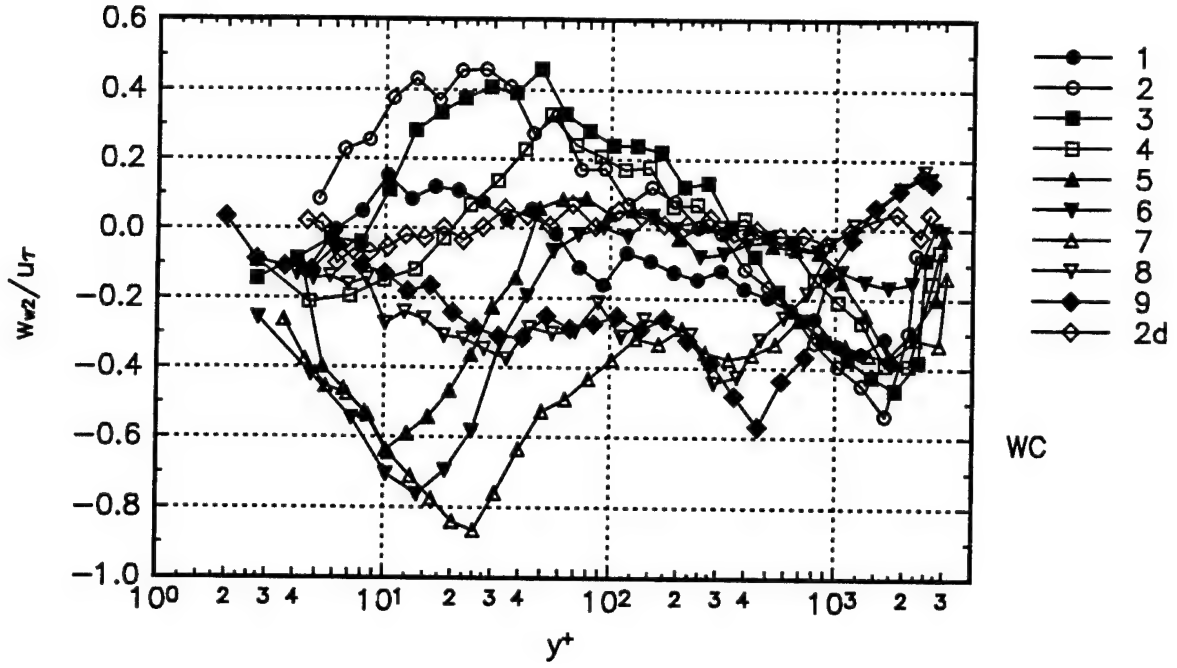
0.6
0.4
0.2
0.0
−0.2
−0.4
−0.6
−0.8
−1.0
w_{w2}/u_τ
10^0 2 3 4 10^1 2 3 4 10^2 2 3 4 10^3 2 3
y^+
1
2
3
4
5
6
7
8
9
2d
WC

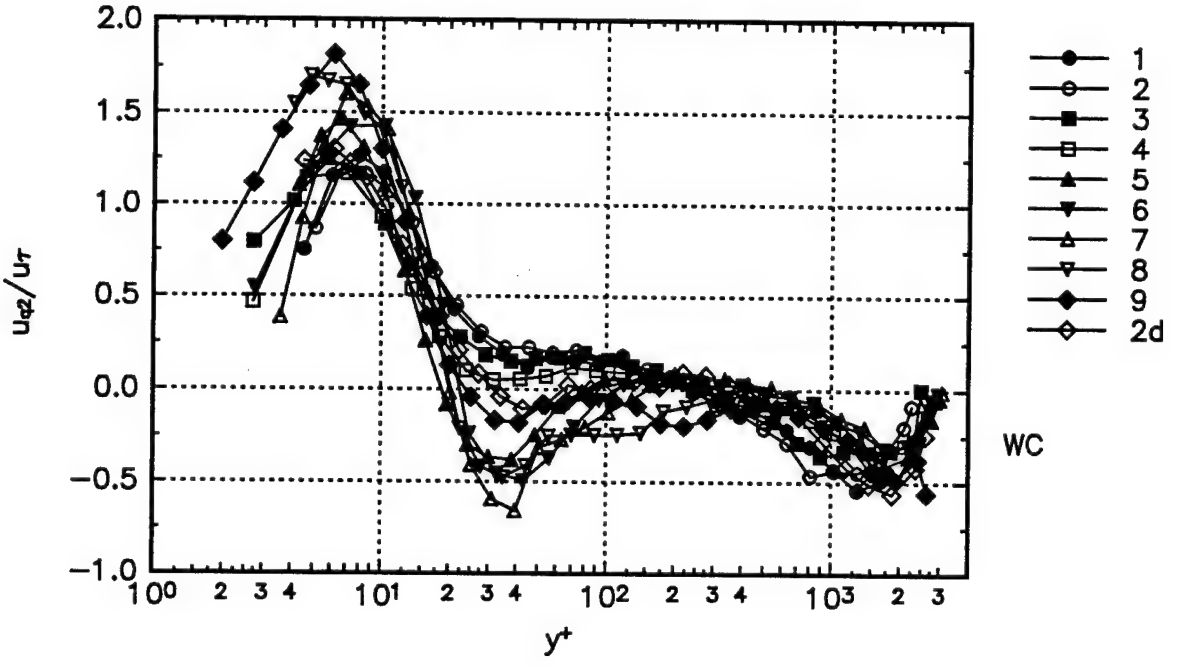
2.0
1.5
1.0
0.5
0.0
−0.5
−1.0
u_{q2}/u_τ
10^0 2 3 4 10^1 2 3 4 10^2 2 3 4 10^3 2 3
y^+
1
2
3
4
5
6
7
8
9
2d
WC

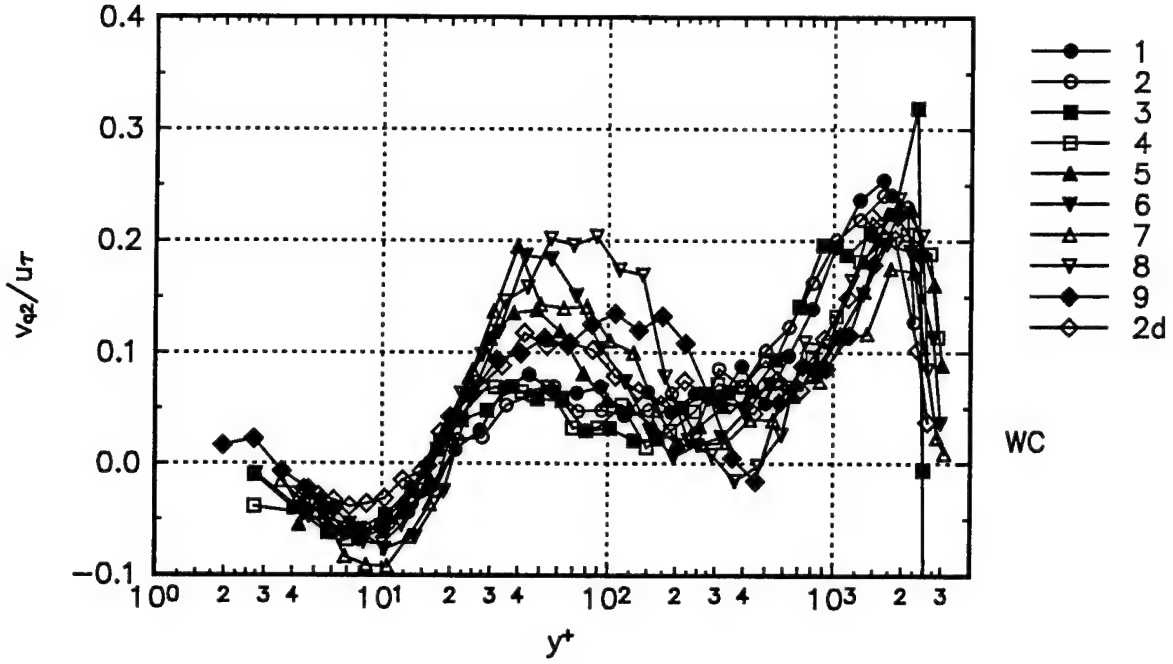
0.4
0.3
0.2
0.1
0.0
−0.1
v_{q2}/u_τ
10^0 2 3 4 10^1 2 3 4 10^2 2 3 4 10^3 2 3
y^+
1
2
3
4
5
6
7
8
9
2d
WC

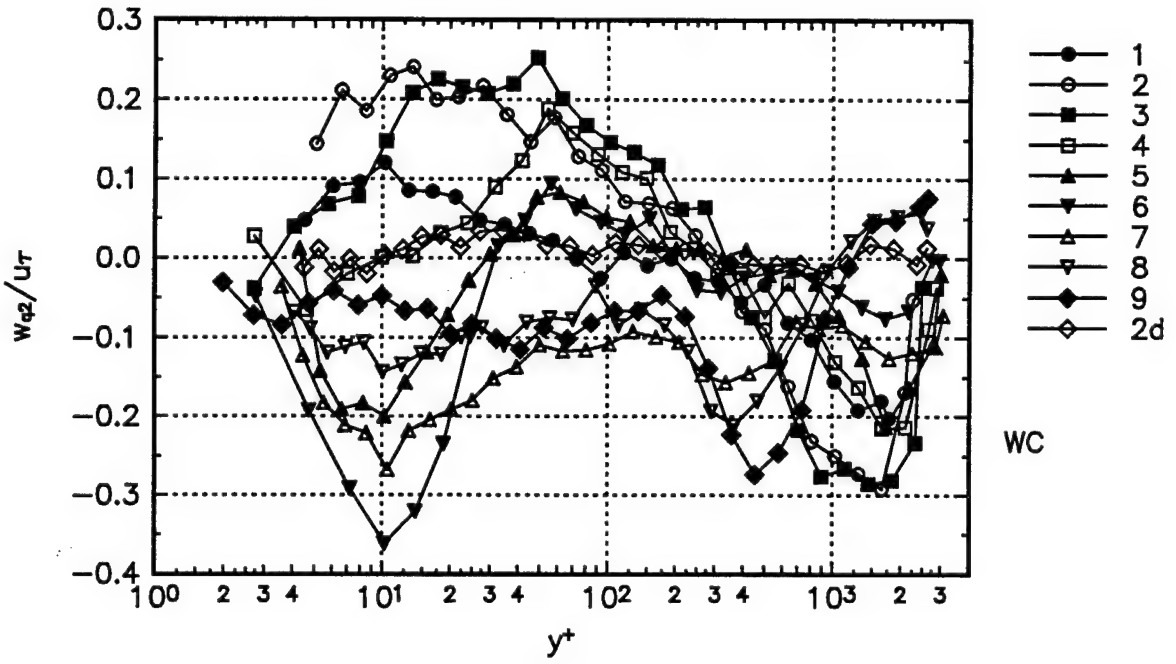
0.3
0.2
0.1
0.0
−0.1
−0.2
−0.3
−0.4
w_{q2}/u_τ
10^0 2 3 4 10^1 2 3 4 10^2 2 3 4 10^3 2 3
y^+
1
2
3
4
5
6
7
8
9
2d
WC

Several other flow parameters:
Non-dimensional "y" derivatives of the mean velocity, Reynolds stress and triple products at Station 5. The velocities are non-dimensionalized by the respective powers of the u_τ. $y^+ = yu_\tau/\nu$.

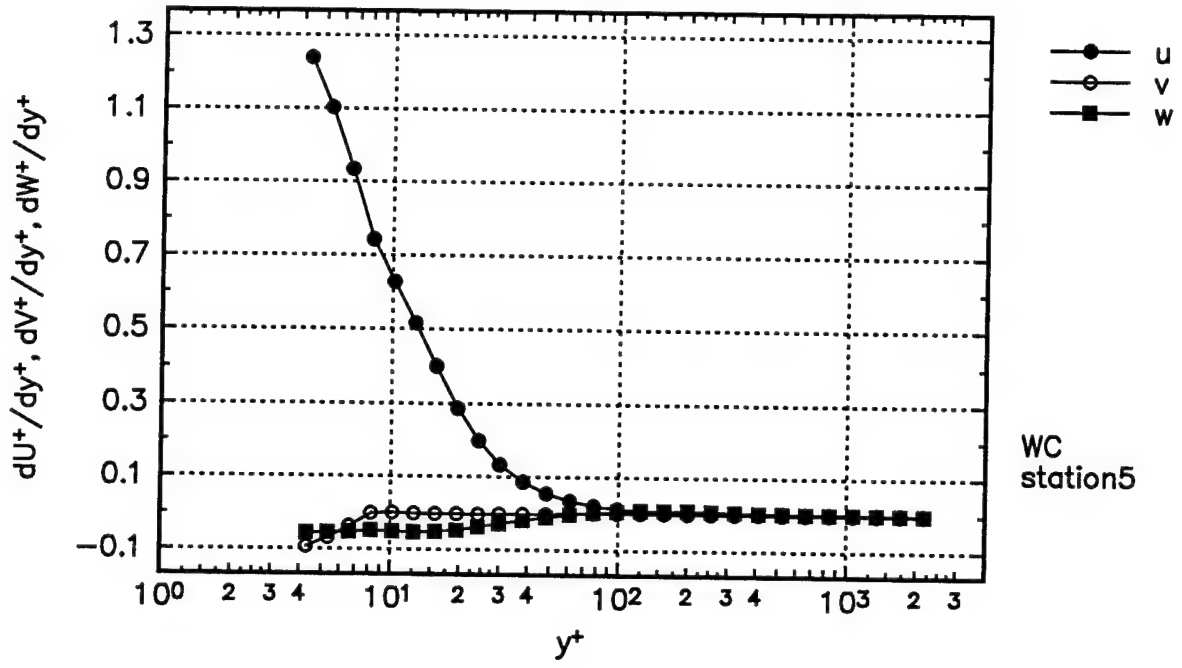

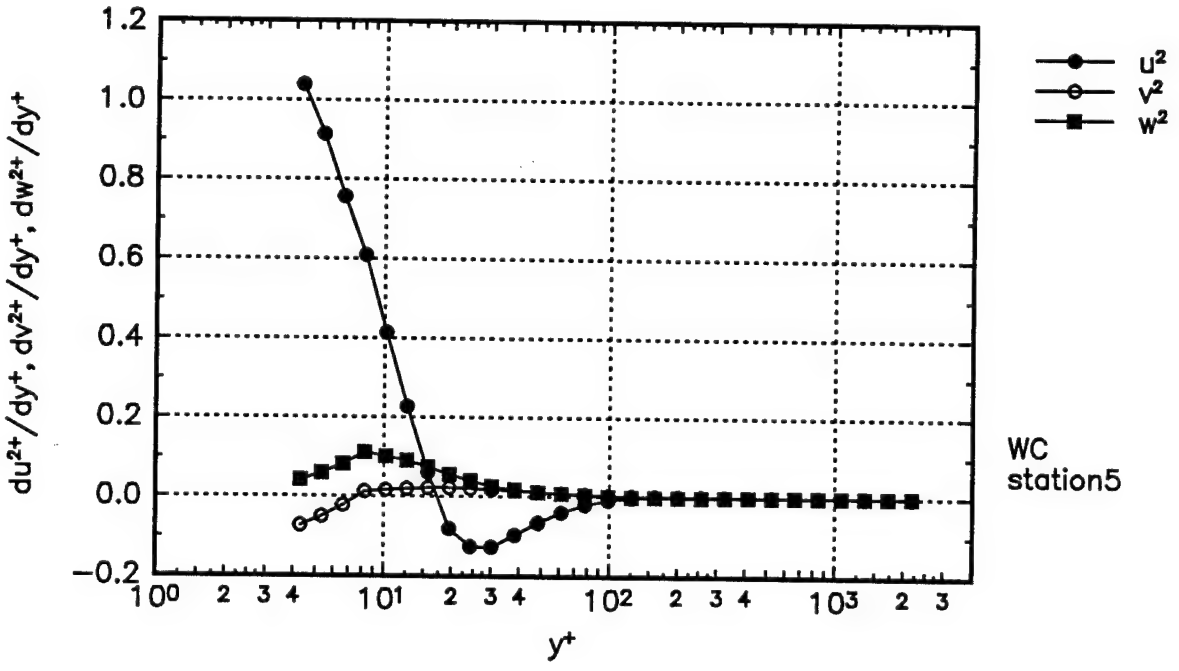

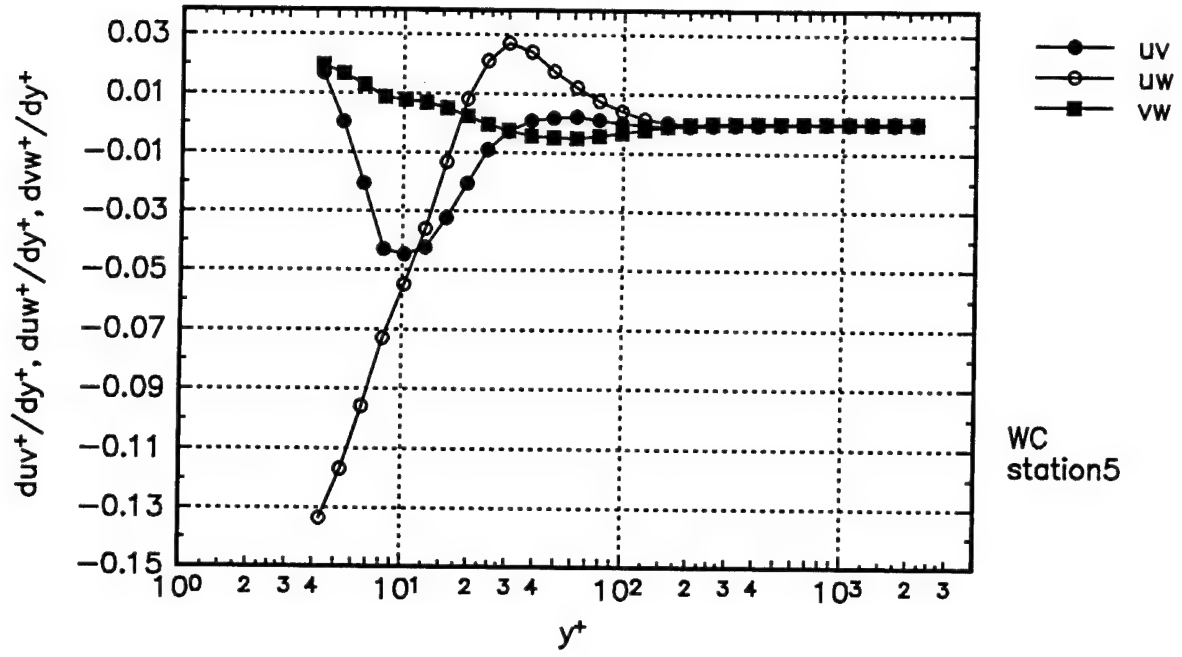
0.03
0.01
−0.01
−0.03
−0.05
−0.07
−0.09
−0.11
−0.13
−0.15
10^0 2 3 4 10^1 2 3 4 10^2 2 3 4 10^3 2 3
y^+
$du^+/dy^+, duw^+/dy^+, dvw^+/dy^+$
uv
uw
vw
WC
station5

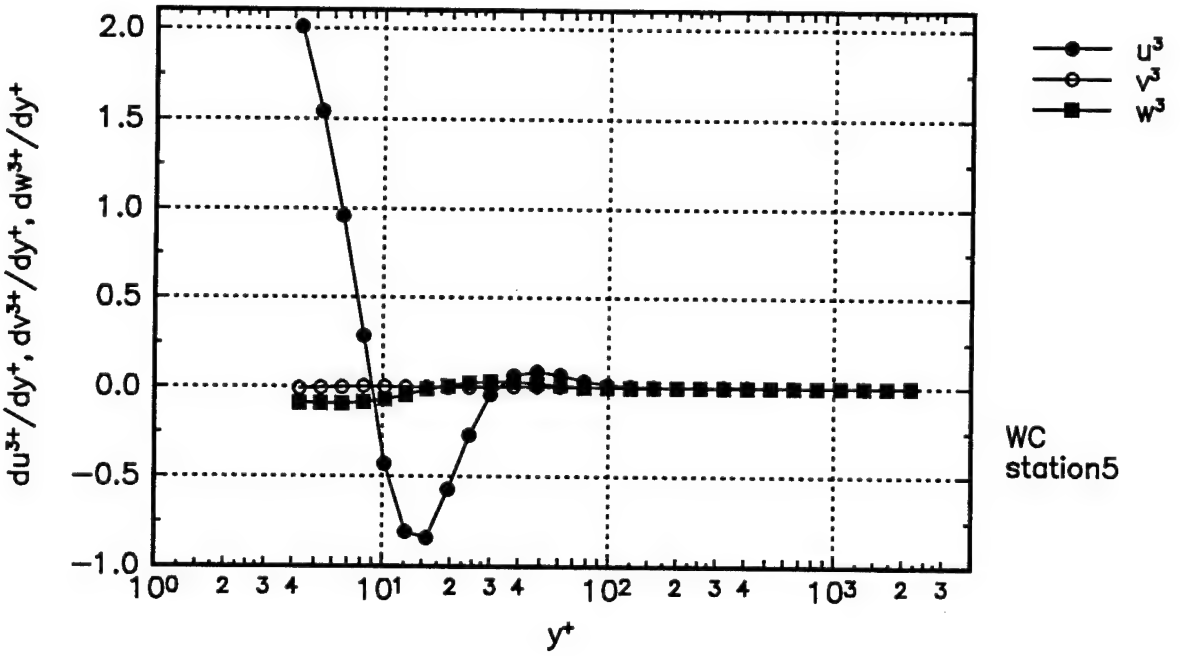
2.0
1.5
1.0
0.5
0.0
−0.5
−1.0
10^0 2 3 4 10^1 2 3 4 10^2 2 3 4 10^3 2 3
y^+
$du^{3+}/dy^+, dv^{3+}/dy^+, dw^{3+}/dy^+$
u^3
v^3
w^3
WC
station5

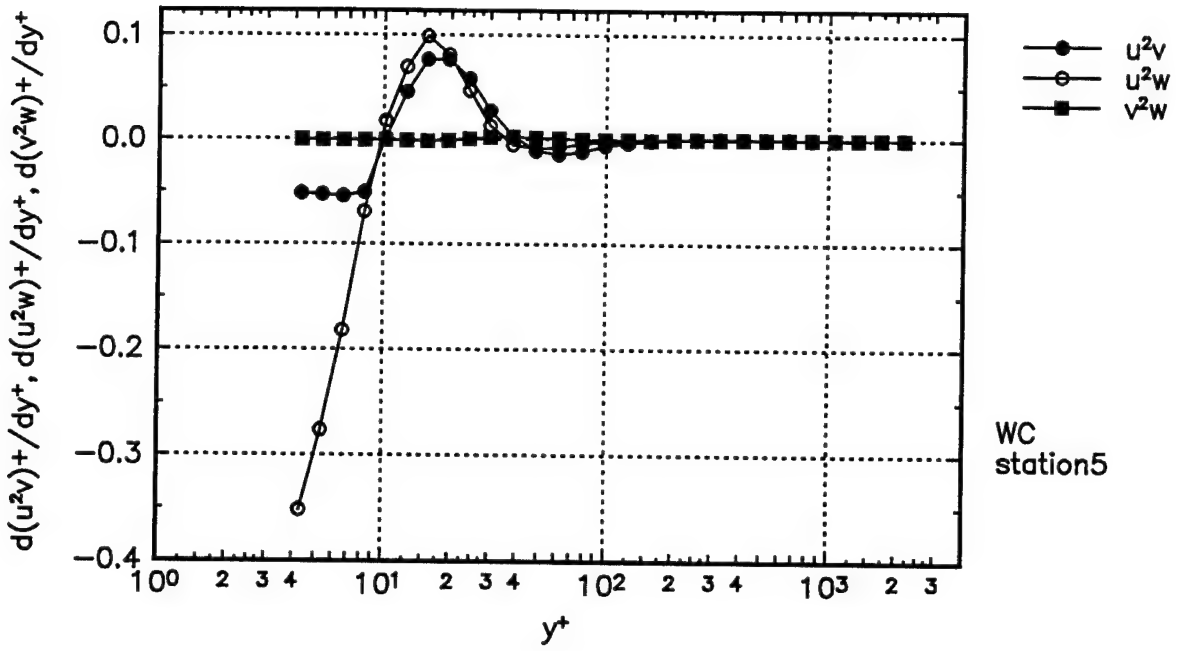
0.1
0.0
−0.1
−0.2
−0.3
−0.4
10^0 2 3 4 10^1 2 3 4 10^2 2 3 4 10^3 2 3
y^+
$d(u^2v)^+/dy^+$, $d(u^2w)^+/dy^+$, $d(v^2w)^+/dy^+$
u^2v
u^2w
v^2w
WC
station5

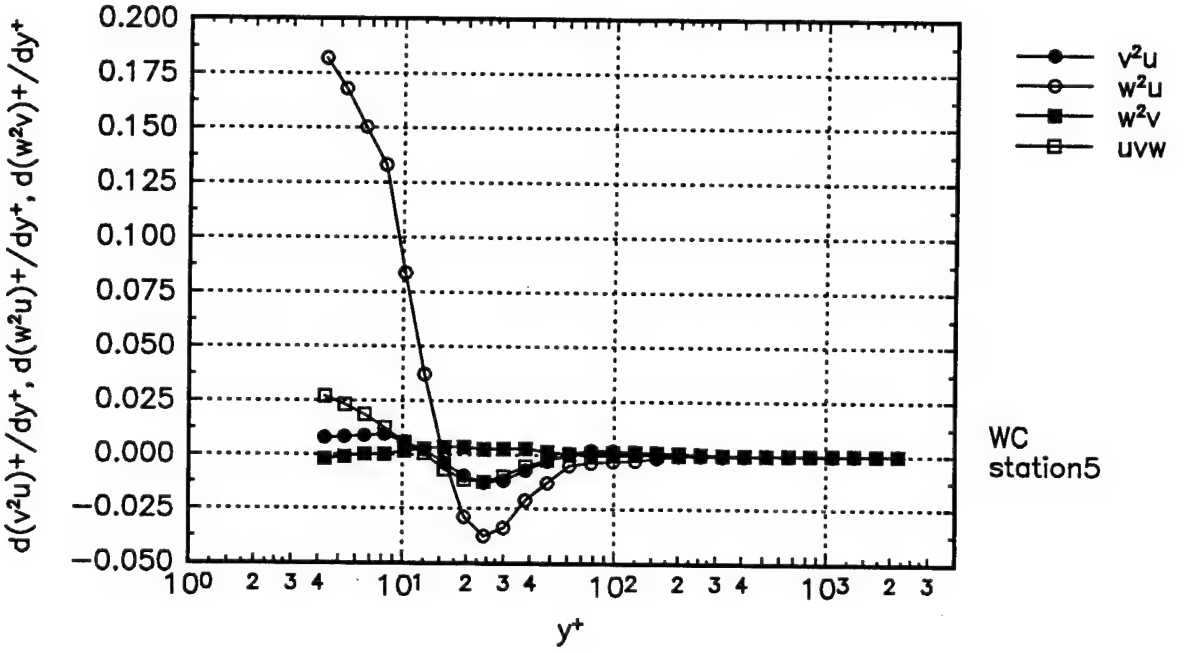
0.200
0.175
0.150
0.125
0.100
0.075
0.050
0.025
0.000
−0.025
−0.050
10^0 2 3 4 10^1 2 3 4 10^2 2 3 4 10^3 2 3
y^+
$d(v^2u)^+/dy^+$, $d(w^2u)^+/dy^+$, $d(w^2v)^+/dy^+$
v^2u
w^2u
w^2v
uvw
WC
station5

Production terms of triple product transport equations using boundary layer approximations at Station 5.

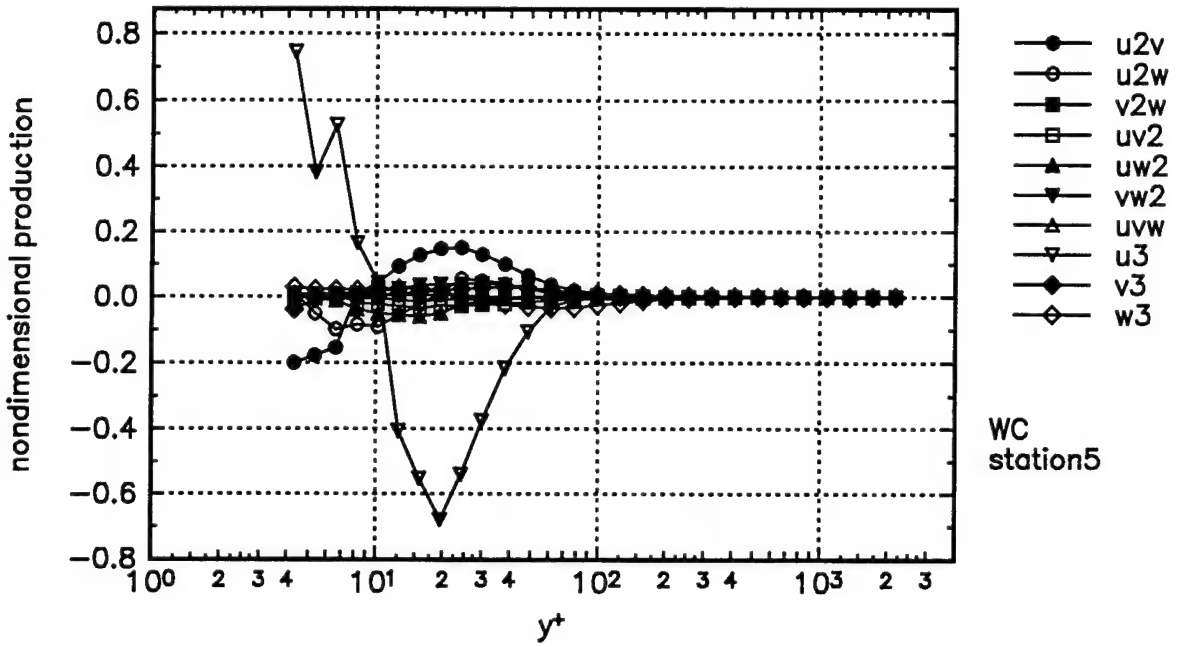

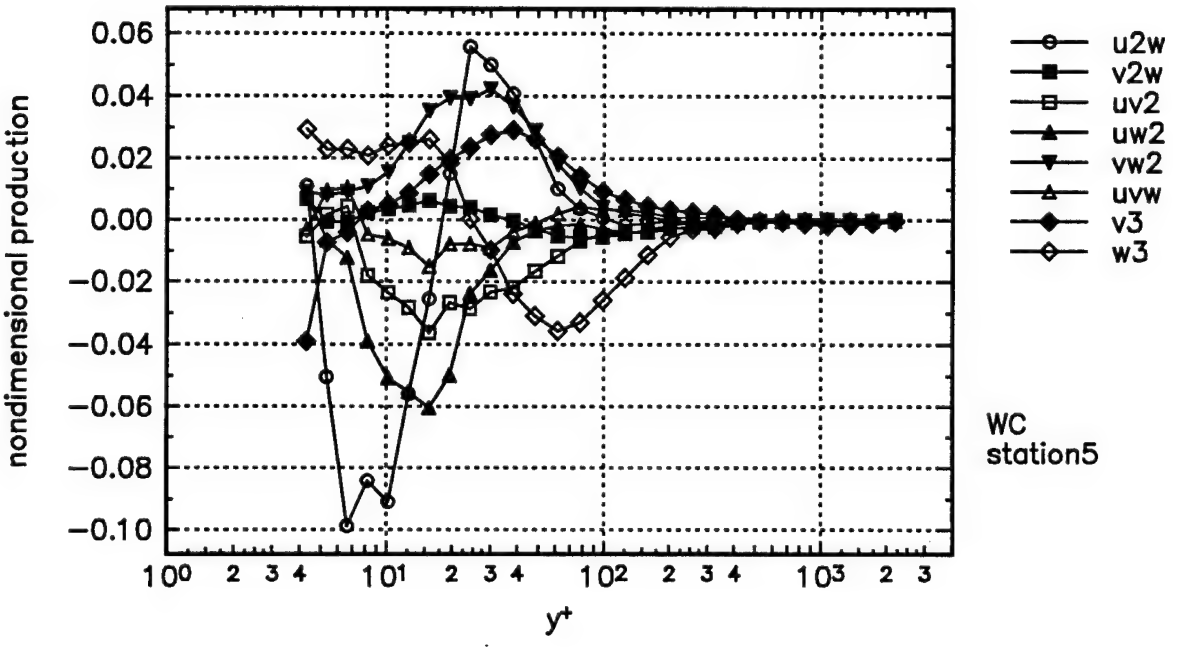

Some structural parameters obtained using the Reynolds' stresses and the triple products.

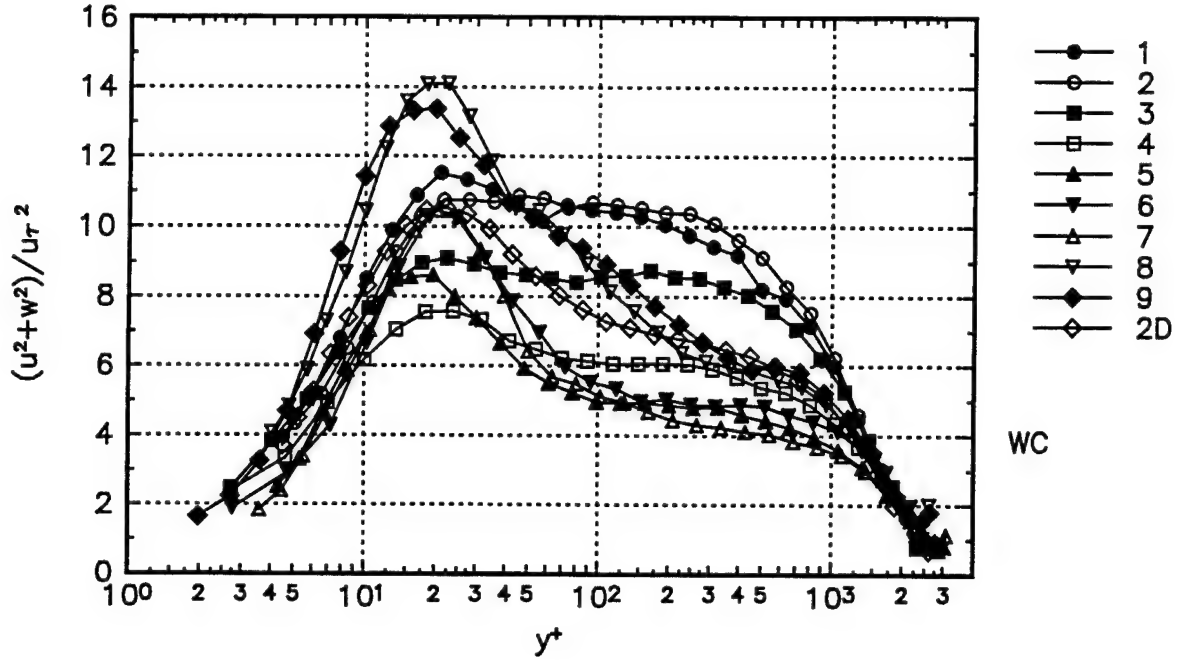

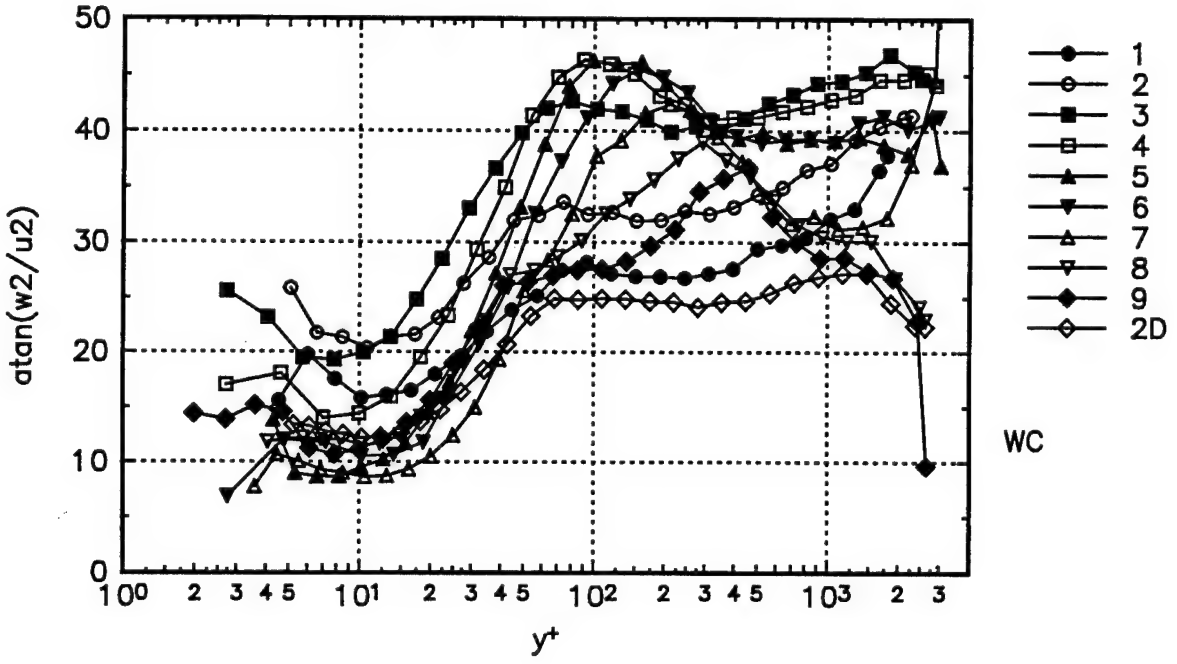

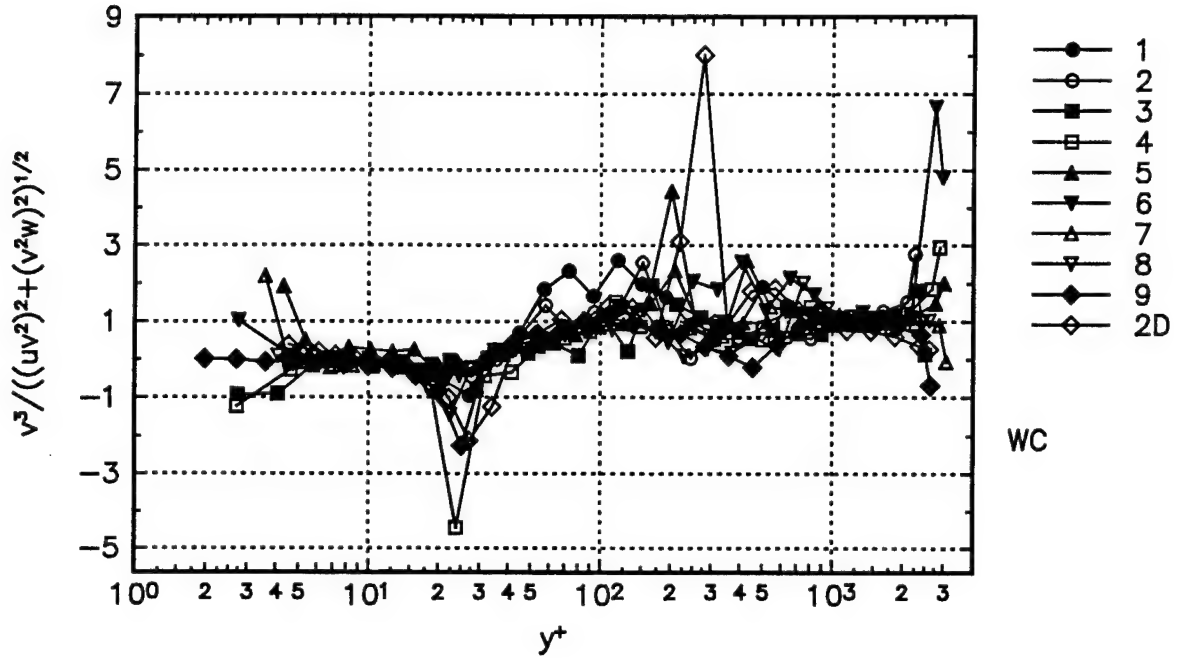
9
7
5
3
1
−1
−3
−5
$v^3/((uv^2)^2+(v^2w)^2)^{1/2}$
10^0 2 3 4 5 10^1 2 3 4 5 10^2 2 3 4 5 10^3 2 3
y^+
1
2
3
4
5
6
7
8
9
2D
WC

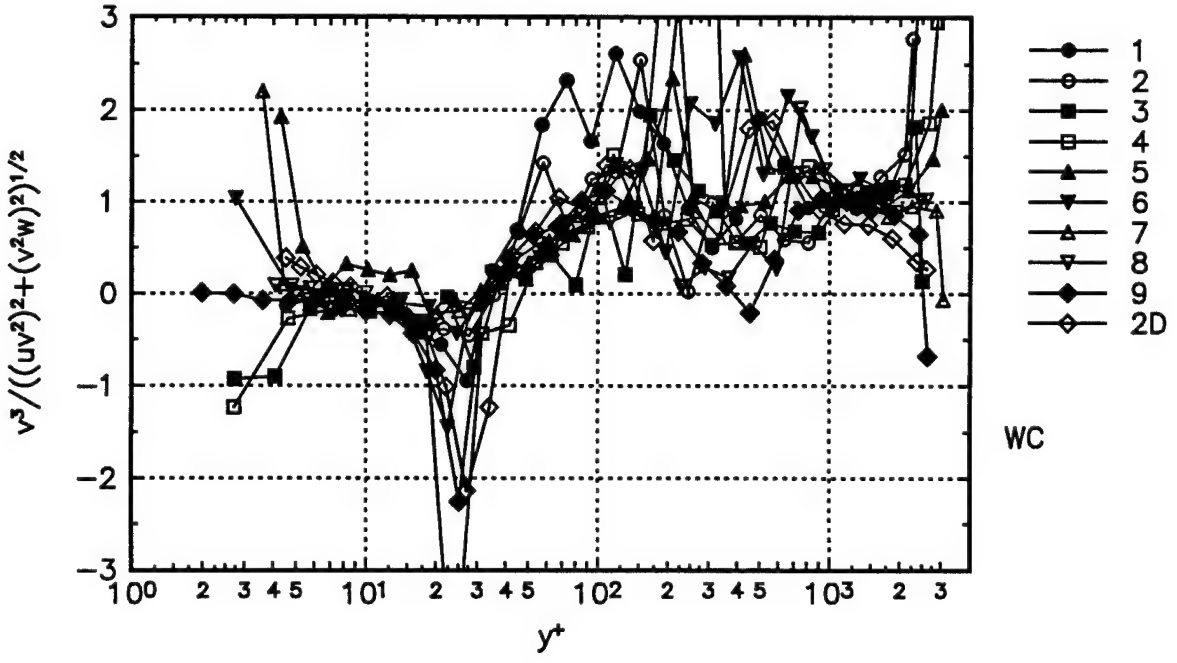
3
2
1
0
−1
−2
−3
$v^3/((uv^2)^2+(v^2w)^2)^{1/2}$
10^0 2 3 4 5 10^1 2 3 4 5 10^2 2 3 4 5 10^3 2 3
y^+
1
2
3
4
5
6
7
8
9
2D
WC

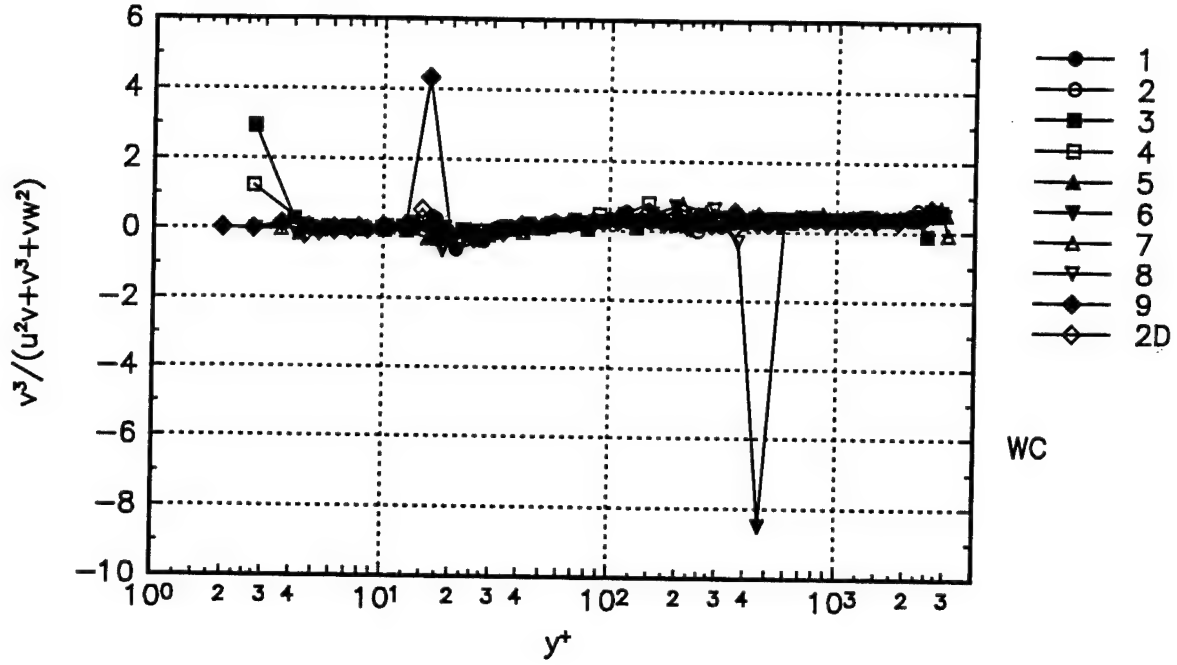
6
4
2
0
−2
−4
−6
−8
−10
$v^3/(u^2v+v^3+vw^2)$
10^0 2 3 4 10^1 2 3 4 10^2 2 3 4 10^3 2 3
y^+
1
2
3
4
5
6
7
8
9
2D
WC

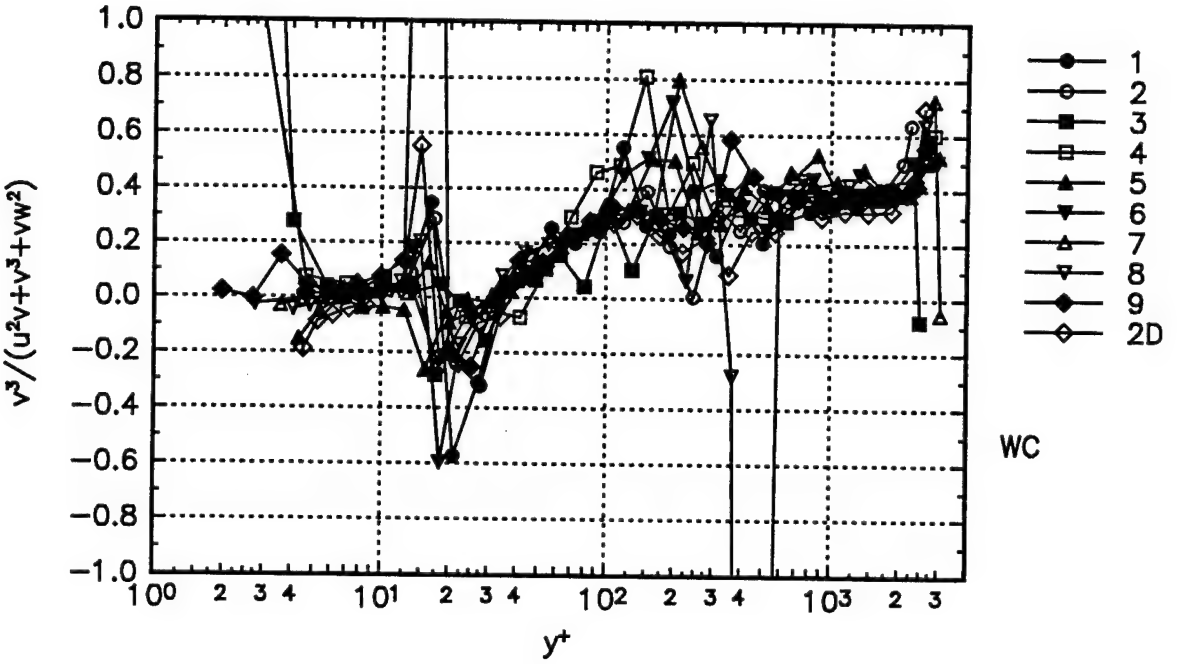
1.0
0.8
0.6
0.4
0.2
0.0
−0.2
−0.4
−0.6
−0.8
−1.0
$v^3/(u^2v+v^3+vw^2)$
10^0 2 3 4 10^1 2 3 4 10^2 2 3 4 10^3 2 3
y^+
1
2
3
4
5
6
7
8
9
2D
WC

Mean velocity profiles in a compact presentation. Velocities are nondimensionalized with the u_τ.

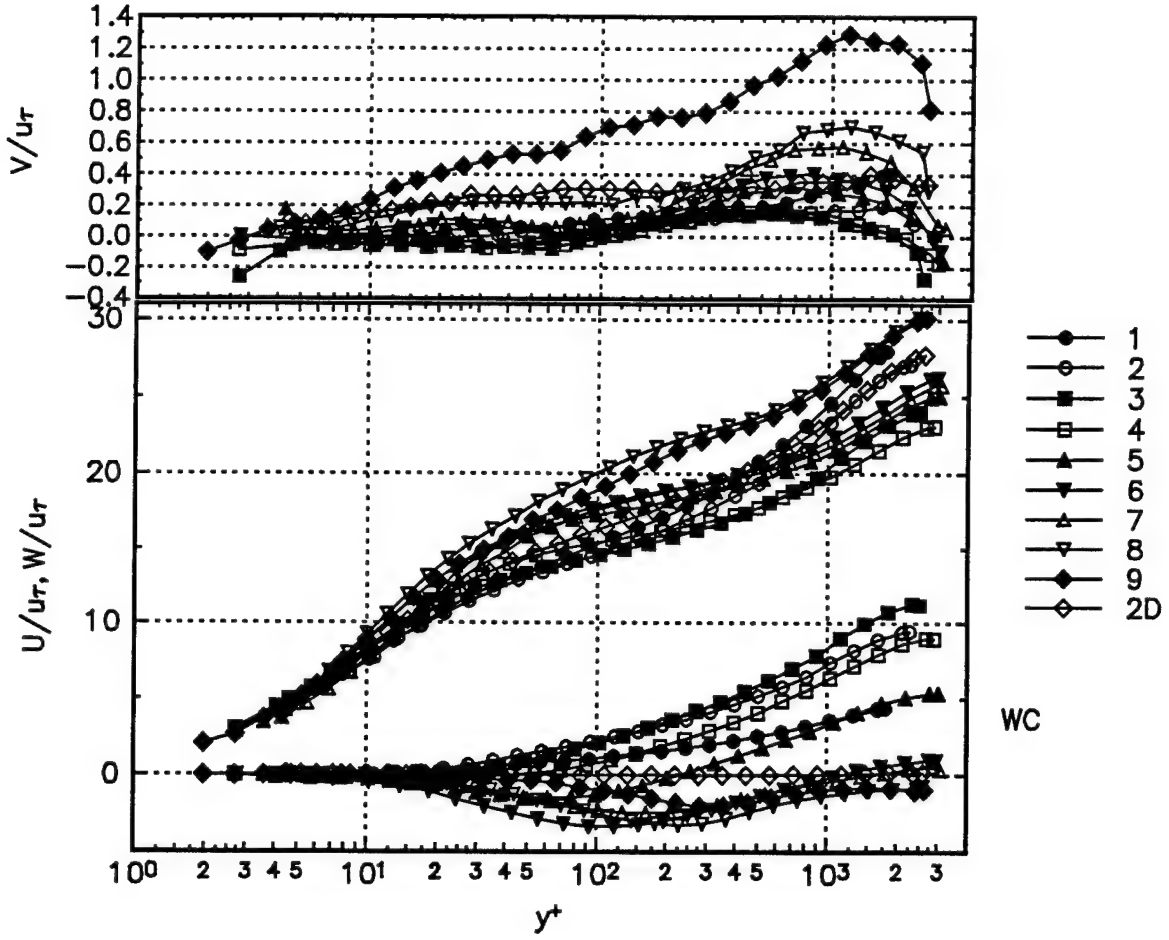

Appendix B: Tunnel Coordinates

In this Appendix the data are presented in tunnel coordinates. The "x" axis of the coordinate system is aligned with the tunnel centerline. The "y" axis is perpendicular to the tunnel wall and the "z" axis completes a right handed coordinate system. The mean velocity, Reynolds' stresses and triple products are nondimensionalized with the relative powers of U_{ref}. Also in this Appendix the correlation coefficient form of the second and third order velocity products are presented.

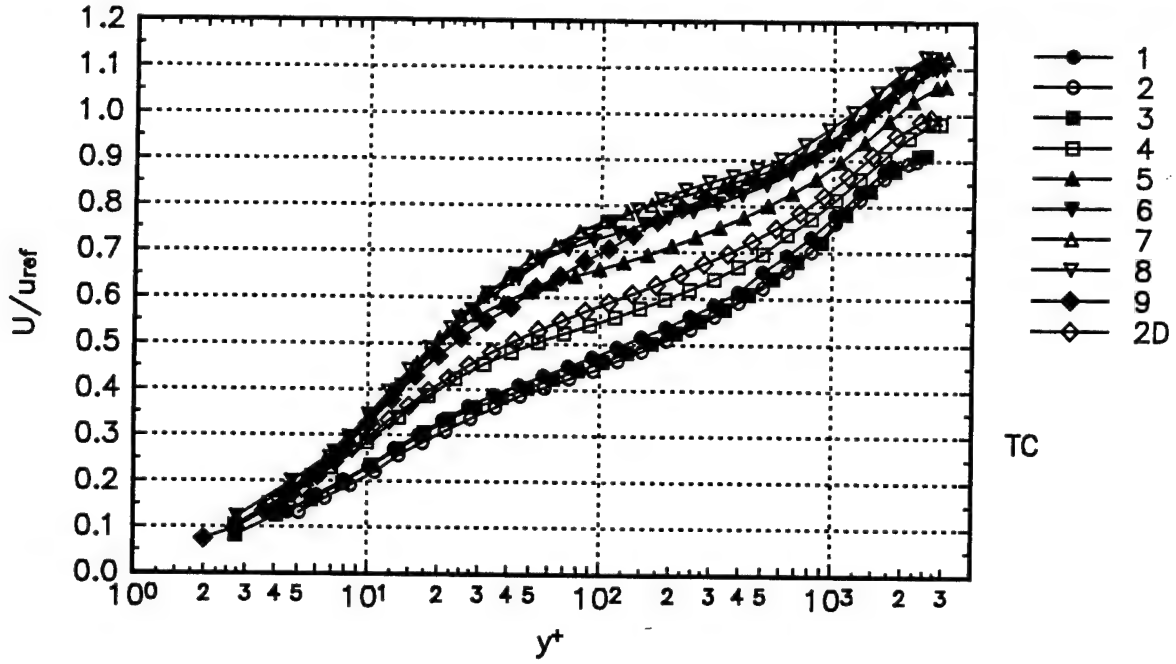

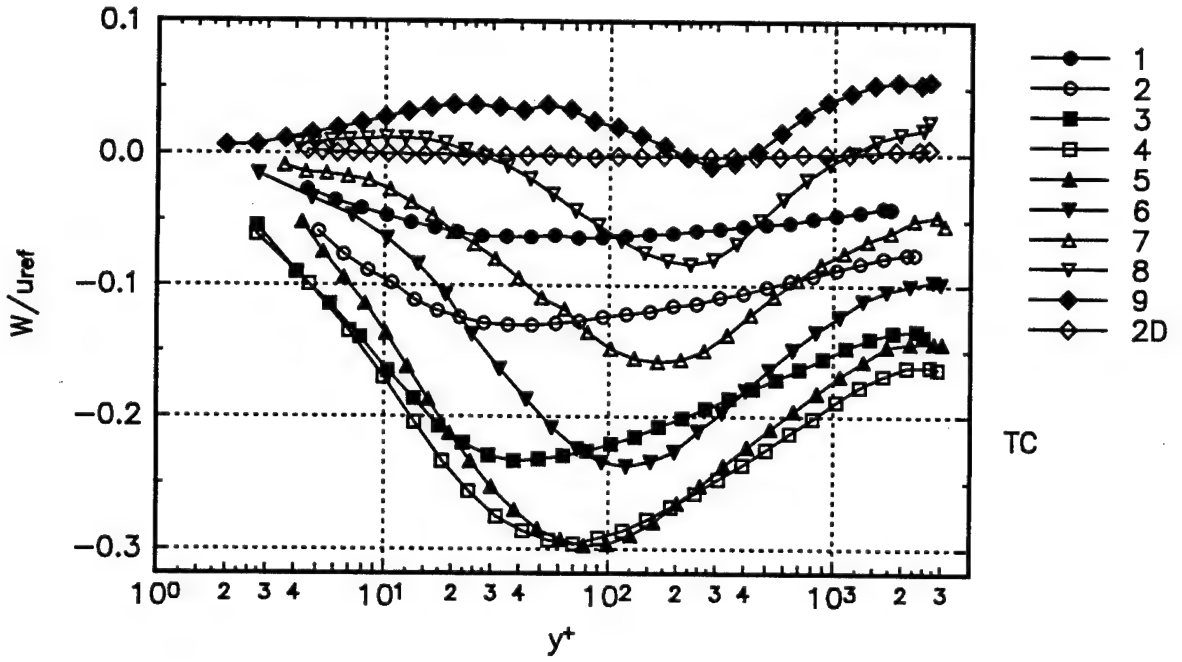

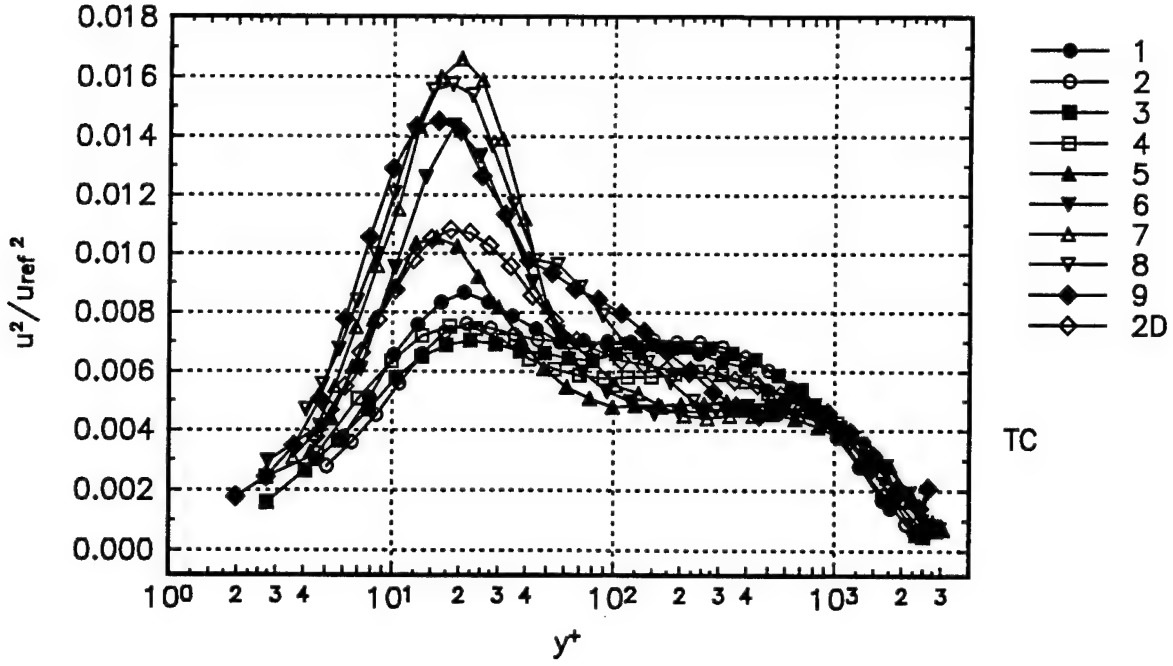
0.018
0.016
0.014
0.012
0.010
0.008
0.006
0.004
0.002
0.000
u²/Uref²
10⁰ 2 3 4 10¹ 2 3 4 10² 2 3 4 10³ 2 3
y+
1
2
3
4
5
6
7
8
9
2D
TC

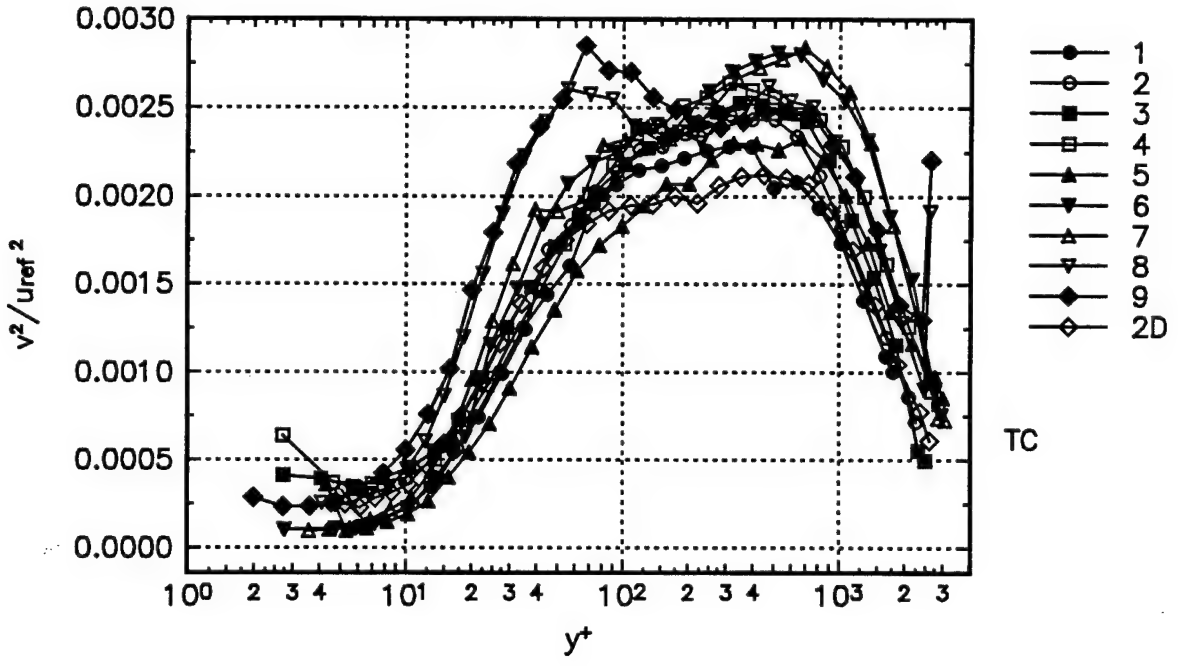
0.0030
0.0025
0.0020
0.0015
0.0010
0.0005
0.0000
v²/Uref²
10⁰ 2 3 4 10¹ 2 3 4 10² 2 3 4 10³ 2 3
y+
1
2
3
4
5
6
7
8
9
2D
TC

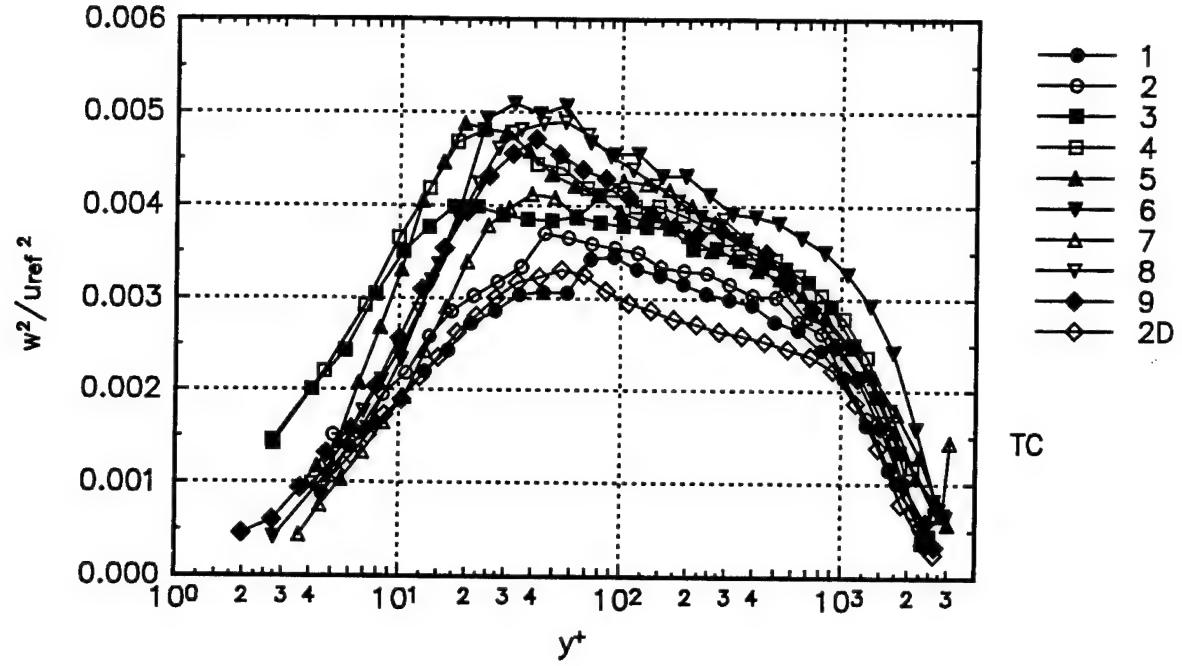
0.006
0.005
0.004
0.003
0.002
0.001
0.000
w²/Uref²
10⁰ 2 3 4 10¹ 2 3 4 10² 2 3 4 10³ 2 3
y+
1
2
3
4
5
6
7
8
9
2D
TC

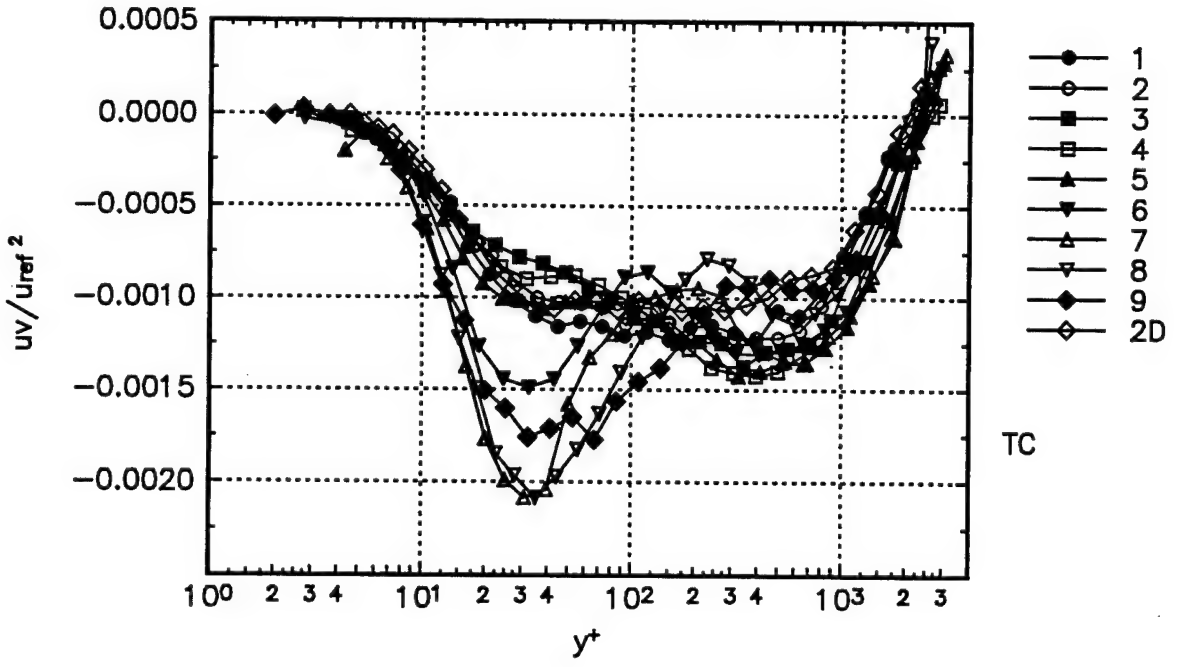
0.0005
0.0000
−0.0005
−0.0010
−0.0015
−0.0020
UV/Uref²
10⁰ 2 3 4 10¹ 2 3 4 10² 2 3 4 10³ 2 3
y+
1
2
3
4
5
6
7
8
9
2D
TC

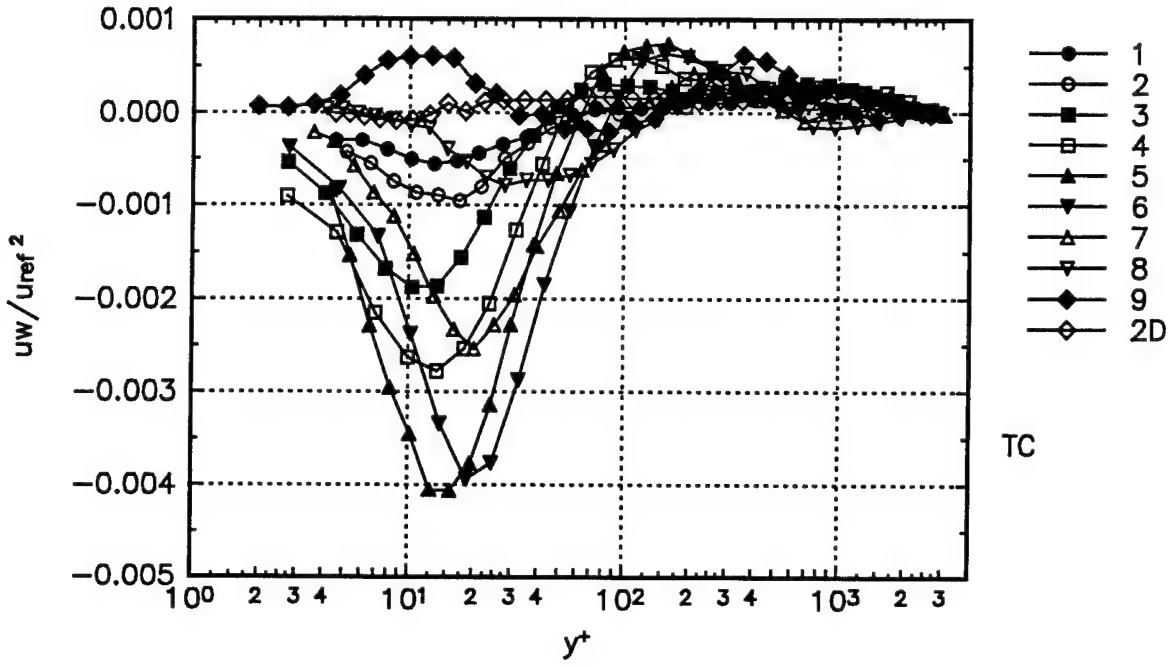
0.001
0.000
−0.001
−0.002
−0.003
−0.004
−0.005
UW/Uref 2
10^0 2 3 4 10^1 2 3 4 10^2 2 3 4 10^3 2 3
y+
1
2
3
4
5
6
7
8
9
2D
TC

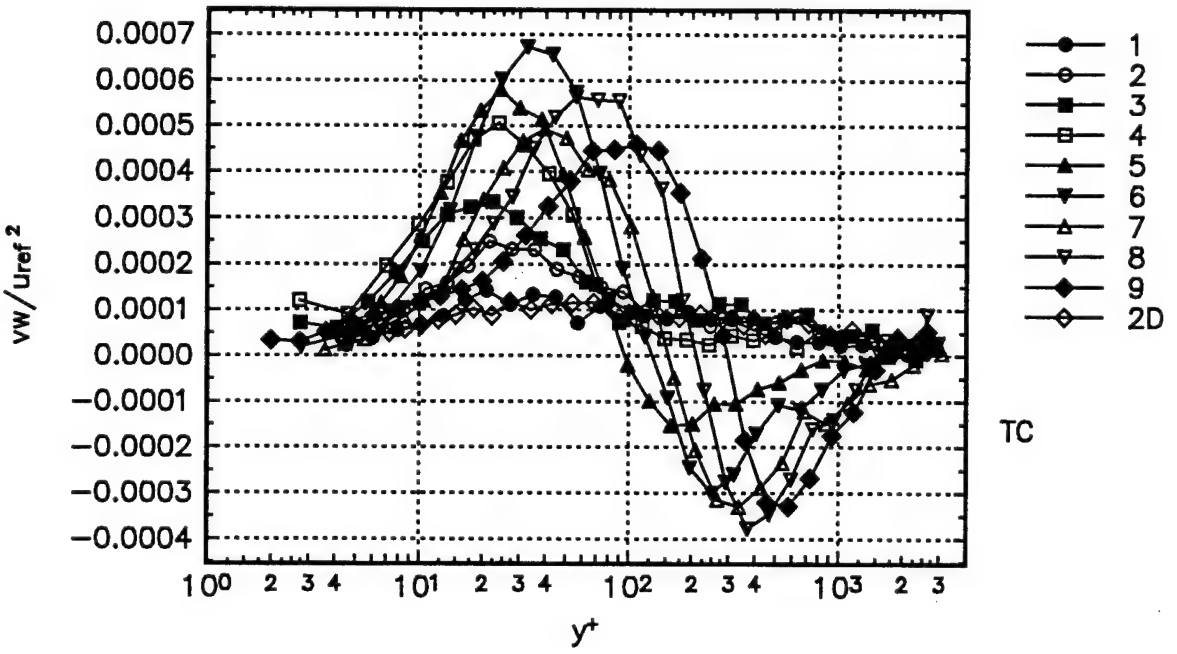
0.0007
0.0006
0.0005
0.0004
0.0003
0.0002
0.0001
0.0000
−0.0001
−0.0002
−0.0003
−0.0004
VW/Uref 2
10^0 2 3 4 10^1 2 3 4 10^2 2 3 4 10^3 2 3
y+
1
2
3
4
5
6
7
8
9
2D
TC

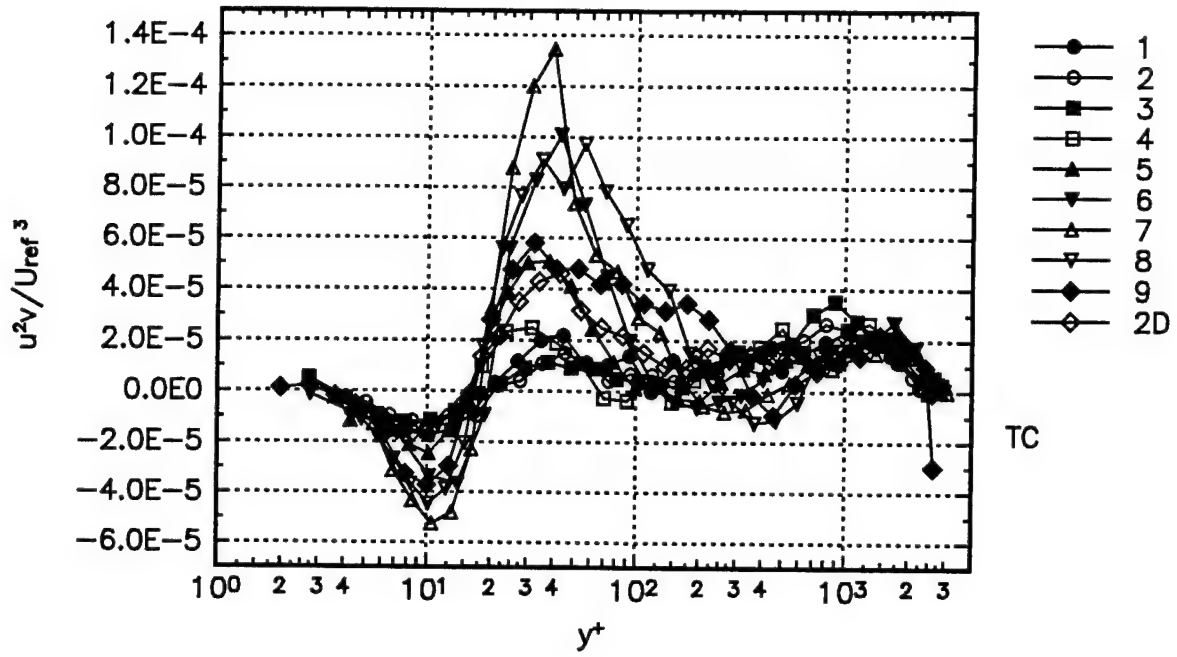
1.4E−4
1.2E−4
1.0E−4
8.0E−5
6.0E−5
4.0E−5
2.0E−5
0.0E0
−2.0E−5
−4.0E−5
−6.0E−5
u²v/Uref³
10⁰ 2 3 4 10¹ 2 3 4 10² 2 3 4 10³ 2 3
y+
1
2
3
4
5
6
7
8
9
2D
TC

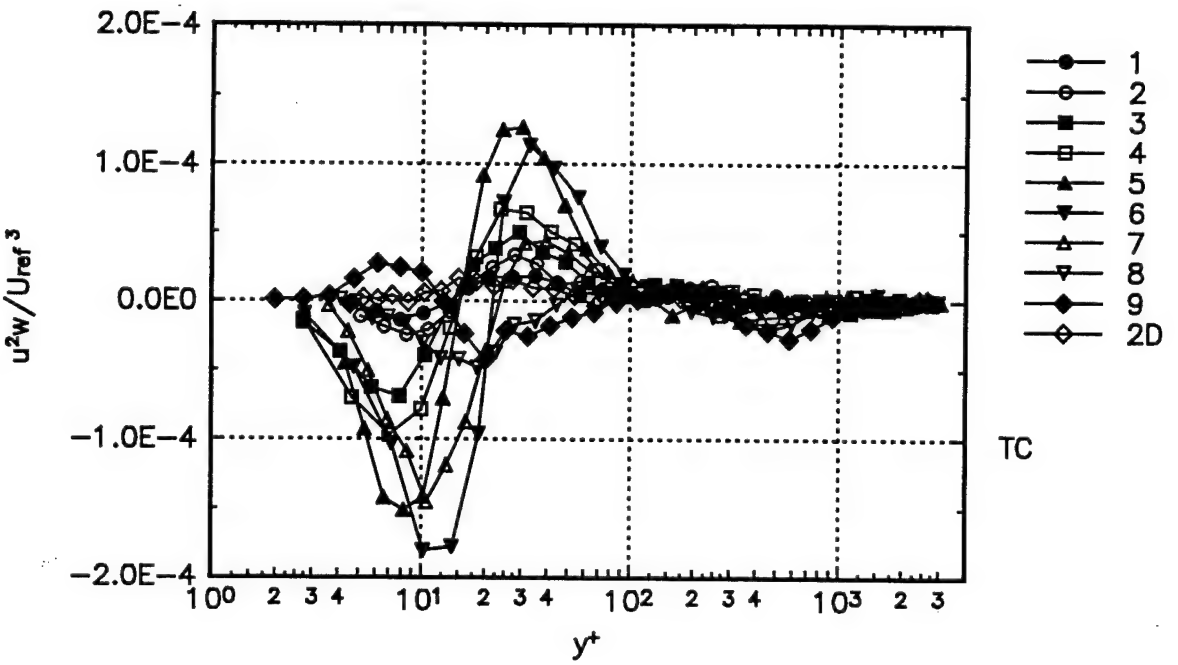
2.0E−4
1.0E−4
0.0E0
−1.0E−4
−2.0E−4
u²w/Uref³
10⁰ 2 3 4 10¹ 2 3 4 10² 2 3 4 10³ 2 3
y+
1
2
3
4
5
6
7
8
9
2D
TC

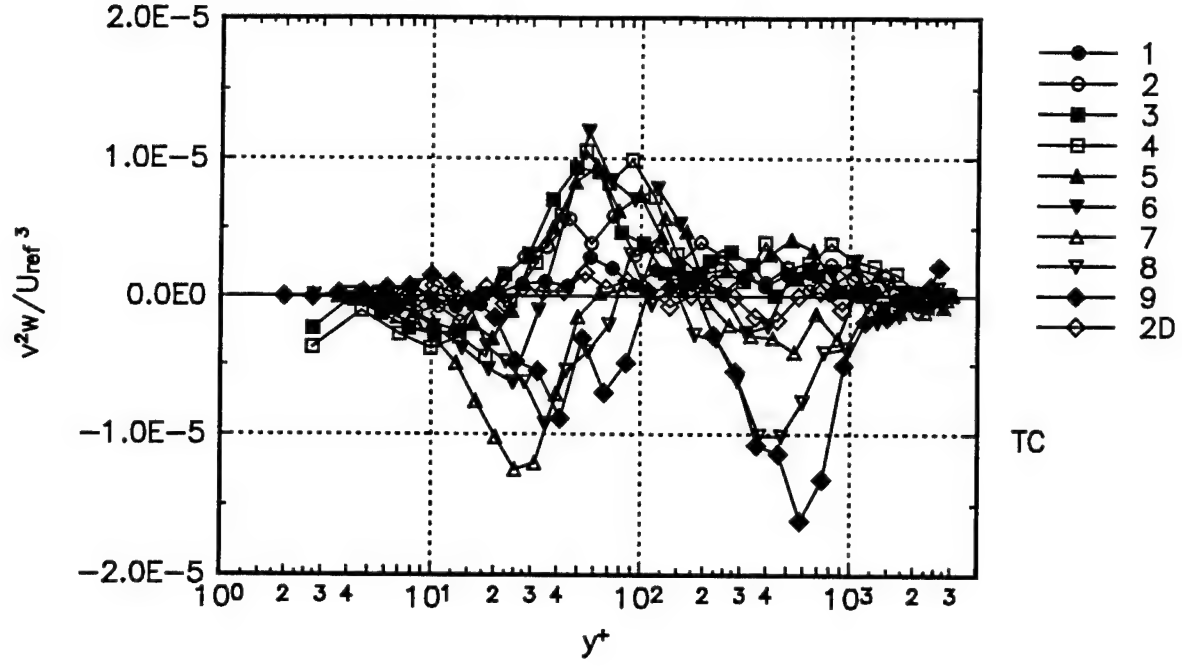
2.0E−5
1.0E−5
0.0E0
−1.0E−5
−2.0E−5
v^2w/U_{ref}^3
10^0 2 3 4 10^1 2 3 4 10^2 2 3 4 10^3 2 3
y^+
1
2
3
4
5
6
7
8
9
2D
TC

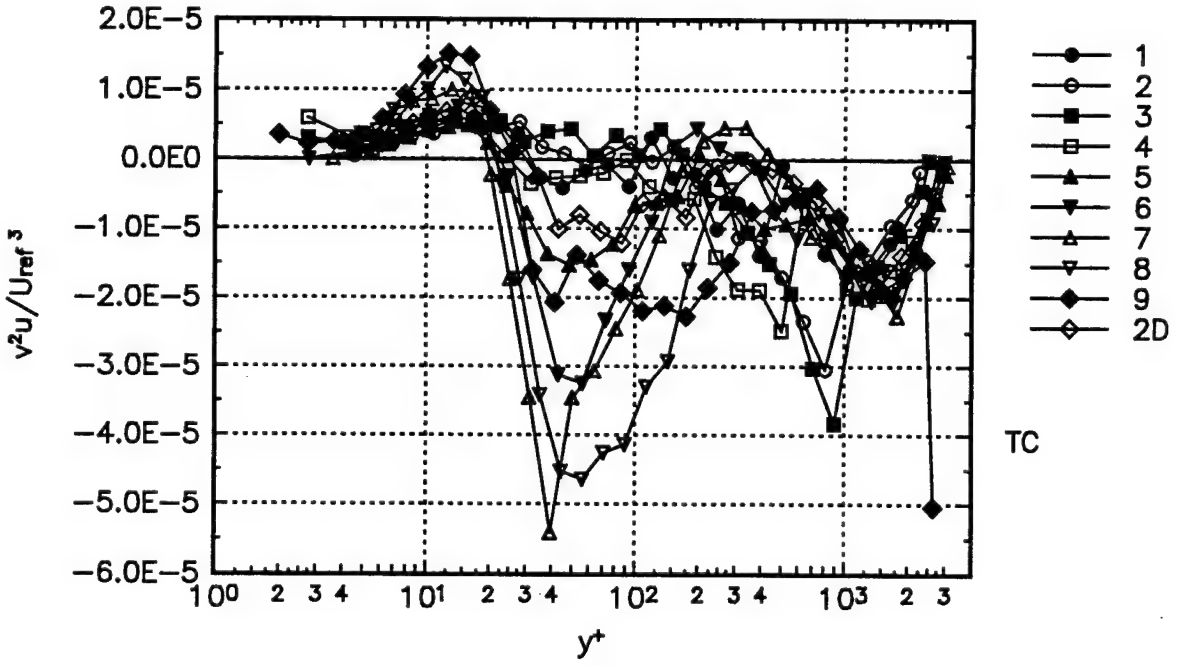
2.0E−5
1.0E−5
0.0E0
−1.0E−5
−2.0E−5
−3.0E−5
−4.0E−5
−5.0E−5
−6.0E−5
v^2u/U_{ref}^3
10^0 2 3 4 10^1 2 3 4 10^2 2 3 4 10^3 2 3
y^+
1
2
3
4
5
6
7
8
9
2D
TC

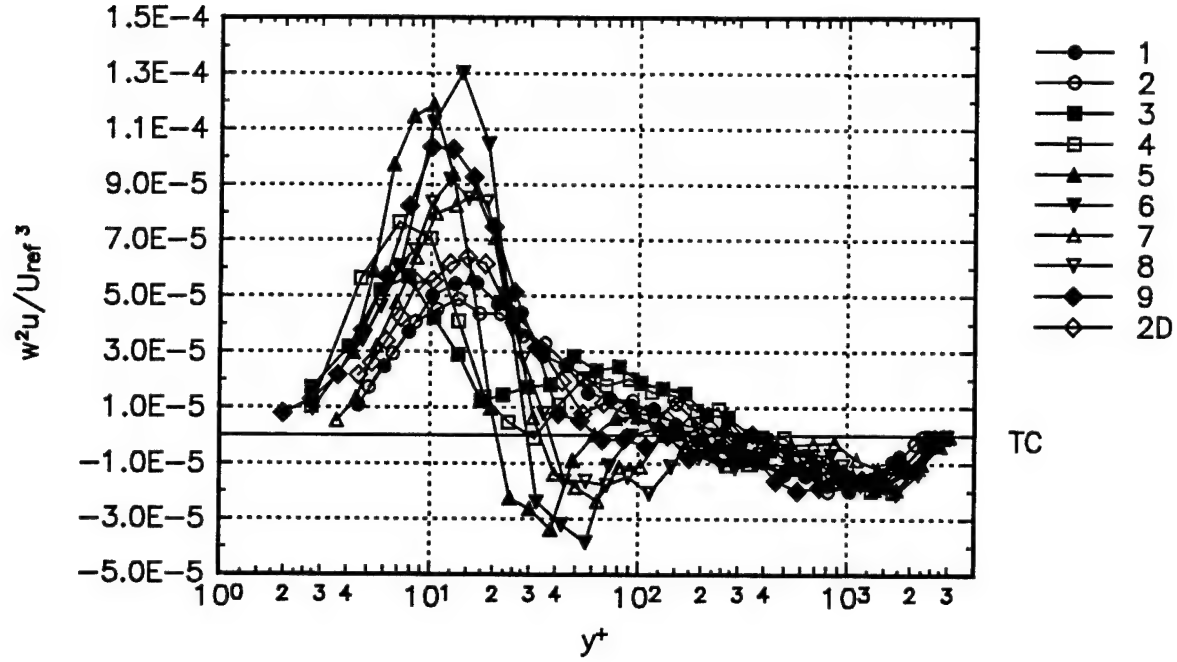
1.5E−4
1.3E−4
1.1E−4
9.0E−5
7.0E−5
5.0E−5
3.0E−5
1.0E−5
−1.0E−5
−3.0E−5
−5.0E−5
w²u/Uref³
10⁰ 2 3 4 10¹ 2 3 4 10² 2 3 4 10³ 2 3
y+
1
2
3
4
5
6
7
8
9
2D
TC

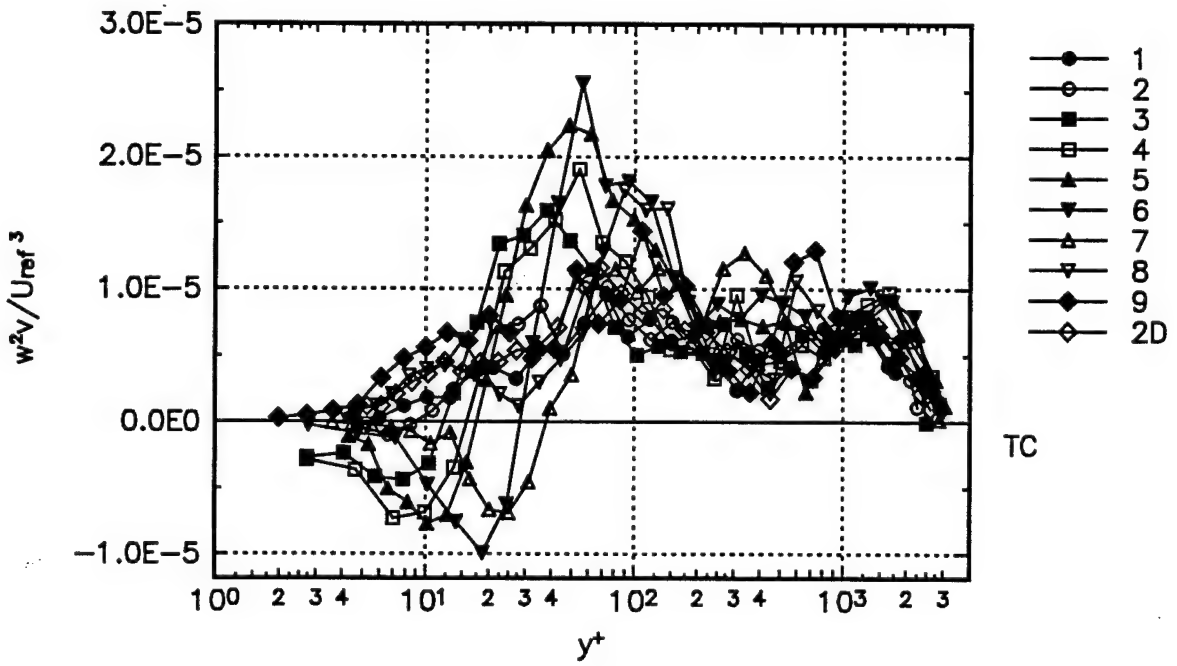
3.0E−5
2.0E−5
1.0E−5
0.0E0
−1.0E−5
w²v/Uref³
10⁰ 2 3 4 10¹ 2 3 4 10² 2 3 4 10³ 2 3
y+
1
2
3
4
5
6
7
8
9
2D
TC

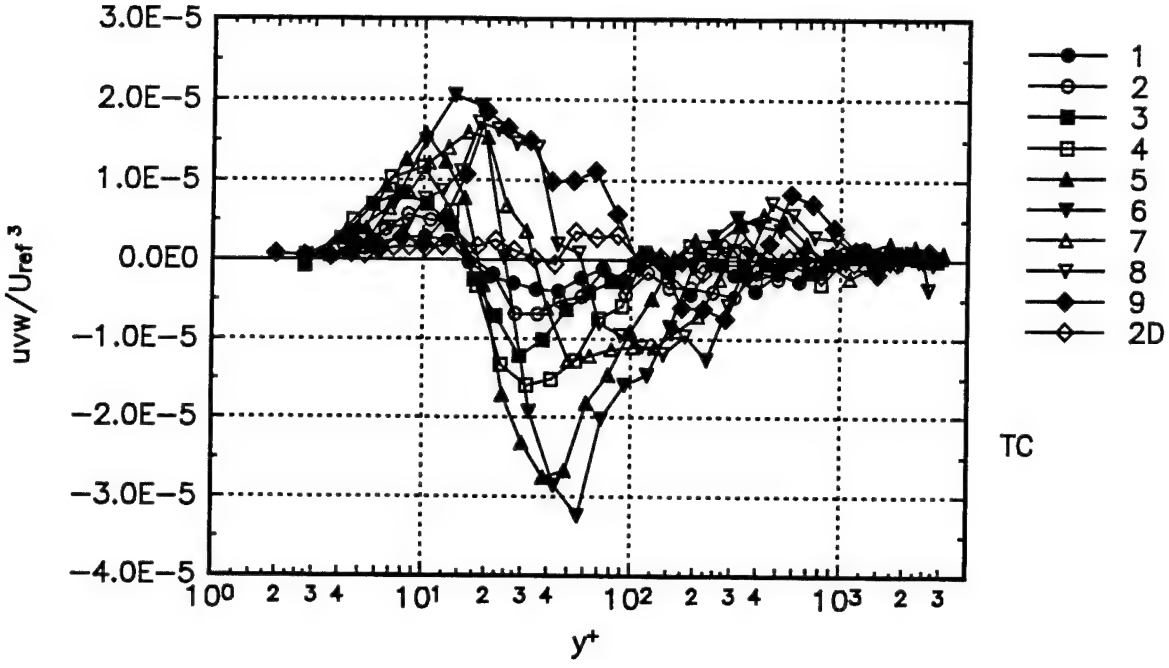
3.0E−5
2.0E−5
1.0E−5
0.0E0
−1.0E−5
−2.0E−5
−3.0E−5
−4.0E−5
uvw/Uref 3
100 2 3 4 101 2 3 4 102 2 3 4 103 2 3
y+
1
2
3
4
5
6
7
8
9
2D
TC

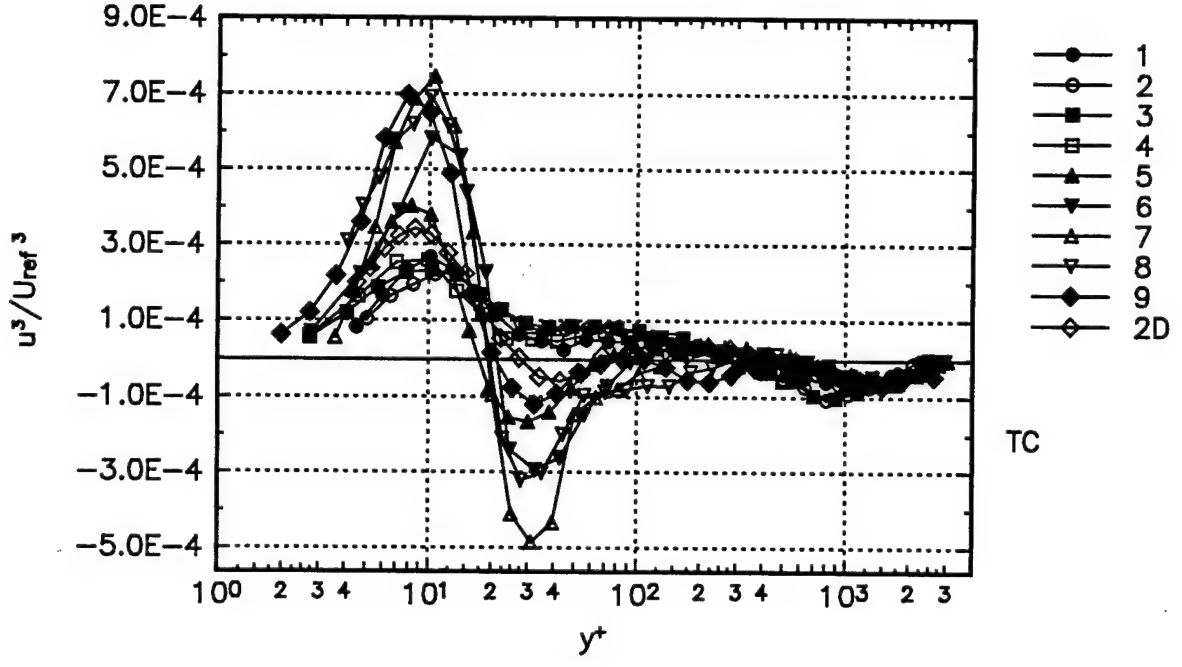
9.0E−4
7.0E−4
5.0E−4
3.0E−4
1.0E−4
−1.0E−4
−3.0E−4
−5.0E−4
u3/Uref 3
100 2 3 4 101 2 3 4 102 2 3 4 103 2 3
y+
1
2
3
4
5
6
7
8
9
2D
TC

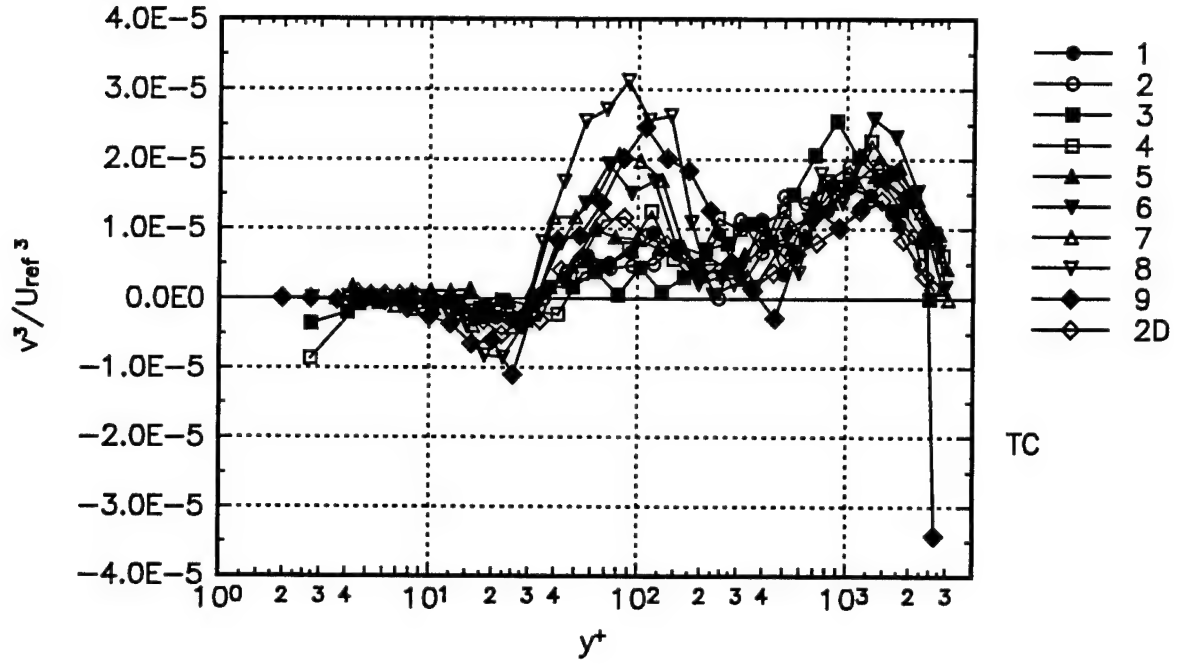
4.0E−5
3.0E−5
2.0E−5
1.0E−5
0.0E0
−1.0E−5
−2.0E−5
−3.0E−5
−4.0E−5
v³/Uref³
10⁰ 2 3 4 10¹ 2 3 4 10² 2 3 4 10³ 2 3
y+
1
2
3
4
5
6
7
8
9
2D
TC

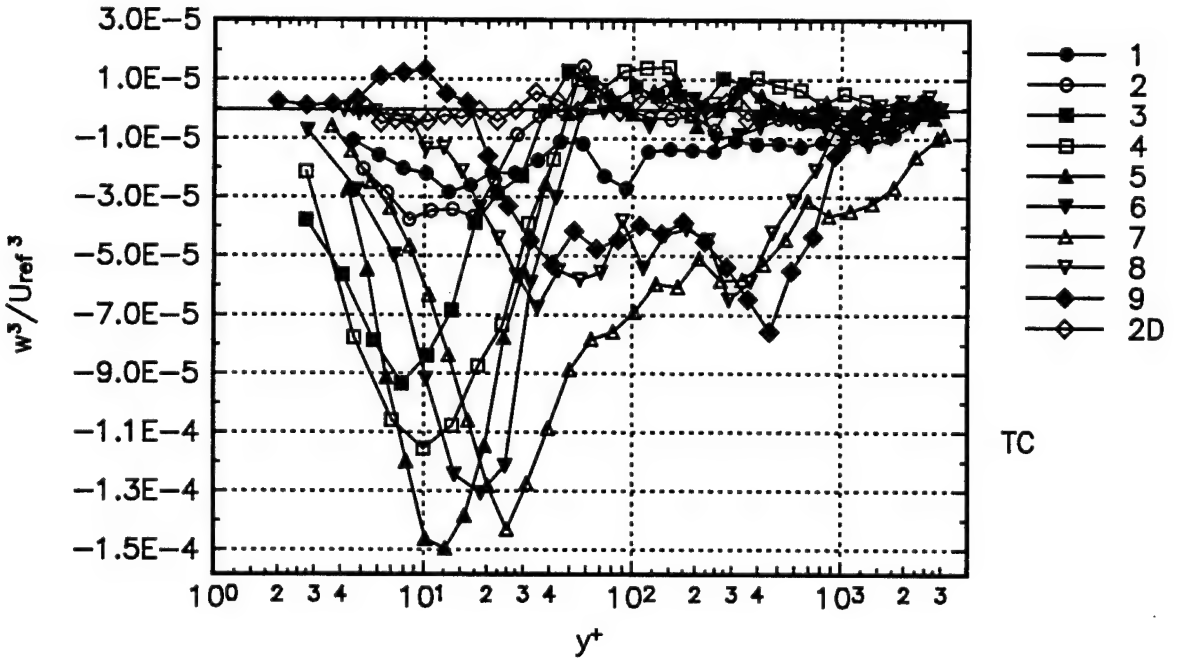
3.0E−5
1.0E−5
−1.0E−5
−3.0E−5
−5.0E−5
−7.0E−5
−9.0E−5
−1.1E−4
−1.3E−4
−1.5E−4
w³/Uref³
10⁰ 2 3 4 10¹ 2 3 4 10² 2 3 4 10³ 2 3
y+
1
2
3
4
5
6
7
8
9
2D
TC

Correlation coefficient form of the second and third order products in tunnel coordinates.

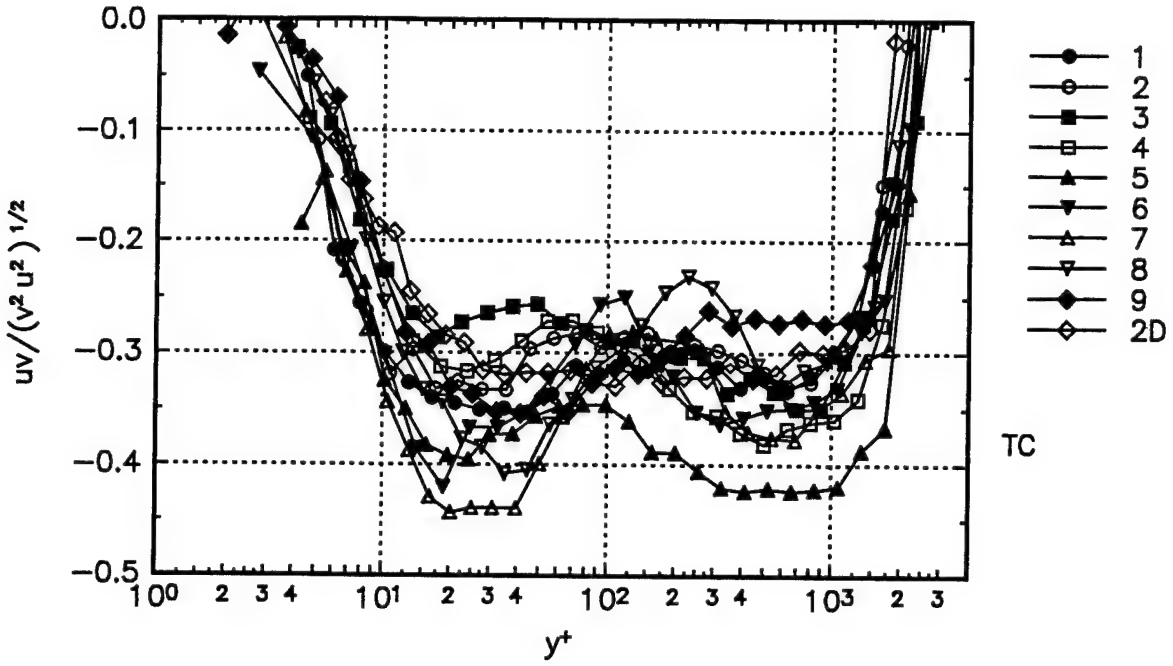

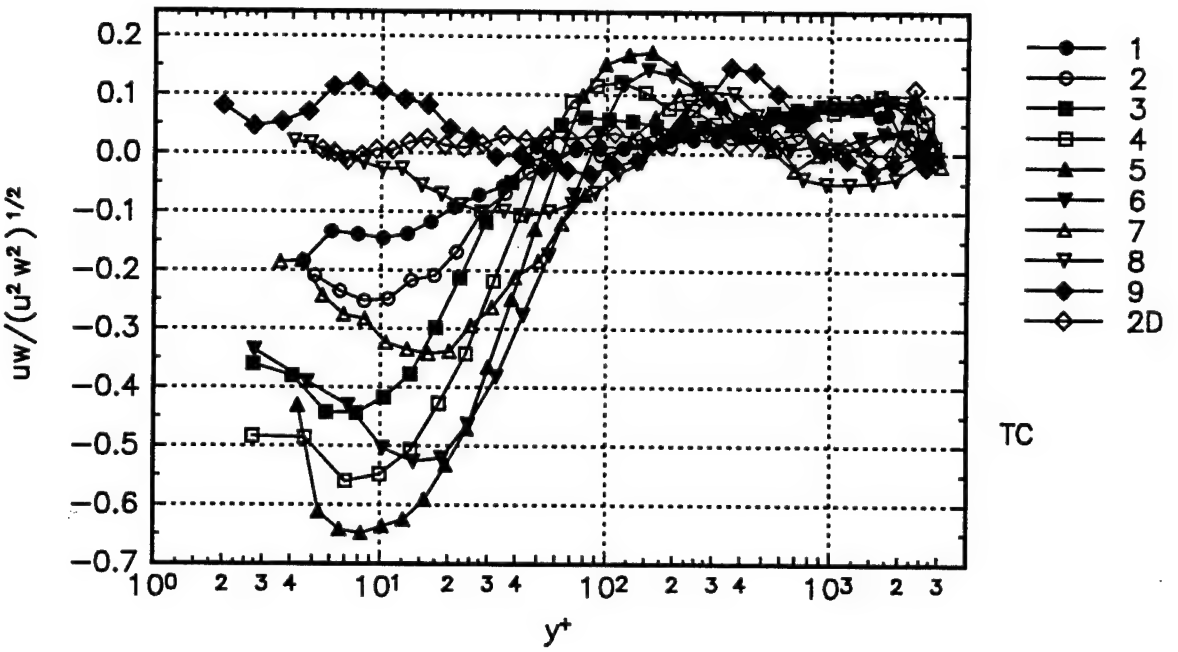

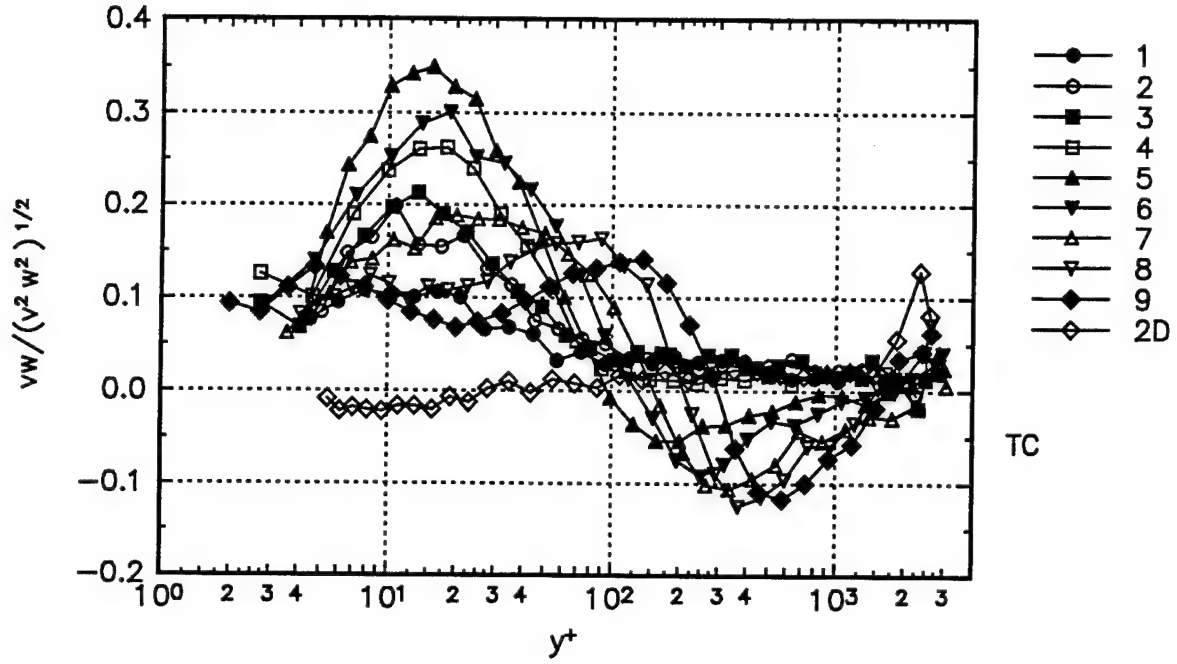
0.4
0.3
0.2
0.1
0.0
−0.1
−0.2
10^0 2 3 4 10^1 2 3 4 10^2 2 3 4 10^3 2 3
y^+
$vw/(v^2 w^2)^{1/2}$
1
2
3
4
5
6
7
8
9
2D
TC

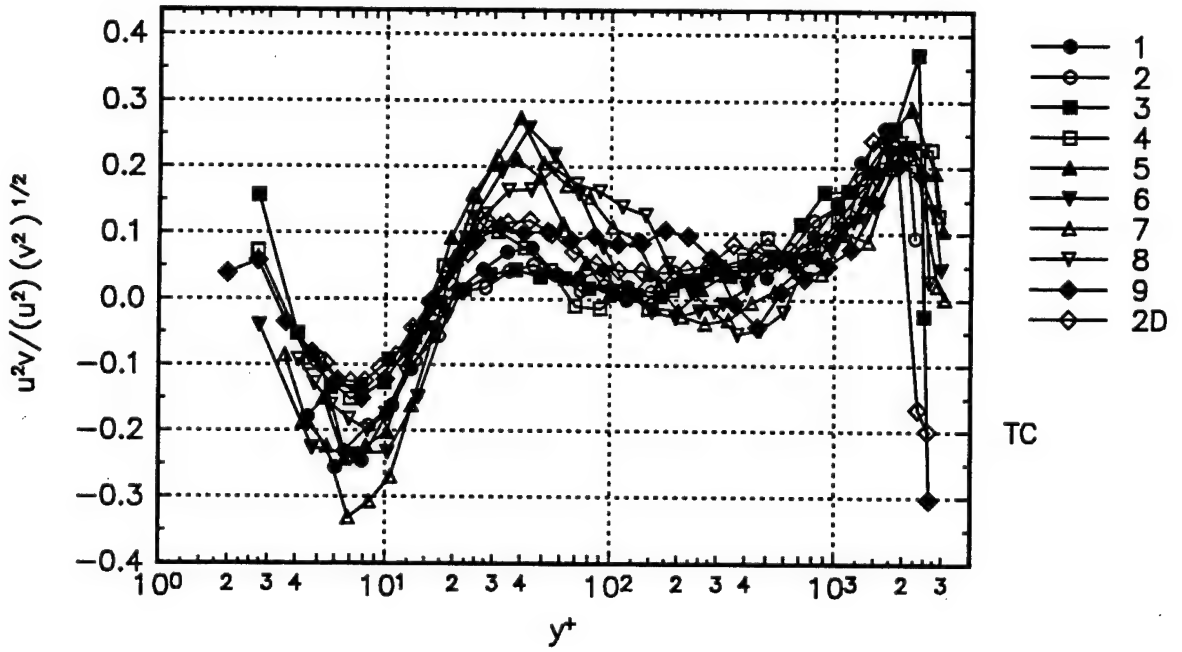
0.4
0.3
0.2
0.1
0.0
−0.1
−0.2
−0.3
−0.4
10^0 2 3 4 10^1 2 3 4 10^2 2 3 4 10^3 2 3
y^+
$u^2v/(u^2)(v^2)^{1/2}$
1
2
3
4
5
6
7
8
9
2D
TC

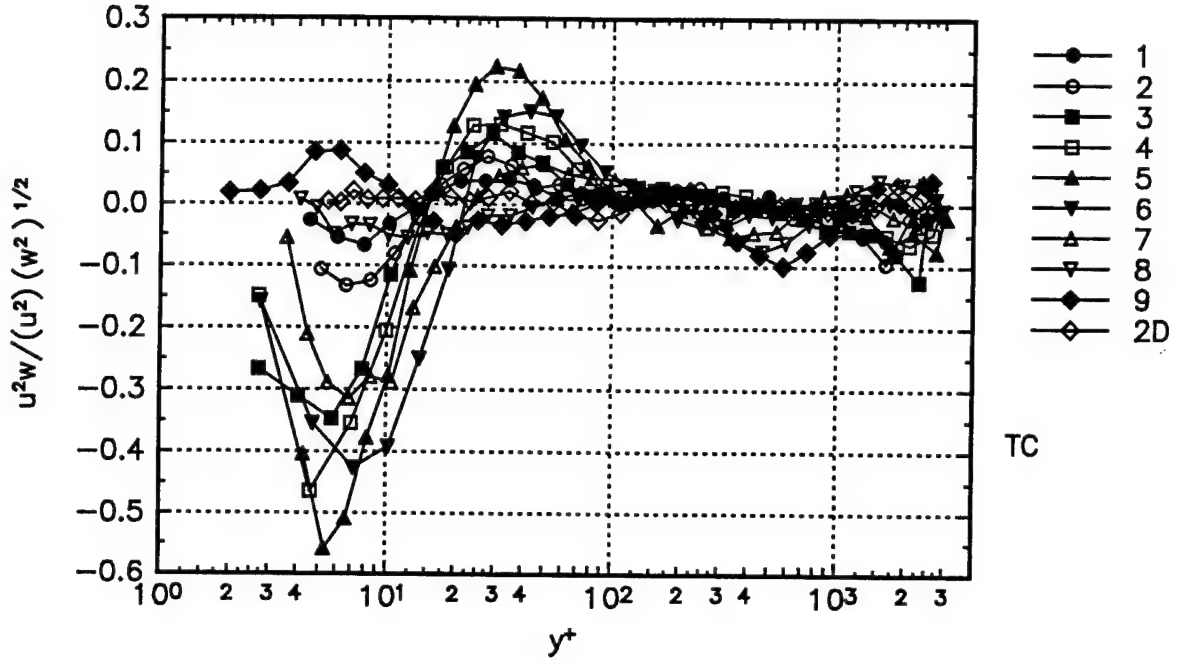
0.3
0.2
0.1
0.0
−0.1
−0.2
−0.3
−0.4
−0.5
−0.6
$u^2w/(u^2)(w^2)^{1/2}$
10^0 2 3 4 10^1 2 3 4 10^2 2 3 4 10^3 2 3
y^+
1
2
3
4
5
6
7
8
9
2D
TC

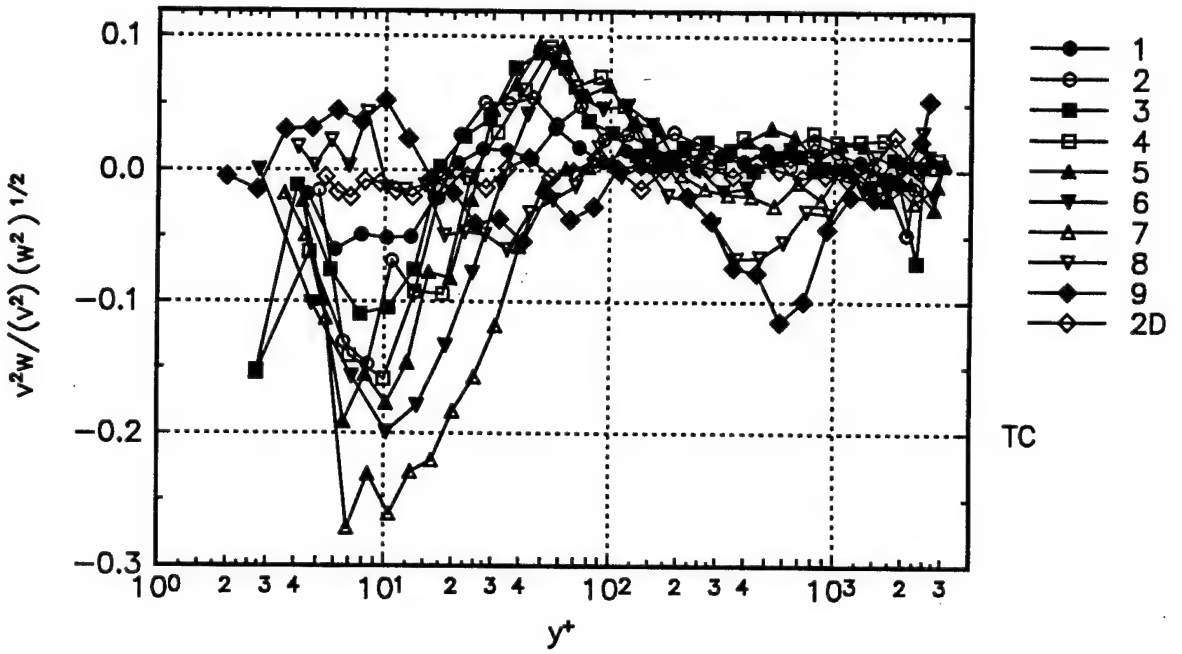
0.1
0.0
−0.1
−0.2
−0.3
$v^2w/(v^2)(w^2)^{1/2}$
10^0 2 3 4 10^1 2 3 4 10^2 2 3 4 10^3 2 3
y^+
1
2
3
4
5
6
7
8
9
2D
TC

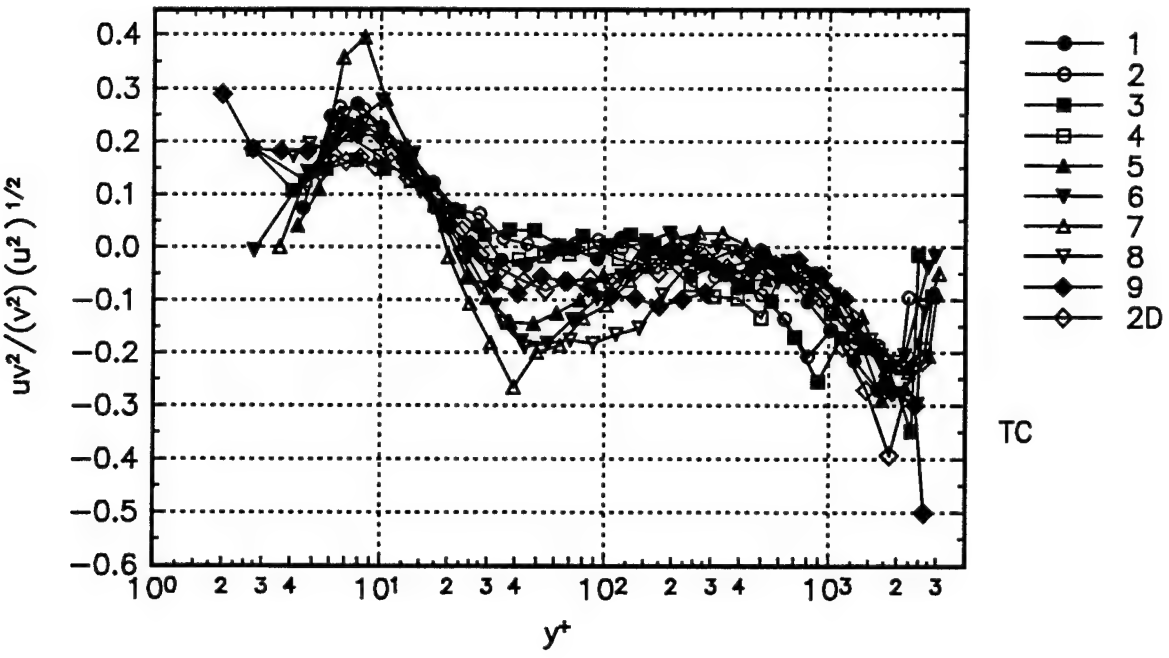
0.4
0.3
0.2
0.1
0.0
−0.1
−0.2
−0.3
−0.4
−0.5
−0.6
$uv^2/(v^2)\,(u^2)^{1/2}$
10^0 2 3 4 10^1 2 3 4 10^2 2 3 4 10^3 2 3
y^+
1
2
3
4
5
6
7
8
9
2D
TC

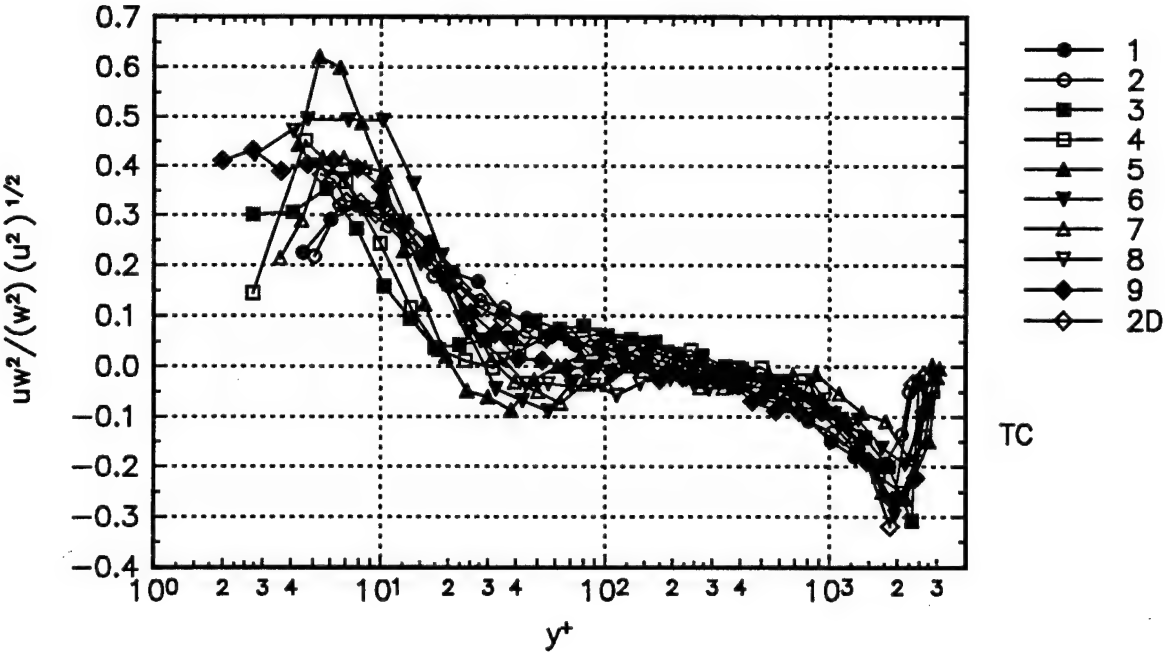
0.7
0.6
0.5
0.4
0.3
0.2
0.1
0.0
−0.1
−0.2
−0.3
−0.4
$uw^2/(w^2)\,(u^2)^{1/2}$
10^0 2 3 4 10^1 2 3 4 10^2 2 3 4 10^3 2 3
y^+
1
2
3
4
5
6
7
8
9
2D
TC

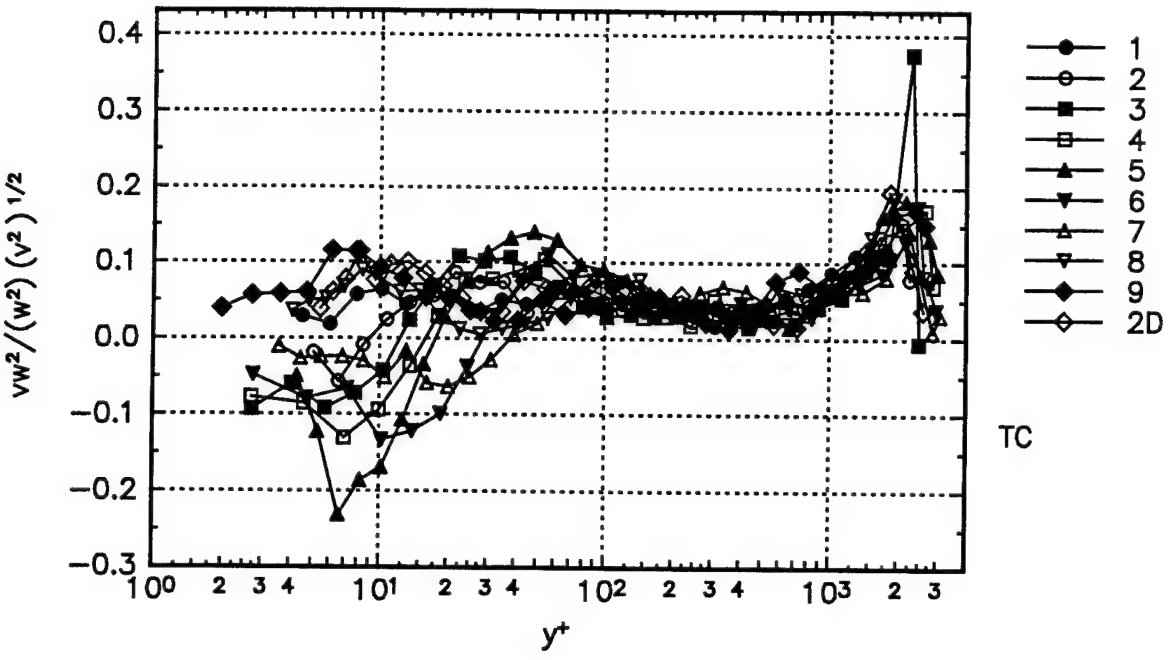
0.4
0.3
0.2
0.1
0.0
−0.1
−0.2
−0.3
$vw^2/(w^2)(v^2)^{1/2}$
10^0 2 3 4 10^1 2 3 4 10^2 2 3 4 10^3 2 3
y^+
1
2
3
4
5
6
7
8
9
2D
TC

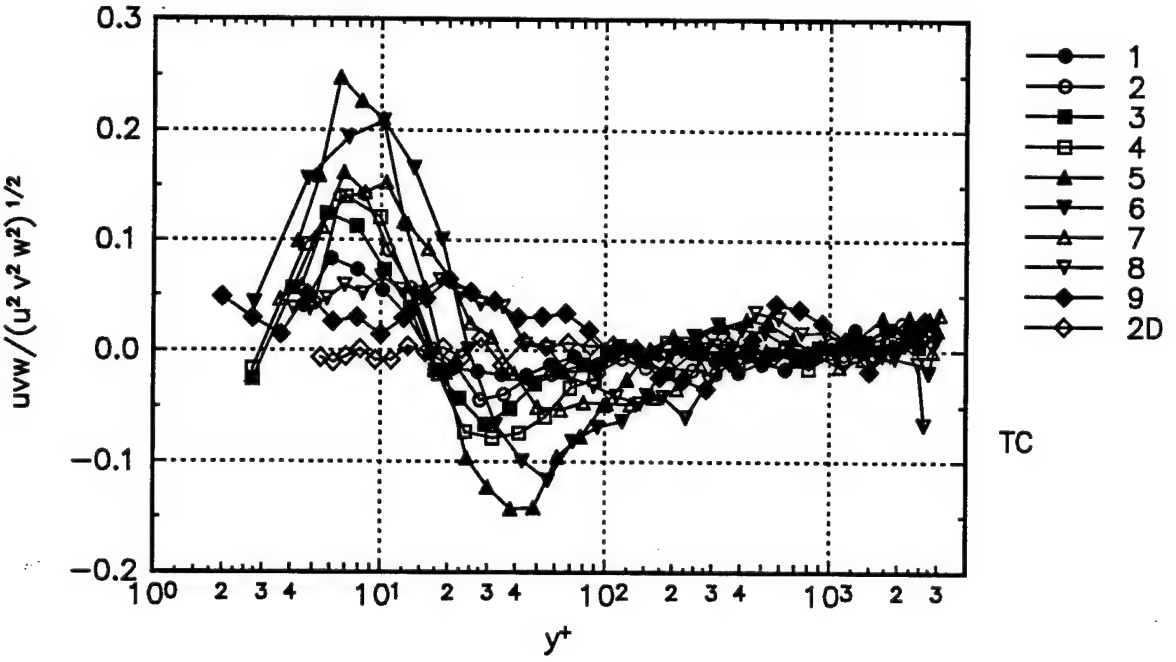
0.3
0.2
0.1
0.0
−0.1
−0.2
$uvw/(u^2v^2w^2)^{1/2}$
10^0 2 3 4 10^1 2 3 4 10^2 2 3 4 10^3 2 3
y^+
1
2
3
4
5
6
7
8
9
2D
TC

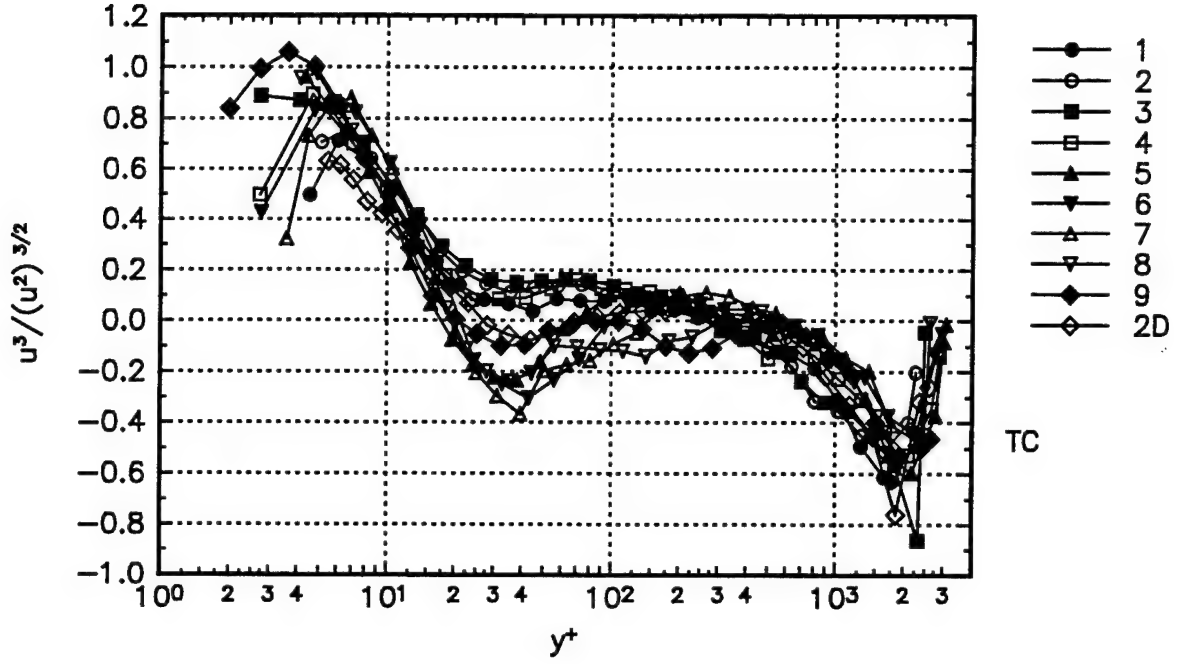
1.2
1.0
0.8
0.6
0.4
0.2
0.0
−0.2
−0.4
−0.6
−0.8
−1.0
$u^3/(u^2)^{3/2}$
10^0 2 3 4 10^1 2 3 4 10^2 2 3 4 10^3 2 3
y^+
1
2
3
4
5
6
7
8
9
2D
TC

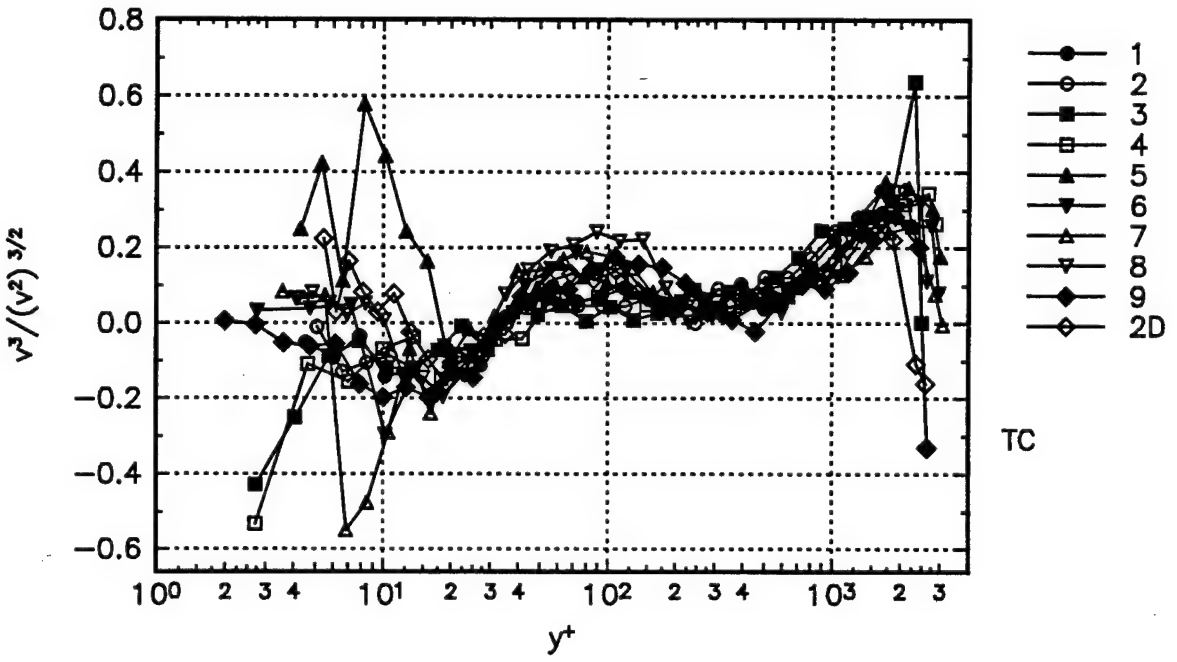
0.8
0.6
0.4
0.2
0.0
−0.2
−0.4
−0.6
$v^3/(v^2)^{3/2}$
10^0 2 3 4 10^1 2 3 4 10^2 2 3 4 10^3 2 3
y^+
1
2
3
4
5
6
7
8
9
2D
TC

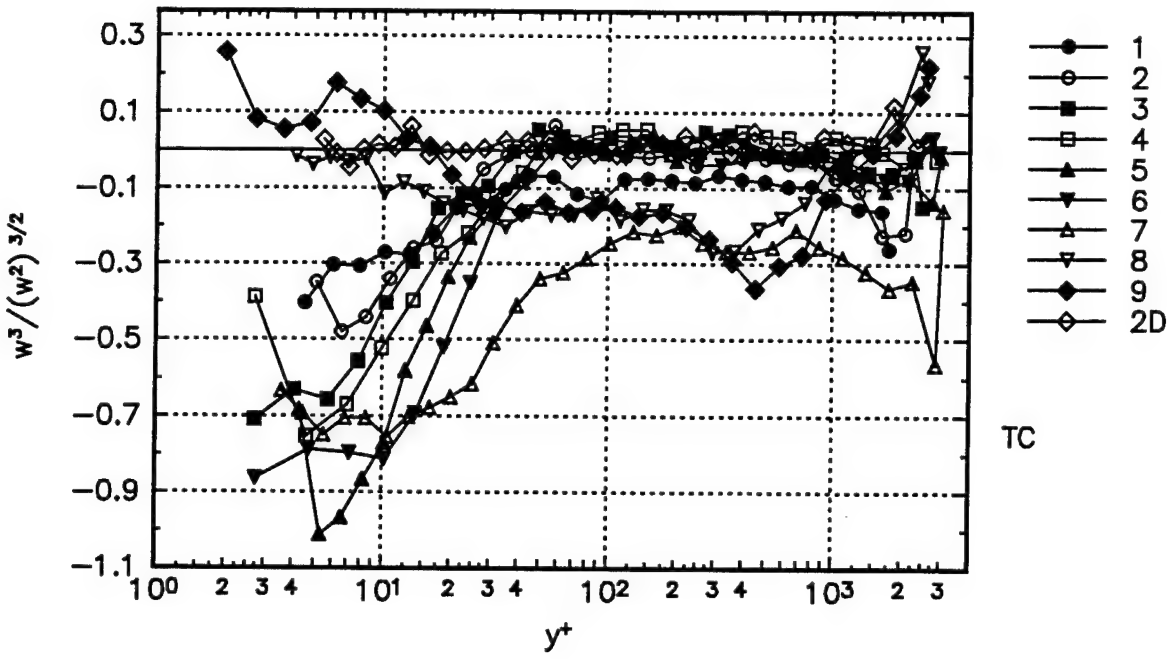
0.3
0.1
−0.1
−0.3
−0.5
−0.7
−0.9
−1.1
$w^3/(w^2)^{3/2}$
10^0 2 3 4 10^1 2 3 4 10^2 2 3 4 10^3 2 3
y^+
1
2
3
4
5
6
7
8
9
2D
TC

Appendix C: Free-stream Coordinates

In this Appendix the data are presented in free-stream coordinates coordinates. The "x" coordinate direction of the free-stream coordinates is in the direction of the flow at the outer edge of the boundary layer, "y" coordinate is perpendicular to the wall and the "z" axis completes a right handed coordinate system. The mean velocity, Reynolds' stresses and triple products are nondimensionalized with the relative powers of U_{ref}. Also in this Appendix the correlation coefficient form of the second and third order velocity products are presented.

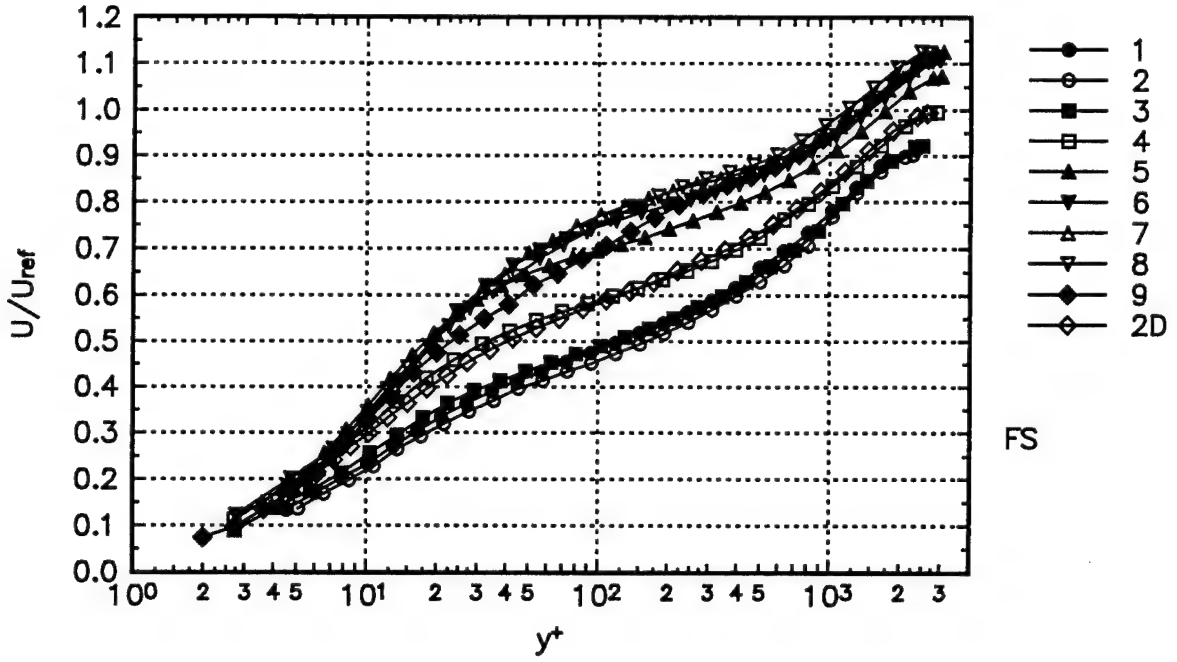

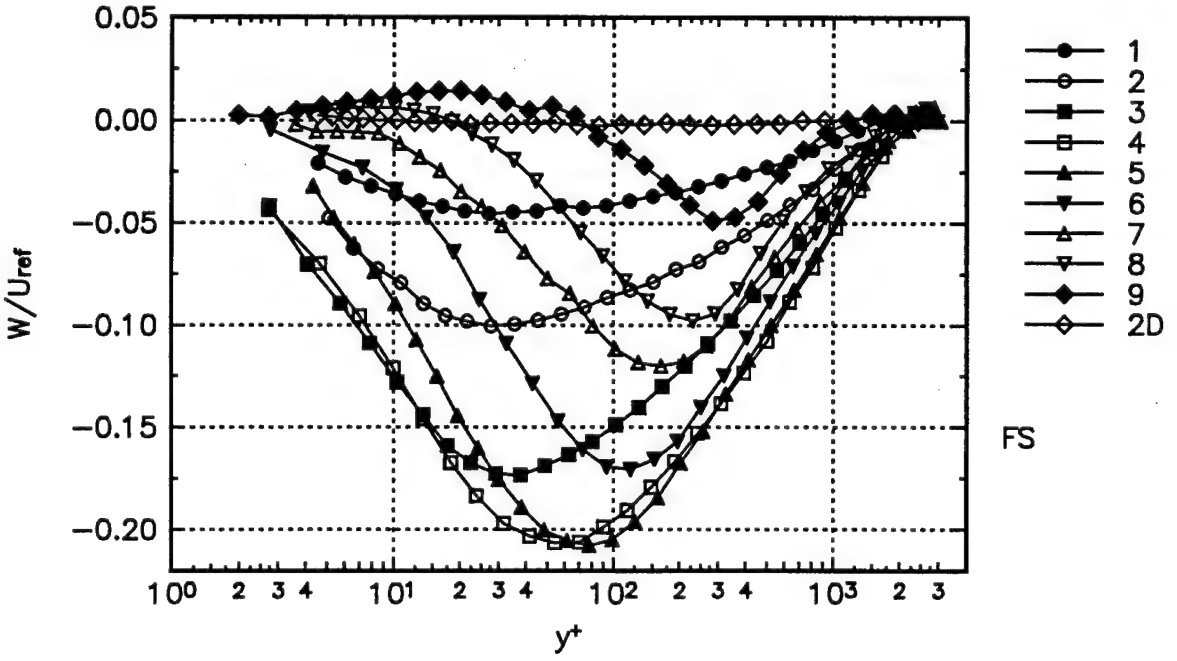

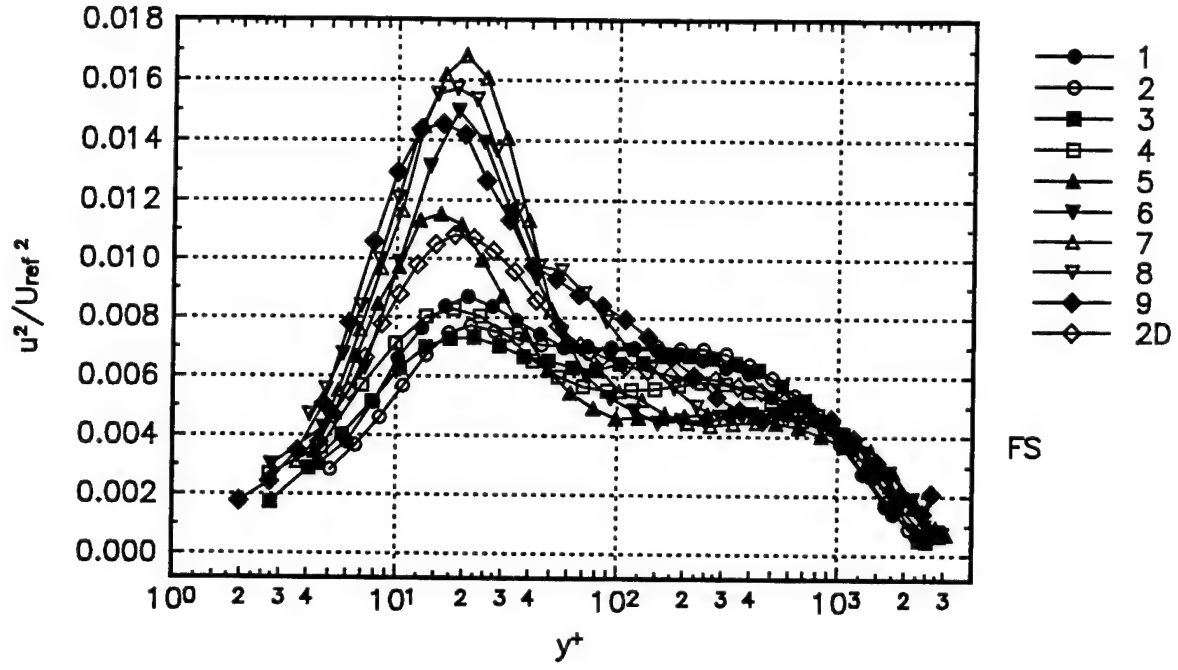
0.018
0.016
0.014
0.012
0.010
0.008
0.006
0.004
0.002
0.000
u²/Uref²
10⁰ 2 3 4 10¹ 2 3 4 10² 2 3 4 10³ 2 3
y+
1
2
3
4
5
6
7
8
9
2D
FS

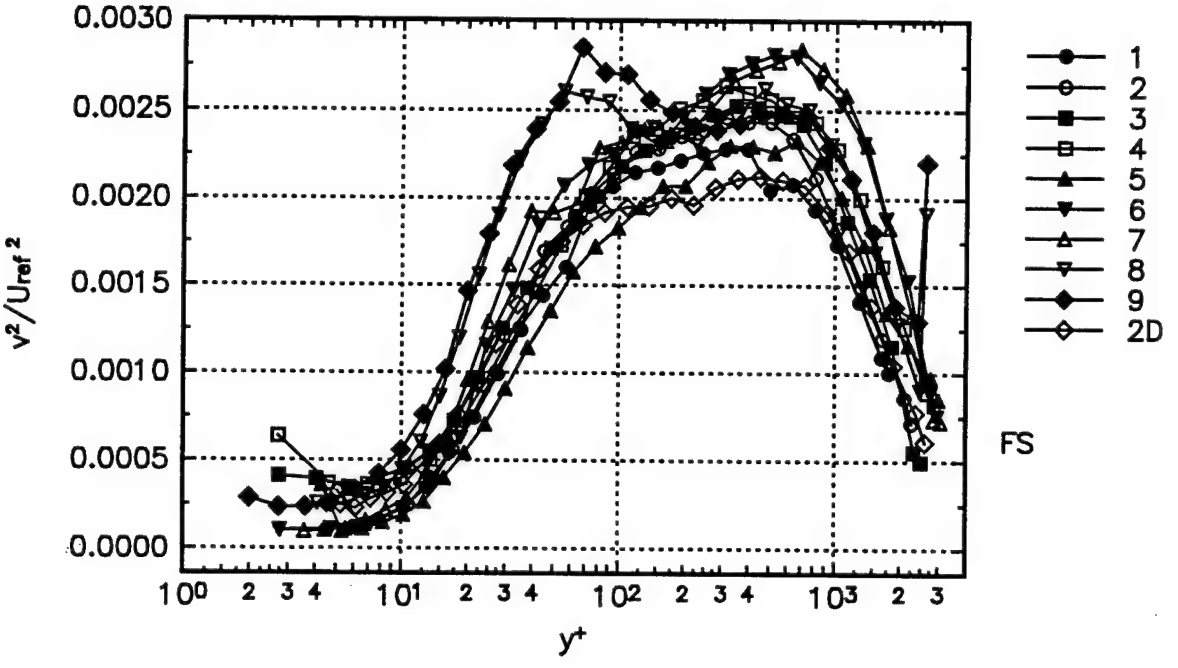
0.0030
0.0025
0.0020
0.0015
0.0010
0.0005
0.0000
v²/Uref²
10⁰ 2 3 4 10¹ 2 3 4 10² 2 3 4 10³ 2 3
y+
1
2
3
4
5
6
7
8
9
2D
FS

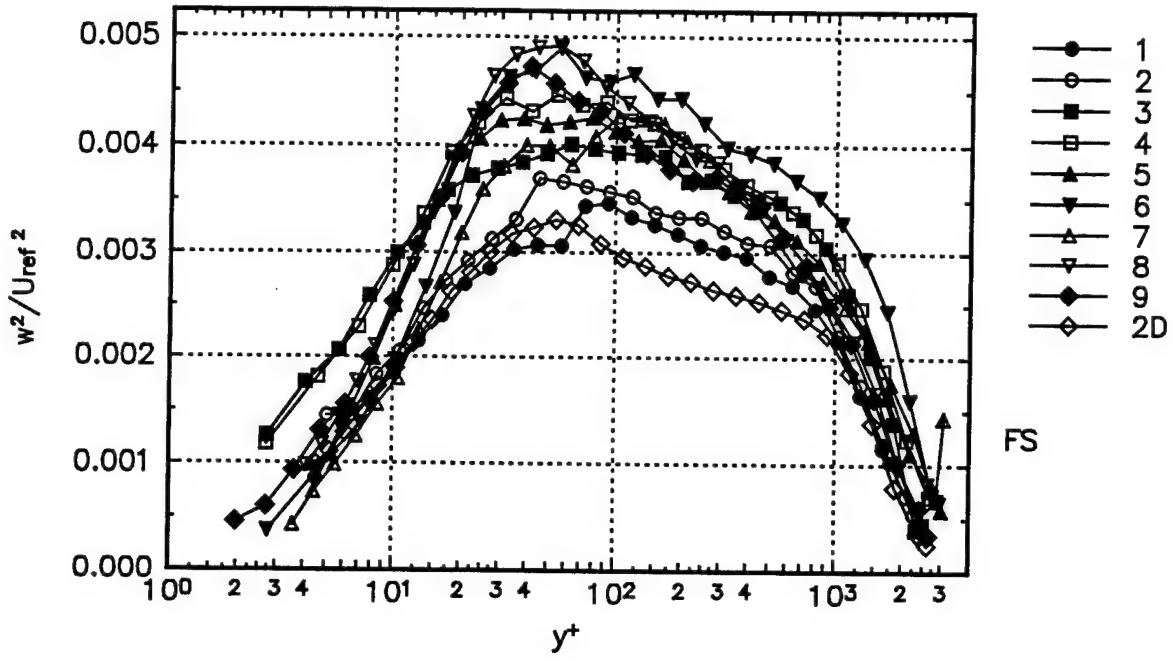
0.005
0.004
0.003
0.002
0.001
0.000
w^2/U_{ref}^2
10^0 2 3 4 10^1 2 3 4 10^2 2 3 4 10^3 2 3
y^+
1
2
3
4
5
6
7
8
9
2D
FS

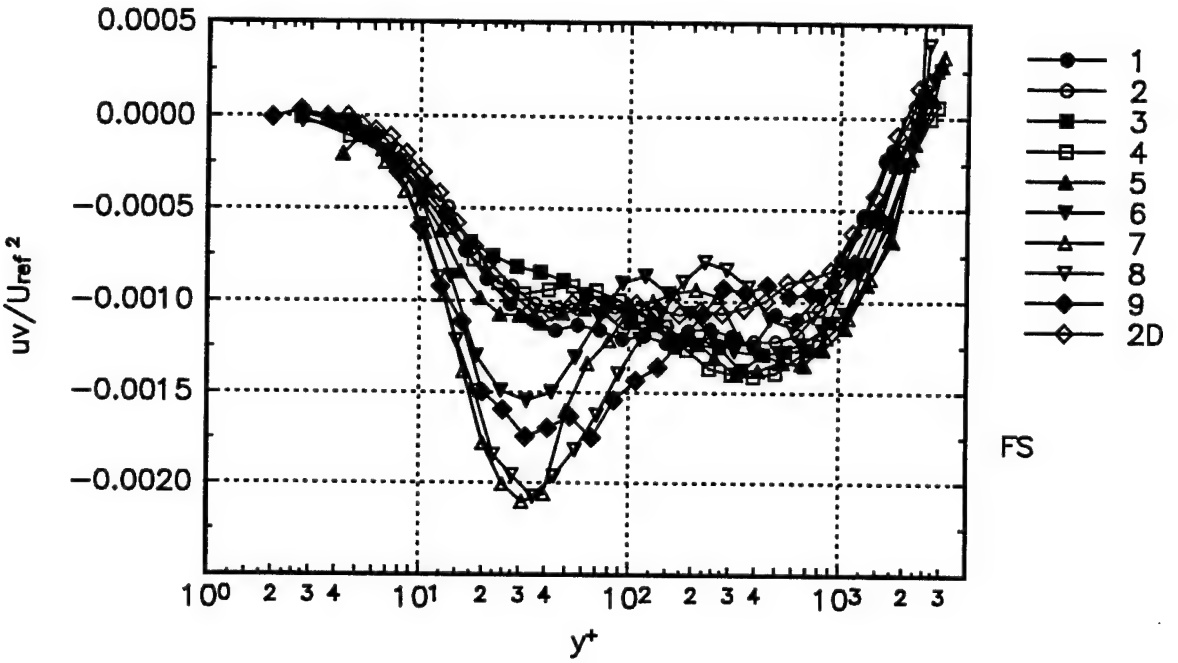
0.0005
0.0000
−0.0005
−0.0010
−0.0015
−0.0020
uv/U_{ref}^2
10^0 2 3 4 10^1 2 3 4 10^2 2 3 4 10^3 2 3
y^+
1
2
3
4
5
6
7
8
9
2D
FS

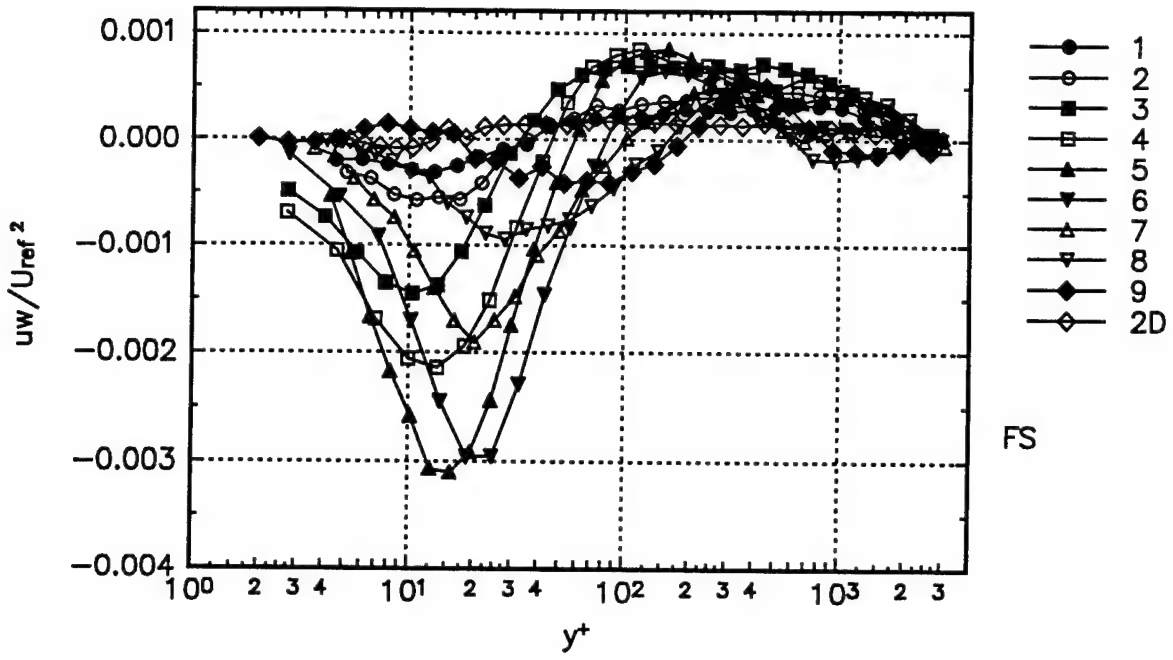
0.001
0.000
−0.001
−0.002
−0.003
−0.004
uw/Uref 2
10^0 2 3 4 10^1 2 3 4 10^2 2 3 4 10^3 2 3
y+
1
2
3
4
5
6
7
8
9
2D
FS

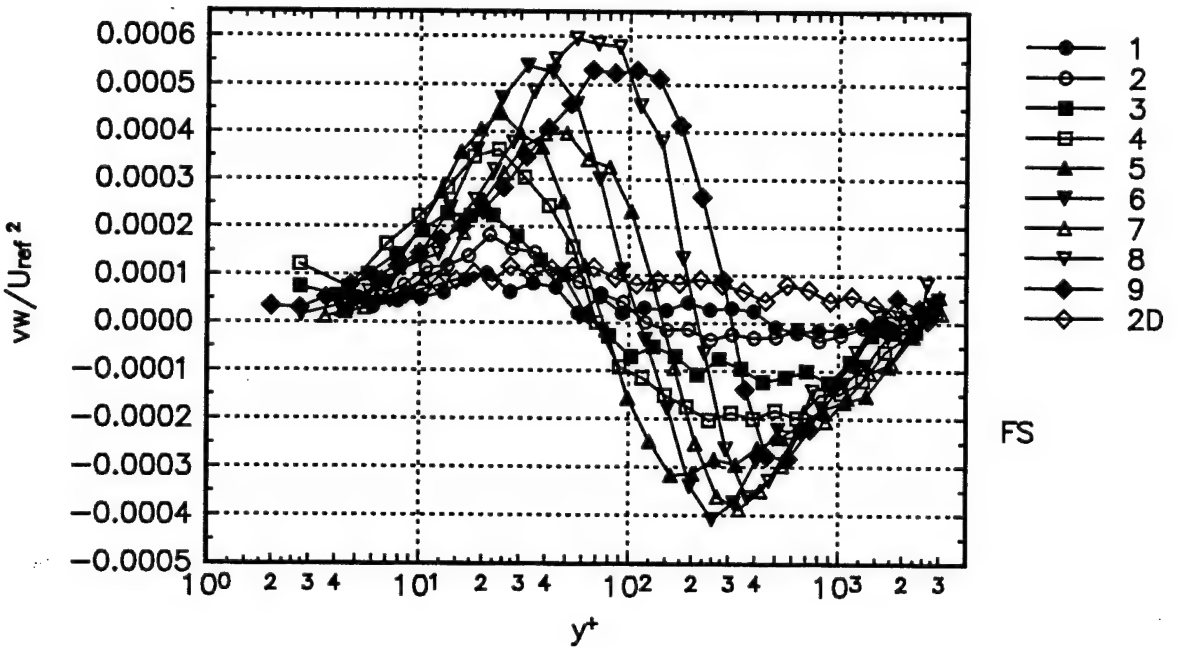
0.0006
0.0005
0.0004
0.0003
0.0002
0.0001
0.0000
−0.0001
−0.0002
−0.0003
−0.0004
−0.0005
vw/Uref 2
10^0 2 3 4 10^1 2 3 4 10^2 2 3 4 10^3 2 3
y+
1
2
3
4
5
6
7
8
9
2D
FS

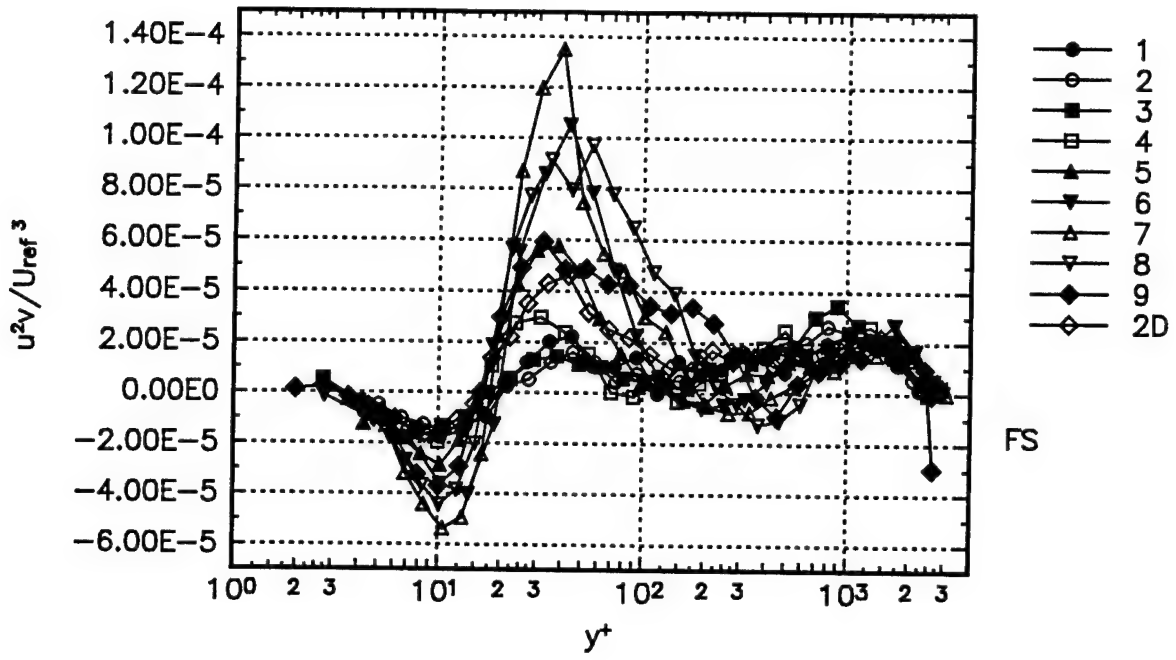
1.40E−4
1.20E−4
1.00E−4
8.00E−5
6.00E−5
4.00E−5
2.00E−5
0.00E0
−2.00E−5
−4.00E−5
−6.00E−5
u²v/Uref³
10⁰ 2 3 10¹ 2 3 10² 2 3 10³ 2 3
y+
1
2
3
4
5
6
7
8
9
2D
FS

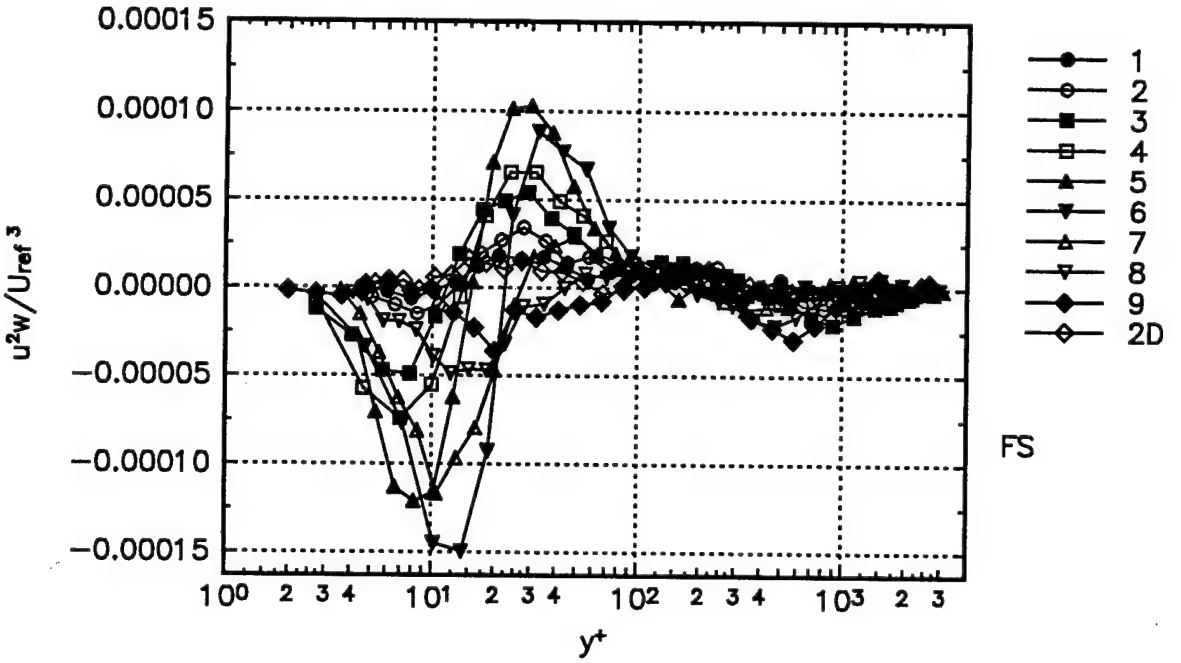
0.00015
0.00010
0.00005
0.00000
−0.00005
−0.00010
−0.00015
u²w/Uref³
10⁰ 2 3 4 10¹ 2 3 4 10² 2 3 4 10³ 2 3
y+
1
2
3
4
5
6
7
8
9
2D
FS

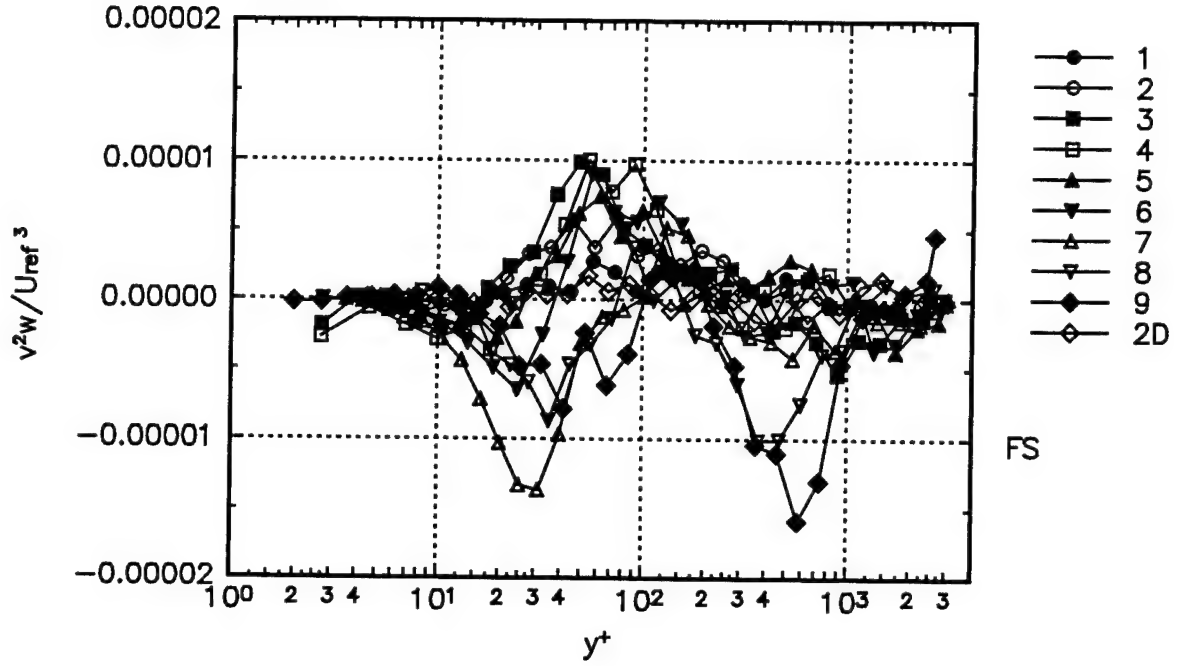
0.00002
0.00001
0.00000
−0.00001
−0.00002
v^2w/U_{ref}^3
10^0 2 3 4 10^1 2 3 4 10^2 2 3 4 10^3 2 3
y^+
1
2
3
4
5
6
7
8
9
2D
FS

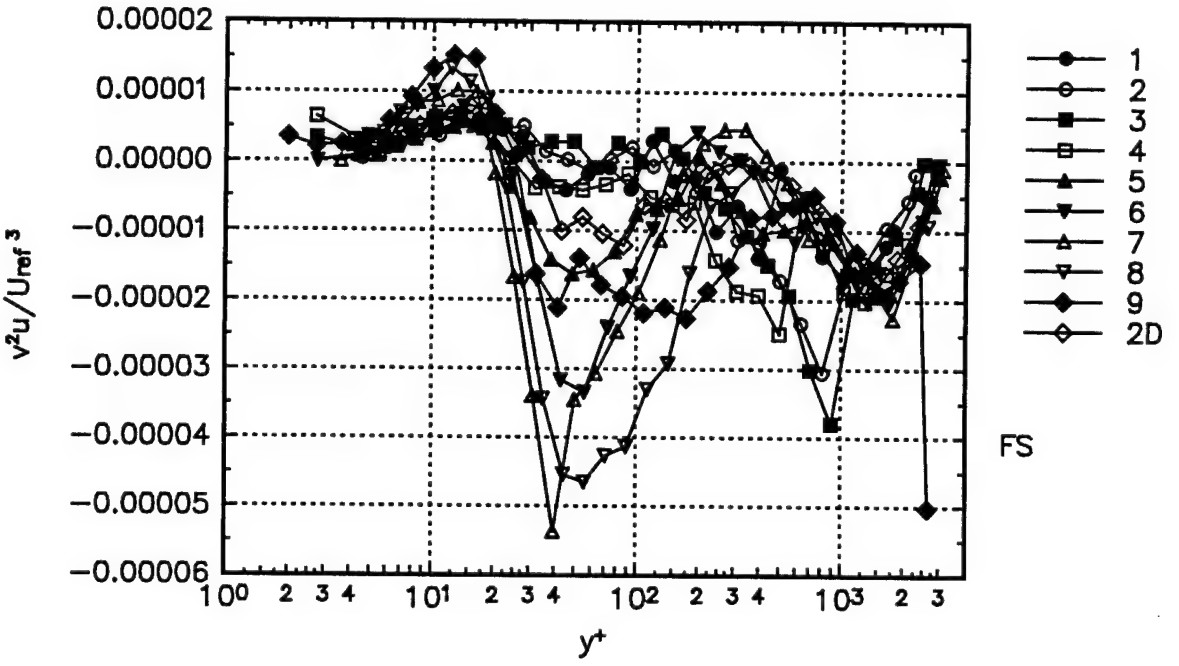
0.00002
0.00001
0.00000
−0.00001
−0.00002
−0.00003
−0.00004
−0.00005
−0.00006
v^2u/U_{ref}^3
10^0 2 3 4 10^1 2 3 4 10^2 2 3 4 10^3 2 3
y^+
1
2
3
4
5
6
7
8
9
2D
FS

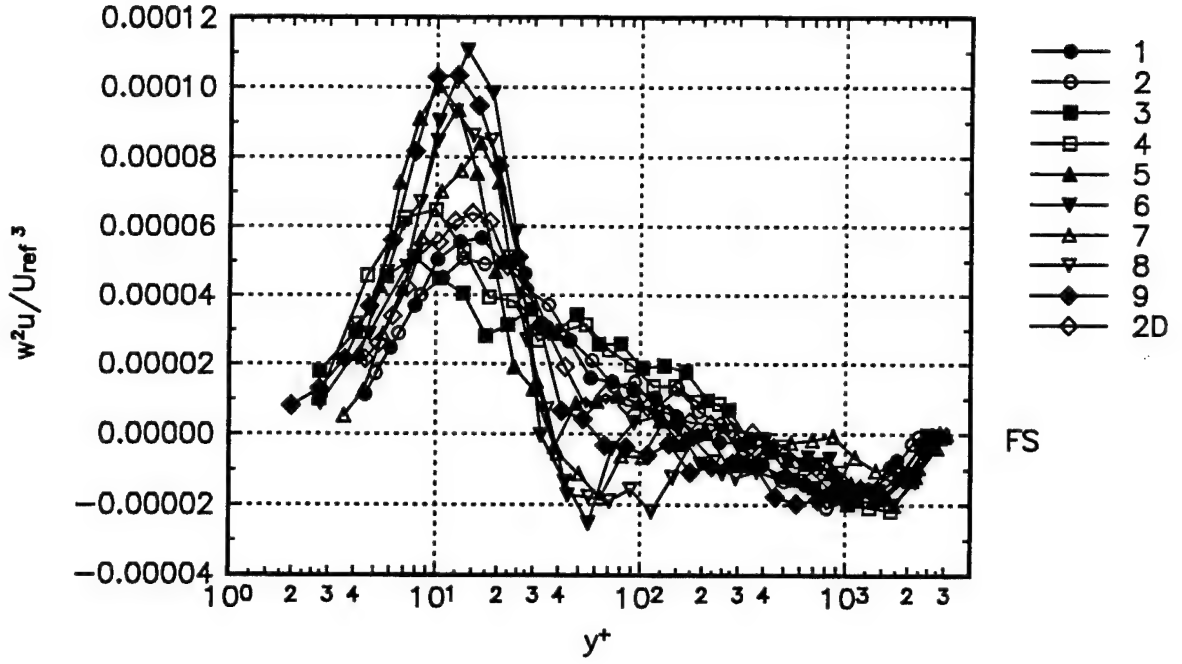
0.00012
0.00010
0.00008
0.00006
0.00004
0.00002
0.00000
−0.00002
−0.00004
w²u/Uref³
10⁰ 2 3 4 10¹ 2 3 4 10² 2 3 4 10³ 2 3
y+
1
2
3
4
5
6
7
8
9
2D
FS

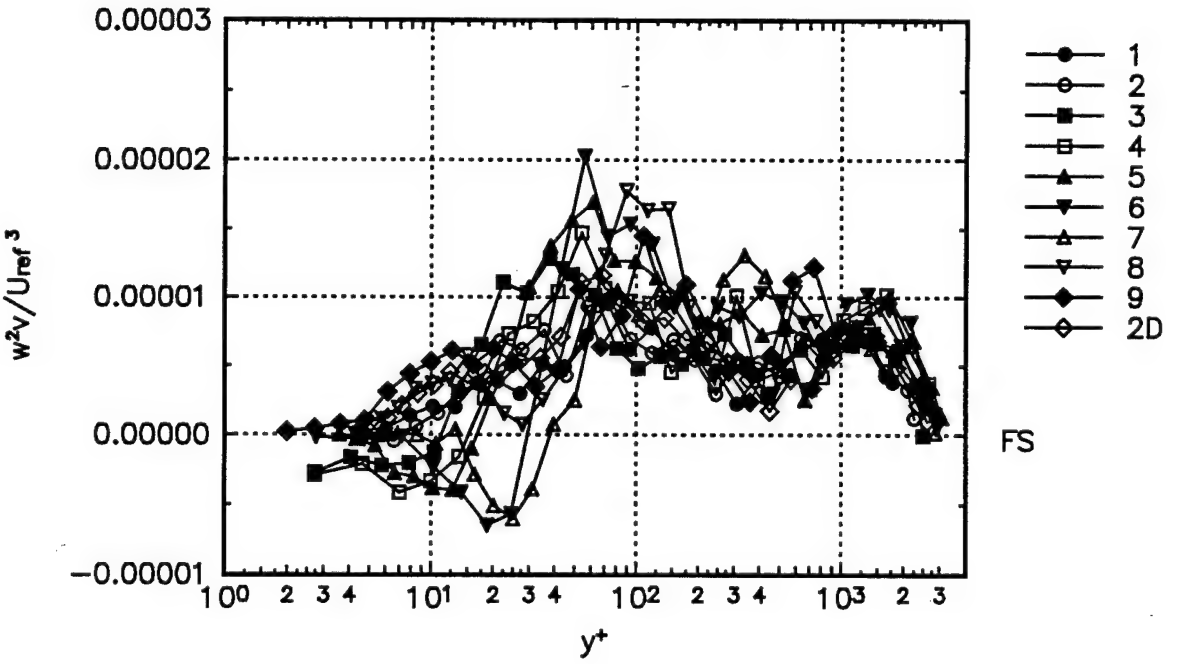
0.00003
0.00002
0.00001
0.00000
−0.00001
w²v/Uref³
10⁰ 2 3 4 10¹ 2 3 4 10² 2 3 4 10³ 2 3
y+
1
2
3
4
5
6
7
8
9
2D
FS

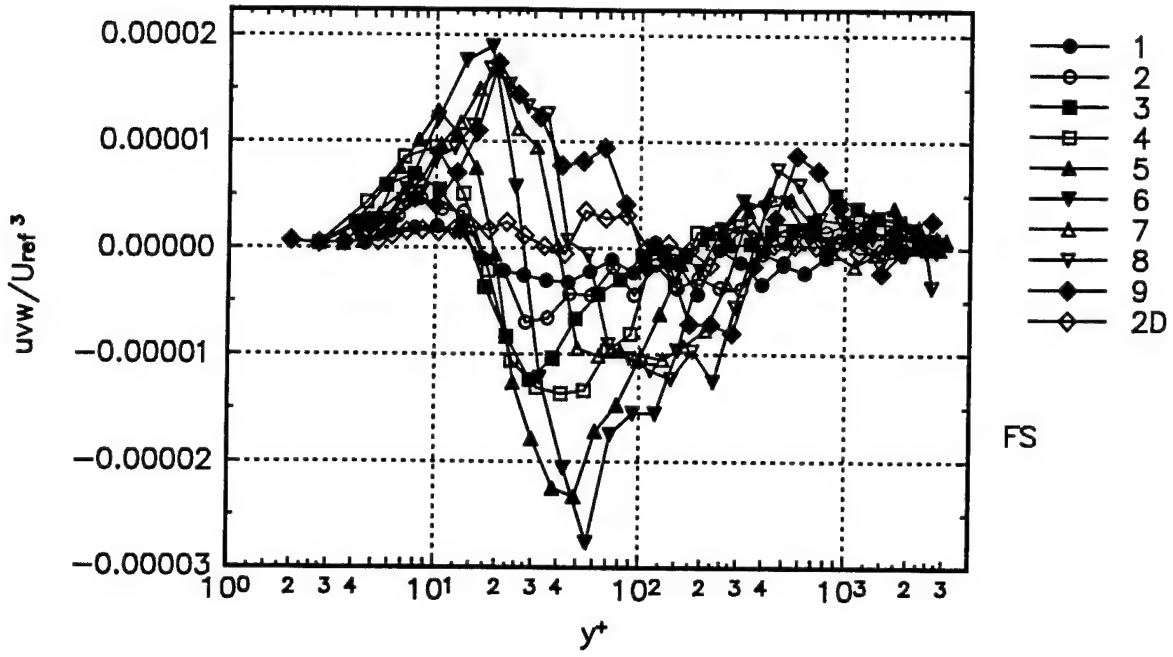
0.00002
0.00001
0.00000
−0.00001
−0.00002
−0.00003
uvw/Uref 3
100 2 3 4 101 2 3 4 102 2 3 4 103 2 3
y+
1
2
3
4
5
6
7
8
9
2D
FS

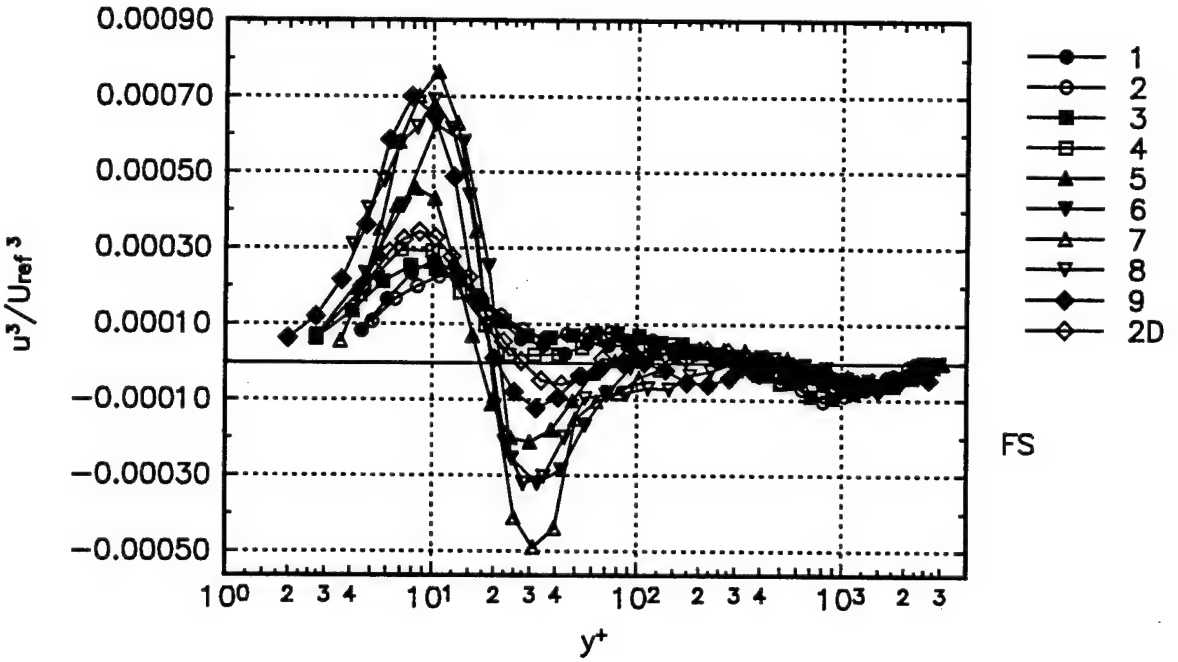
0.00090
0.00070
0.00050
0.00030
0.00010
−0.00010
−0.00030
−0.00050
u3/Uref 3
100 2 3 4 101 2 3 4 102 2 3 4 103 2 3
y+
1
2
3
4
5
6
7
8
9
2D
FS

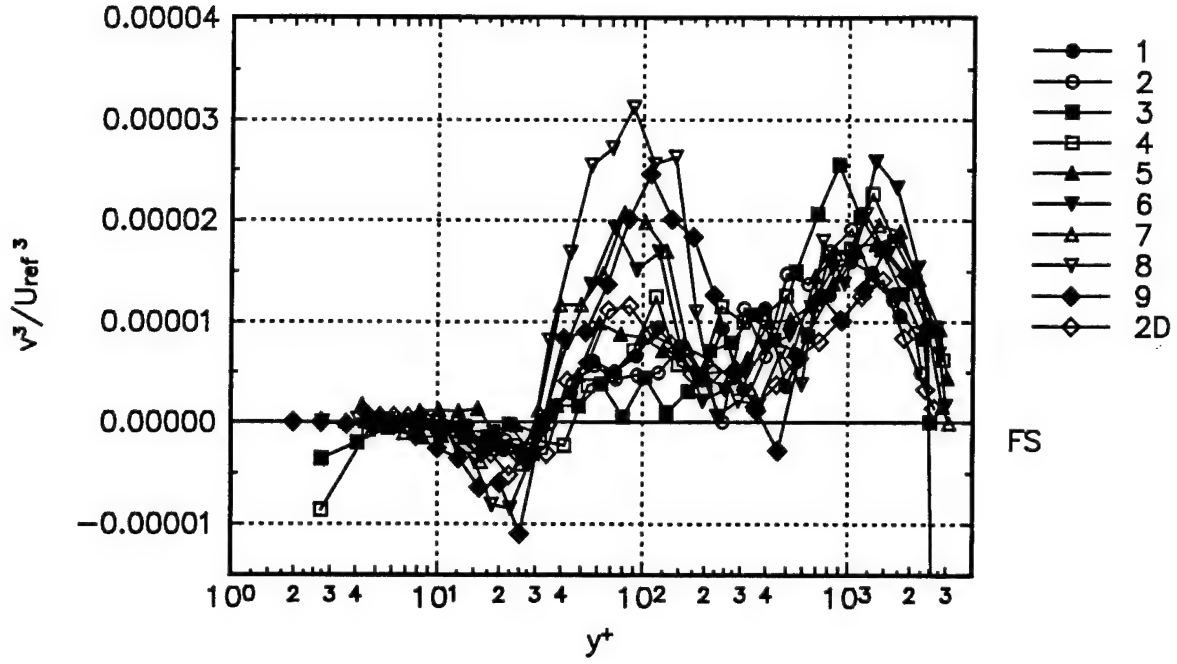
0.00004
0.00003
0.00002
0.00001
0.00000
−0.00001
$v^3/U_{ref}{}^3$
10^0 2 3 4 10^1 2 3 4 10^2 2 3 4 10^3 2 3
y^+
1
2
3
4
5
6
7
8
9
2D
FS

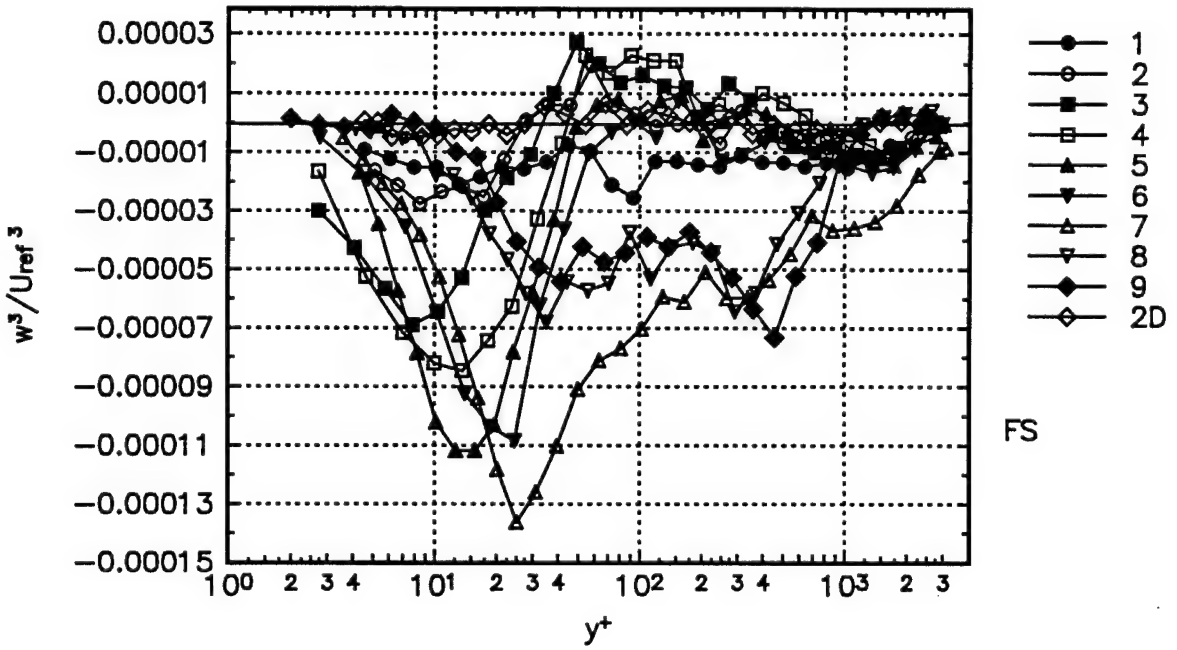
0.00003
0.00001
−0.00001
−0.00003
−0.00005
−0.00007
−0.00009
−0.00011
−0.00013
−0.00015
$w^3/U_{ref}{}^3$
10^0 2 3 4 10^1 2 3 4 10^2 2 3 4 10^3 2 3
y^+
1
2
3
4
5
6
7
8
9
2D
FS

Correlation coefficient form of the second and third order products in free-stream coordinates.

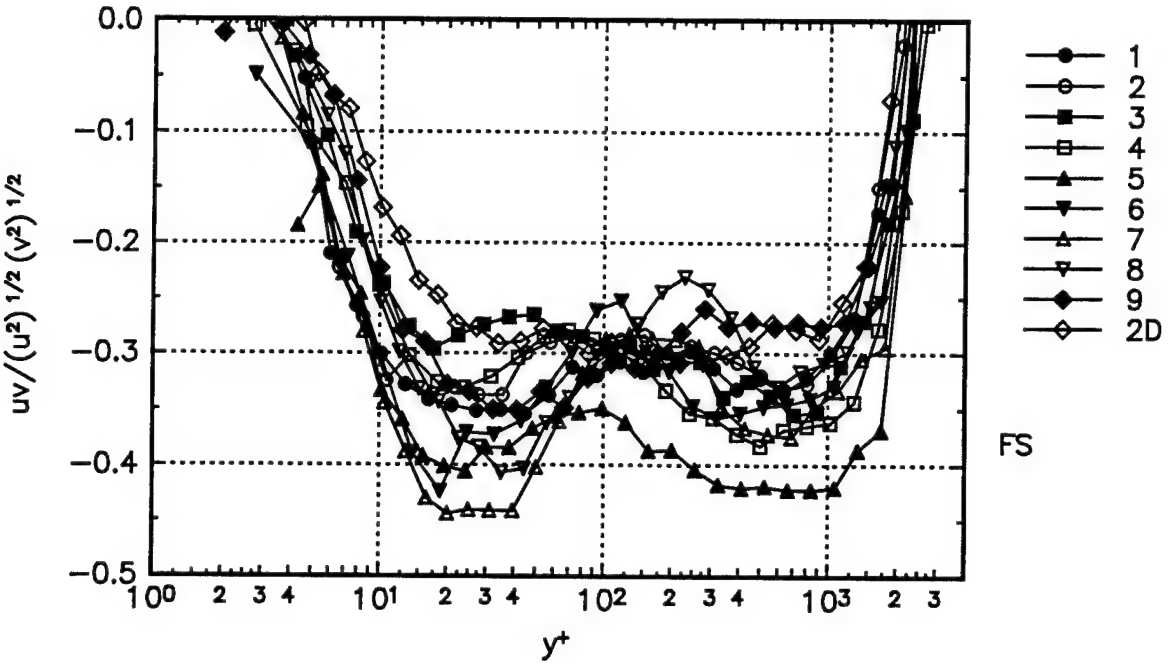

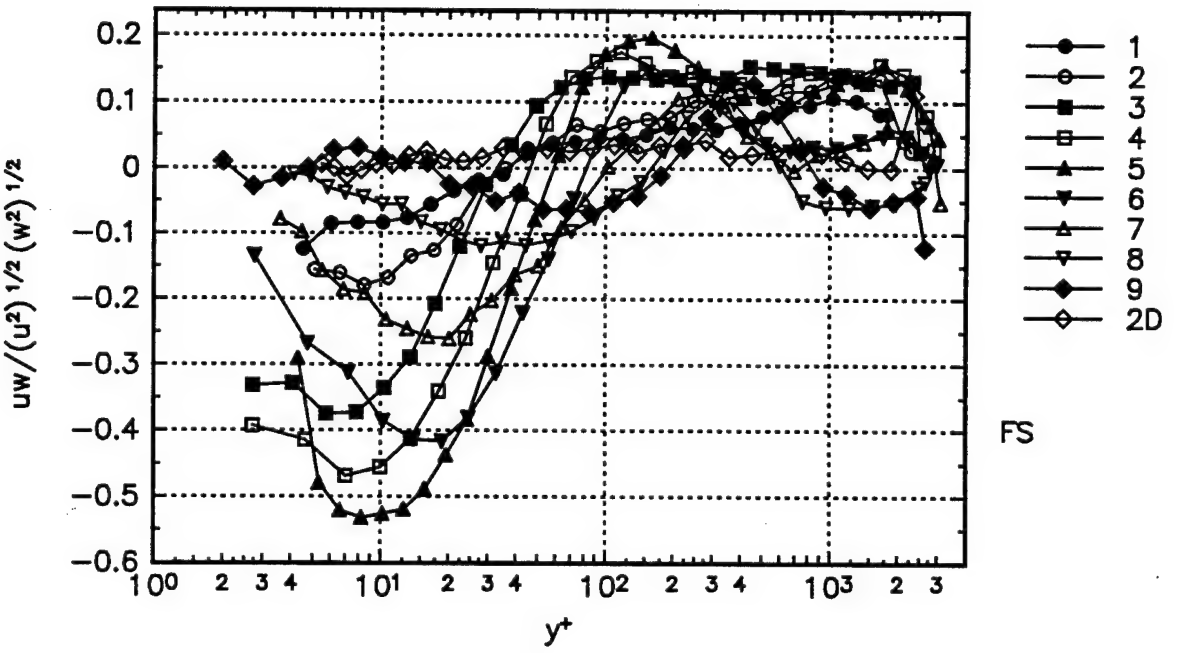

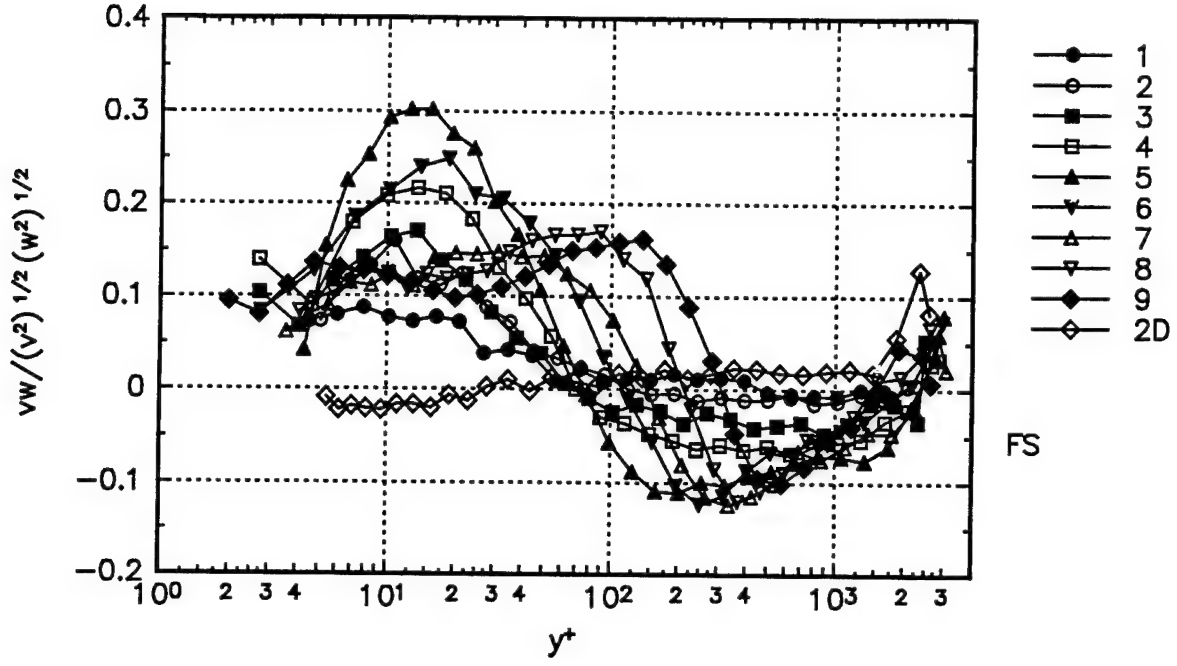
0.4
0.3
0.2
0.1
0
−0.1
−0.2
10^0 2 3 4 10^1 2 3 4 10^2 2 3 4 10^3 2 3
y^+
$vw/(v^2)^{1/2}(w^2)^{1/2}$
1
2
3
4
5
6
7
8
9
2D
FS

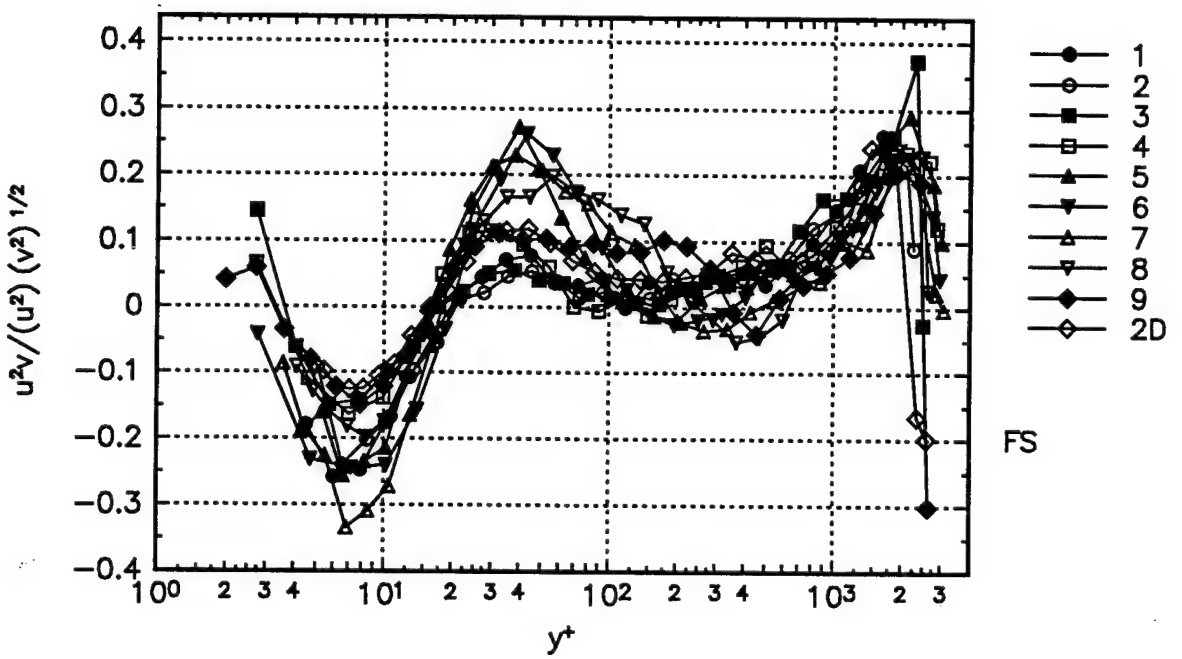
0.4
0.3
0.2
0.1
0
−0.1
−0.2
−0.3
−0.4
10^0 2 3 4 10^1 2 3 4 10^2 2 3 4 10^3 2 3
y^+
$u^2v/(u^2)(v^2)^{1/2}$
1
2
3
4
5
6
7
8
9
2D
FS

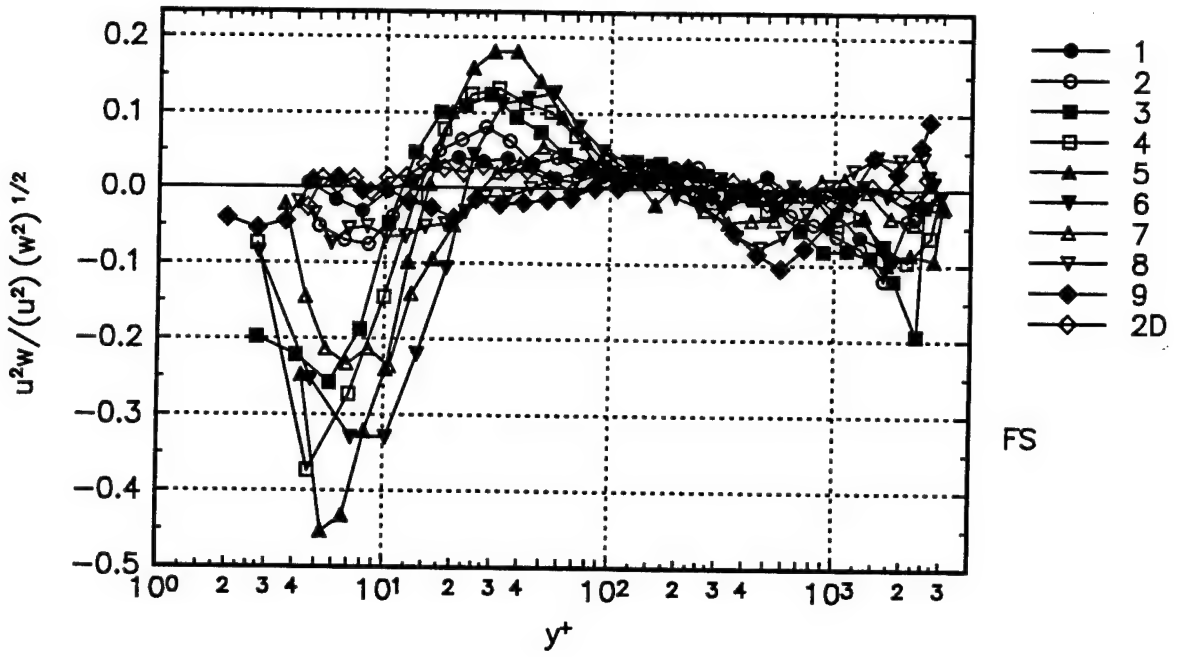
0.2
0.1
0.0
−0.1
−0.2
−0.3
−0.4
−0.5
$u^2w/(u^2)\,(w^2)^{1/2}$
10^0 2 3 4 10^1 2 3 4 10^2 2 3 4 10^3 2 3
y^+
1
2
3
4
5
6
7
8
9
2D
FS

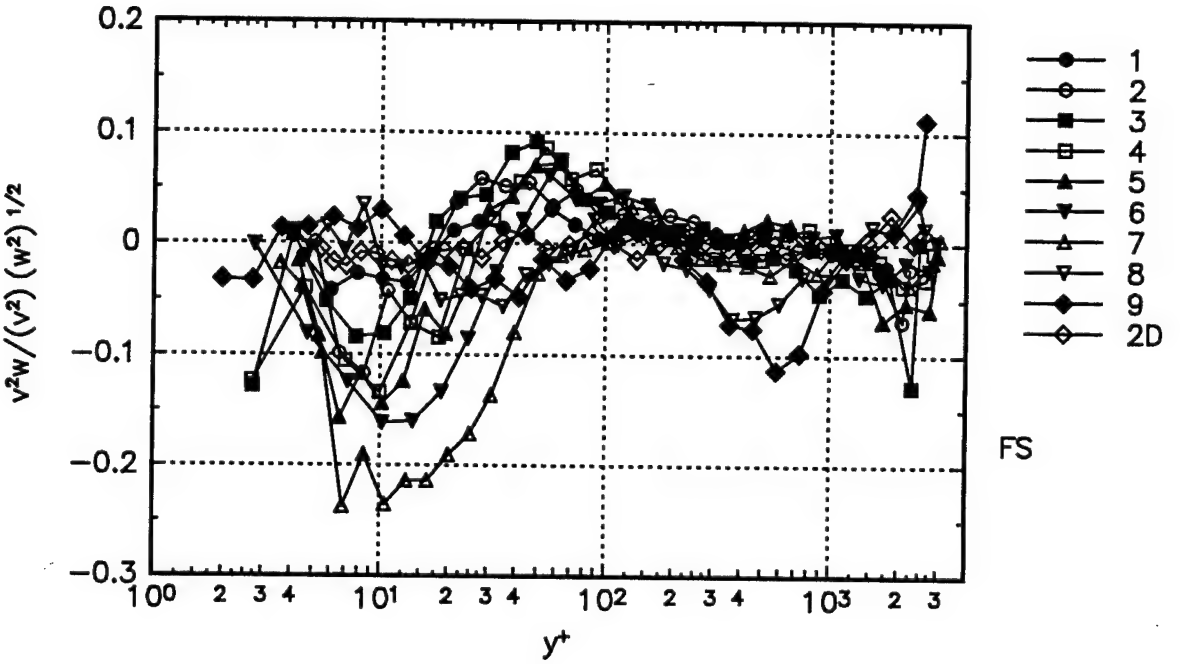
0.2
0.1
0
−0.1
−0.2
−0.3
$v^2w/(v^2)\,(w^2)^{1/2}$
10^0 2 3 4 10^1 2 3 4 10^2 2 3 4 10^3 2 3
y^+
1
2
3
4
5
6
7
8
9
2D
FS

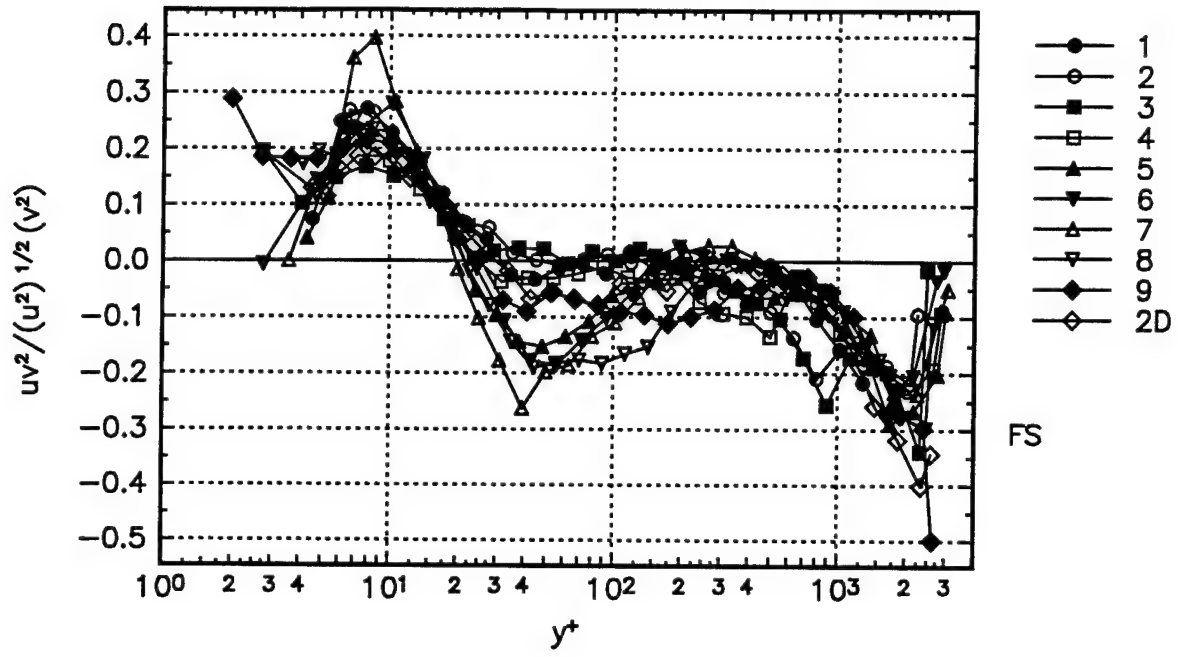
0.4
0.3
0.2
0.1
0.0
−0.1
−0.2
−0.3
−0.4
−0.5
10^0 2 3 4 10^1 2 3 4 10^2 2 3 4 10^3 2 3
y^+
$uv^2/(u^2)^{1/2}(v^2)$
1
2
3
4
5
6
7
8
9
2D
FS

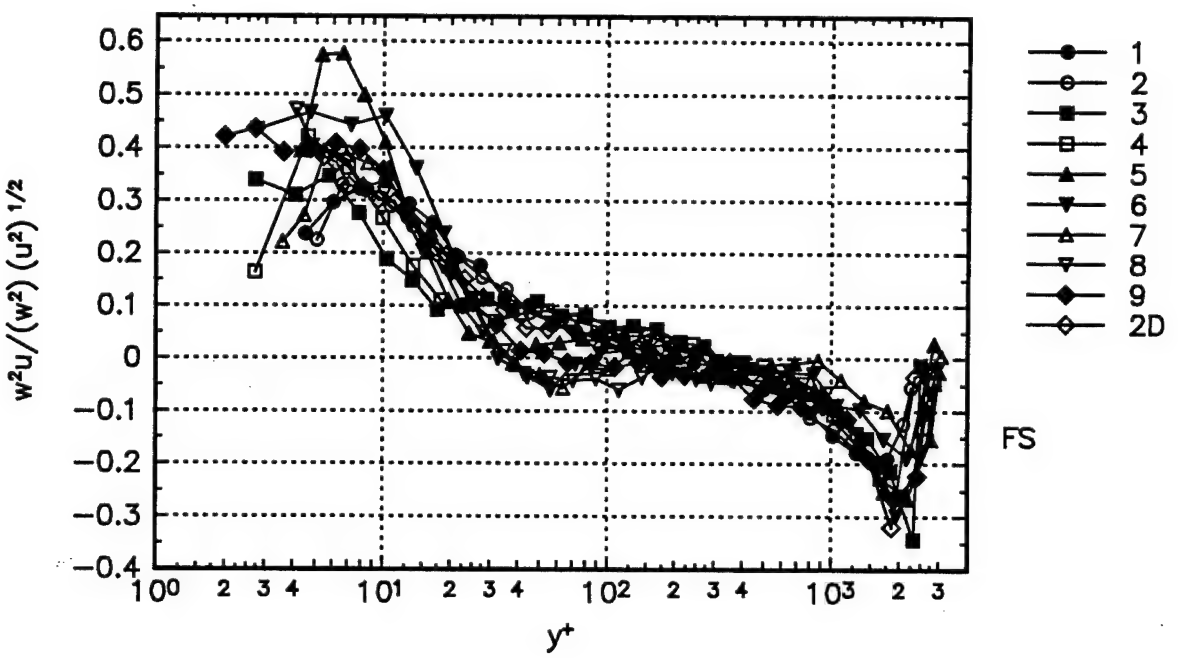
0.6
0.5
0.4
0.3
0.2
0.1
0
−0.1
−0.2
−0.3
−0.4
10^0 2 3 4 10^1 2 3 4 10^2 2 3 4 10^3 2 3
y^+
$w^2u/(w^2)(u^2)^{1/2}$
1
2
3
4
5
6
7
8
9
2D
FS

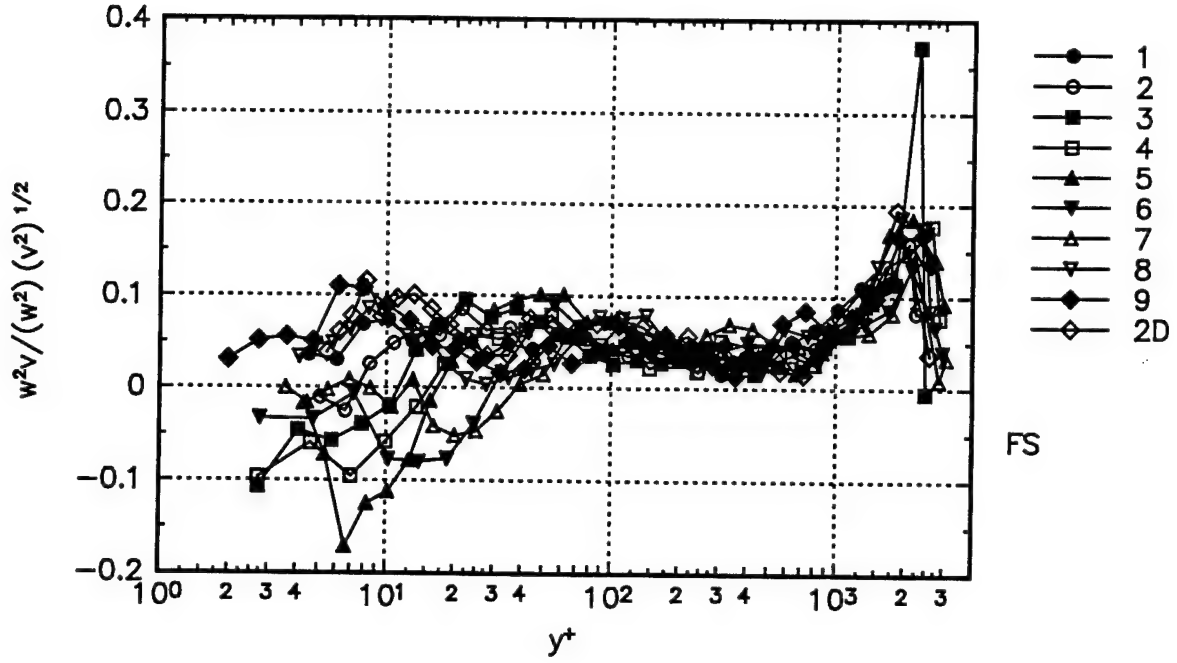
0.4
0.3
0.2
0.1
0
−0.1
−0.2
$w^2v/(w^2)(v^2)^{1/2}$
10^0 2 3 4 10^1 2 3 4 10^2 2 3 4 10^3 2 3
y^+
1
2
3
4
5
6
7
8
9
2D
FS

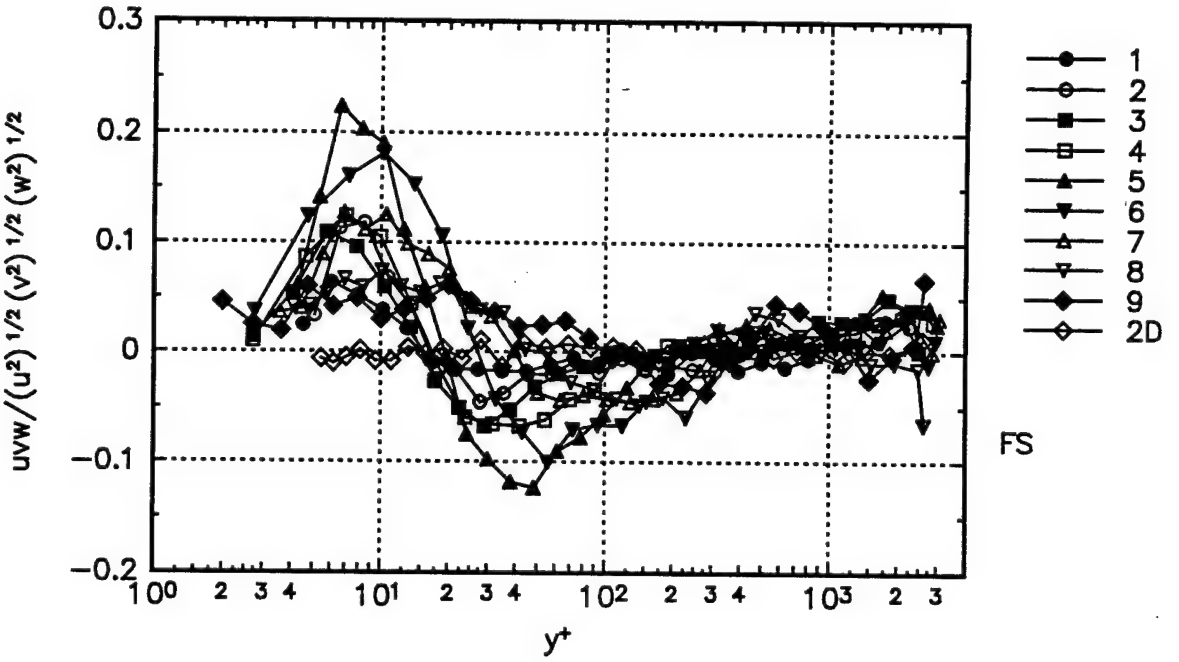
0.3
0.2
0.1
0
−0.1
−0.2
$uvw/(u^2)^{1/2}(v^2)^{1/2}(w^2)^{1/2}$
10^0 2 3 4 10^1 2 3 4 10^2 2 3 4 10^3 2 3
y^+
1
2
3
4
5
6
7
8
9
2D
FS

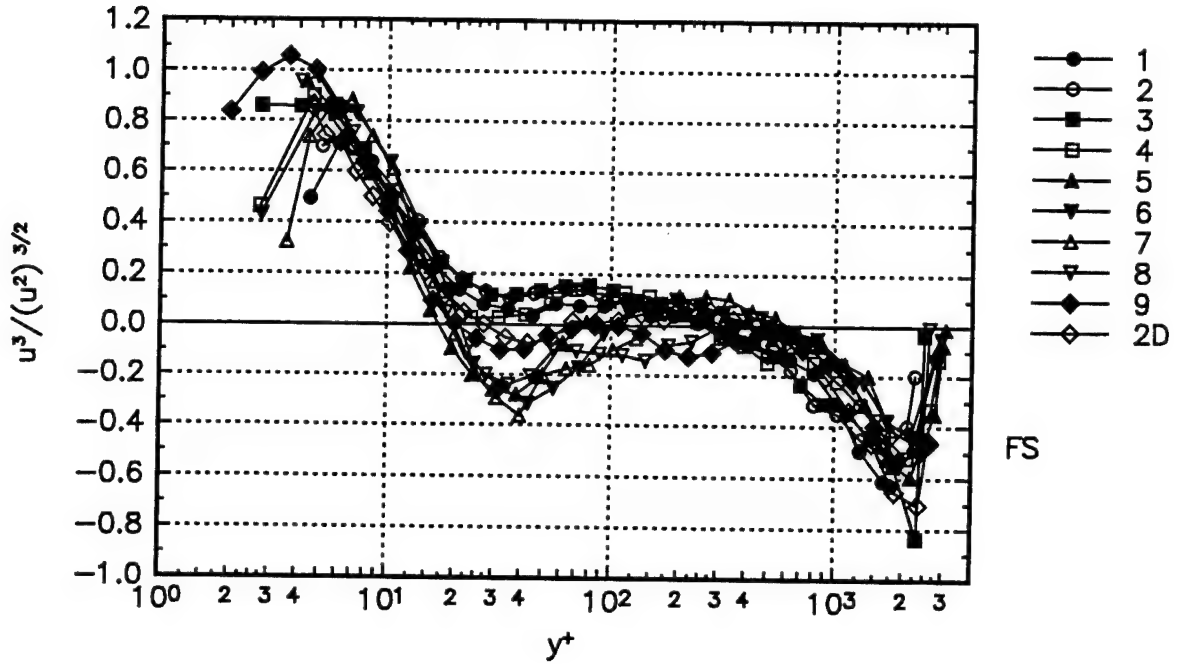
1.2
1.0
0.8
0.6
0.4
0.2
0.0
−0.2
−0.4
−0.6
−0.8
−1.0
$u^3/(u^2)^{3/2}$
10^0 2 3 4 10^1 2 3 4 10^2 2 3 4 10^3 2 3
y^+
1
2
3
4
5
6
7
8
9
2D
FS

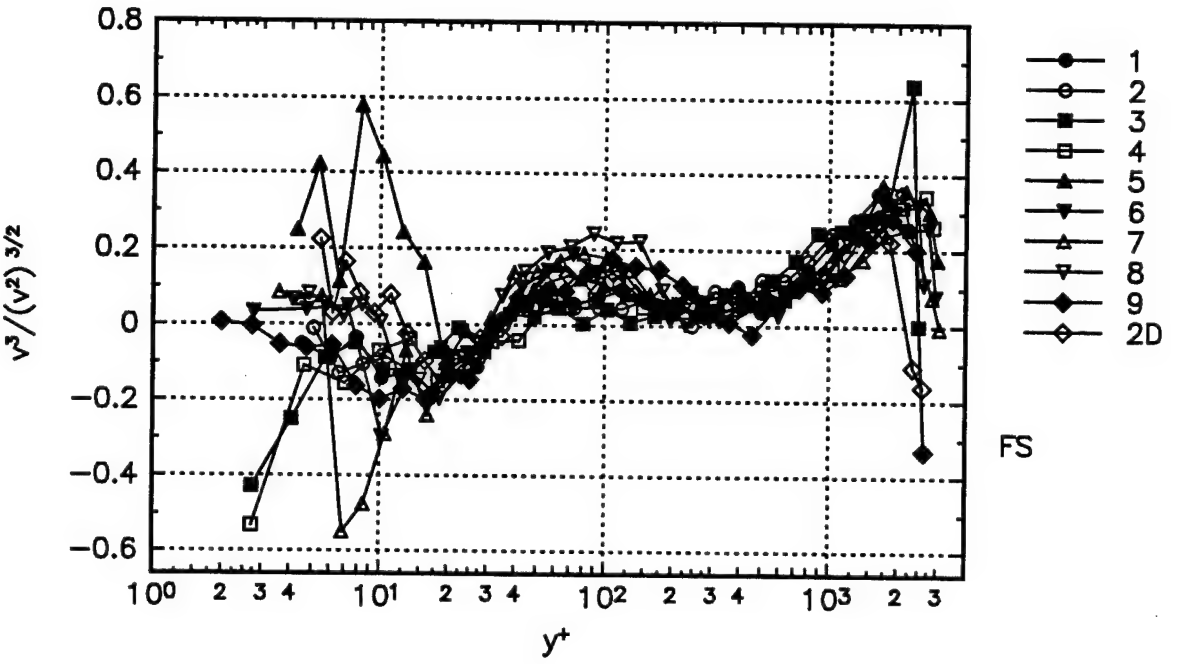
0.8
0.6
0.4
0.2
0
−0.2
−0.4
−0.6
$v^3/(v^2)^{3/2}$
10^0 2 3 4 10^1 2 3 4 10^2 2 3 4 10^3 2 3
y^+
1
2
3
4
5
6
7
8
9
2D
FS

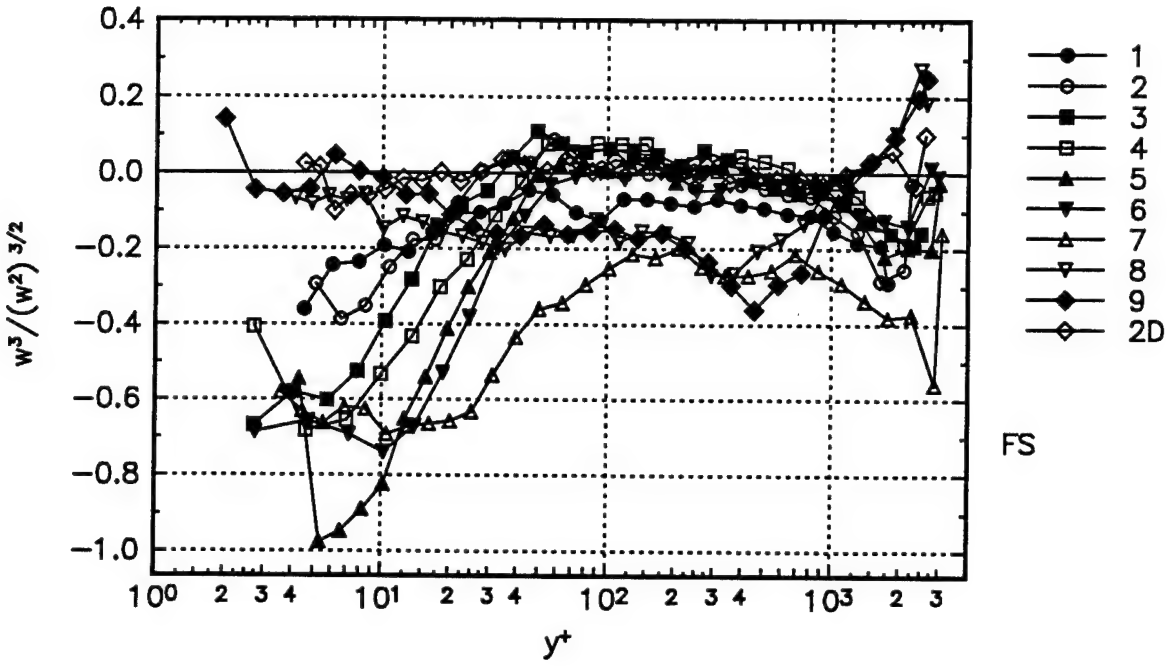
0.4
0.2
0.0
−0.2
−0.4
−0.6
−0.8
−1.0
$w^3/(w^2)^{3/2}$
10^0 2 3 4 10^1 2 3 4 10^2 2 3 4 10^3 2 3
y^+
1
2
3
4
5
6
7
8
9
2D
FS

Appendix D: Natural Coordinates

In this Appendix the data are presented in natural coordinates. The "x" coordinate direction of the natural coordinates is in the direction of the mean velocity vector at that point. The "x" coordinate direction varies at each profile location. The "y" coordinate is perpendicular to the "x" axis and lies within the plane of the "x" axis and the tunnel coordinates "y" axis. Therefore the "y" axis in natural coordinates also varies from location to location. The "z" axis completes a right handed coordinate system. The mean velocity, Reynolds' stresses and triple products are nondimensionalized with the relative powers of U_{ref}. Also in this Appendix the correlation coefficient form of the second and third order velocity products are presented.

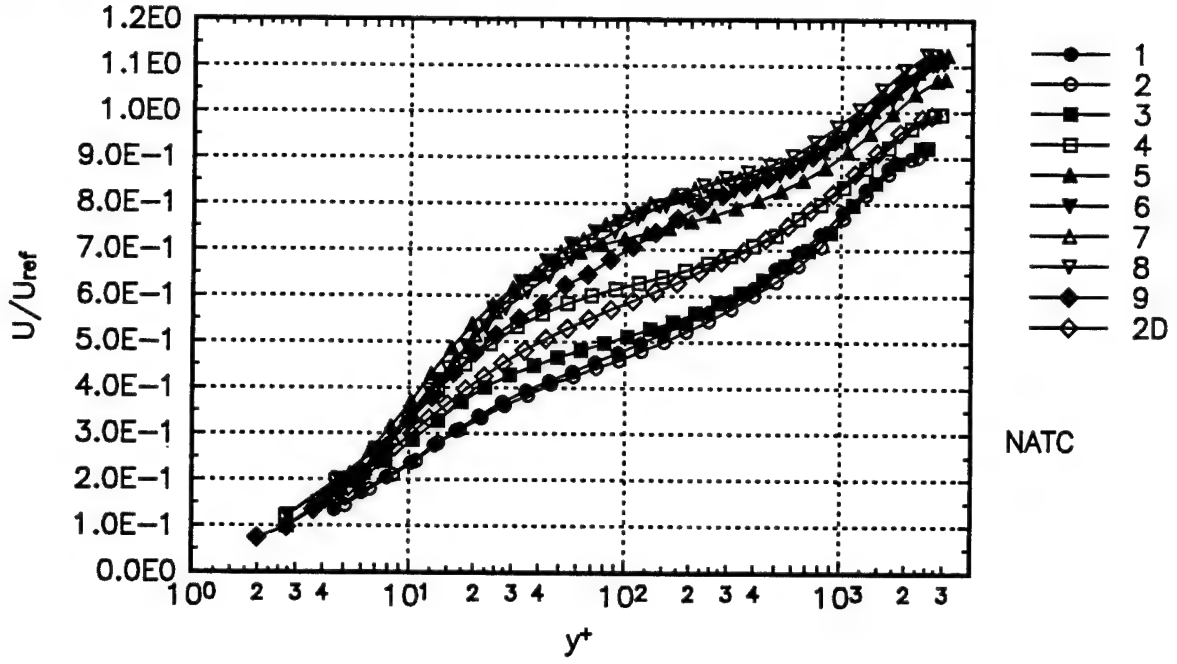

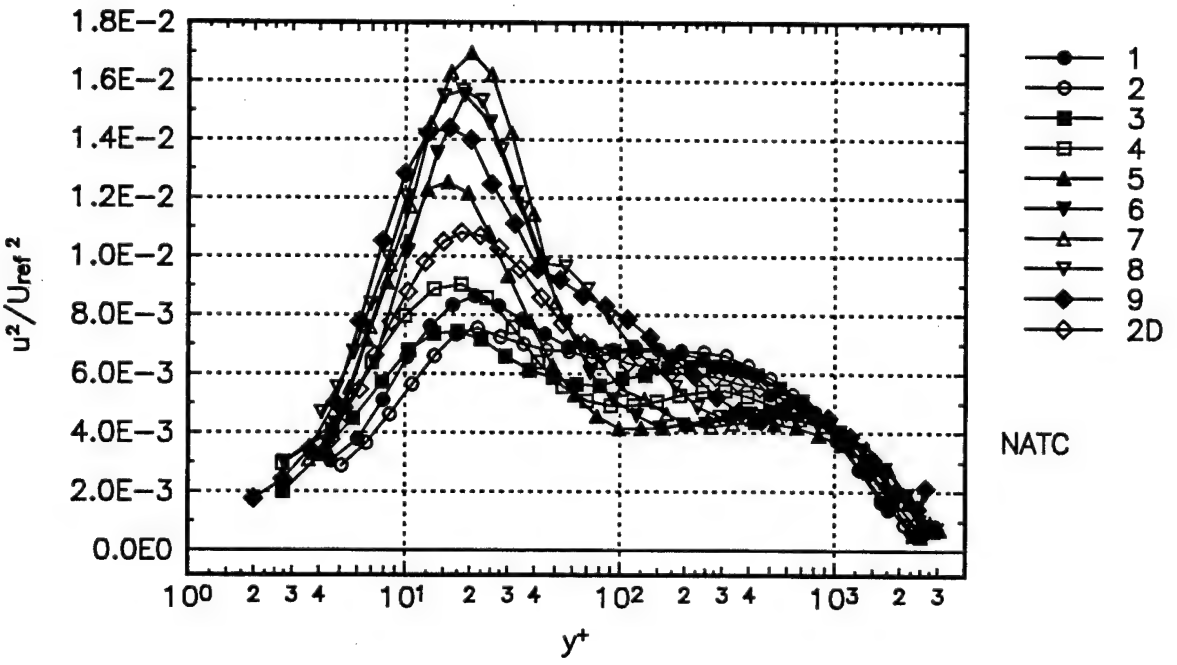

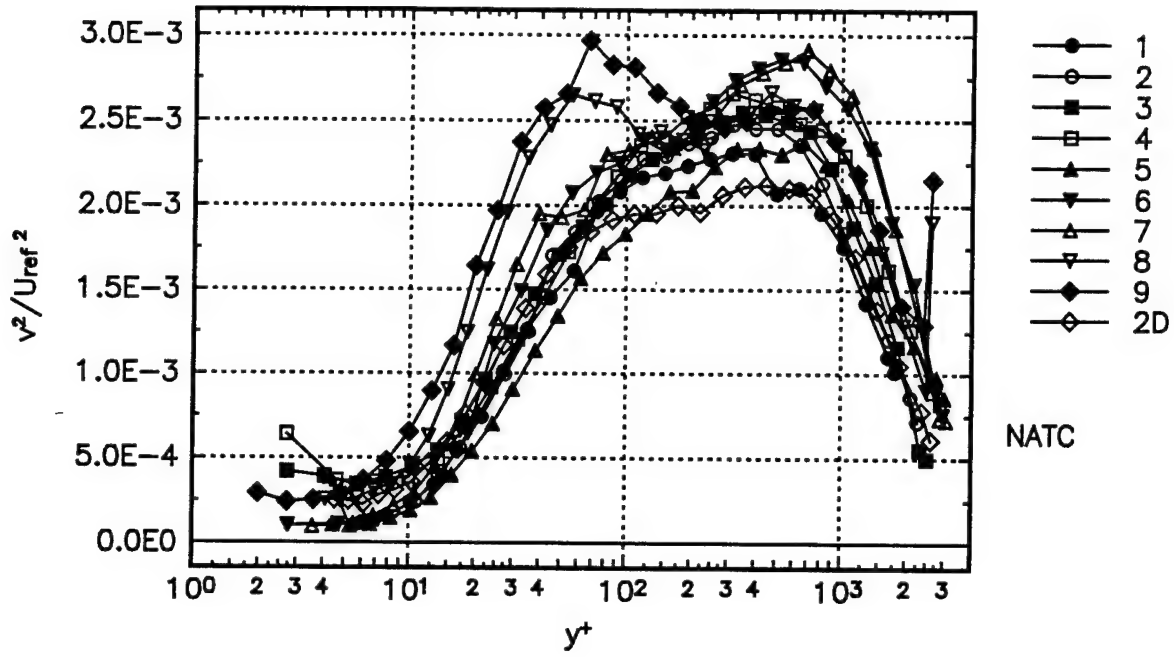
3.0E−3
2.5E−3
2.0E−3
1.5E−3
1.0E−3
5.0E−4
0.0E0
v^2/U_{ref}^2
10^0 2 3 4 10^1 2 3 4 10^2 2 3 4 10^3 2 3
y^+
1
2
3
4
5
6
7
8
9
2D
NATC

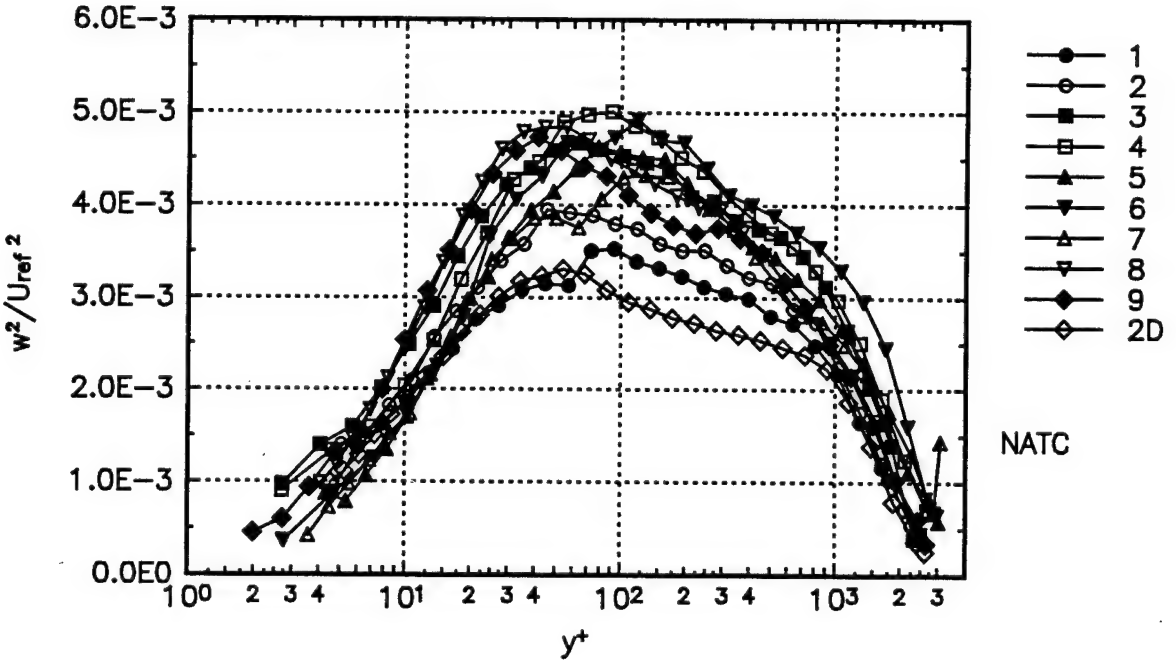
6.0E−3
5.0E−3
4.0E−3
3.0E−3
2.0E−3
1.0E−3
0.0E0
w^2/U_{ref}^2
10^0 2 3 4 10^1 2 3 4 10^2 2 3 4 10^3 2 3
y^+
1
2
3
4
5
6
7
8
9
2D
NATC

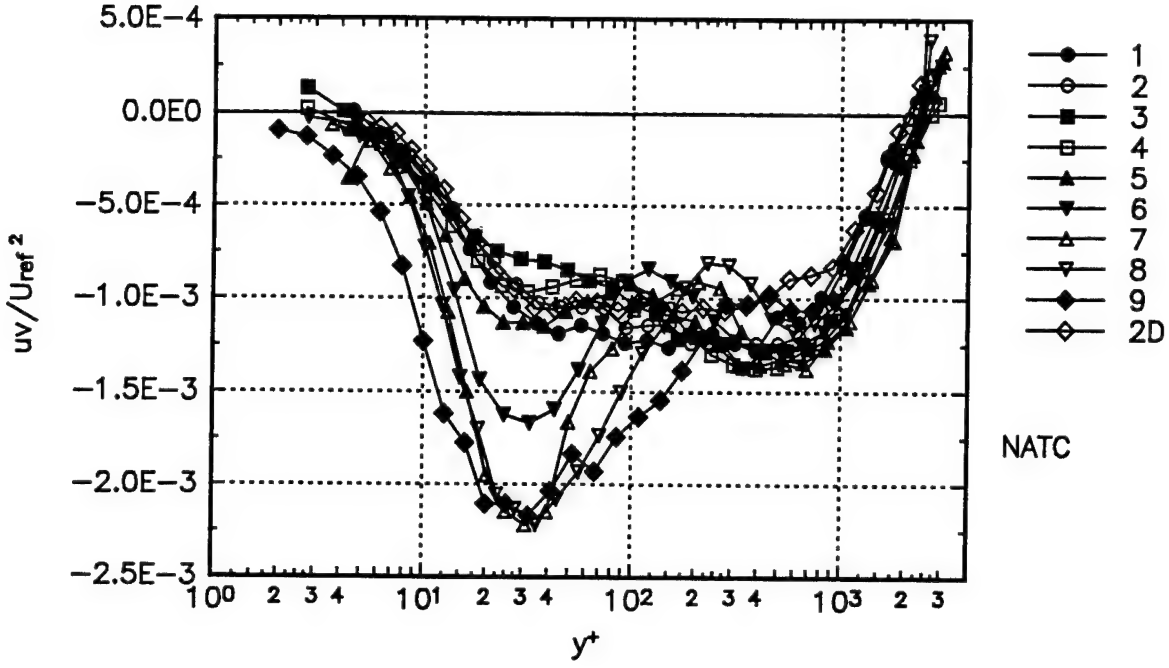
5.0E−4
0.0E0
−5.0E−4
−1.0E−3
−1.5E−3
−2.0E−3
−2.5E−3
uv/Uref²
10⁰ 2 3 4 10¹ 2 3 4 10² 2 3 4 10³ 2 3
y+
1
2
3
4
5
6
7
8
9
2D
NATC

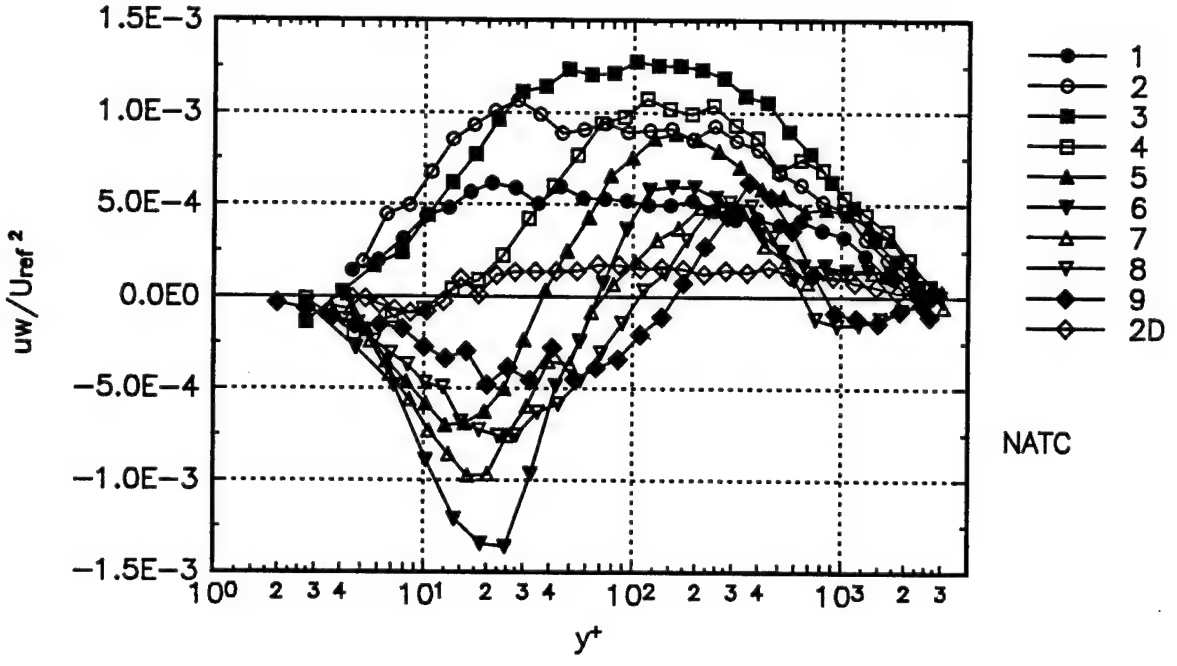
1.5E−3
1.0E−3
5.0E−4
0.0E0
−5.0E−4
−1.0E−3
−1.5E−3
uw/Uref²
10⁰ 2 3 4 10¹ 2 3 4 10² 2 3 4 10³ 2 3
y+
1
2
3
4
5
6
7
8
9
2D
NATC

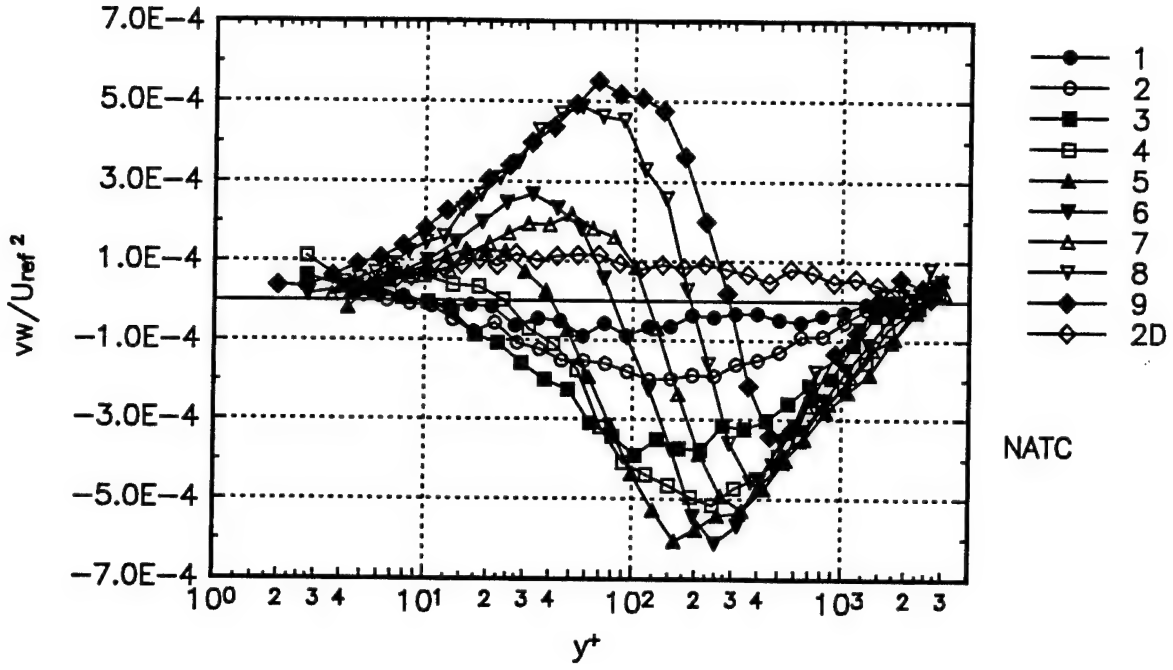
7.0E−4
5.0E−4
3.0E−4
1.0E−4
−1.0E−4
−3.0E−4
−5.0E−4
−7.0E−4
vw/Uref 2
10^0 2 3 4 10^1 2 3 4 10^2 2 3 4 10^3 2 3
y+
1
2
3
4
5
6
7
8
9
2D
NATC

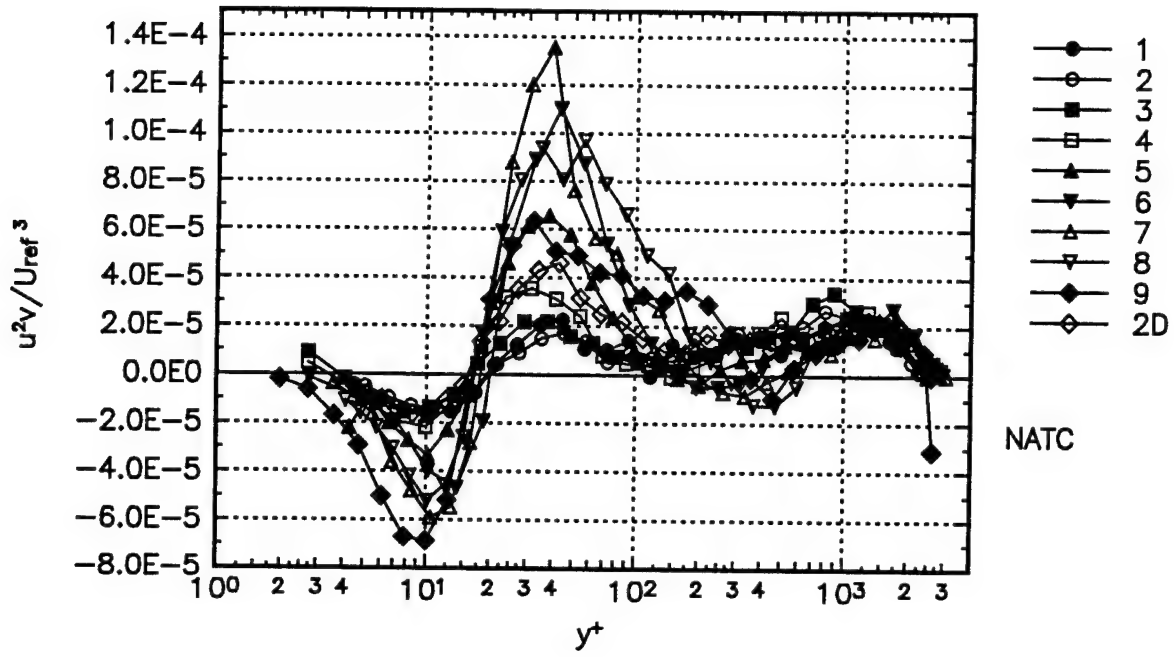
1.4E−4
1.2E−4
1.0E−4
8.0E−5
6.0E−5
4.0E−5
2.0E−5
0.0E0
−2.0E−5
−4.0E−5
−6.0E−5
−8.0E−5
u^2v/U_{ref}^3
10^0 2 3 4 10^1 2 3 4 10^2 2 3 4 10^3 2 3
y^+
1
2
3
4
5
6
7
8
9
2D
NATC

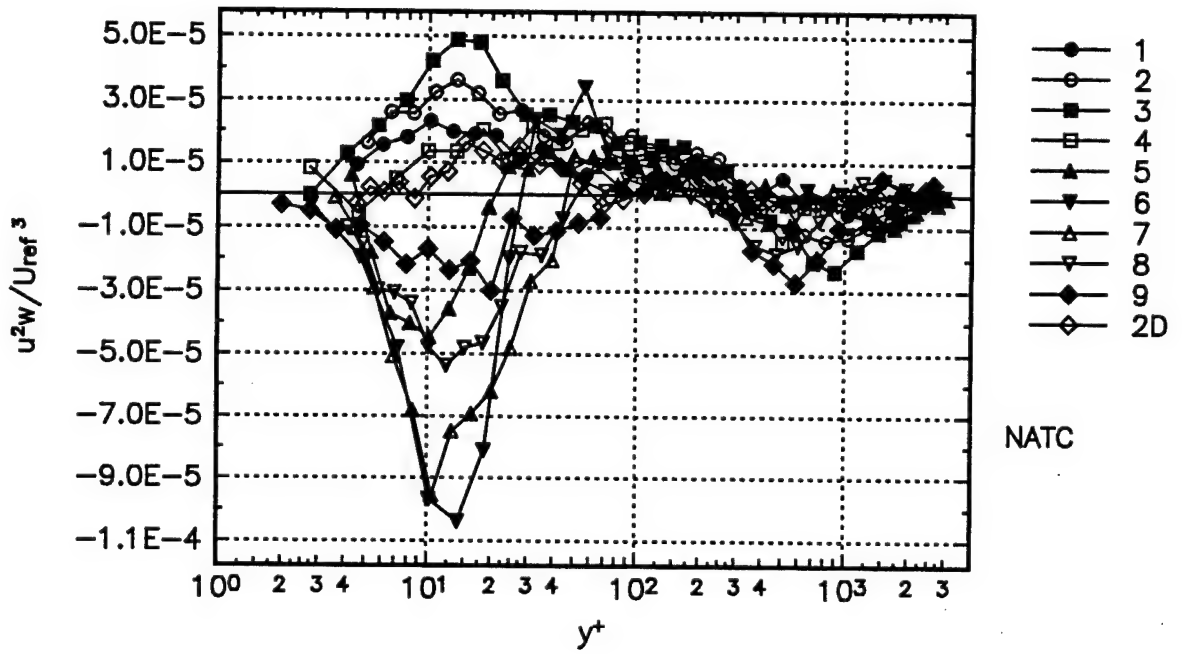
5.0E−5
3.0E−5
1.0E−5
−1.0E−5
−3.0E−5
−5.0E−5
−7.0E−5
−9.0E−5
−1.1E−4
u^2w/U_{ref}^3
10^0 2 3 4 10^1 2 3 4 10^2 2 3 4 10^3 2 3
y^+
1
2
3
4
5
6
7
8
9
2D
NATC

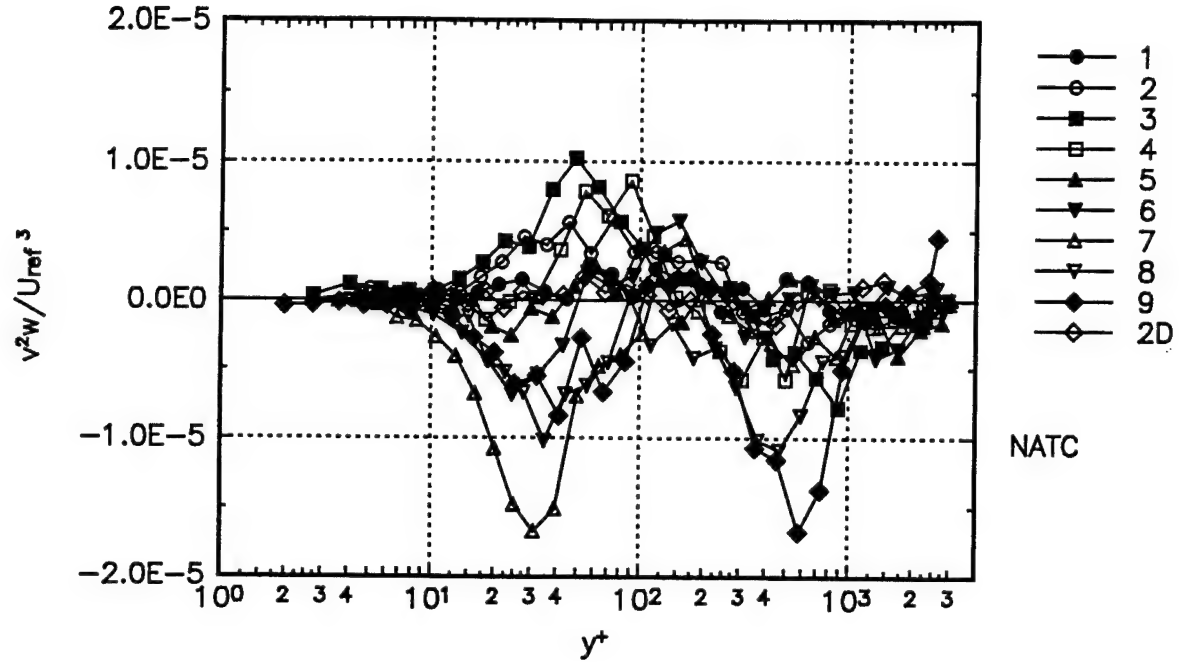
2.0E−5
1.0E−5
0.0E0
−1.0E−5
−2.0E−5
v^2w/U_{ref}^3
10^0 2 3 4 10^1 2 3 4 10^2 2 3 4 10^3 2 3
y^+
1
2
3
4
5
6
7
8
9
2D
NATC

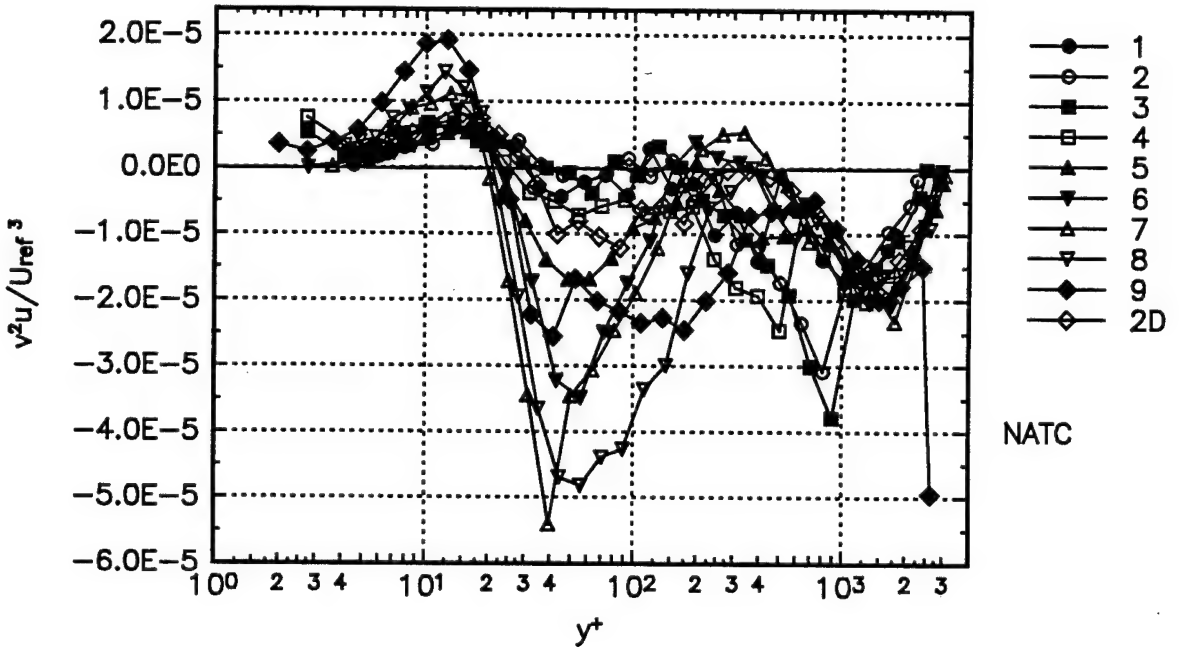
2.0E−5
1.0E−5
0.0E0
−1.0E−5
−2.0E−5
−3.0E−5
−4.0E−5
−5.0E−5
−6.0E−5
v^2u/U_{ref}^3
10^0 2 3 4 10^1 2 3 4 10^2 2 3 4 10^3 2 3
y^+
1
2
3
4
5
6
7
8
9
2D
NATC

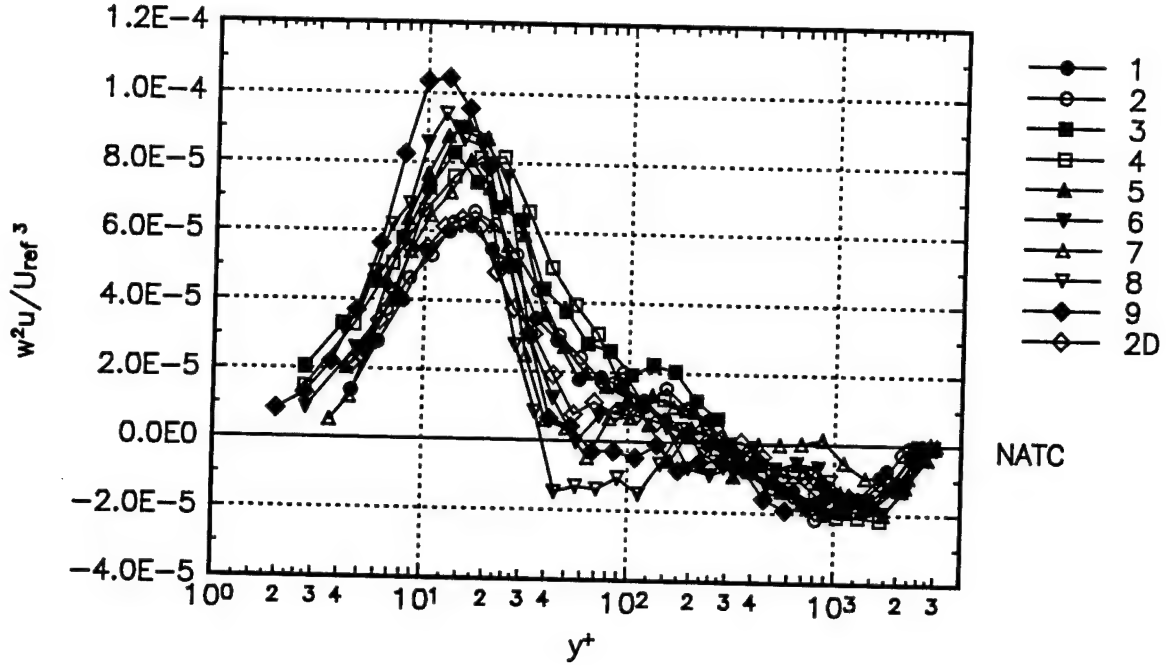
1.2E−4
1.0E−4
8.0E−5
6.0E−5
4.0E−5
2.0E−5
0.0E0
−2.0E−5
−4.0E−5
w²U/Uref³
10⁰ 2 3 4 10¹ 2 3 4 10² 2 3 4 10³ 2 3
y+
1
2
3
4
5
6
7
8
9
2D
NATC

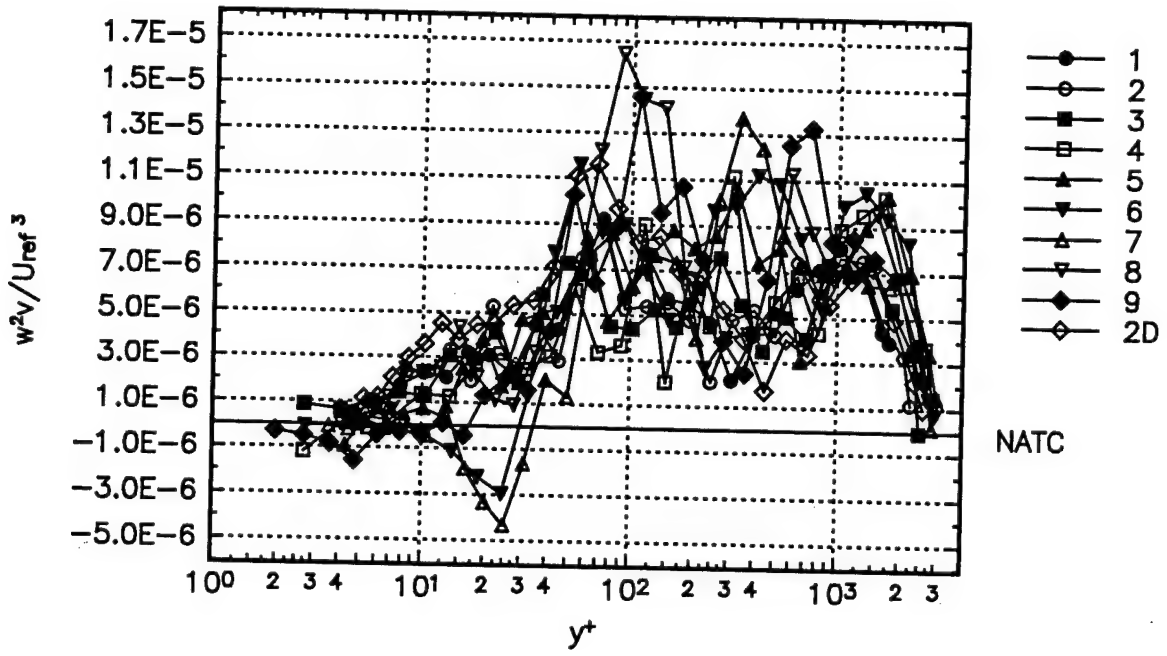
1.7E−5
1.5E−5
1.3E−5
1.1E−5
9.0E−6
7.0E−6
5.0E−6
3.0E−6
1.0E−6
−1.0E−6
−3.0E−6
−5.0E−6
w²V/Uref³
10⁰ 2 3 4 10¹ 2 3 4 10² 2 3 4 10³ 2 3
y+
1
2
3
4
5
6
7
8
9
2D
NATC

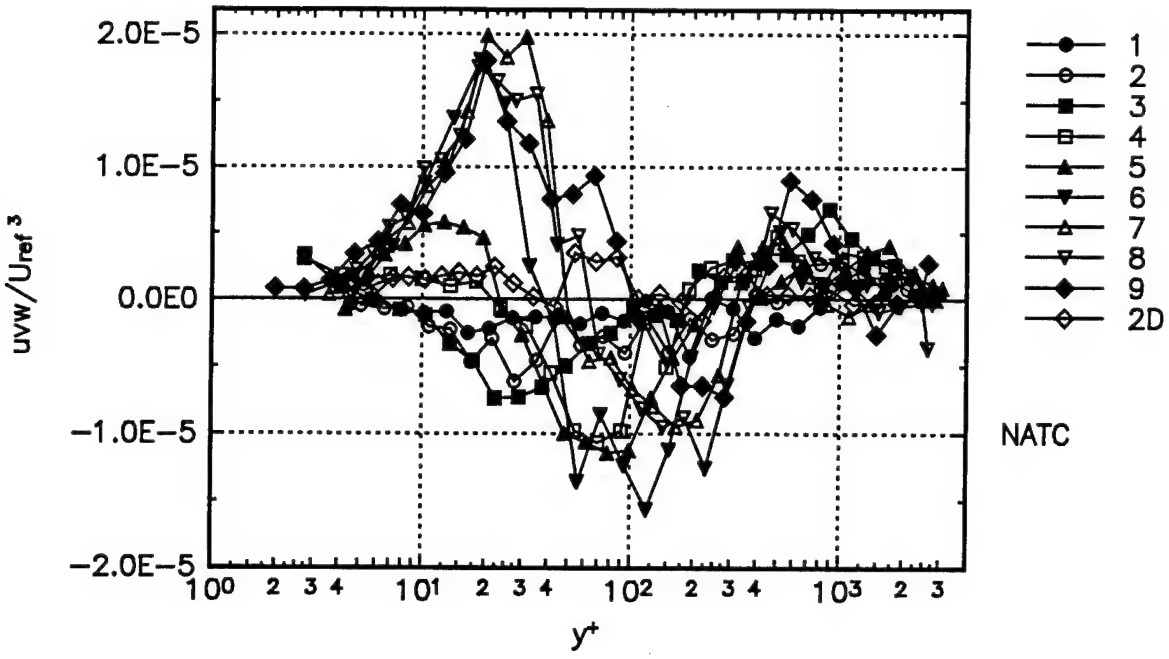
2.0E−5
1.0E−5
0.0E0
−1.0E−5
−2.0E−5
uvw/Uref 3
10^0 2 3 4 10^1 2 3 4 10^2 2 3 4 10^3 2 3
y+
1
2
3
4
5
6
7
8
9
2D
NATC

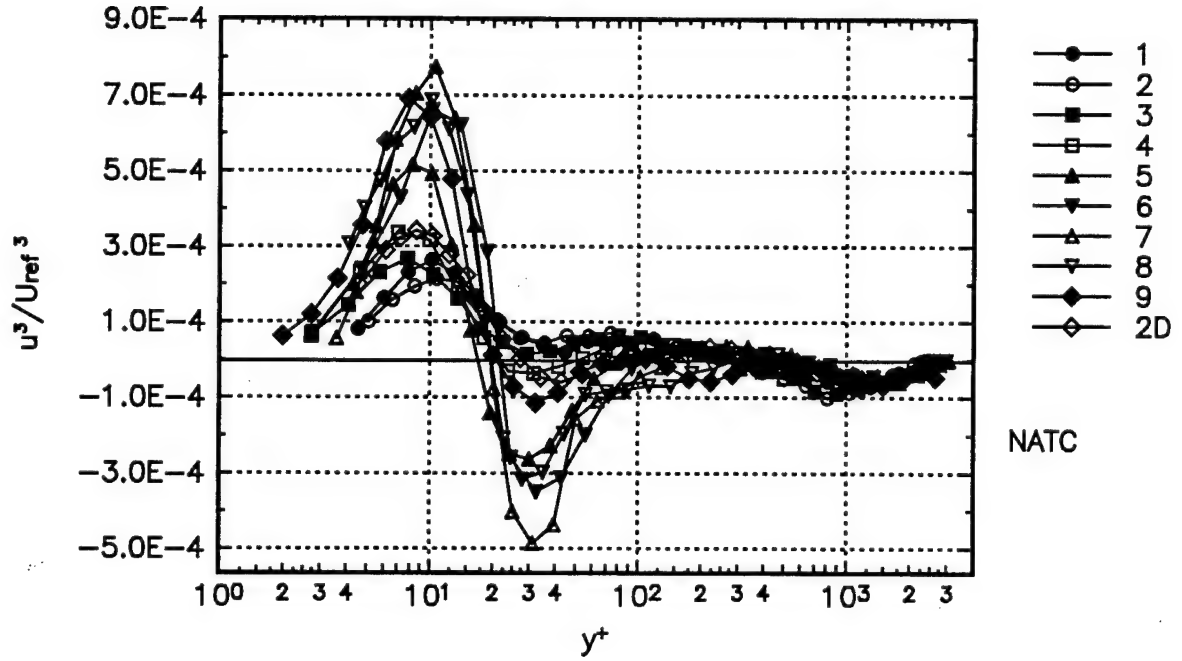
9.0E−4
7.0E−4
5.0E−4
3.0E−4
1.0E−4
−1.0E−4
−3.0E−4
−5.0E−4
u3/Uref 3
10^0 2 3 4 10^1 2 3 4 10^2 2 3 4 10^3 2 3
y+
1
2
3
4
5
6
7
8
9
2D
NATC

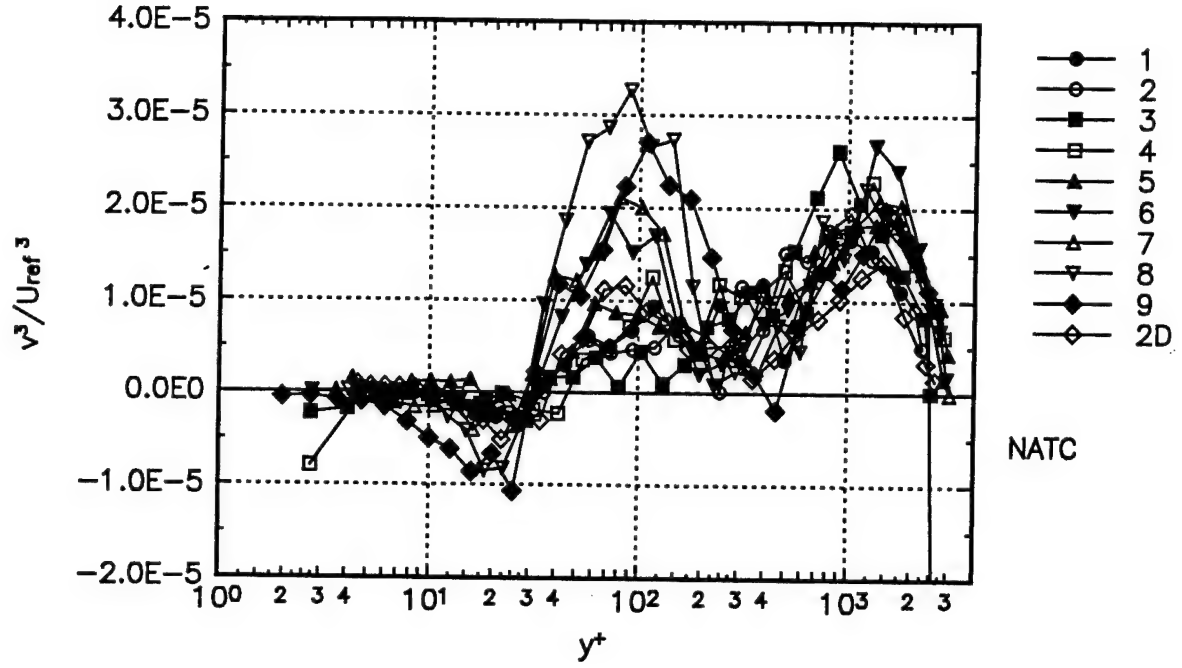
4.0E−5
3.0E−5
2.0E−5
1.0E−5
0.0E0
−1.0E−5
−2.0E−5
v³/Uref³
10⁰ 2 3 4 10¹ 2 3 4 10² 2 3 4 10³ 2 3
y+
1
2
3
4
5
6
7
8
9
2D
NATC

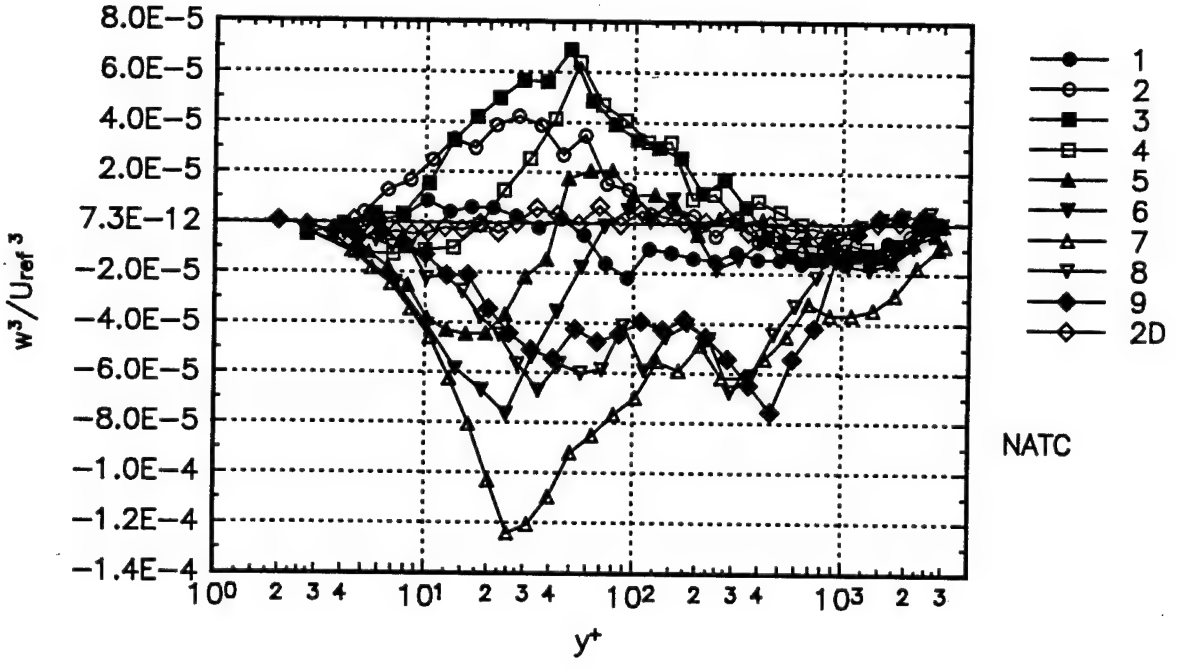
8.0E−5
6.0E−5
4.0E−5
2.0E−5
7.3E−12
−2.0E−5
−4.0E−5
−6.0E−5
−8.0E−5
−1.0E−4
−1.2E−4
−1.4E−4
w³/Uref³
10⁰ 2 3 4 10¹ 2 3 4 10² 2 3 4 10³ 2 3
y+
1
2
3
4
5
6
7
8
9
2D
NATC

Correlation coefficient form of the second and third order products in natural coordinates.

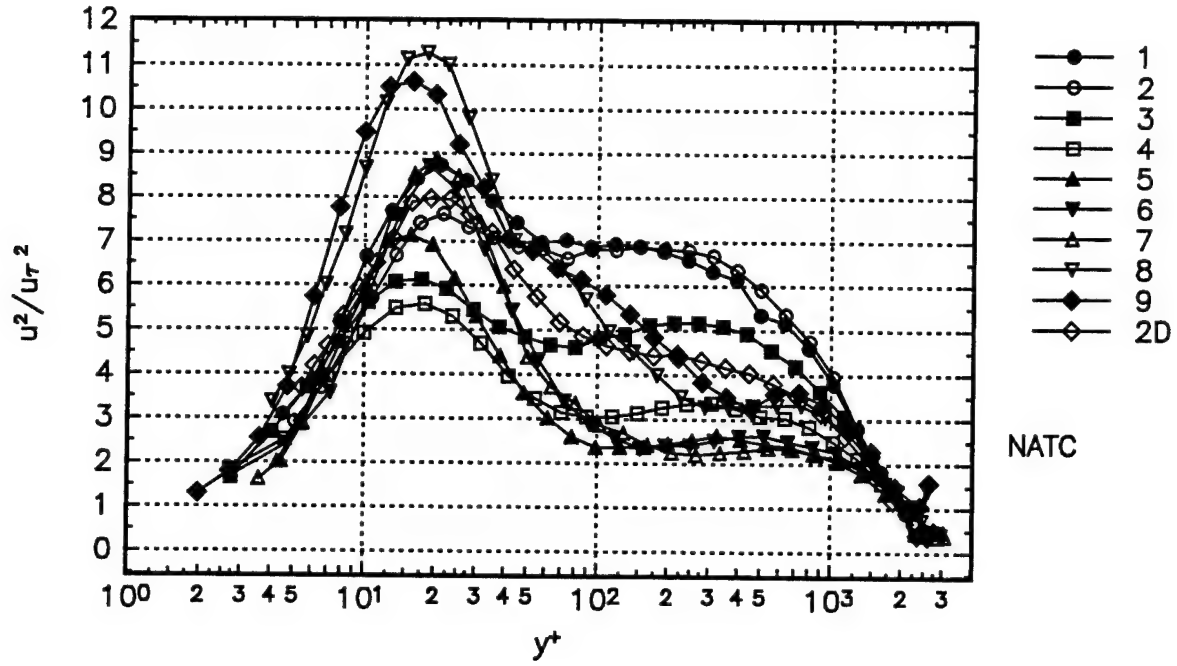

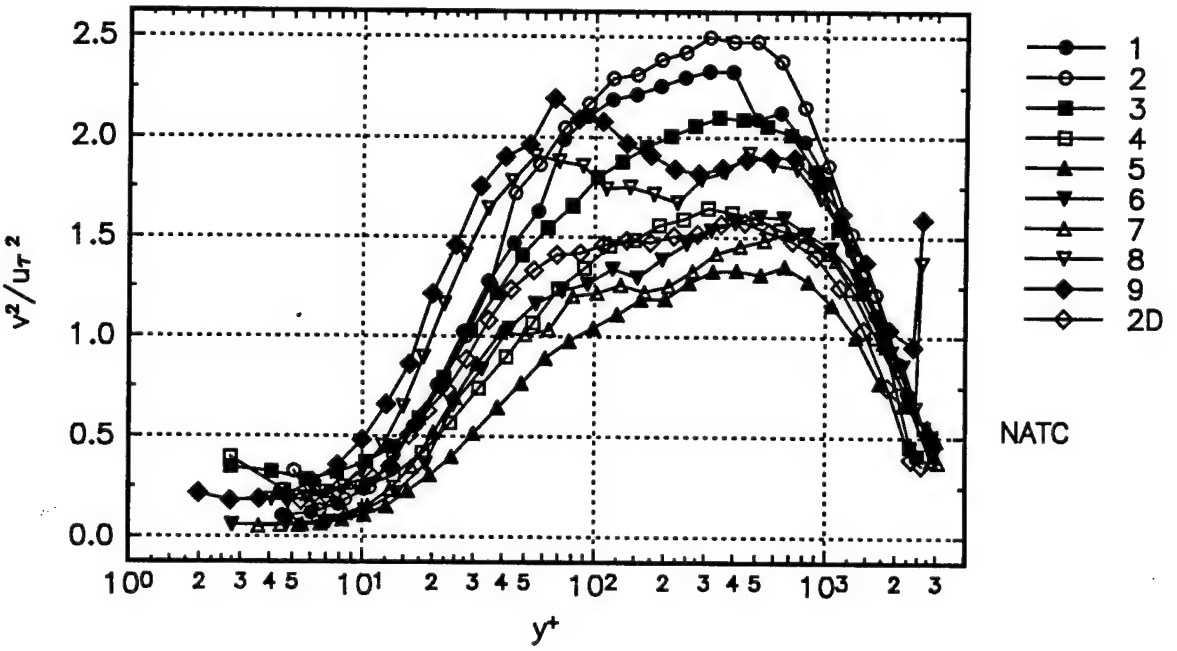

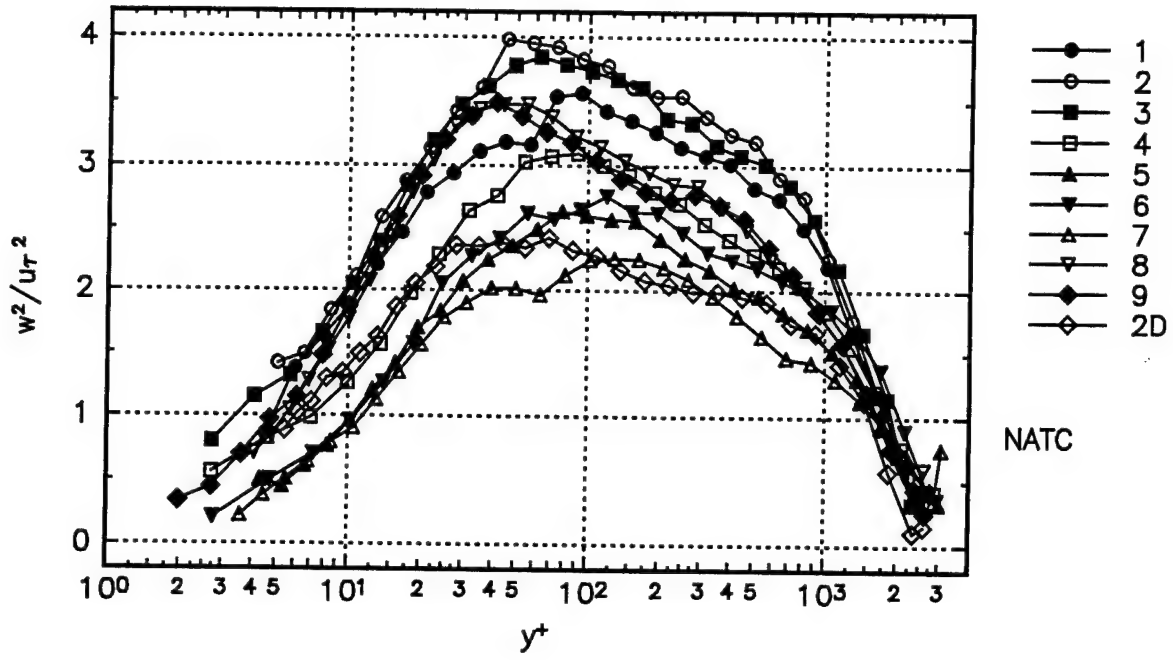
4
3
2
1
0
w^2/u_τ^2
10^0 2 3 4 5 10^1 2 3 4 5 10^2 2 3 4 5 10^3 2 3
y^+
1
2
3
4
5
6
7
8
9
2D
NATC

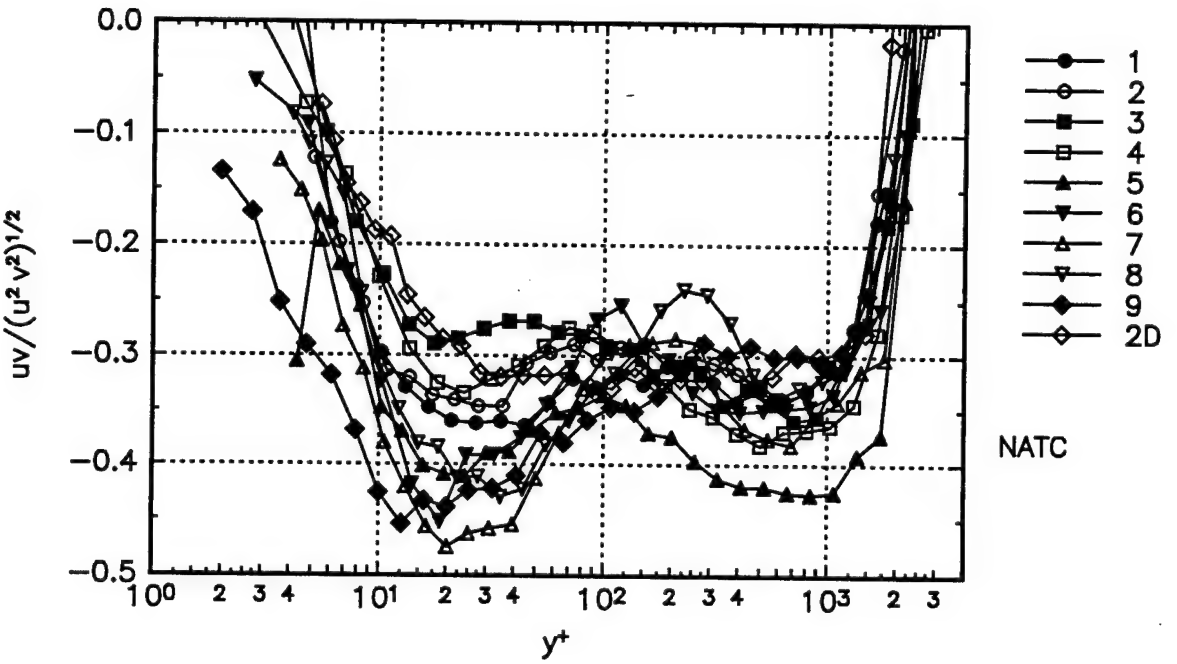
0.0
−0.1
−0.2
−0.3
−0.4
−0.5
$uv/(u^2v^2)^{1/2}$
10^0 2 3 4 10^1 2 3 4 10^2 2 3 4 10^3 2 3
y^+
1
2
3
4
5
6
7
8
9
2D
NATC

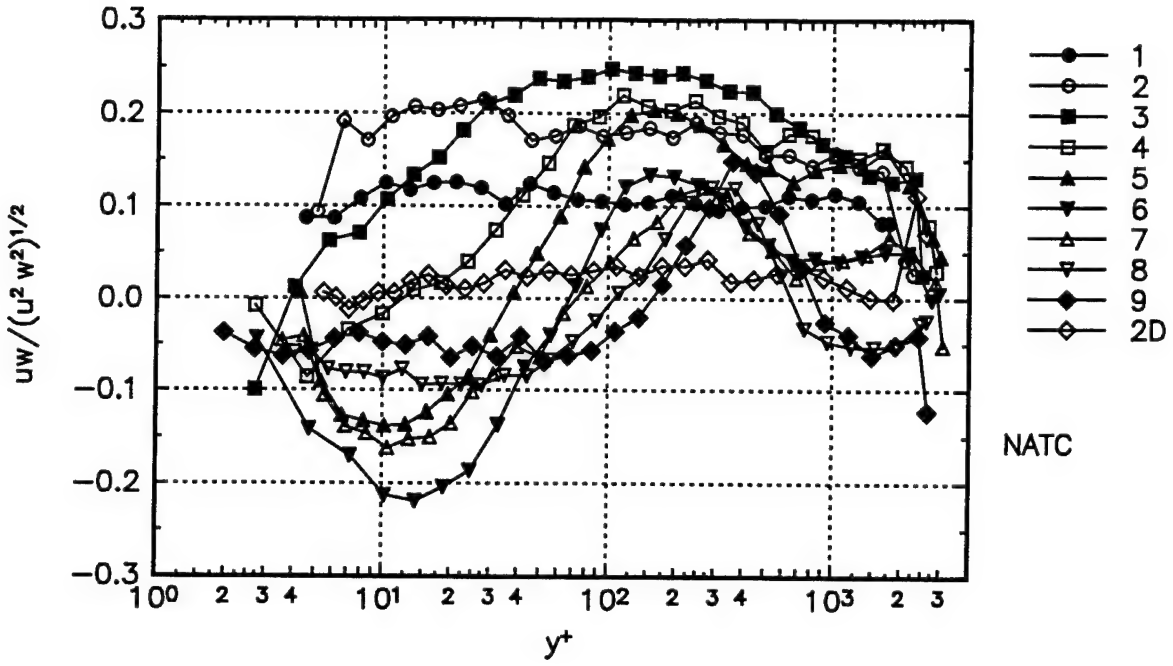
0.3
0.2
0.1
0.0
−0.1
−0.2
−0.3
uw/(u² w²)^1/2
10⁰ 2 3 4 10¹ 2 3 4 10² 2 3 4 10³ 2 3
y+
1
2
3
4
5
6
7
8
9
2D
NATC

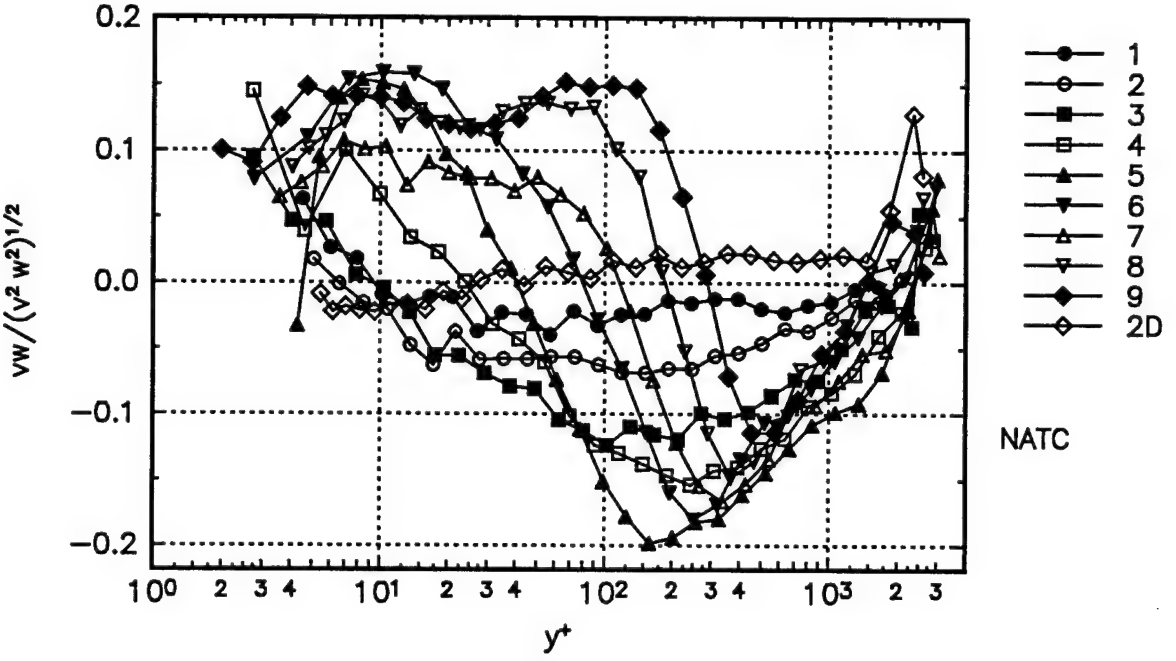
0.2
0.1
0.0
−0.1
−0.2
vw/(v² w²)^1/2
10⁰ 2 3 4 10¹ 2 3 4 10² 2 3 4 10³ 2 3
y+
1
2
3
4
5
6
7
8
9
2D
NATC

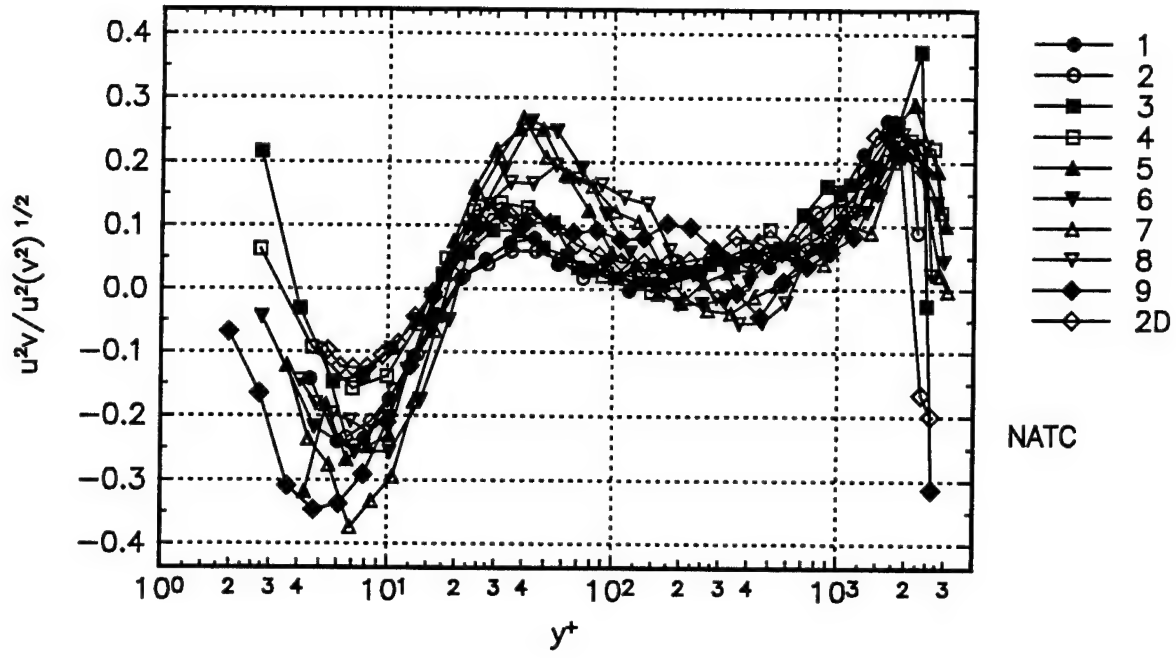
0.4
0.3
0.2
0.1
0.0
−0.1
−0.2
−0.3
−0.4
$u^2v/u^2(v^2)^{1/2}$
10^0 2 3 4 10^1 2 3 4 10^2 2 3 4 10^3 2 3
y^+
1
2
3
4
5
6
7
8
9
2D
NATC

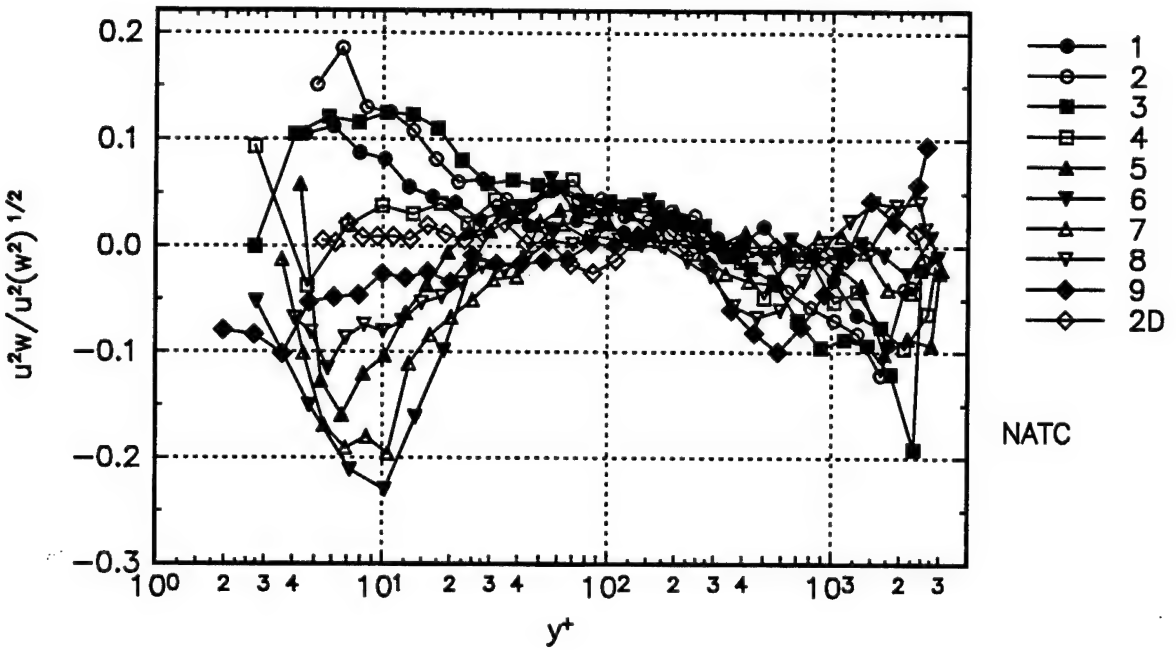
0.2
0.1
0.0
−0.1
−0.2
−0.3
$u^2w/u^2(w^2)^{1/2}$
10^0 2 3 4 10^1 2 3 4 10^2 2 3 4 10^3 2 3
y^+
1
2
3
4
5
6
7
8
9
2D
NATC

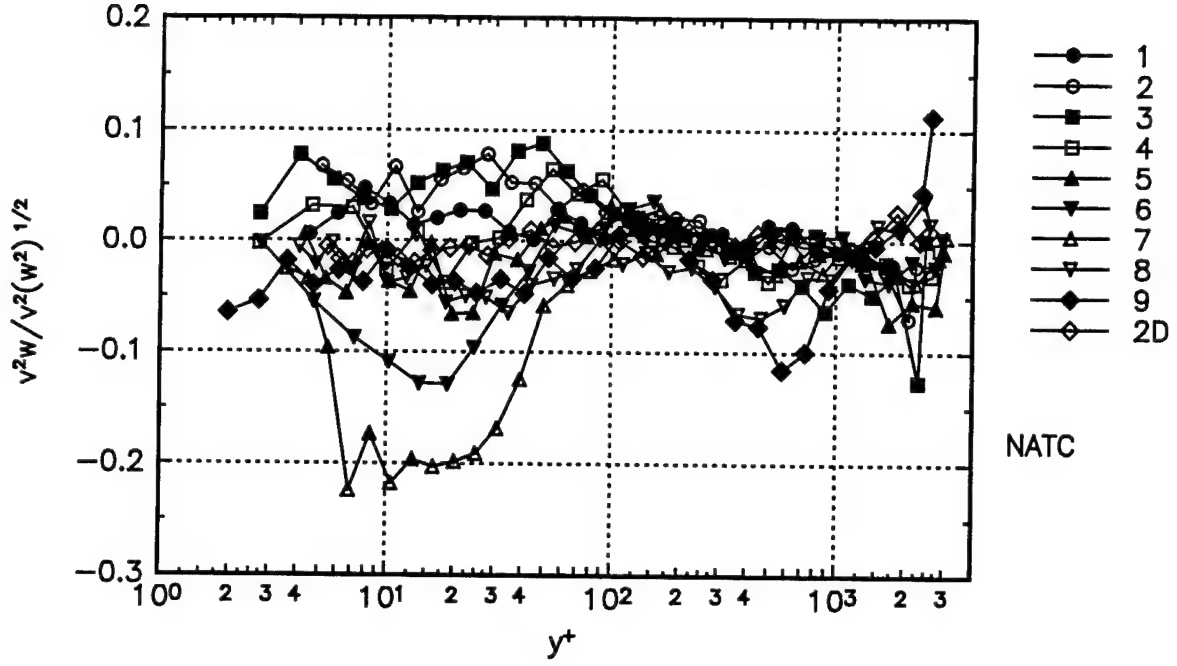
0.2
0.1
0.0
−0.1
−0.2
−0.3
$v^2w/v^2(w^2)^{1/2}$
10^0 2 3 4 10^1 2 3 4 10^2 2 3 4 10^3 2 3
y^+
1
2
3
4
5
6
7
8
9
2D
NATC

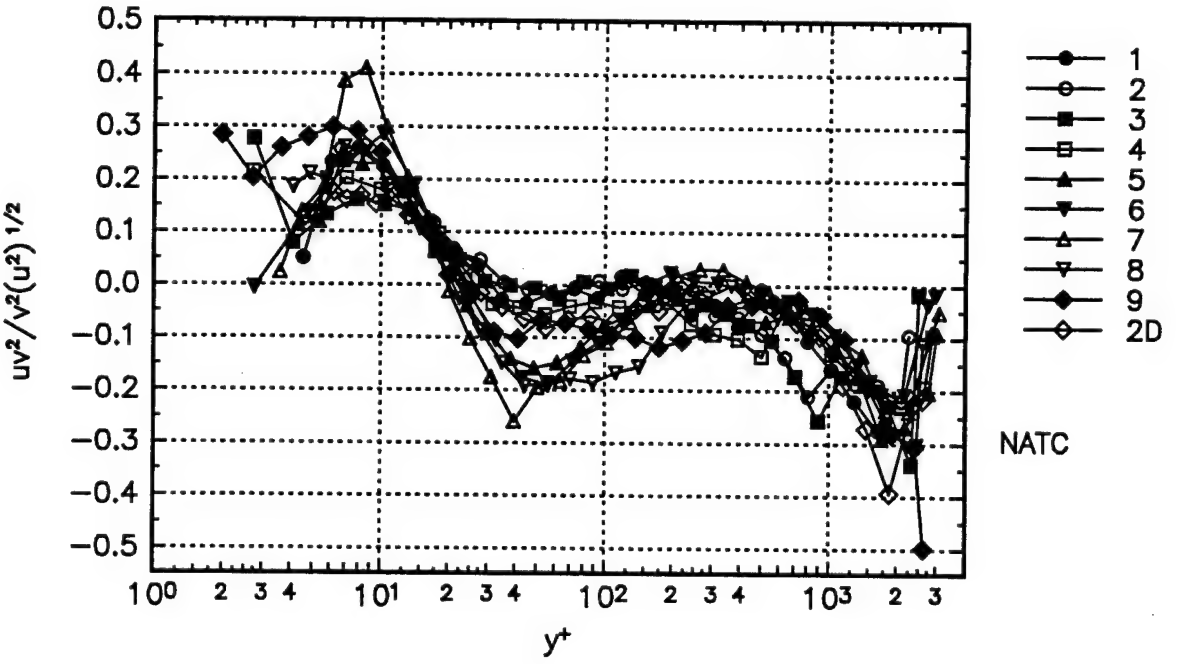
0.5
0.4
0.3
0.2
0.1
0.0
−0.1
−0.2
−0.3
−0.4
−0.5
$uv^2/v^2(u^2)^{1/2}$
10^0 2 3 4 10^1 2 3 4 10^2 2 3 4 10^3 2 3
y^+
1
2
3
4
5
6
7
8
9
2D
NATC

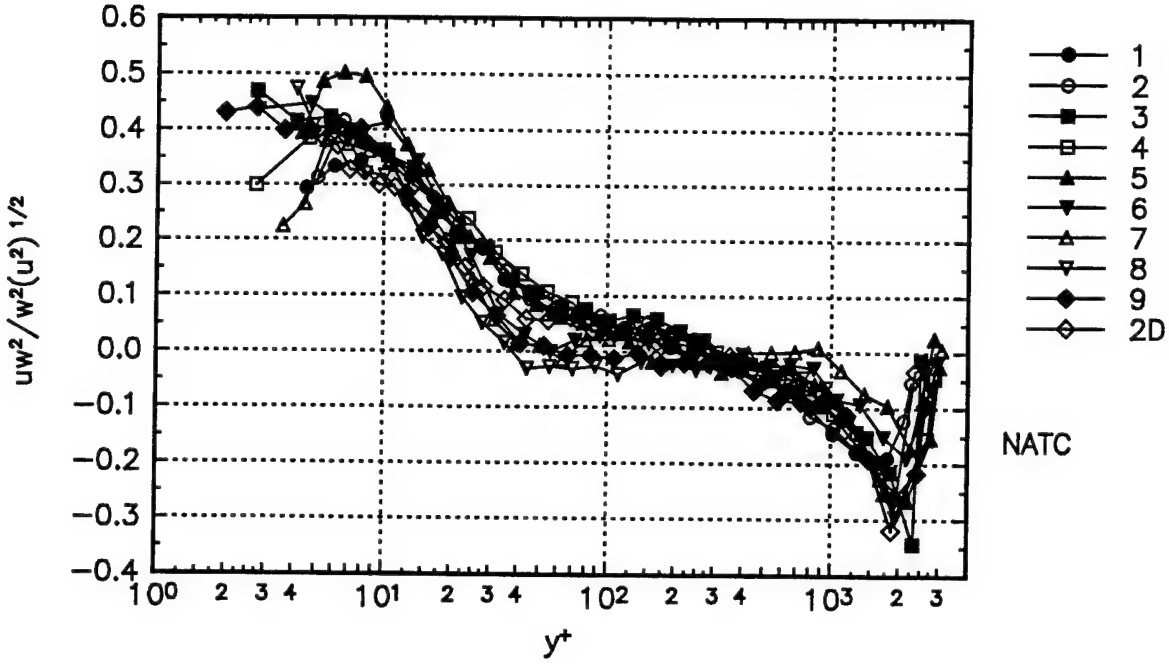
0.6
0.5
0.4
0.3
0.2
0.1
0.0
−0.1
−0.2
−0.3
−0.4
uw²/w²(u²) 1/2
10⁰ 2 3 4 10¹ 2 3 4 10² 2 3 4 10³ 2 3
y+
1
2
3
4
5
6
7
8
9
2D
NATC

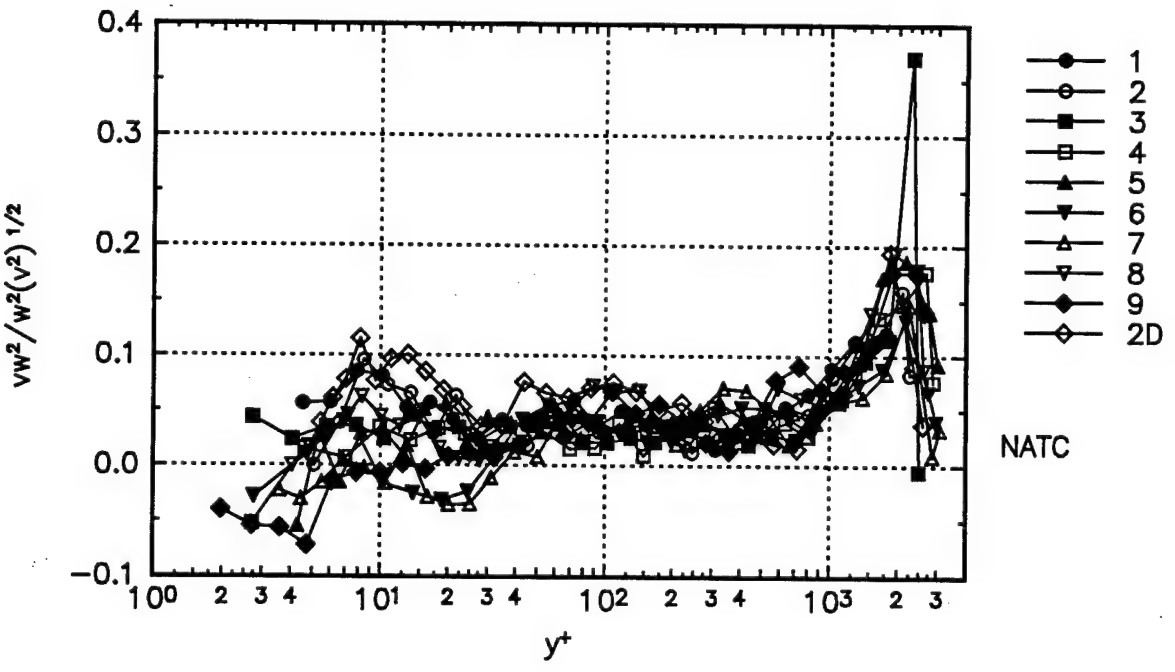
0.4
0.3
0.2
0.1
0.0
−0.1
vw²/w²(v²) 1/2
10⁰ 2 3 4 10¹ 2 3 4 10² 2 3 4 10³ 2 3
y+
1
2
3
4
5
6
7
8
9
2D
NATC

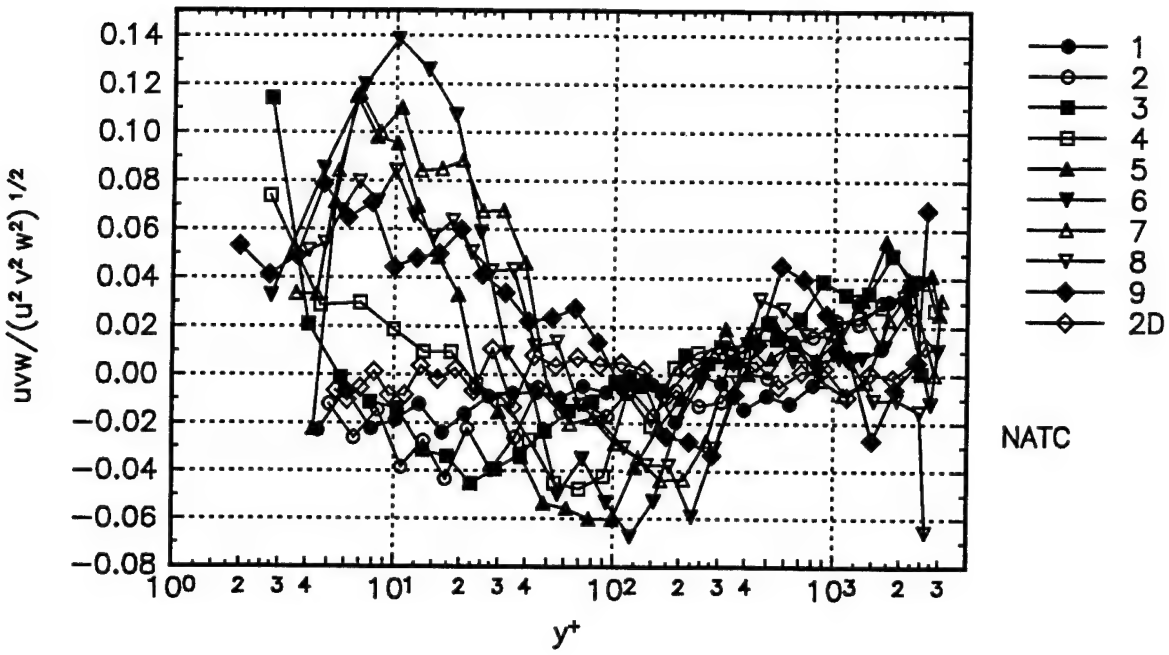
0.14
0.12
0.10
0.08
0.06
0.04
0.02
0.00
−0.02
−0.04
−0.06
−0.08
uvw/(u² v² w²) 1/2
10⁰ 2 3 4 10¹ 2 3 4 10² 2 3 4 10³ 2 3
y+
1
2
3
4
5
6
7
8
9
2D
NATC

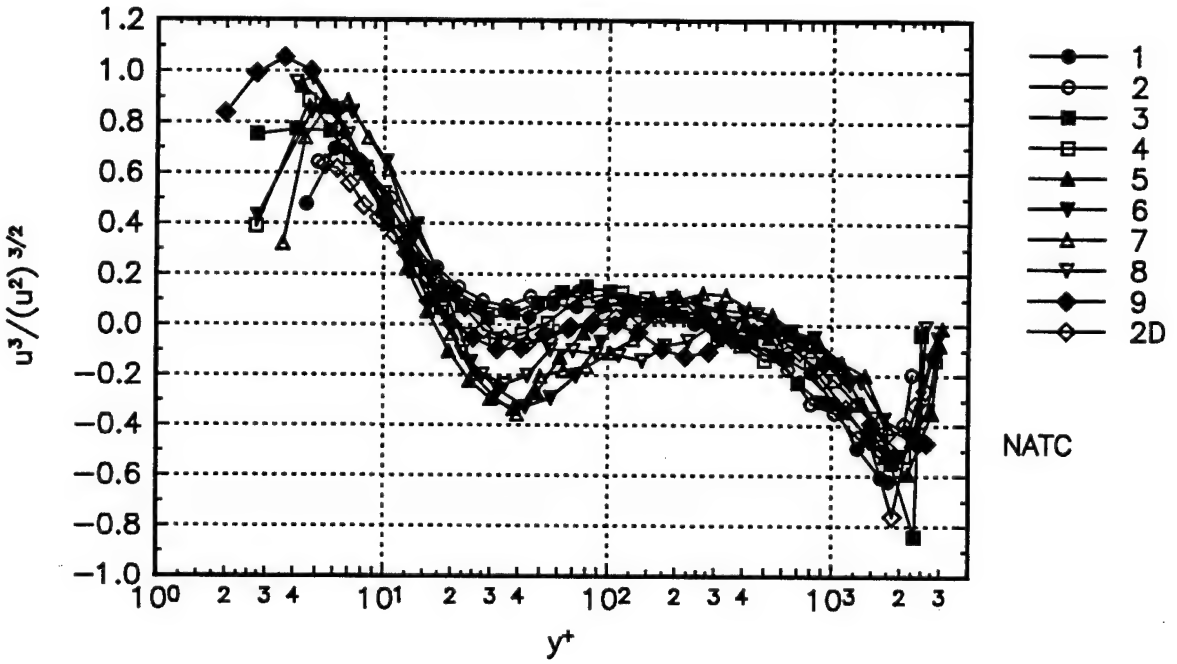
1.2
1.0
0.8
0.6
0.4
0.2
0.0
−0.2
−0.4
−0.6
−0.8
−1.0
u³/(u²) 3/2
10⁰ 2 3 4 10¹ 2 3 4 10² 2 3 4 10³ 2 3
y+
1
2
3
4
5
6
7
8
9
2D
NATC

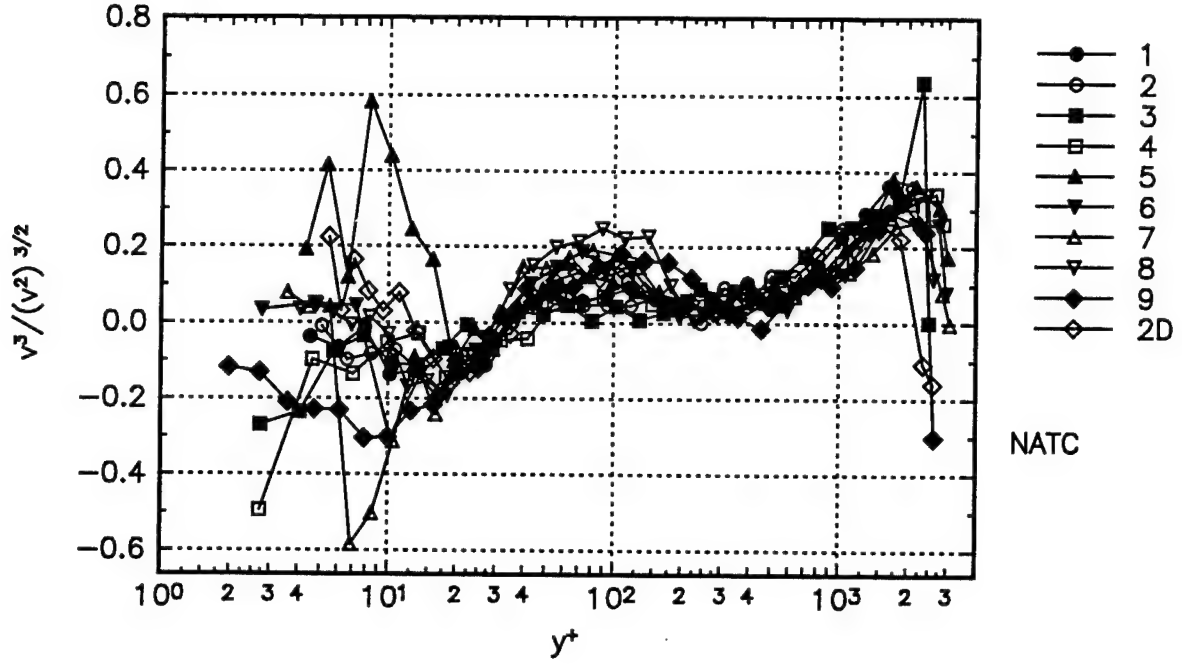
0.8
0.6
0.4
0.2
0.0
−0.2
−0.4
−0.6
$v^3/(v^2)^{3/2}$
10^0 2 3 4 10^1 2 3 4 10^2 2 3 4 10^3 2 3
y^+
1
2
3
4
5
6
7
8
9
2D
NATC

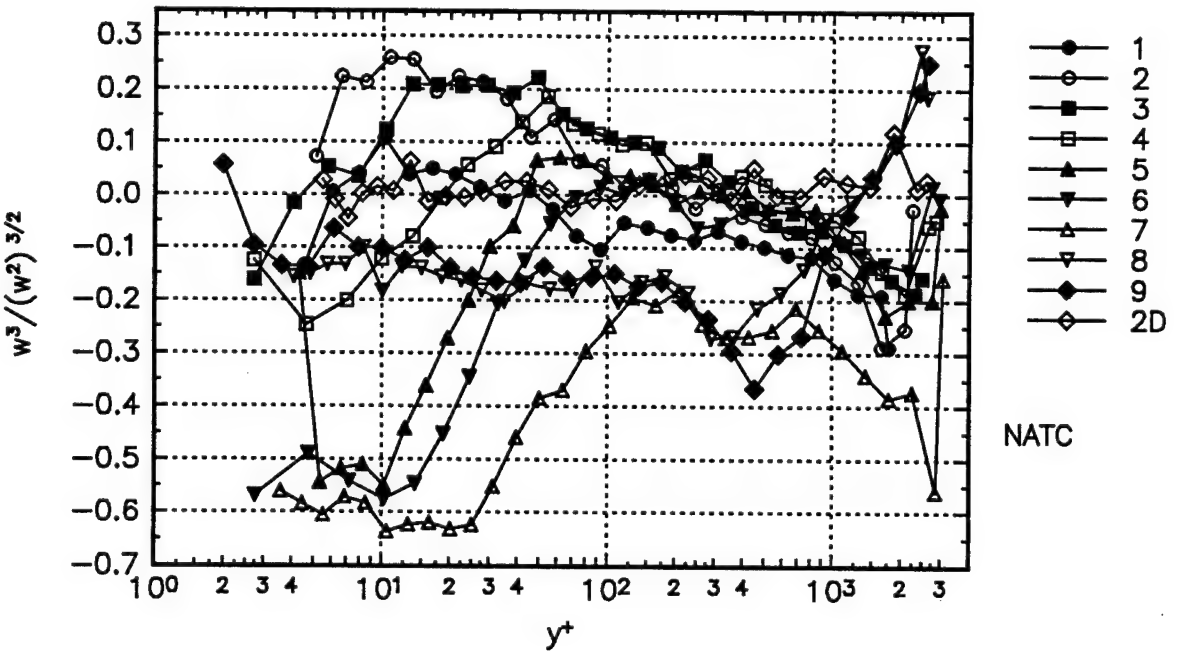
0.3
0.2
0.1
0.0
−0.1
−0.2
−0.3
−0.4
−0.5
−0.6
−0.7
$w^3/(w^2)^{3/2}$
10^0 2 3 4 10^1 2 3 4 10^2 2 3 4 10^3 2 3
y^+
1
2
3
4
5
6
7
8
9
2D
NATC

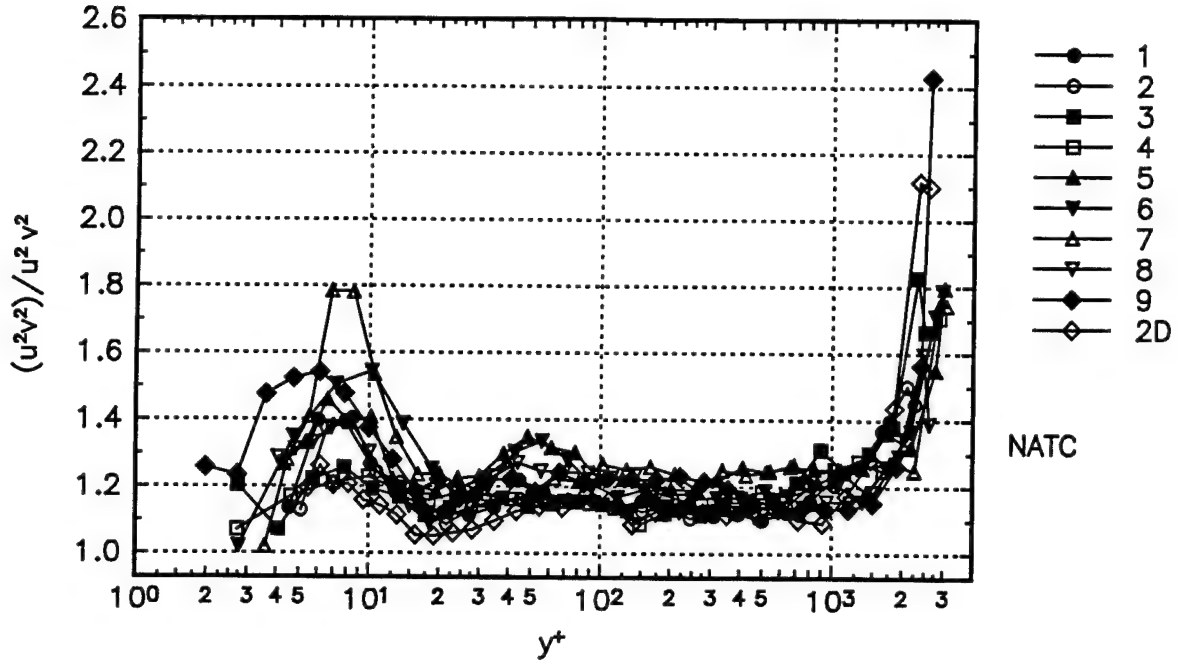
2.6
2.4
2.2
2.0
1.8
1.6
1.4
1.2
1.0
$(u^2v^2)/u^2v^2$
10^0 2 3 4 5 10^1 2 3 4 5 10^2 2 3 4 5 10^3 2 3
y^+
1
2
3
4
5
6
7
8
9
2D
NATC

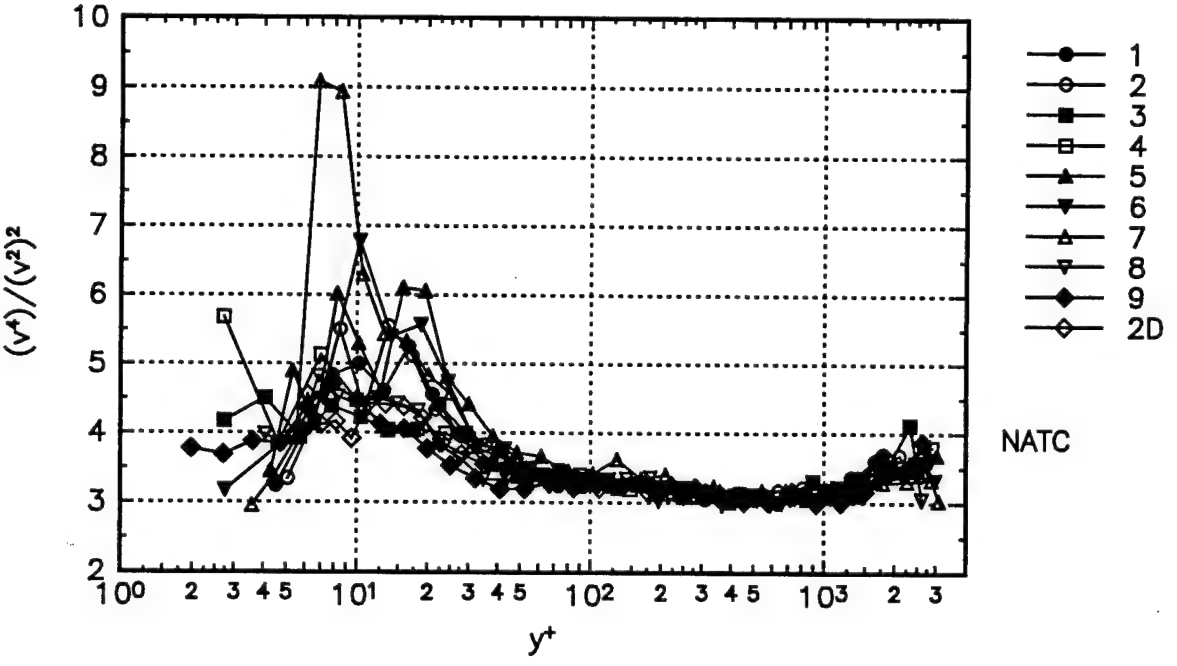
10
9
8
7
6
5
4
3
2
$(v^4)/(v^2)^2$
10^0 2 3 4 5 10^1 2 3 4 5 10^2 2 3 4 5 10^3 2 3
y^+
1
2
3
4
5
6
7
8
9
2D
NATC

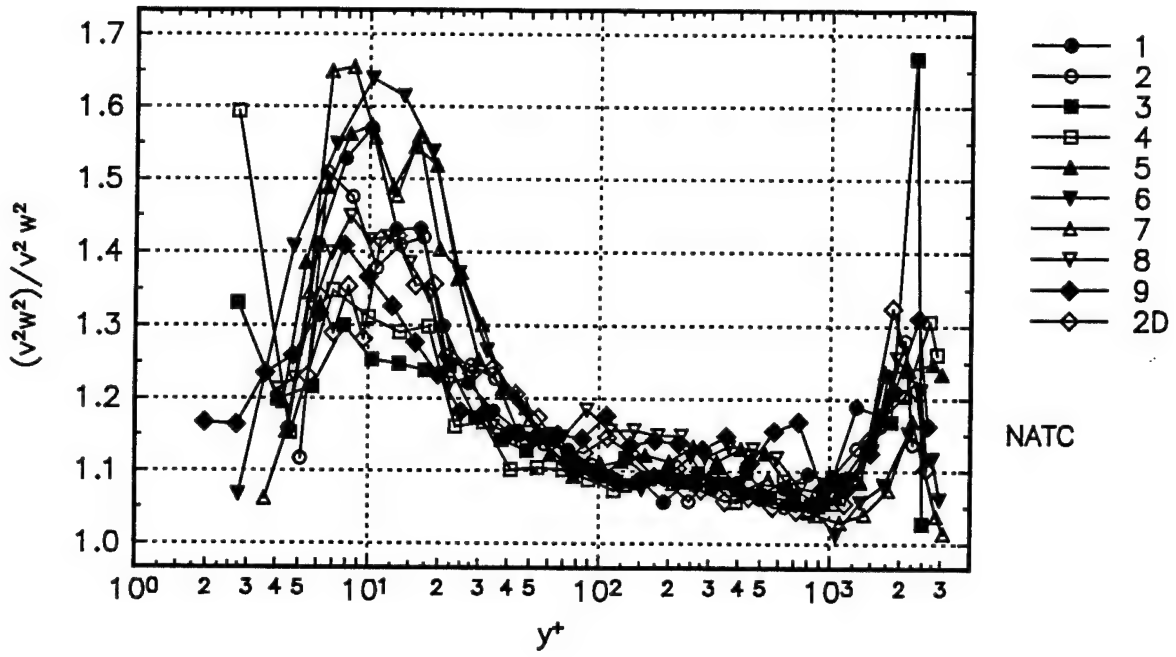
1.7
1.6
1.5
1.4
1.3
1.2
1.1
1.0
$(v^2w^2)/v^2\,w^2$
10^0 2 3 4 5 10^1 2 3 4 5 10^2 2 3 4 5 10^3 2 3
y^+
1
2
3
4
5
6
7
8
9
2D
NATC

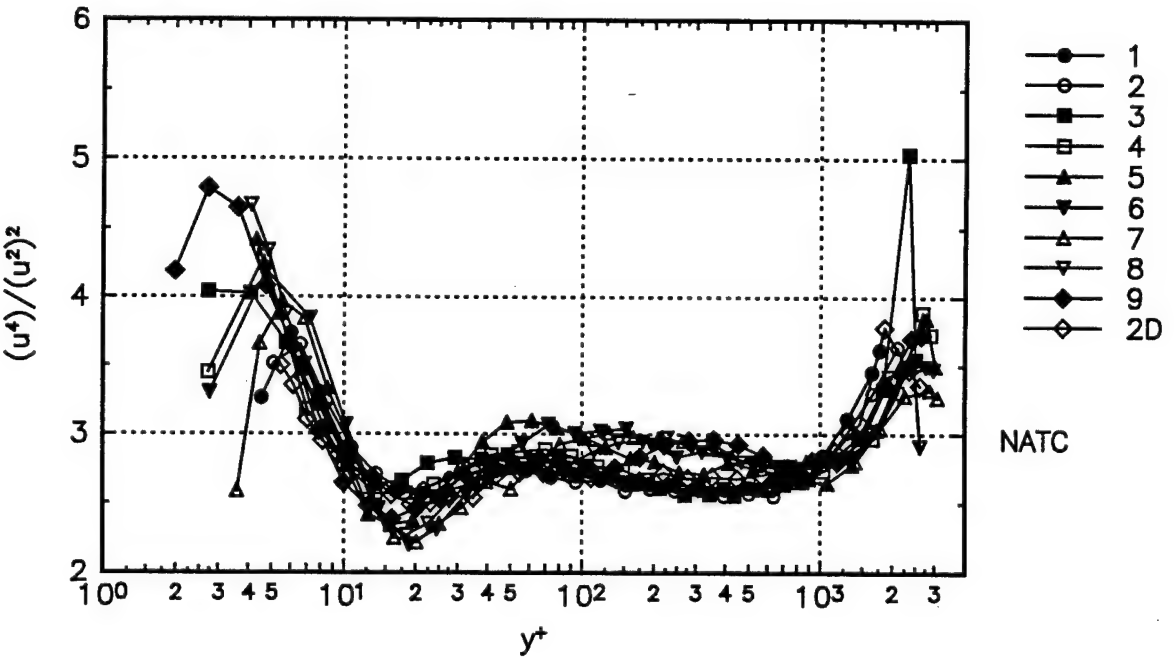
6
5
4
3
2
$(u^4)/(u^2)^2$
10^0 2 3 4 5 10^1 2 3 4 5 10^2 2 3 4 5 10^3 2 3
y^+
1
2
3
4
5
6
7
8
9
2D
NATC

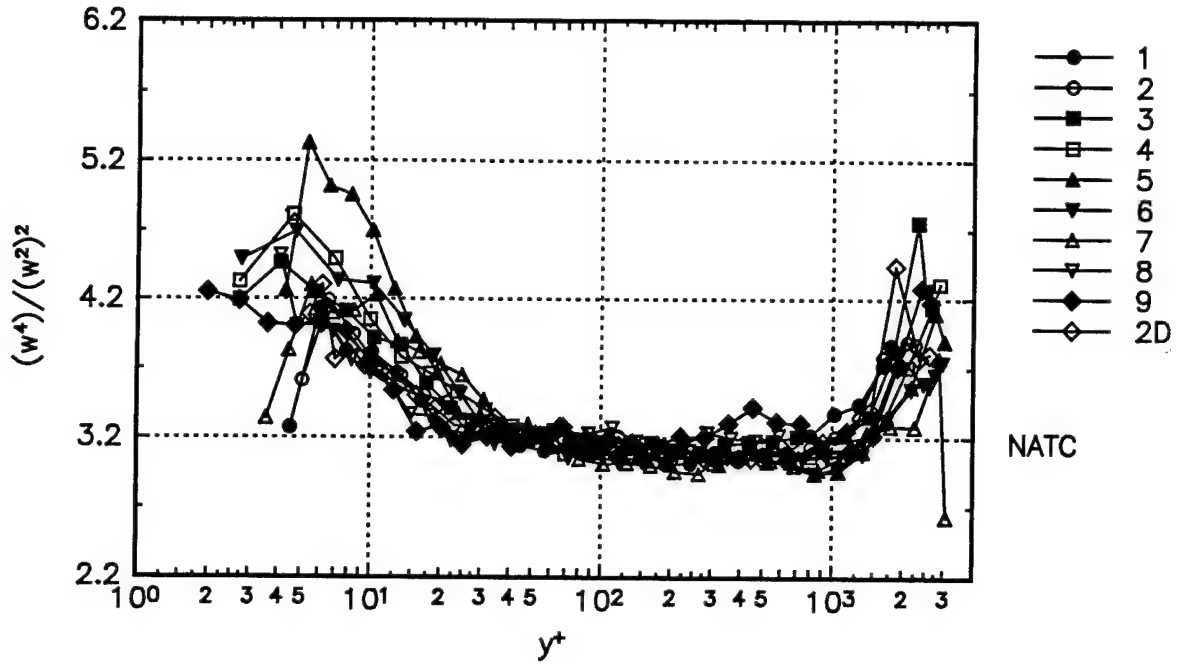
6.2
5.2
4.2
3.2
2.2
$(w^+)/(w^2)^2$
10^0 2 3 4 5 10^1 2 3 4 5 10^2 2 3 4 5 10^3 2 3
y^+
1
2
3
4
5
6
7
8
9
2D
NATC

Appendix E: Principal Stress Coordinates

In this Appendix the normal stresses are presented in the principal stress corrdinates. The normal stresses are nondimensionalized with the u_τ. In the principal stress coordinates the coordinate system is defined such that all the shear stresses are zero.

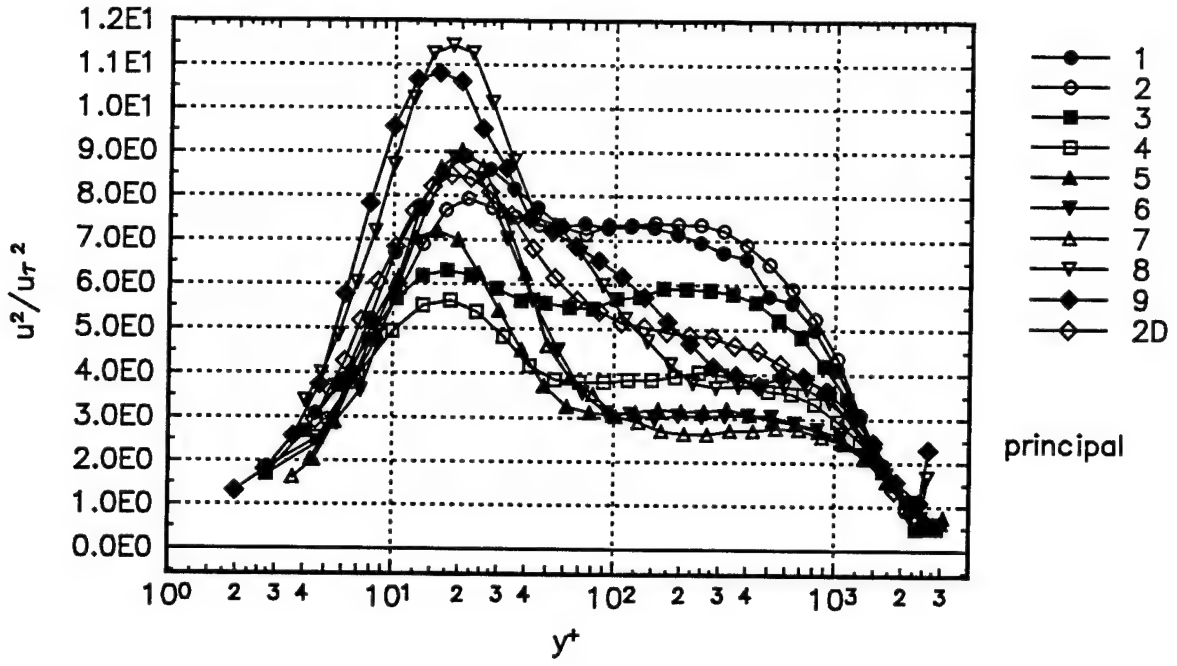

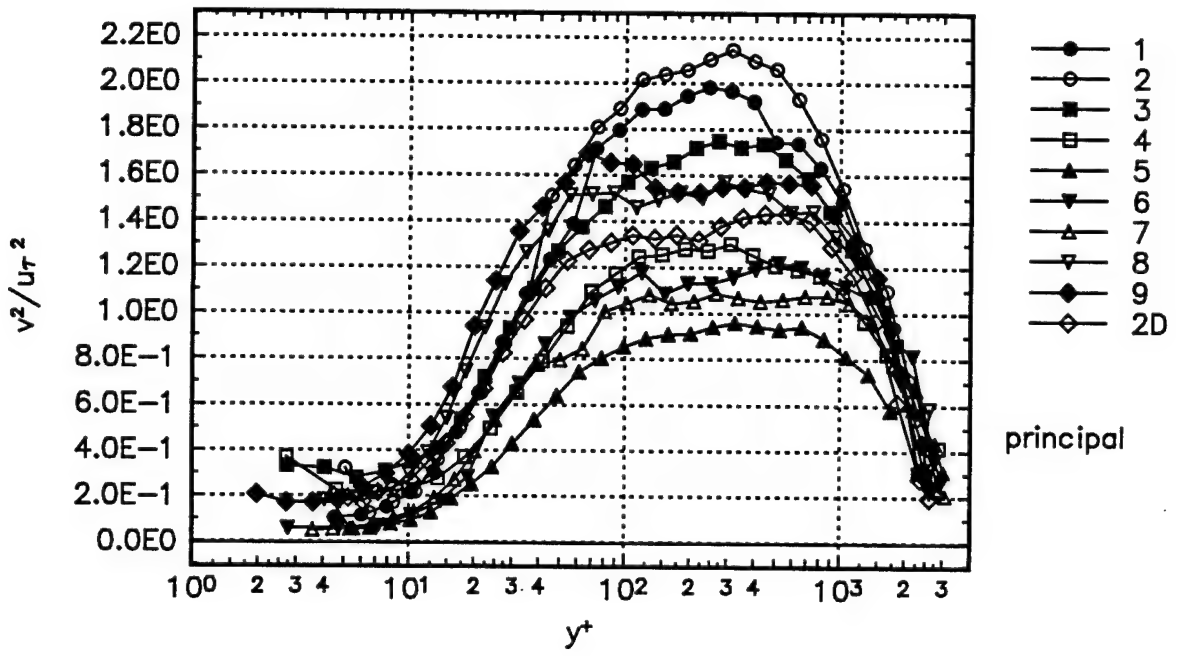

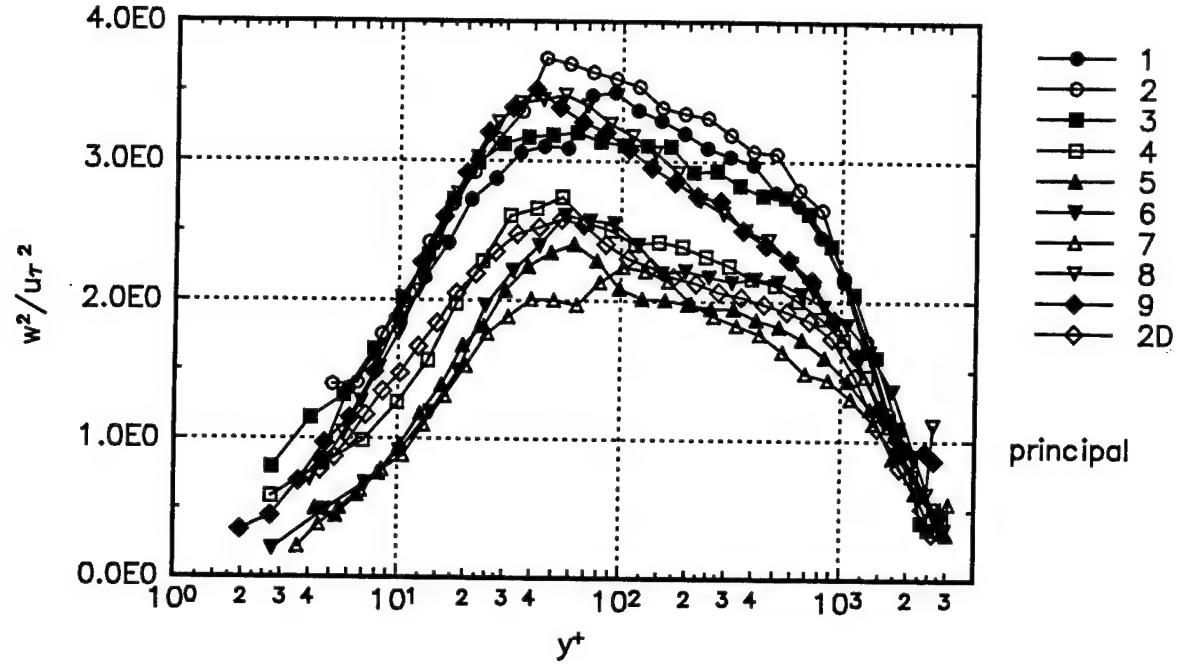

In principal stress coordinates by definition shear stresses are zero. The following shear stress values are the maxiumum shear stresses that are calculated as half of the sum of the normal stresses.

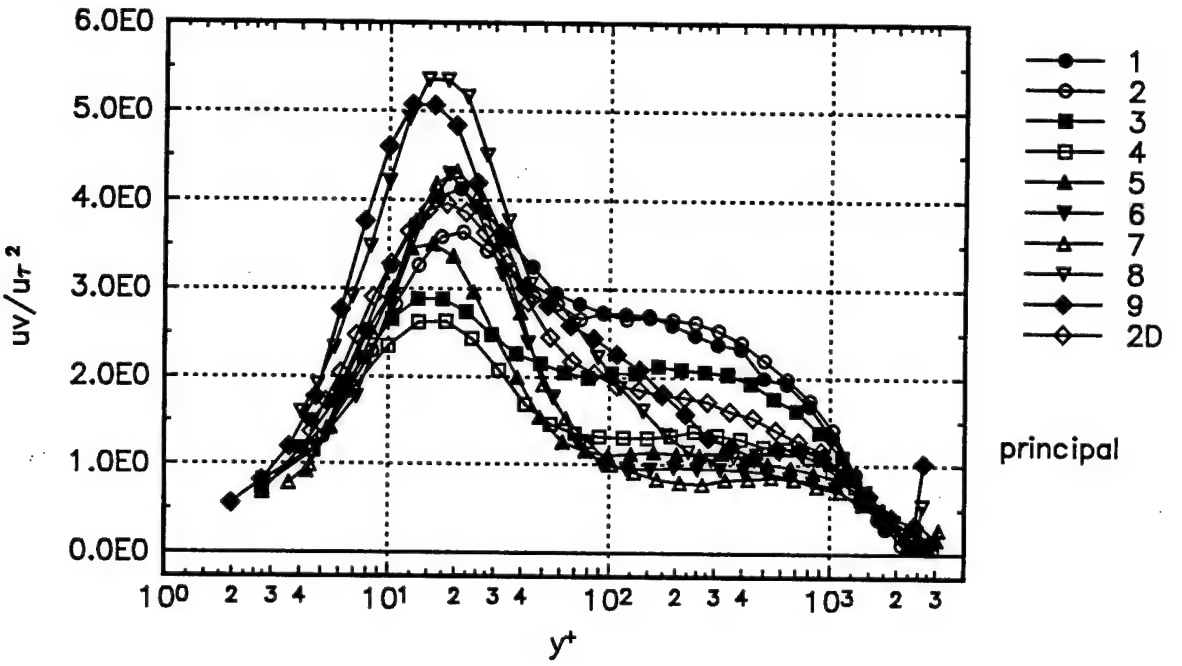

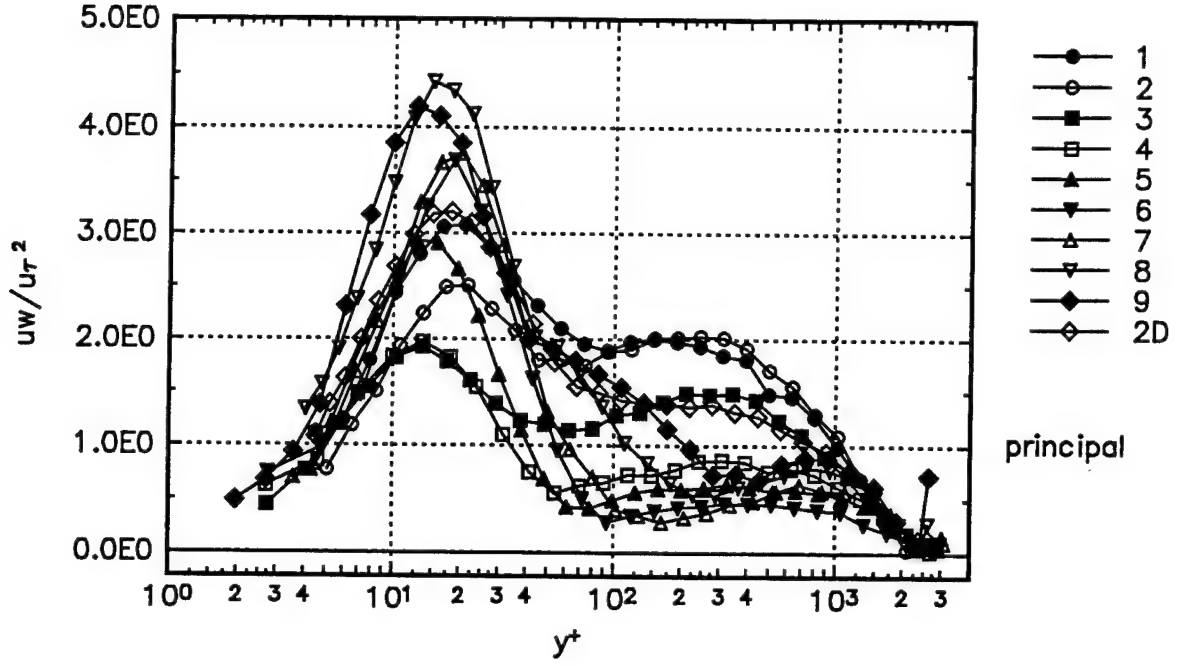
5.0E0
4.0E0
3.0E0
2.0E0
1.0E0
0.0E0
uw/u_τ²
10⁰ 2 3 4 10¹ 2 3 4 10² 2 3 4 10³ 2 3
y⁺
1
2
3
4
5
6
7
8
9
2D
principal

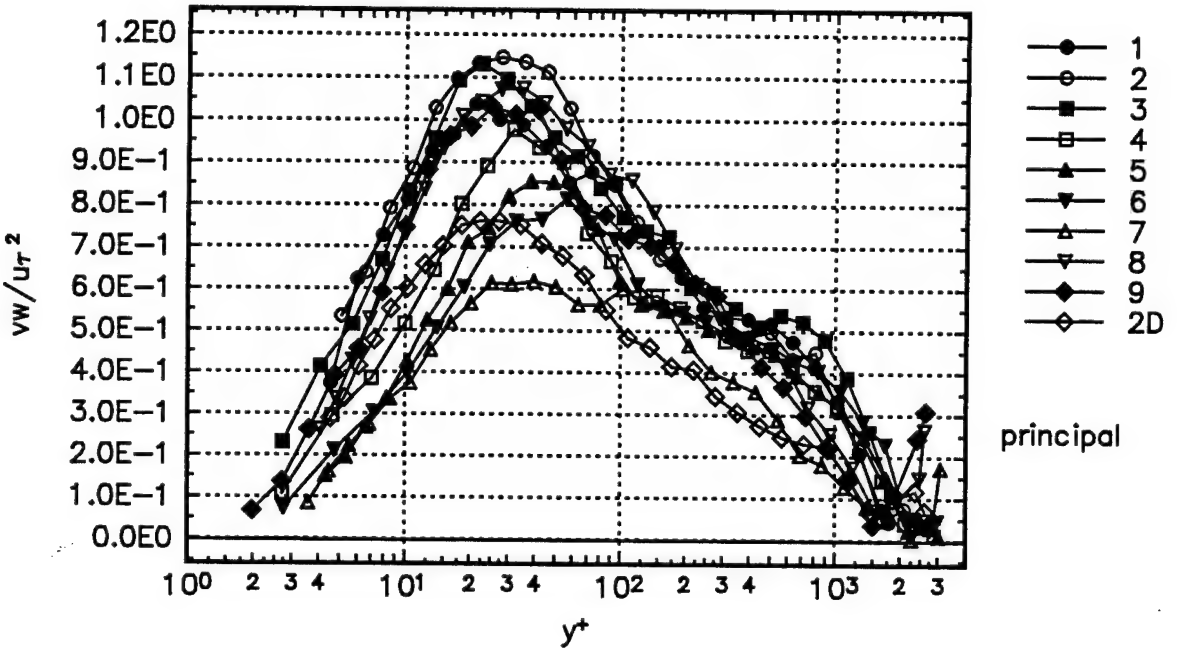
1.2E0
1.1E0
1.0E0
9.0E−1
8.0E−1
7.0E−1
6.0E−1
5.0E−1
4.0E−1
3.0E−1
2.0E−1
1.0E−1
0.0E0
vw/u_τ²
10⁰ 2 3 4 10¹ 2 3 4 10² 2 3 4 10³ 2 3
y⁺
1
2
3
4
5
6
7
8
9
2D
principal

Appendix F: All Negative $\overline{vw}$ Coordinates

In this Appendix the flow variables are presented nondimensionalized by the respective powers of the u_τ. The coordinate system is defined such that the largest $\overline{vw}$ shear stress in a profile is equal to zero.

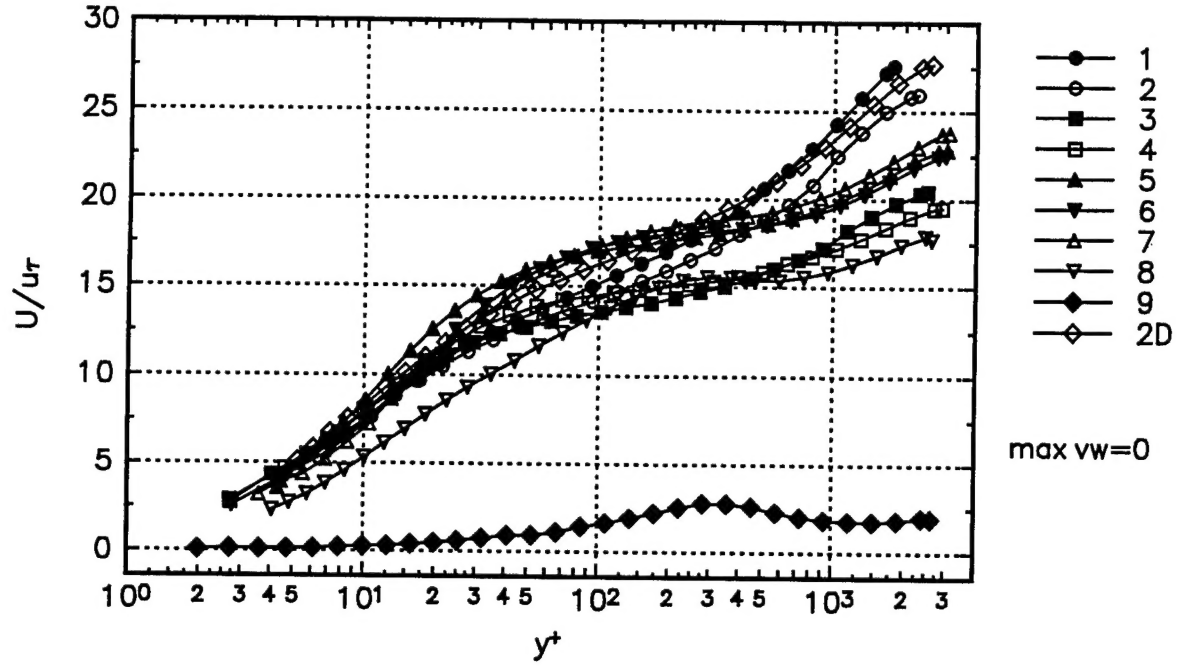

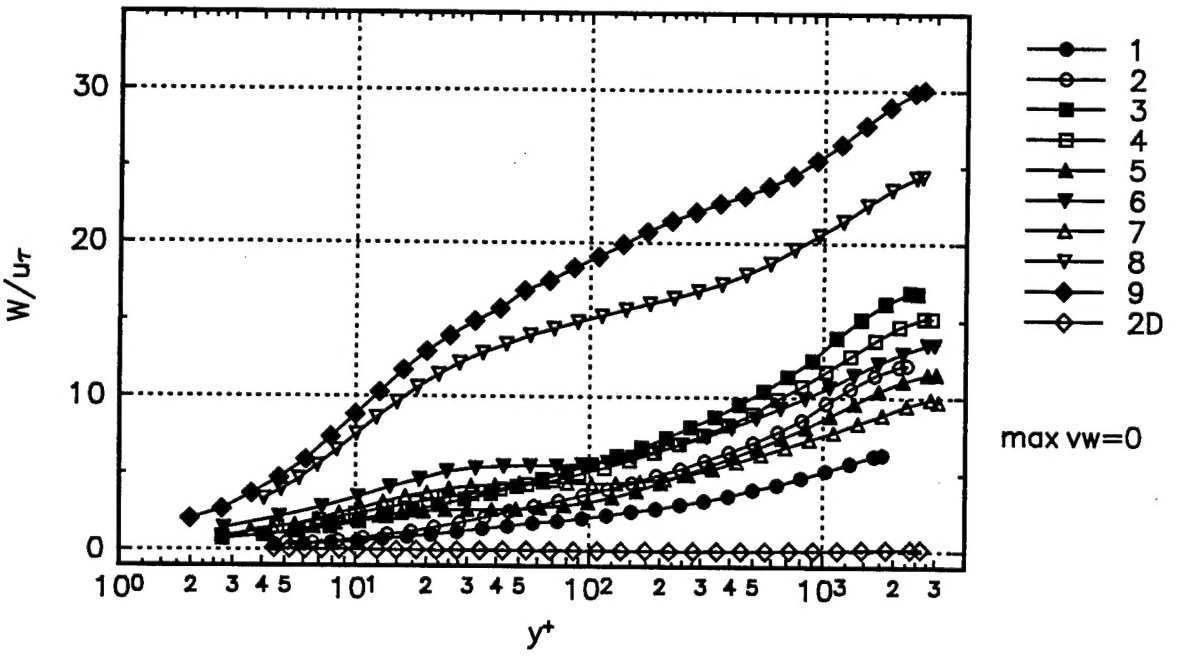

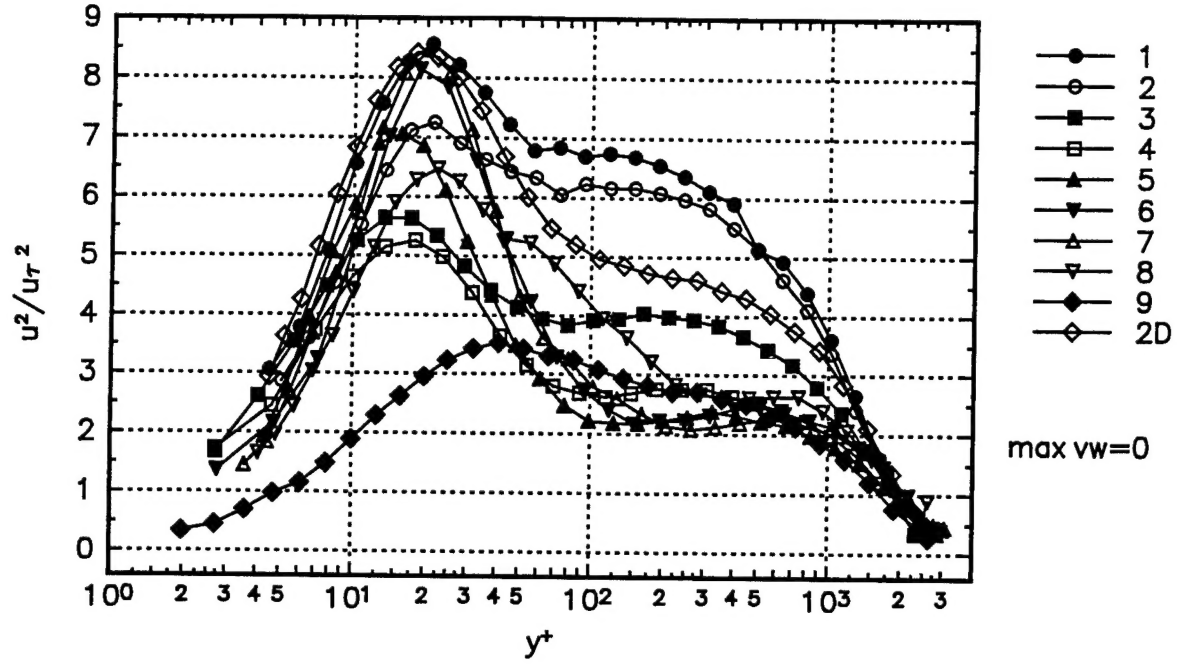
9
8
7
6
5
4
3
2
1
0
u^2/u_τ^2
10^0 2 3 4 5 10^1 2 3 4 5 10^2 2 3 4 5 10^3 2 3
y^+
1
2
3
4
5
6
7
8
9
2D
max vw=0

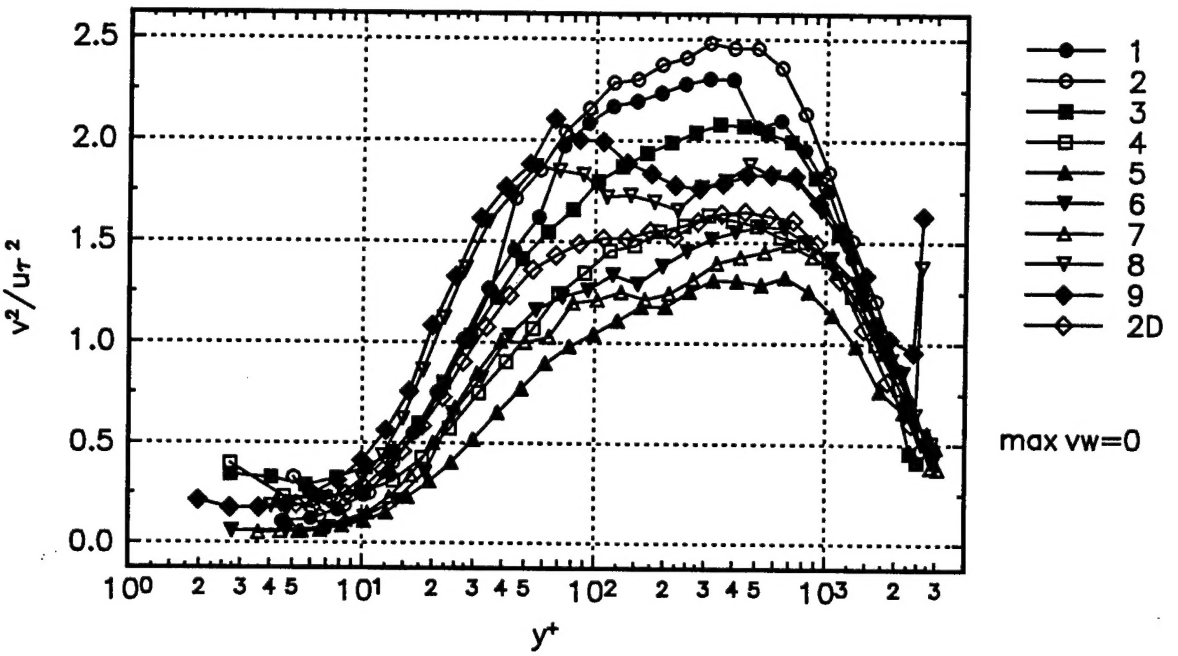
2.5
2.0
1.5
1.0
0.5
0.0
v^2/u_τ^2
10^0 2 3 4 5 10^1 2 3 4 5 10^2 2 3 4 5 10^3 2 3
y^+
1
2
3
4
5
6
7
8
9
2D
max vw=0

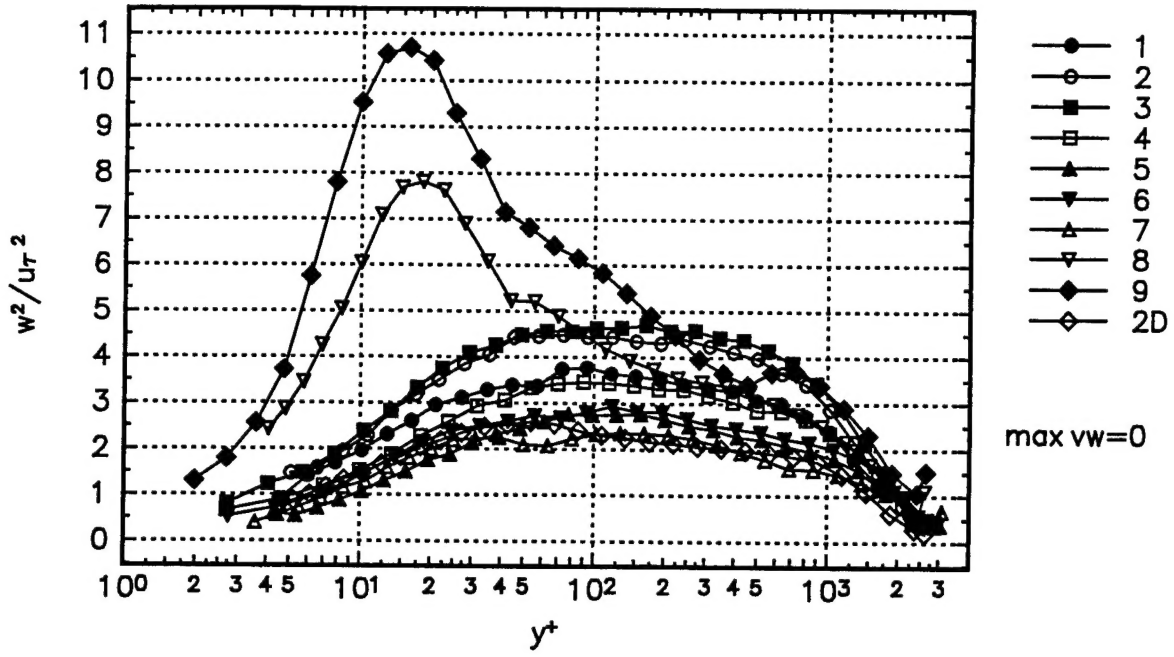
11
10
9
8
7
6
5
4
3
2
1
0
$w^2/u_\tau{}^2$
10^0 2 3 4 5 10^1 2 3 4 5 10^2 2 3 4 5 10^3 2 3
y^+
1
2
3
4
5
6
7
8
9
2D
max vw=0

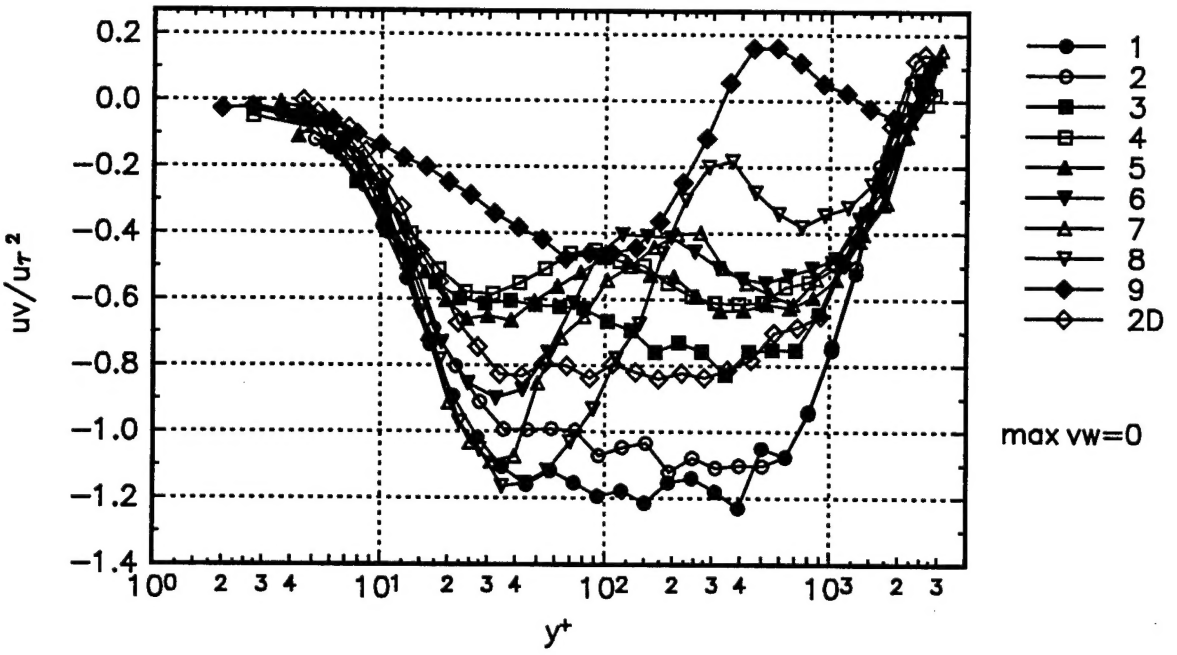
0.2
0.0
−0.2
−0.4
−0.6
−0.8
−1.0
−1.2
−1.4
$uv/u_\tau{}^2$
10^0 2 3 4 10^1 2 3 4 10^2 2 3 4 10^3 2 3
y^+
1
2
3
4
5
6
7
8
9
2D
max vw=0

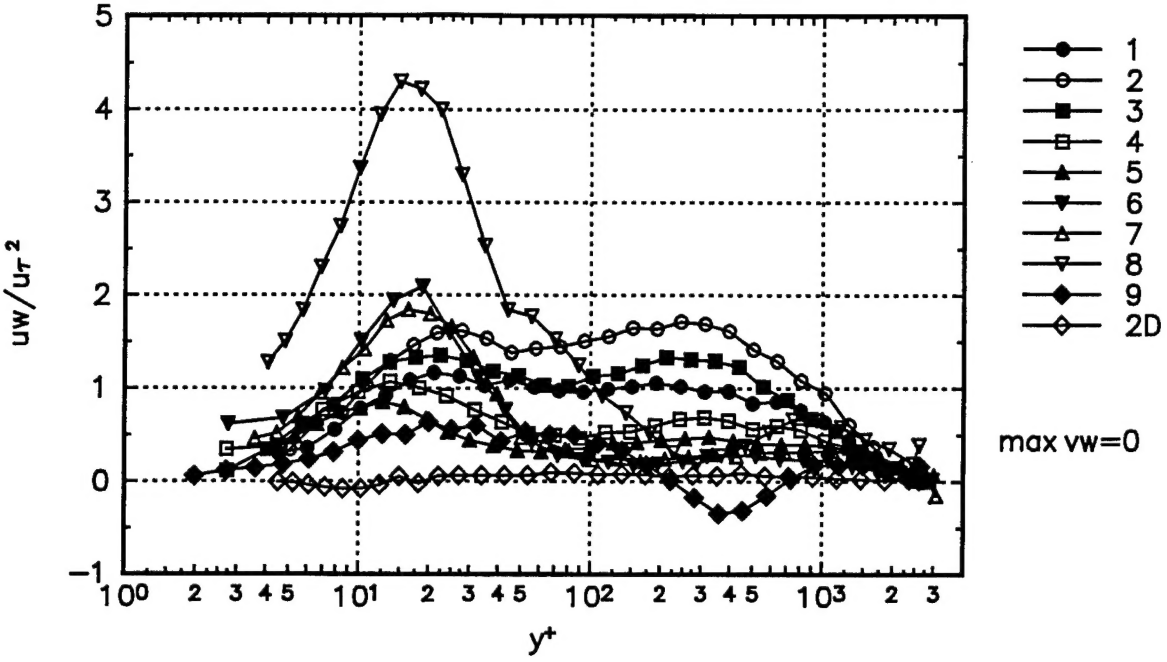
5
4
3
2
1
0
−1
uw/u_τ²
10⁰ 2 3 4 5 10¹ 2 3 4 5 10² 2 3 4 5 10³ 2 3
y⁺
1
2
3
4
5
6
7
8
9
2D
max vw=0

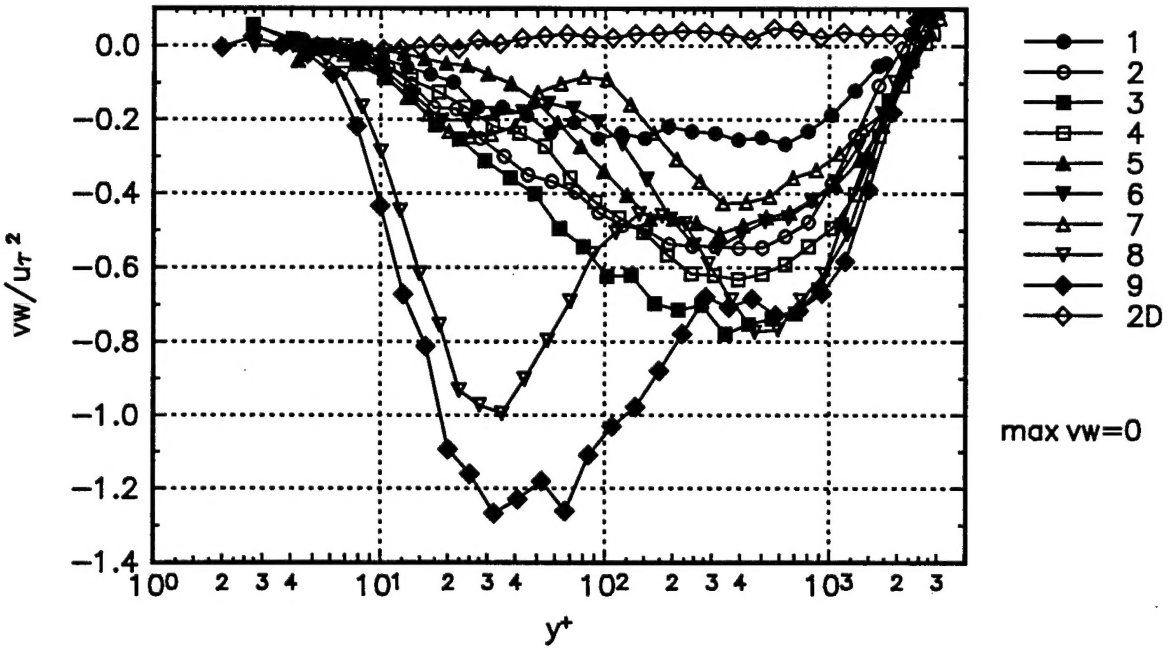
0.0
−0.2
−0.4
−0.6
−0.8
−1.0
−1.2
−1.4
vw/u_τ²
10⁰ 2 3 4 10¹ 2 3 4 10² 2 3 4 10³ 2 3
y⁺
1
2
3
4
5
6
7
8
9
2D
max vw=0